

**Dissecting the role of the *HAWAIIAN SKIRT* gene in
the regulation of floral development using a suppressor
analysis strategy**

By

Dasuni Jayaweera; BSc, MSc

**Thesis submitted to University of Nottingham for the degree of
Doctor of Philosophy, June 2013**



IMAGING SERVICES NORTH

Boston Spa, Wetherby

West Yorkshire, LS23 7BQ

www.bl.uk

BEST COPY AVAILABLE.

VARIABLE PRINT QUALITY

ABSTRACT

HAWAIIAN SKIRT (HWS) is an F-box gene in *Arabidopsis* that plays a key role in plant floral organ development. *HWS* has been identified due to sepal fusion along their basal margins resulting in failure to shed its floral organs (Gonzalez-Carranza *et al.*, 2007). Similar phenotypic characteristics can be seen in the ectopically expressed microRNA *miR164* (Mallory *et al.*, 2004; Lauf *et al.*, 2004) and in the double mutants *cup-shaped cotyledon 1 cuc1/cuc2* (Aida *et al.*, 1997). Previous studies carried out by Gonzalez-Carranza *et al.* (unpublished) using genetic crosses between *hws-1* and other floral mutants has revealed that *HWS* may play a crucial role in the microRNA biogenesis.

In an effort to identify potential substrates of *HWS* and to identify the role of *HWS* in the miRNA pathway, a population of EMS mutagenized *hws-1* was used for isolation and characterization of suppressors of *hws-1*. Screening a number of EMS mutagenized *hws-1* populations has identified several suppressor lines that are currently under study. From the identified mutants, two lines 43.1 and 80.5 were selected for further characterization analysis. These suppressor lines rescue the distinctive sepal fusion phenotype of *hws-1* as well as displaying other phenotypic characteristics.

Characterization of the suppressor lines has identified that 43.1 is an allele of *HST* gene, which is involved in miRNA biogenesis, and 80.5 is an allele of *AS2* gene, which is an adaxial cell fate determinant. Expression analyses have revealed that loss of *HWS* gene function leads to the repression of both 43.1 and 80.5. Genetic analyses have also confirmed that loss of *HWS* gene function results in an upregulation of *CUC1* and *CUC2* gene expression. The results obtained in this project have shown that *HWS* is involved in miRNA, adaxial-abaxial and Organ boundary signalling, concluding that *HWS* may have a wider function in different signalling pathways than previously proposed.

ACKNOWLEDGEMENTS

I would like to thank my supervisor; Professor Jeremy Roberts who provided me with the opportunity to join his research group and for his unwavering support, advice and supervision throughout my doctoral degree. I would also like to thank Dr. Zinnia Gonzalez-Carranza for her supervision, suggestions and support as well as vital laboratory knowledge and techniques. Their continued support and friendship are valuable in completing my research at Sutton Bonington.

Many thanks to Dr. Janny Peters, University of Nijmegen, for her mapping using InDel markers. I am also grateful to Dr. Jean-Luc Verdeil for providing me with the opportunity to carry out some of my research in his laboratory in CIRAD, Montpellier and to Fabienne Lapeyre-Montes for her laboratory support while I was in CIRAD, Montpellier. I owe thanks to Dr. Timothy Tranbarger, IRD and Dr. Fabienne Morcillo, IRD for their support and discussions while I was in Montpellier. I would also like to thank Morag Whitworth for laboratory services and techniques as well as all the staff and friends in Division of Plant Sciences who have help me during my research.

I owe special thanks to my husband and brother for their everlasting love, support and encouragement. I would like to express my deepest gratitude to my father and mother, without whom this doctoral degree would not be possible and for there abiding support and advice throughout my life. Finally I would like to thank the University of Nottingham for providing me with a scholarship to pursue my doctoral degree.

CONTENTS

Contents	i
Tables	iv
Figures	v
Abbreviations	ix

Chapter 1 General Introduction

1.1	<i>Arabidopsis thaliana</i> as a model plant	1
1.2	Regulation of floral development and cell division.....	4
1.3	Regulation of boundary formation throughout floral development.....	10
1.4	Abscission of floral organs in <i>Arabidopsis</i>	15
1.5	Ubiquitin-mediated protein degradation.....	18
1.6	MicroRNAs in plants.....	23
1.7	Leaf formation and patterning in <i>Arabidopsis</i>	30
1.8	Aims and objectives of project	35

Chapter 2 Materials and Methods

2.1	Plant materials and growth conditions.....	36
2.2	Phenotypic analysis and light microscopy.....	37
2.2.1	Tissue fixation and embedding	38
2.2.2	Tissue sectioning	38
2.2.3	Tissue staining	39
2.3	DNA extraction.....	39
2.4	RNA extraction.....	40
2.5	Nucleic acid concentration measurement	41
2.6	Image processing and statistical analysis	41
2.7	Polymerase Chain Reaction (PCR) amplification	42
2.7.1	PCR amplification via Taq DNA polymerase	42
2.7.2	First-strand cDNA synthesis for reverse transcription-PCR	42
2.7.3	Gel electrophoresis	43

2.7.4	Purification of PCR product	43
2.8	Gel extraction for DNA recovery	43
2.9	The <i>hws-1</i> suppressor line mapping	44
2.9.1	InDel (insertion, deletion) marker polymorphism.	44
2.10	Plasmid construction and transformation	46
2.10.1	<i>AS2_{pro}::AS2</i> line generation	46
2.10.2	<i>AS2_{pro}::GUS</i> line generation.....	48
2.10.3	DNA digestion using restriction enzymes	48
2.10.4	<i>AS2</i> gene fragment and pBI101.2 vector ligation.....	48
2.10.5	Bacterial transformation using DH5 α	49
2.10.6	<i>Agrobacterium</i> transformation using C58	50
2.10.7	<i>Arabidopsis</i> transformation using floral dip.....	50
2.10.8	Selecting for plant transformation	51
2.10.9	Histochemical analysis of <i>GUS</i> activity	51
2.11	Bioinformatics analysis	52

Chapter 3 Characterisation of 43.1

3.1	Introduction.....	53
3.1.1	Strategies to identify the substrate(s) of <i>HWS</i>	53
3.1.2	Interaction of <i>HWS</i> and microRNA genes	56
3.1.3	Chapter aims and objectives	57
3.2	Results	58
3.2.1	Morphological analysis of EMS populations	58
3.2.2	Phenotypic analysis of <i>43.1</i>	62
3.2.3	Identifying the nature of <i>43.1</i> mutation	75
3.3	Chapter discussion	80
3.3.1	Flower morphology of <i>43.1</i>	80
3.3.2	Leaf phenotype of <i>43.1</i>	81
3.3.3	Root growth of <i>43.1</i>	82
3.3.4	Isolation and mapping of <i>43.1</i> locus.....	83
3.3.5	Interaction between <i>HWS</i> and <i>HST</i>	84

Chapter 4 Characterisation of 80.5

4.1	Introduction.....	86
4.1.1	The <i>LATERAL ORGAN BOUNDARIES DOMAIN (LBD)</i> gene family.....	86
4.1.2	Adaxial-abaxial polarity	88
4.1.3	Chapter aims and objectives	94
4.2	Results	95
4.2.1	Phenotypic characteristics of 80.5	95
4.2.2	Mapping the gene responsible for the 80.5 phenotype	106
4.2.3	Complementation analysis of 80.5	113
4.2.3.1	Plasmid construction.....	113
4.2.3.2	<i>Agrobacterium</i> and <i>Arabidopsis</i> transformation	116
4.2.3.3	Screening for plant transformants.....	120
4.2.4	Expression analysis of <i>AS2_{pro}::GUS</i> transgenic lines.....	123
4.2.5	Gene expression analysis of 80.5.....	131
4.2.6	Genetic interactions of 80.5 and <i>Pro_{35S}::HWS</i>	132
4.2.7	Genetic interactions of 80.5 and <i>UFO</i>	136
4.3	Chapter discussion	139
4.3.1	Phenotype of the 80.5 mutant	139
4.3.2	Isolation and mapping of the 80.5 locus.....	141
4.3.3	Expression analysis of 80.5	142
4.3.4	Genetic Crosses between 80.5 and selected <i>Arabidopsis</i> mutants.....	144

Chapter 5 General Discussion

5.1	The role of the <i>HWS</i> gene in miRNA biogenesis	144
5.2	The role of the <i>HWS</i> gene in adaxial-abaxial polarity.....	149
5.3	<i>HWS</i> and meristem-to-organ boundary	150
5.4	Conclusion	151
5.5	Future work.....	152
	References.....	154
	Appendix	173

TABLES

1.1	Stages of development of <i>Arabidopsis thaliana</i> Col-0 wild type plants from seed germination to senescence.....	2
2.1	Mutant alleles used in this project obtained from NASC.....	36
3.1	Forty six M2 EMS mutagenized <i>hws-1</i> populations were analysed and twenty suppressor lines have been isolated (shown in white)..	59

FIGURES

1.1	Forward and reverse genetic approaches used to establish gene function by mutagenesis..	4
1.2	Floral meristem developments.....	5
1.3	<i>ABC+E</i> model of <i>Arabidopsis thaliana</i>	7
1.4	Fused floral organ (<i>ffo</i>) alleles.....	12
1.5	Flower phenotype of the <i>hws-1</i> mutant.	13
1.6	The <i>HWS</i> gene and its expression.....	14
1.7	Abscission of floral organs in <i>Arabidopsis</i>	16
1.8	Different stages of development from <i>IDA:GUS</i> flowers.	18
1.9	The process of ubiquitination	20
1.10	MicroRNA biogenesis.	25
1.11	Flowers of miRNA pathway mutants.	26
1.12	MicroRNAs gene regulation and their subsequent functions in different systems are shown in the above pie chart.....	27
1.13	MicroRNA gene regulations in leaf development.....	28
1.14	Col-0 wild type, <i>Cuc1cuc2</i> double mutant, ectopically expressing <i>miR164b</i> and <i>hws-1</i> mutant flower phenotype..	29
1.15	SAM and leaf primordia signalling pathway.....	32
1.16	Theoretical model of interaction between <i>CUC2</i> , <i>PIN1</i> and auxin in the leaf margins.	34
2.1	InDel marker polymorphism with two flanking InDel markers.	45
2.2	<i>AS2</i> promoter and gene sequence..	47
2.3	pBI101.2 T-DNA region.....	49
3.1	PCR analysis of some of the suppressor lines indicating the presence of the <i>HWS</i> gene with a 172 bp band.....	60
3.2	The different types of suppressor mutations, showing an effect on floral organ development.....	61
3.3	Various phenotypic characteristics of <i>43.1/hws-1</i>	63
3.4	F2 progeny PCR amplification of the cross between Col-0 wild type and <i>43.1/hws-1</i>	64

3.5	Phenotypic comparisons of flower at stage 6.90 (table 1.1, section 1.1) and inflorescence morphology of Col-0 wild type, <i>hws-1</i> , <i>43.1/hws-1</i> and <i>43.1/colwt</i>	66
3.6	The average number of sepals and petals from the first ten flowers at stage 6.90 (table 1.1, stage 1.1) out of twenty five flowers analysed from six Col-0 wild type, <i>43.1/colwt</i> and <i>43.1/hws-1</i> plants.....	67
3.7	Stage 6.5 flower comparisons between <i>43.1/hws-1</i> , <i>43.1/colwt</i> and <i>hst-1</i> at stage 6.90	68
3.8.	Abnormal phyllotaxis in <i>43.1/hws-1</i> , <i>43.1/colwt</i> and <i>hst-1</i> compared to Col-0 wild type and <i>hws-1</i>	69
3.9	Comparison of the phenotypic characteristics between Col-0 wild type, <i>hws-1</i> , <i>43.1/hws-1</i> and <i>43.1/colwt</i>	71
3.10	Seedling comparison between <i>43.1/hws-1</i> , <i>43.1/colwt</i> and <i>hst-1</i>	72
3.11	Comparison between Col-0 wild type, <i>hws-1</i> and <i>43.1/hws-1</i> seedling on MS media plates	73
3.12	Root growth over a time course of 10 days of Col-0 wild type, <i>hws-1</i> , <i>43.1/hws-1</i> and <i>hst-1</i>	74
3.13	Part of the multiple sequence alignment of <i>43.1</i> and <i>HST</i> using ClustalW (EMBL-EBI) program.....	76
3.14	Protein translation of <i>HST</i> coding region showing <i>43.1</i> stop codon.....	77
3.15	Genomic structure of <i>HST</i> showing the locations of various <i>hst</i> alleles	84
4.1	Expression of <i>AS2</i> various tissues of <i>Arabidopsis</i>	87
4.2	An illustration of Abaxial-adaxial polarity.....	89
4.3	Adaxial-abaxial genetic network in leaves.....	91
4.4	Adaxial-abaxial polarity in stamen development.....	93
4.5	PCR amplifications of members of the F2 population from the cross between Col-0 wild type and <i>80.5/hws-1</i> using <i>HWS</i> specific primers	96
4.6	Comparisons between 20 day old seedlings of Col-0 wild type, <i>hws-1</i> , <i>80.5/hws-1</i> and <i>80.5/colwt</i>	98

4.7	Comparisons between 24 day old seedlings of (A) <i>80.5/hws-1</i> , <i>80.5/colwt</i> and (B) <i>as2-1</i> , <i>as2-4</i> , <i>as2-101</i>	99
4.8	Comparable phenotypic analysis of flower at stage 6.90 (table 1.1, section 1.1) and inflorescence morphology of Col-0 wild type, <i>hws-1</i> , <i>80.5/hws-1</i> and <i>80.5/colwt</i>	101
4.9	Flower at stage 6.90 (table 1.1, section 1.1) and inflorescence morphology of (A and D) <i>as2-1</i> , (B and E) <i>as2-4</i> and (C and F). <i>as2-101</i>).	102
4.10	Root growth over a time course of 19 days of Col-0 wild type, <i>hws-1</i> , <i>80.5/hws-1</i> and <i>80.5/colwt</i>	103
4.11	Anatomy of transverse sections stage 1.06 (table 1.1, section 1.1), 6 rosette leaves > 1mm in length, Col-0 wild type, <i>hws-1</i> , <i>80.5/hws-1</i> and <i>80.5/colwt</i> rosette leaves.	105
4.12	Genomic DNA of plant tissue extracted from 64 F2 plants out of 384 of the cross between <i>80.5/hws-1</i> (Columbia ecotype) and <i>ffo1</i> (Landsberg ecotype).	107
4.13	Mapping structure of <i>80.5</i>	108
4.14	Multiple sequence alignment of <i>AS2</i> and <i>80.5</i> 5'UTR using ClustalW (EMBL-EBI) program.	109
4.15	Protein translations of <i>AS2</i> and <i>80.5</i>	111
4.16	Protein translation of <i>AS2</i>	112
4.17	<i>AS2</i> gene sequence.....	114
4.18	The structure of the <i>AS2_{pro}::AS2</i> construct for complementation analysis in <i>80.5/hws-1</i> including Col-0 wild type and <i>hws-1</i> as controls	115
4.19	Ligation and transformation of the <i>AS2_{pro}::AS2::pBI101.2</i> construct.....	117
4.20	The pattern of <i>AS2_{pro}::AS2::pBI101.2</i> construct (positive colony 3) digestion.....	118
4.21	Sequence alignment of <i>AS2_{pro}::AS2::pBI101.2</i> construct with the primers used for PCR amplification of purified positive colony 3.....	119
4.22	PCR amplification of the positive colonies from the <i>AS2_{pro}::AS2::pBI101.2</i> plasmid transformation via <i>Agrobacterium tumefaciens</i> C58.....	120

4.23	PCR amplification of the T1 transformants. Primers used for PCR amplification include (A) <i>AS2_{pro}::AS2::pBI101.2</i> plasmid primers (pBI101.2for and AS2rev4), (B) <i>HWS</i> primers (SSLPHSfor and SSLPHSrev), (C) specific primers design to amplify wild type (WTfor and MISMATCHrev) and (D) <i>80.5</i> mutant (MUTANTfor and MISMATCHrev).....	122
4.24	The structure of the <i>AS2_{pro}::GUS</i> construct and PCR amplification of the DH5 α cell transformation.....	124
4.25	Sequence alignment of <i>AS2_{pro}::GUS</i> construct with the primers used for PCR amplification of purified positive colony 22 using ClustalW (EMBL-EBI) program.	125
4.26	PCR amplification of the positive colonies from the <i>AS2_{pro}::GUS</i> plasmid transformation via <i>Agrobacterium tumefaciens</i> C58..	126
4.27	PCR amplification of the T1 transformants.....	127
4.28	Expression analysis of <i>AS2_{pro}::GUS</i> transformed <i>hws-1</i> T1 progeny..	129
4.29	Expression analysis of <i>AS2_{pro}::GUS</i> transformed Col-0 wild type T1 progeny.....	130
4.30	<i>GUS</i> expression in two week old seedlings of <i>AS2_{pro}::GUS</i> transformed Col-0 wild type and <i>hws-1</i>	131
4.31	Gene expression analysis of inflorescence and leaves of Col-0 wild type, <i>hws-1</i> , <i>Pro35S::HWS</i> , <i>80.5/hws-1</i> , <i>80.5/colwt</i> and <i>as2-1</i> cDNA using RT-PCR analysis..	132
4.32	PCR amplification for the selection of <i>80.5/Pro35S::HWS</i> double mutant..	133
4.33	Phenotypic characteristics of <i>Pro35S::HWS</i> , <i>80.5/colwt</i> and <i>80.5/Pro35S::HWS</i> double mutant.	135
4.34	PCR amplification for the selection of <i>80.5/ufo-2</i> double mutant.....	137
4.35	Phenotypic characteristics of <i>80.5/colwt</i> , <i>ufo-2</i> and <i>80.5/ufo-2</i> double mutant.	138
5.1	<i>HWS</i> and <i>HST</i> gene interactions.	147
5.2	<i>HWS</i> and adaxial-abaxial gene interactions.....	151

ABBREVIATIONS

α	alpha
β	beta
μg	microgram
μl	microlitre
μM	micromolar
AD	activation domain
AG	<i>AGAMOUS</i>
<i>AGO1</i>	<i>ARGONAUTE1</i>
<i>AP1</i>	<i>APETALA1</i>
<i>AP2</i>	<i>APETALA 2</i>
<i>AP3</i>	<i>APETALA 3</i>
<i>ARF</i>	<i>AUXIN RESPONSE FACTOR</i>
<i>AS1</i>	<i>ASYMMETRIC LEAVES1</i>
<i>AS2</i>	<i>ASYMMETRIC LEAVES2</i>
ASK	<i>Arabidopsis</i> Skp-1 related
<i>ASL</i>	<i>AS2-like</i>
AZ	abscission zone
BD	binding domain
<i>BOP1</i>	<i>BLADE-ON-PETIOLE1</i>
bp	base pair
<i>BP</i>	<i>BREVIPEDICELLUS</i>
CaMV35S	cauliflower mosaic virus 35S promoter
CBP	CAP-BINDING PROTEIN
cDNA	complementary deoxyribonucleic acid
<i>CLV</i>	<i>CLAVATA</i>
cm	centimeter
Col-0	Columbia-0-wild type
<i>CRC</i>	<i>CRAB CLAW</i>
<i>CUC</i>	<i>CUP-SHAPED COTYLEDON</i>
CUL1	Cullin1
DCL1	Dicer-like 1
<i>DLC4</i>	<i>DICER-LIKE4</i>
DNA	deoxyribonucleic acid
DNase	deoxyribonuclease
dNTP	deoxyribonucleoside triphosphates
dsRNA	double stranded RNA
E1	ubiquitin activating enzyme
E2	ubiquitin conjugating enzyme
E3	ubiquitin ligase
<i>EEP1</i>	<i>EARLY EXTRA PETALS1</i>
EMS	Ethyl methane sulfonate
<i>ETT</i>	<i>ETTIN</i>

<i>FIL</i>	<i>FILAMENTOUS FLOWER</i>
FM	floral meristem
g	gram
GUS	β -glucuronidase
<i>HD-ZIPIII</i>	<i>HOMEODOMAIN-LEUCINE ZIPPER III</i>
<i>HEA</i>	<i>HAESA</i>
<i>HEN1</i>	<i>HUA ENHENCER1</i>
<i>HSL2</i>	<i>HEASA-LIKE 2</i>
<i>HST</i>	<i>HASTY</i>
<i>HWS</i>	<i>HAWAIIAN SKIRT</i>
<i>HYL1</i>	<i>HYPONASTIC LEAVES1</i>
IAA	Indole-3-acetic acid
<i>IDA</i>	<i>INFLORESCENCE DEFICIENT IN ABSCISSION</i>
IM	inflorescence meristem
<i>INO</i>	<i>INNER NO OUTER</i>
<i>KAN</i>	<i>KANADI</i>
Kb	kilobase
<i>KNOX</i>	<i>KNOTTED</i> -like homeobox
L	litre
LB	.
medium	Luria and Bertani medium
<i>LBD</i>	<i>LOB DOMAIN</i>
Ler	Landsberg erecta
<i>LFY</i>	<i>LEAFY</i>
LLRs	Leucine rich repeats
<i>LOB</i>	<i>LATERAL ORGAN BOUNDARIES</i>
mg	milligram
miRNA	microRNA
ml	millilitre
mM	millimolar
mRNA	messenger RNA
MS	
medium	Murashige and Skoog Basal medium
NBB	Naphthol blue black
ORF	open reading frame
<i>PAN</i>	<i>PERIANTHIA</i>
PAS	periodic acid-Schiff's reagent
PCR	Polymerase Chain Reaction
PGs	polygalacturonases
<i>PHAN</i>	<i>PHANTASTICA</i>
<i>PHB</i>	<i>PHABULOSA</i>
<i>PHV</i>	<i>PHAVOLUTA</i>
<i>PI</i>	<i>PISTILLATA</i>
<i>PID</i>	<i>PINOID</i>

<i>PIN1</i>	<i>PINFORMED1</i>
pri-miRNA	primary miRNA
<i>PRS</i>	<i>PRESSED FLOWER</i>
<i>PTL</i>	<i>PETAL LOSS</i>
<i>RBE</i>	<i>RABBIT EARS</i>
RBX1	RING-BOX1
<i>RDR6</i>	<i>RNA-DEPENDENT RNA POLYMERASE6</i>
<i>REV</i>	<i>REVOLUTA</i>
RLK5	receptor-like protein kinase 5
RNA	ribonucleic acid
RNAi	RNA interference
RNase	ribonuclease
<i>RS2</i>	<i>ROUGH SHEATH2</i>
RT-PCR	<i>Reverse Transcriptase-Polymerase Chain Reaction</i>
SAM	shoot apical meristem
SCF	SKP1-CUL1-F-box
<i>SE</i>	<i>SERRATE</i>
<i>SEP</i>	<i>SEPALLATA</i>
<i>SGS3</i>	<i>SUPPRESSOR OF GENE SILENCING3</i>
SKP1	SUPPRESSOR OF KINETOCHORE PROTEIN1
sRNAs	small RNAs
ssRNAs	single stranded RNAs
<i>STM</i>	<i>SHOOT MERISTEMLESS</i>
<i>SUP</i>	<i>SUPERMAN</i>
ta-siRNA	trans-acting short interfering RNAs
TBE	Tris-Borate-EDTA
TCP	TEOSINTE BRANCHED1 CYCLOIDEA, PCF
T-DNA	transfer DNA
<i>TFL1</i>	<i>TERMINAL FLOWER1</i>
TILLING	targeting induced local lesions in genomes
Ub	ubiquitin
<i>UFO</i>	<i>UNUSUAL FLORAL ORGAN</i>
UTR	untranslated region
UV	ultraviolet
V/V	volume per volume
W/V	weight per volume
W/W	weight per weight
<i>WUS</i>	<i>WUSCHEL</i>
<i>YUC</i>	<i>YUCCA</i>

CHAPTER 1

General Introduction

1.1 *Arabidopsis thaliana* as a model plant

As a small dicotyledonous plant belonging to the *Brassicaceae* or mustard family, *Arabidopsis thaliana* is well known for its research in paving the way for development of many genetics approaches for gene function determination (Meinke et al., 1998). Various ecotypes have been accumulated from the natural population of *Arabidopsis*. The common ecotypes used for molecular and genetic studies are the Columbia (Col-0) and the Landsberg (*Ler*) ecotypes. The *Arabidopsis* life cycle takes six weeks to complete making it easy to study over a short period of time. The life cycle includes the germination of seeds, rosette plant formation, main stem bolting, floral development and seed maturation. The wild type flowers have a length of 2 mm and have the capability to self pollinate. It can also be cross pollinated by applying pollen from a donor plant to the stigma surface. Seed diameter is known to be 0.5 mm and the plant generates siliques as it matures with approximately 51 seeds per silique (Meinke et al., 1998; Crawford and Yanofsky, 2011). Depending on the growth conditions, the standard rosette plants have a diameter of 2-10 cm. The surface of *Arabidopsis* leaves is populated with trichomes which are used in the study of cellular differentiation and morphogenesis (Meinke et al., 1998). The understanding of plant development and growth is made possible by focusing on the molecular genetics of the *Arabidopsis* plant. In an effort to rapidly identify gene functions, Boyes *et al* (2001) have created developmental landmarks and triggers for the accumulation of morphological data (Table 1.1)

Stages of development	Average day from sowing date		Description
Stage 0 Seed germination			
	0.10	3	Seed imbibition
	0.50	4.3	Radical emergence
	0.70	5.5	Hypocotyl and cotyledon emergence
Stage 1 Leaf development			
	1.0	6	Cotyledons fully opened
	1.02	12.5	2 rosette leaves > 1mm in length
	1.03	15.9	3 rosette leaves > 1mm in length
	1.04	16.5	4 rosette leaves > 1mm in length
	1.05	17.7	5 rosette leaves > 1mm in length
	1.06	18.4	6 rosette leaves > 1mm in length
	1.07	19.4	7 rosette leaves > 1mm in length
	1.08	20	8 rosette leaves > 1mm in length
	1.09	21.1	9 rosette leaves > 1mm in length
	1.10	21.6	10 rosette leaves > 1mm in length
	1.11	22.2	11 rosette leaves > 1mm in length
	1.12	23.3	12 rosette leaves > 1mm in length
	1.13	24.8	13 rosette leaves > 1mm in length
	1.14	25.5	14 rosette leaves > 1mm in length
Stage 3 Rosette development			
	3.20	18.9	Rosette is 20% of final size
	3.50	24	Rosette is 50% of final size
	3.70	27.4	Rosette is 70% of final size
	3.90	29.3	Rosette development is complete
Stage 5 Emergence of inflorescence			
	5.10	26	First flower buds are visible
Stage 6 Production of flowers			
	6.0	31.8	First flower opens
	6.10	35.9	10% of flower to be produced have opened
	6.30	40.1	30% of flower to be produced have opened
	6.50	43.5	50% of flower to be produced have opened
	6.90	49.4	Flowering complete
Stage 8 Silique ripening			
	8.00	48	First silique shattered
Stage 9 Senescence			
	9.70		Senescence complete, ready for seed harvest

Table 1.1 Stages of development of *Arabidopsis thaliana* Col-0 wild type plants from seed germination to senescence showing a time course to reach each growth stage. Each stage was noted by taking the average day from the date of sowing, including 3 day stratification at 4°C in order to synchronize germination. The plants were grown under standard environmental conditions during a 16 hour light cycle. Illustration from Boyes et al., 2001.

Arabidopsis gene function can be determined through forward or reverse genetics (Figure 1.1). Forward genetics is used in the identification of genes that are associated with specific biological processes (Østergaard and Yanofsky, 2004). It involves the use of mutagenesis via chemical, physical or biological agents such as Ethyl methane sulfonate (EMS), fast neutron bombardment and insertion elements (T-DNA) (Alonso and Ecker, 2006). When the mutant possessing the desired phenotype is identified, the gene responsible is isolated using map and clone based analysis. Chemical agents such as EMS are highly efficient due to the high frequency of mutations (approximately 400 mutations per genome) that can be obtained compared to T-DNA transposon insertions which generate an average of 1.5 insertions per T-DNA mutant. However one of the disadvantages of EMS is finding the mutant phenotype DNA alteration, which is often a single base change in a large genome (Alonso *et al.*, 2003). T-DNA or transposon insertion alleles on the other hand can easily be isolated through the sequence flanking the insertion site simplifying the identification of the gene responsible for a mutant phenotype (Alonso and Ecker, 2006). Fast neutron bombardment typically induces chromosomal rearrangements and deletions. Comparative to EMS, fast neutron bombardment also yields high mutagenicity resulting fewer plants being screened to identify the desired mutant phenotype. However this would require unrelated mutations being removed via backcrossing several times to the non-mutagenized parental line prior to analysis of the mutant phenotype (Alonso and Ecker, 2006). The aim of forward genetics is to identify all the genes that are associated with a particular biological process.

Reverse genetics involves the study of the gene of interest and the identification of mutations within it. This approach is useful in scrutinizing gene families where functional redundancy of closely related gene members obscures their phenotype. Reverse genetics allows detection of mutations in all gene family members (Østergaard and Yanofsky, 2004). Reverse genetics approaches include T-DNA insertional mutagenesis; targeting induced local lesions in genomes (TILLING), which allows loss-of-function allele identification, and RNA-mediated interference (RNAi), which is involved in generating a silencing signal throughout the plant resulting in a decrease in

transcription levels of genes in manner that is sequence specific (Reviewed in Gilchrist and Haughn, 2010).

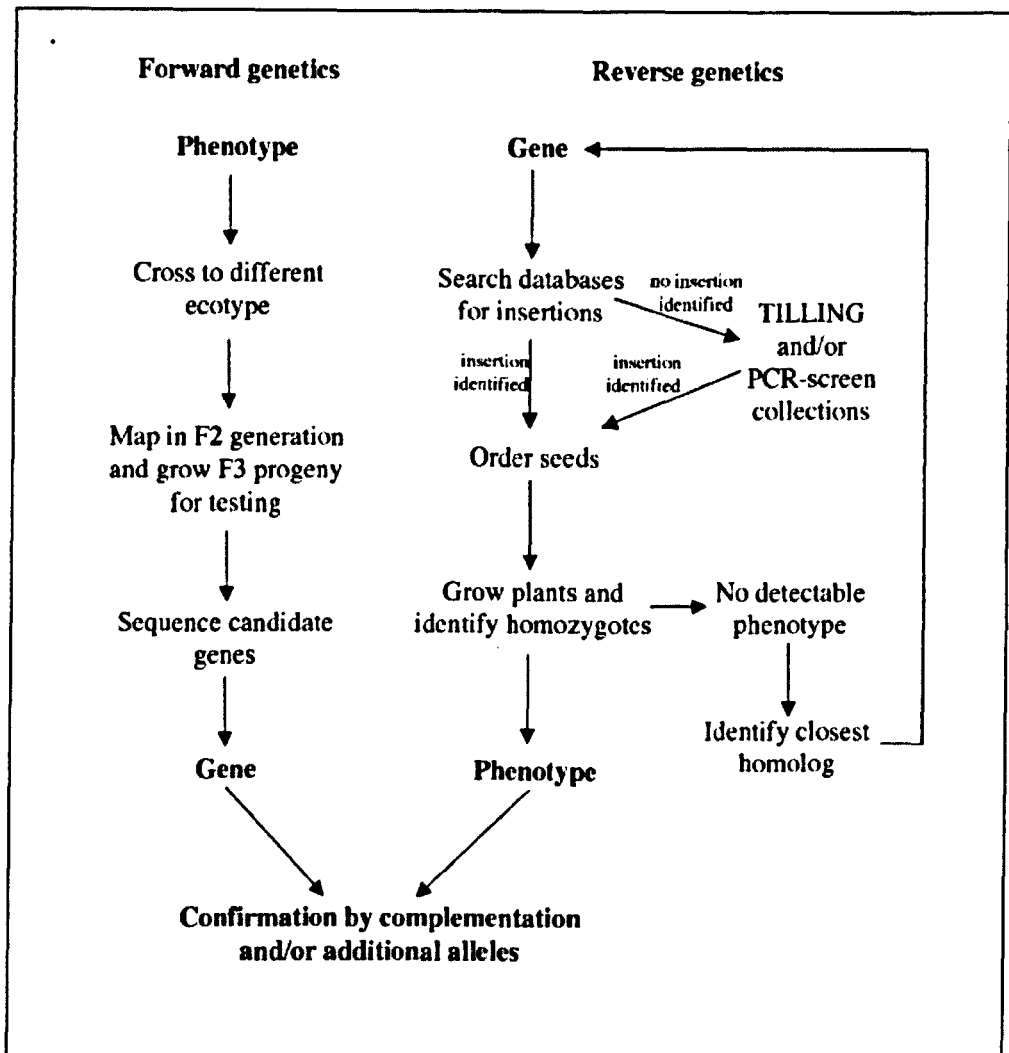


Figure 1.1 Forward and reverse genetic approaches used to establish gene function by mutagenesis. Illustration by Østergaard and Yanofsky (2004).

1.2 Regulation of floral development and cell division

The vegetative development of *Arabidopsis* involves the shoot apical meristem (SAM) producing leaves on its flanks. During flower development, the SAM converts to the inflorescence meristem (IM) (Alvarez-Buylla *et al.*, 2010). A flower can be produced by a sequence of developmental phases from the floral meristem (FM). The transition from vegetative to reproductive

development results in the apical meristem generating the FM (Figure 1.2A), subsequently activating floral-meristem identity genes such as *LEAFY* (*LFY*) and *APETALA1* (*API*). *LFY*, a floral meristem identity gene in flower organ development, interacts with *API* to endorse the transition from inflorescence to floral meristem. *API* is associated with regulation of genes that are promoting floral organ formation (Yu *et al.*, 2004). Loss-of-function of *LFY* by mutation results in severe effects on meristem identity. The *lfy* mutants persist to generate leaves and associated lateral shoots when wild type plants generate flowers, thus the inactivation of *LFY* gene results in conversion of flowers into shoot like structures (Blázquez *et al.*, 1997). The double mutant *ap1/lfy* demonstrates a more severe conversion of flowers into shoot-like structures (Figure 1.2B) than the single mutants alone, indicating that *LFY* and *API* encode transcription factors that have partly overlapping functions in specifying a floral-meristem fate (Weigel *et al.*, 1992). *LFY* and *API* are known to repress expression of the inflorescence-meristem fate specifying gene *TERMINAL FLOWER1* (*TFL1*) in the floral meristem. However *TFL1* is known to repress expression of *LFY* and *API* in the inflorescence meristem due to their ectopic expression in the IM (Liljegrén *et al.*, 1999).

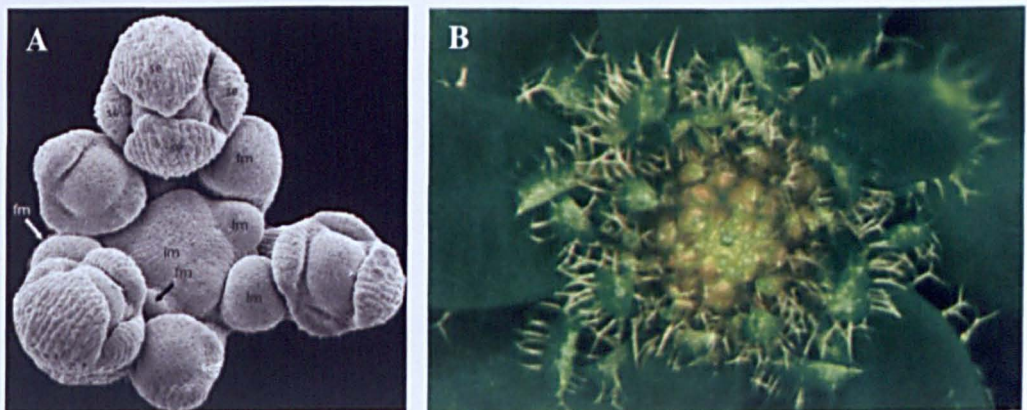


Figure 1.2 Floral meristem developments. (A) Scanning electron micrograph of the wild type inflorescence meristem (im) and floral meristem (fm). Sepal primordia (se) is indicated in the more mature flower. (B) Inflorescence apex of *ap1/lfy*. Illustration from Krizek, 2009.

Different stages in floral development include floral meristem identity, floral organ identity and flowering time. Floral organ identity is characterized by the ABC model of *Arabidopsis* (Figure 1.3), formulated by Coen and Meyerowitz (1991), attributing the homeotic transformation of one floral organ into another. There are four concentric whorls in an *Arabidopsis* flower which consists of two carpels fused together, six stamens, four petals and four sepals (Ni et al., 2004). There are various types of genes that regulate floral architecture in *Arabidopsis*. The correct number of floral organs in the outer three whorls during floral development is ensured by the Bzip transcription factor gene *PERIANTHIA* (*PAN*). Mutants of *pan* result in five sepals, petals and stamens (Running and Meyerowitz, 1996; Chuang et al., 1999). Floral organ number also increases in mutants of *clavata* (*clv*) due to the broadened floral meristem (Clark et al., 1993; Clark et al., 1995).

The ABC+E gene expression describes the type of floral organ that differentiates in each whorl (Figure 1.3). Sepal identity is controlled by the class A genes, *API* (Bowman et al., 1993) and *APETALA 2* (*AP2*), containing carpels where sepals are normally occupied and stamens in place of petals (Kunst et al., 1989). Petal identity is specified by class A and B genes such as *APETALA 3* (*AP3*) (Jack et al., 1992), and *PISTILLATA* (*PI*) where loss-of-function results in sepal formation in place of petals (Hill and Lord, 1989). Stamen identity is controlled by both class B and C gene, *AGAMOUS* (*AG*) (Drews et al., 1991; Bowman et al., 1989) where loss-of-function generates stamens that are homeotically transformed into petals and sepals in place of carpels. Carpel identity is controlled by class C gene, *AG* activity (Ni et al., 2004; Krizek et al., 2006). Classes A, B and C genes act together with class E genes, *SEPALLATA* (*SEP*) to confer sepal, petal, stamen and carpel identities (Krizek et al., 2006) given that *sep1sep2sep3* triple mutant flowers consists of just sepals. Sepal identity is conferred also by *SEP4* along with the other three *SEP* genes, thus indicating that the *sep* quadruple mutants (Figure 1.2) have alterations of all four floral-organ types into leaf-like organs (Ditta et al., 2004; Krizek and Fletcher, 2005). The ABC genes, except for *AP2*, are known to encode MADs-box transcription factors (Yanofsky et al., 1990; Coen and Meyerowitz, 1991; Jack et al., 1992; Mandel et al., 1992; Pelaz et al., 2000).

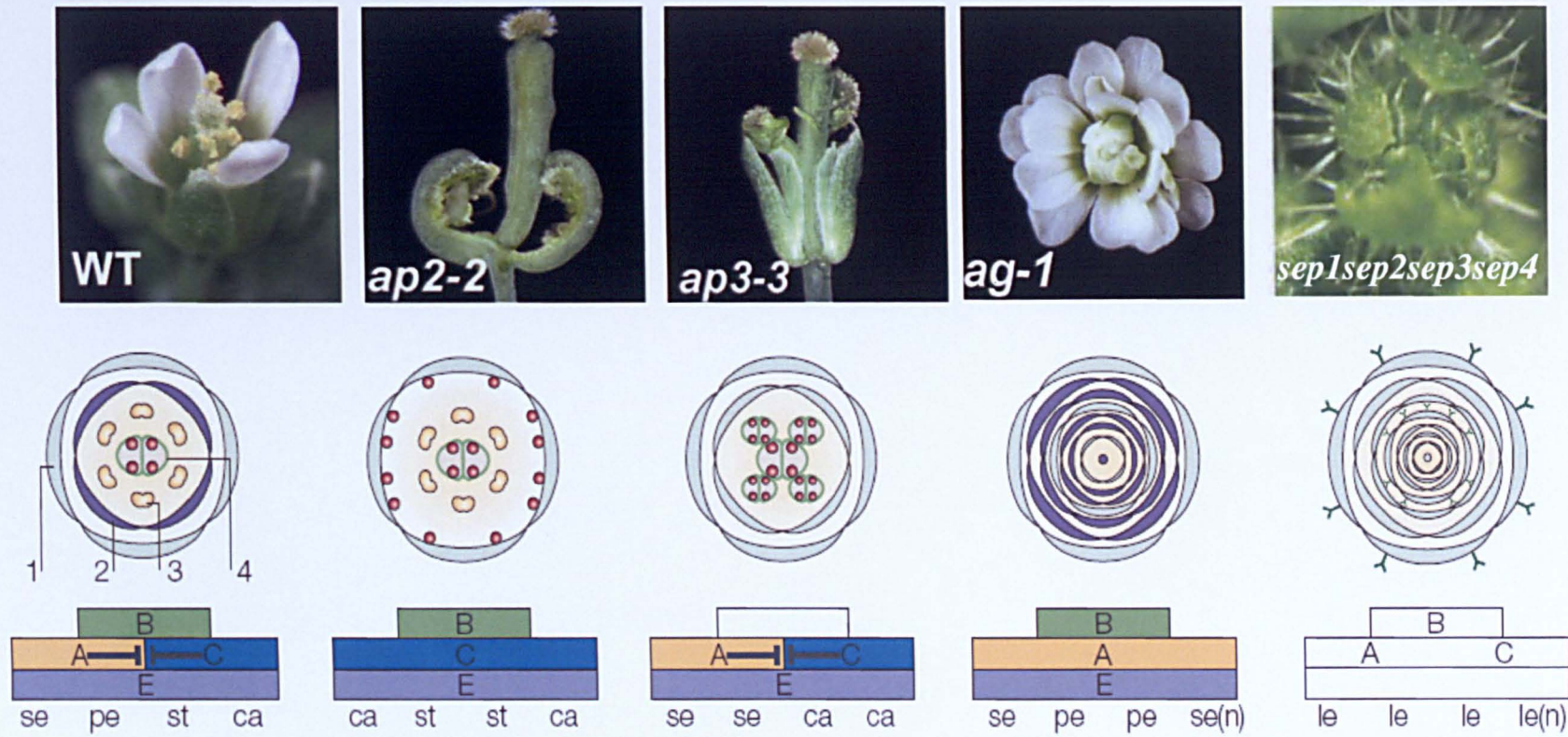


Figure 1.3 ABC+E model of *Arabidopsis thaliana* Model showing the four different whorls and some of the genes involved. Illustration modified from Krizek and Fletcher (2005) and Riechmann and Meyerowitz (1997)

Various genes that regulate flower development have been identified. These include genes involved in floral organ and floral meristem identity as well as flowering time (reviewed in Irish, 2010). Genes such as the *PRESSED FLOWER (PRS)* gene, functions by defining the flower primordium lateral region. In mutants of *prs*, there is a deficiency in lateral sepals (Matsumoto and Okada, 2001). The appropriate number of organs in the second and third whorls is ensured by *UNUSUAL FLORAL ORGAN (UFO)*, an F-box gene. *UFO* also has the ability to promote the outgrowth of petals (Laufs *et al.*, 2003; Durfee *et al.*, 2003). A zinc finger encoding gene, *RABBIT EARS (RBE)*, has the ability to promote petal growth given that petals are absent in plant mutants that are null *rbe* (Takeda *et al.*, 2004).

Other genes such as *SUPERMAN (SUP)*, a zinc finger gene, have the ability to manage cell proliferation in the boundary between carpels and stamens (Sakai *et al.*, 1995). The *CUP-SHAPED COTYLEDON (CUC)* gene *CUC1* and *CUC2*, which encode NAM (no apical meristem)-ATAF (*Arabidopsis* transcription activation factor)-CUC (NAC) transcription factors, control individual organ boundaries. These genes enable adjacent floral organ primordia to stay separate (Aida *et al.*, 1997).

The *UFO* gene is involved in determining floral organ whorled pattern and determining the floral meristem identity. It has the ability to control B function gene *AP3* expression in conjugation with *LFY* (Levin and Meyerowitz, 1995; Samach *et al.*, 1999). Aside from determining floral meristem identity, *UFO* also has a role in controlling the propagation of cells in a developing flower or determining the boundaries between floral organs. Thus far, ten alleles of *ufo* have been identified in *Arabidopsis* and all of these alleles are phenotypically similar to one another except for *ufo-6*, which has a less severe phenotype than the others. The identification of a set of weak *ufo* alleles where petals are absent or substituted by staminoid filaments or petals, has indicated that *UFO* is a key regulator of second-whorl organ growth (Durfee *et al.*, 2003).

Petal loss (ptl) mutants also have similar defects to *ufo* mutants; however they exhibit fusion between the first-whorl sepals and variations in orientation of petal (Griffith *et al.*, 1999). Even though in some circumstances, petals do arise, their average size is less than normal petals and result in trumpet-shaped petals. *PTL* is a trihelix transcription factor gene and has the aptitude to regulate perianth morphogenesis (Griffith *et al.*, 1999; Brewer *et al.*, 2004). The expression of *PTL* is mainly in the first-whorl sepals and is not expressed in the second-whorl cells. This signifies that the second-whorl defect may indirectly affect expansion in the first whorl (Brewer *et al.*, 2004). The distortion in petal primordia orientation leads to some petals in a reversed orientation and others facing sideways resulting from the disturbance of response to another signal in *ptl* mutants (Griffith *et al.*, 1999). In *ptl* mutants, the disturbance in petal orientation and initiation can result indirectly since *PTL* is not expressed in developing petal primordia. This may be due to inter-sepal zone overgrowth since expression of *PTL* is at its greatest in the inter-sepal zones during premature development of flowers. *PTL* keeps sepals separate by suppressing development between sepal primordia and permits petal development signals to be properly distinguished (Griffith *et al.*, 1999; Brewer *et al.*, 2004). Consistent with the theory that *PTL* maintains sepal separation due to its expression between newly occurring sepals, ectopic expression of *PTL* results in growth suppression between initiating sepals (Brewer *et al.*, 2004).

Even in the absence of *PTL* expression, four sepals still arise in the correct location. This suggests that other genes are involved in this function. Genes such as *PINOID (PID)* are expressed in developing sepal primordia; however it is not expressed in the sepal boundaries. *PID* encodes a serine/threonine kinase that is involved in auxin signalling (Christensen *et al.*, 2000). Expression of *PID* in sepal primordia is initiated as sepals occur and develop. The initiation of sepals is facilitated by auxin acting through *PID*, since the initiation site of organ primordia is known to be defined by auxin involvement (Benjamins *et al.*, 2001; Reinhardt *et al.*, 2003). The absence of *PID* expression allows *PTL* to be expressed in the inter-sepal zones, therefore causing repression of growth at these zones. The expression of *PTL* is not apparent in petal primordia until

their expansion at stage eight (Brewer *et al.*, 2004). Although *PTL* is thought to inhibit growth and provide more space for petals to arise, *ptl* mutants show a decrease in the number of petals per flower, suggesting that the petal initiation signal may be weakened by the diffusion of overgrowth in inter-sepal zones. Therefore they rarely appear (Griffith *et al.*, 1999). So far there have been twenty-eight plant-specific trihelix genes identified in the genome of *Arabidopsis*. *PTL* is the first trihelix transcription factor gene that has been shown to function in flower morphogenesis (Brewer *et al.*, 2004).

1.3 Regulation of boundary formation throughout floral development

Morphological boundary formation is a crucial step in plant development. Such boundary formation occurs between whorls of organs and between organs within whorls. The creation of boundaries involves the formation of lateral organ primordia from the shoot apical meristem that separates the surrounding tissue from the primordium. Morphological boundaries are formed between the meristem and organs (M-O boundary), or between adjacent organs (O-O boundary) due to suppression of local growth in the outermost region of the primordium as development progresses (Aida and Tasaka, 2006a). Gene expression and morphological studies have revealed a set of specialized cells that are along the M-O and O-O boundaries (Aida and Tasaka, 2006b). DNA synthesis and cell-cycle-related gene expression were imperceptible in these cells (Breuil-Broyer *et al.*, 2004). These cells display low proliferation rates with distinctly elongated and narrow structures exhibiting decreased growth activity. Thus giving rise to the separation between adjacent tissues or organs. Cell division takes place at a lower frequency at the M-O boundary than at the O-O boundary, indicating the different regulation levels of the cell division rate (Aida and Tasaka, 2006a).

Such special coordination between boundary patterning events is regulated by boundary-specific regulatory genes. Meristem and organ development may be affected by genes expressed in the boundary through

upregulation of cell differentiating genes and downregulation of meristematic genes (Borghi *et al.*, 2007). There are several genes that play a key role in lateral organ separation in flowers and leaves of *Arabidopsis*. Mutations in these genes causes fusion of adjacent organs and tissues which otherwise would be separated. Such genes include *PTL* (Brewer *et al.*, 2004), *FUSED FLORAL ORGANS (FFO)* (Levin *et al.*, 1998), *LATERAL ORGAN BOUNDARIES (LOB)* (Shuai *et al.*, 2002), *RBE* (Krizek *et al.*, 2006) and *HANABA TARANU* (Zhao *et al.*, 2004). There are several other genes in *Arabidopsis* where mutations show floral organ fusion, such as *LFY*, the *CUC* mutants (*CUC1*, *CUC2* and *CUC3*) (Aida *et al.*, 1997; Takada *et al.*, 2001), *UFO* (Samach *et al.*, 1999; Levin and Meyerowitz, 1995) and *HAWAIIAN SKIRT (HWS)* (Gonzalez-Carranza *et al.*, 2007).

The three different *CUC* genes, *CUC1*, *CUC2* and *CUC3*, are members of the NAC-transcription factor family. Mutations in *CUC1* and *CUC2* genes disrupt development of shoot apical meristems during embryogenesis as well as causing defects in sepal, stamen and cotyledon partitioning. The phenotype of *cuc* mutants results in the fusion of cotyledons along the boundaries of their sides. Stronger abnormalities are known to be apparent in the double mutant *cuc1cuc2* indicating the formation of irregular boundary specifications during embryonic development (Aida *et al.*, 1997). There is an extensive amount of sepal fusion in double mutants of *ptl* with either *cuc1* or *cuc2* (Brewer *et al.*, 2004). Lampugnani *et al.* (2012) have shown that *CUC* genes are involved in suppressing sepal tissue growth within the boundaries while *PTL* keeps the boundary size in check.

The *RBE* gene is a transcription factor that is accountable for development of second whorl organ primordia at its early stages. The *rbe* mutant results in petal development defects causing alterations in petal morphology and fusion of sepals (Takeda *et al.*, 2004; Krizek *et al.*, 2006). Similar morphological defects can be observed on the *cuc1cuc2* double mutant (Aida *et al.*, 1997). *RBE* encodes a *SUPERMAN*-like zinc-finger protein which is expressed in cells of second whorl organs. This gene is known to act downstream of *API* and *PTL* genes since it failed to be expressed in *apl-1* and

ptl-1 mutants (Takeda *et al.*, 2004). Krizek *et al* (2006) have identified that *RBE* maintains boundaries of homeotic gene expression between whorls as well as maintaining boundaries within a whorl between organ primordia. *RBE* expression is activated by *UFO* indicating that the development of second whorl organs is promoted by *UFO* and *RBE* genes functioning in the same pathway (Krizek *et al.*, 2006).

FFO genes are derived from an EMS mutagenesis of the *ufo-6* mutant in the Landsberg (*Ler*) background. There are three *FFO* genes that have been identified, *FFO1*, *FFO2* and *FFO3* and mutations in these genes cause fusion of floral organs indicating that they are involved in sustaining floral boundaries during plant development. The *FFO1* and *FFO3* genes may perform at different stages of plant development even though the phenotypes of *ffo1* and *ffo3* (Figure 1.4A and C respectively) mutants are similar. The mutant *ffo2* (Figure 1.4B) occurs mainly in the inflorescence contributing to the fact that *FFO2* acts at an early stage of flower development although organ fusion between boundaries can also be seen elsewhere (Figure 1.4D). Crossing the different *ffo* alleles among themselves to create double mutants resulted in a phenotype that is additive. This signifies that the *FFO* genes may manipulate floral organ separation by functioning in separate pathways. Double mutants of *ffo* alleles with mutants such as *lfy* or *ufo* indicate that *FFO* may perform in a similar procedure in initiation of floral meristem (Levin *et al.*, 1998).

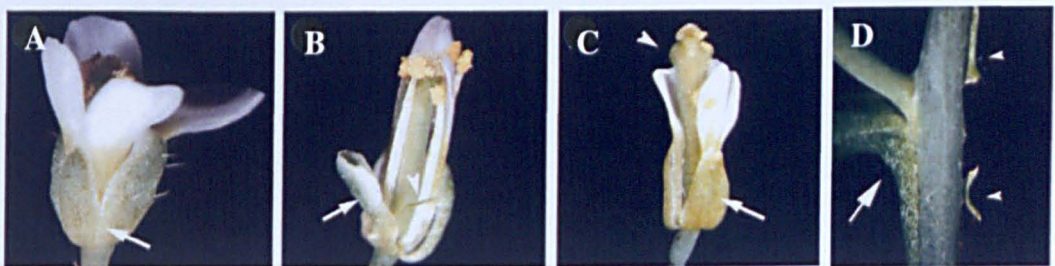


Figure 1.4 Fused floral organ (*ffo*) alleles. (A) Fused sepal margins (arrow) on *ffo1-1* flower. (B) Variable defects in floral organs of *ffo2-1* include characteristics such as petal/sepal organs (arrow). (C) Entirely fused sepals (arrow) and a protuberance just below the stigma head can be observed on *ffo3-1*. (D) Fusion of the cauline leaf to the stem boundary (arrow) on *ffo1-1* plant. Illustration modified from Levin *et al* (1998).

The sepal fusion of *ffo1* and *ffo3* mutant flowers resembles and occurs at a higher frequency than that of *cuc1* and *cuc2* mutants. Sepal fusion in *ffo1* is partial to complete between neighbouring sepals whereas sepal fusion is perceived at lower incidence level in *cuc1* and *cuc2* mutants. *CUC* genes resemble *FFO1* in sustaining boundaries during plant development, but may act at a later stage in development since fusion of sepals are detected at a later phase in plant development in the *cuc1cuc2* double mutant compared to *ffo1* mutants (Levin et al., 1998).

The *HWS* gene encodes a putative F-box protein which is involved in the development of sepal boundaries. It was isolated due to its failure to shed its floral organs following silique desiccation (Figure 1.5C). The *hws-1* mutant is also known to display sepal fusion (Figure 1.5B) along their margins as well as fusion of basal margins, anthers (Figure 1.5D) and cauline leaf lamina (Gonzalez-Carranza *et al.*, 2007).

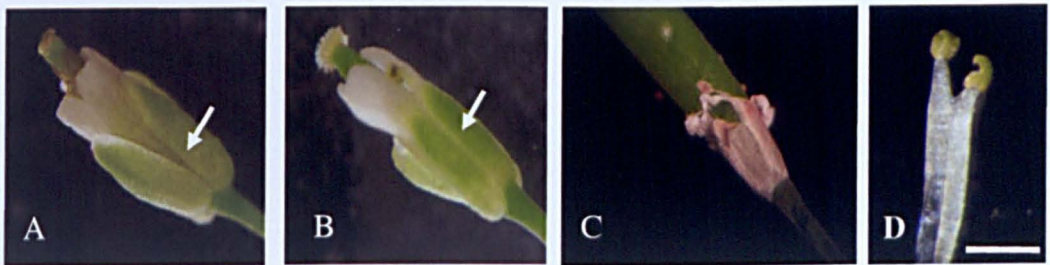


Figure 1.5 Flower phenotype of the *hws-1* mutant Comparison between Col-0 wild type (A) and *hws-1* mutant (B) flowers shows (arrow) fusion on sepal margins in *hws-1* mutant and clear sepal separation in Col-0 wild type flower. (C) Sepals, petals and anthers remain attached as the plant matures. (D) Stamens fused together in the *hws-1* mutant. Bar = 1mm.

Overexpression of the *HWS* gene results in a decrease in root and vegetative shoot growth whereas loss-of-function of *HWS* contributes to an increase in plant size. These analyses signify that the *HWS* degradation target plays an important role in plant organ growth. The *hws-1* mutation results from a 28 bp deletion positioned 966 bp downstream from the open reading frame (ORF) translation start and this brings about a premature termination by an amber stop codon. The *hws-2* mutation, which phenocopies the *hws-1*

mutation, results from two T-DNA insertions introduced in opposite directions positioned 475bp and 491bp downstream from the start of the ORF (Figure 1.6A) (Gonzalez-Carranza *et al.*, unpublished data). *HWS* is known to interact with *ASK1* and *ASK4*, *Arabidopsis Skp1*-like genes 1 and 4, in a yeast two-hybrid library that is anther-specific (Zhang *et al.*, unpublished data). Several *Arabidopsis Skp-1* like genes have been associated with *At3g61590* (the gene encoded by *HWS*) in a targeted yeast (*Saccharomyces cerevisiae*) two-hybrid screen (Takahashi *et al.*, 2004). This indicates evidence that *HWS* functions as an F-box protein. *HWS* is expressed throughout the plant and the greatest amount of expression is located in the inflorescence and floral organs (Figure 1.6B). It has been shown that *hws-1* non-shedding phenomena is due to a delay in timing of cell separation, therefore indicating that *HWS* may contribute to the timing of abscission (Gonzalez-Carranza *et al.*, 2007).

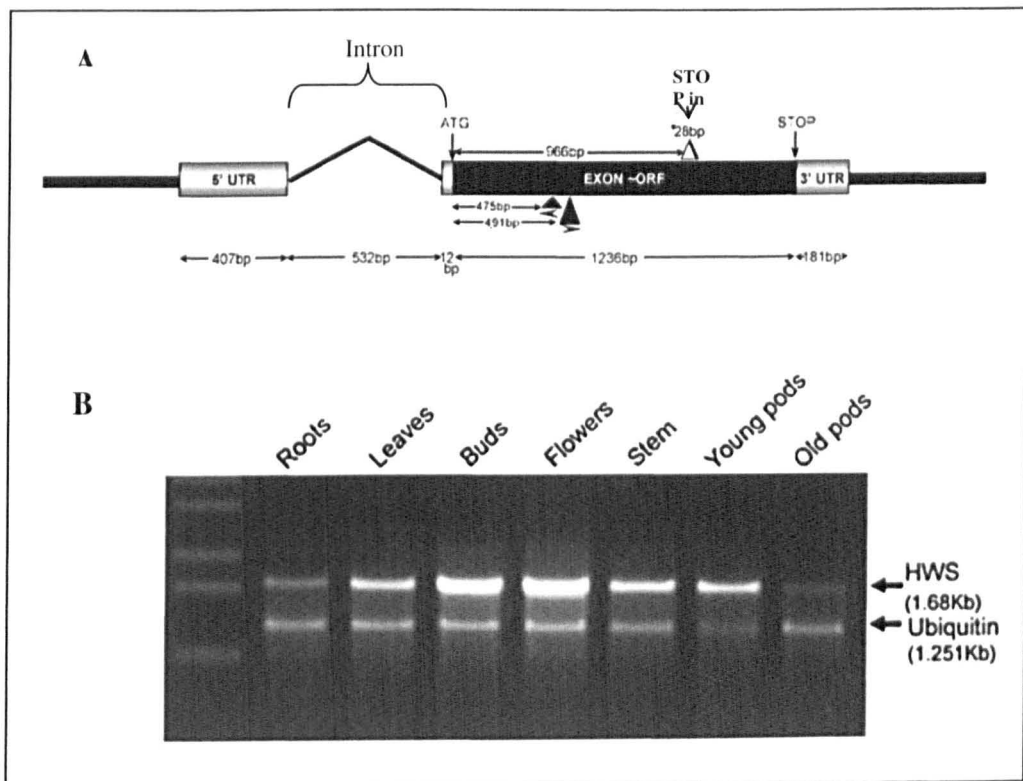


Figure 1.6 The *HWS* gene and its expression. (A) The *HWS* gene consists of a 5' UTR disrupted by 532bp intron, a 1,236bp ORF (Open Reading Frame) and a 181bp 3' UTR. The ORF shows the 28bp deletion which results in *hws-1* mutation and the 2 T-DNA insertions which lead to the *hws-2* mutation. (B) RT-PCR analysis on Col-0 wild type showing the expression of *HWS* is strongest in inflorescence and flowers. Ubiquitin is used as a control. Illustration from Gonzalez-Carranza *et al.*, 2007.

The mutant *hws-1* was crossed with *ffol-1* and *ffo3-1* as both *ffol1-1* and *ffo3-1* showed a fused sepal phenotype. The cross between *hws-1* and *ffol-1* resulted in an *hws* phenotype in the F1 population, although *FFO1* has been proposed to reside on chromosome 5 and *HWS* is located in chromosome 3. The sequencing of the *ffol1-1HWS* locus showed that a single base pair mutation alters the codon TGG to TGA which results in a premature termination on chromosome 3. Therefore it was identified that *ffol-1* is an allele of *HWS* which was confirmed by sequencing (Gonzalez-Carranza *et al.*, unpublished data). The cross between *hws-1* and *ffo3-1* resulted in wild type phenotype in the F1 population (Zhang and Gonzalez-Carranza, unpublished data). Fusion of sepals and basal margins can also be observed in the double mutant *cuc1/cuc2* (Aida *et al.*, 1997) and in ectopically expressed microRNA *miR164b* which is involved in post-transcriptional downregulation of *CUC1* and *CUC2* mRNA (Laufs *et al.*, 2004; Mallory *et al.*, 2004b). These analyses will be described in more detail in the following chapters.

1.4 Abscission of floral organs in *Arabidopsis*

Abscission is an important and complex process of cell separation by which shedding of plant organs, such as leaves, fruits and flowers occur from the main body through a programmed cell separation mechanism. Abscission also enables the removal of infected or non-functional organs from the plant. The process of shedding in plants requires the formation of a morphologically distinct cell layer known as the abscission zone (AZ) (Addicott, 1982). The AZ is determined by several layers of small densely packed cytoplasmic cells between the floral organs and the flower receptacle (Bleecker and Patterson, 1997; van Nocker, 2009).

Cell separation is reported to take place throughout plant development in regions which initiate cell elongation for growth (Cosgrove, 1998; Cosgrove, 2000), fruit ripening (Fisher and Bennett, 1991), dehiscence of anthers (Jenkins *et al.*, 1999) and pods (Meakin and Roberts, 1990), germination of seeds (Sitrit *et al.*, 1999), pollen tube growth (Clarke and Gleeson, 1981) and lateral root

outgrowth (Peretto et al., 1992). The process of cell separation occurs only after the formation of AZ at the floral organ boundary (Figure 1.7A) and after the acquisition of abscission signals. Following this process, cell elongation occurs at the AZ plant body area. The middle lamella between the AZ cells undergoes enzymatic hydrolysis degradation and the AZ plant body region separates followed by the formation of a protective layer (Figure 1.7B and C) (Patterson, 2001; Butenko et al., 2003).

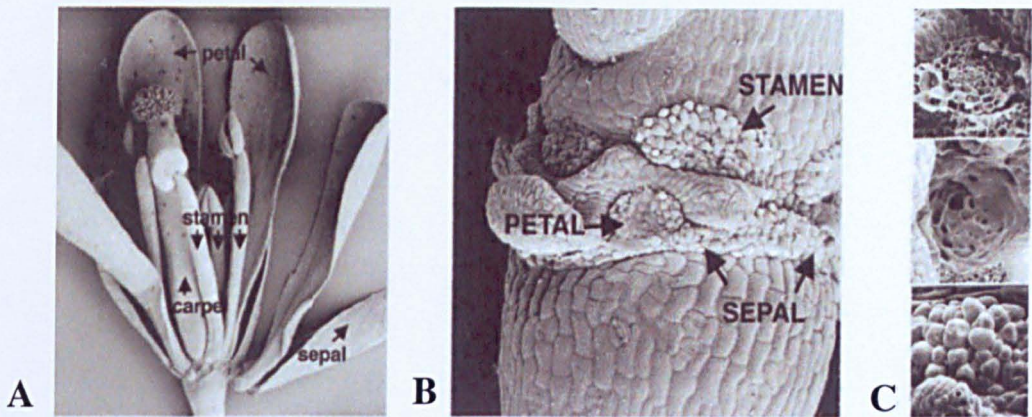


Figure 1.7 Abscission of floral organs in *Arabidopsis*. (A) Scanning electron micrograph of the *Arabidopsis* flower showing floral organ separation at the AZ. (B) electron micrograph of the *Arabidopsis* flower petal, sepal and stamen AZ. (C) Scanning electron micrograph of the petal AZ fracture plane at the flower position 2 (top) showing broken cells, position 3 (middle) showing a fracture plane that is flattened and position 9 (bottom) showing fully rounded cells. Illustration from Patterson (2001).

During abscission, the cell wall is degraded at the AZ by the activity of several hydrolytic enzymes such as polygalacturonases (PGs) (Taylor *et al.*, 1993; Kalaitzis *et al.*, 1995; Brown, 1997), β -1, 4-endo-glucanases (cellulases) (Bonghi *et al.*, 1992; Lashbrook *et al.*, 1994; Del Campillo, 1999) and proteins such as expansins (Cho and Cosgrove, 2000). During leaf and floral organ shedding, PG activity has been known to elevate in AZ tissue (Bonghi *et al.*, 1992). It is known that PG family members are widely detected throughout *Arabidopsis* plant development (Torki *et al.*, 2000).

Arabidopsis does not shed leaves or fruits but it is known to shed intact turgid floral organs (Patterson, 2001), thus identifying that abscission in *Arabidopsis* is not associated with the process of senescence. Previous studies on *Arabidopsis thaliana* have shown that abscission can be controlled due to the involvement of several different genes. One of the first *Arabidopsis* mutants identified that did not undergo abscission is *inflorescence deficient in abscission (ida)*, where floral organs do not abscise even after mature seed shedding, yet the abscission zone does develop (Figure 1.8A-G) (Butenko *et al.*, 2003). It has been demonstrated, by use of overexpressing *35S::IDA* lines, that the AZ is receptive to IDA following flower opening. Premature abscission of floral organs can be observed in the *35S::IDA* flowers due to cell proliferation at the AZ (Stenvik *et al.*, 2006). IDA overexpression also results in ectopic abscission formation between the pedicel-stem junction and base of siliques (Reviewed in Roberts and Gonzalez-Carranza, 2013). Another gene involved in abscission, identified as *HAESA (HAE)* (previously known as receptor-like protein kinase 5 (RLK5)) and *HEASA-LIKE 2 (HSL2)*, is an *Arabidopsis* leucine-rich repeat receptor kinase that controls floral organ abscission. A study carried out by Jinn *et al.* (2000) using an antisense strategy showed that the decrease in function of *HAE* in plants with an antisense construct results in delayed floral organ abscission and the severity of the phenotypic change depends on the *HAE* protein level. *HAE-GUS* construct studies support these results by showing gene expression of *HAE* in the floral organ AZ (Jinn *et al.*, 2000). Double mutants of *HEA* and *HSL2* have been shown to phenocopy the *ida* mutant (Reviewed in Roberts and Gonzalez-Carranza, 2013).

The process of abscission can be accelerated via the plant growth regulator ethylene and delayed by the hormone auxin (IAA) (Osbourne, 1989). However it is debated whether ethylene is entirely necessary for the process of abscission. While the ethylene-insensitive *Arabidopsis* mutant, *etr1-1* demonstrates a delay in abscission, the expression of *HAESA* does not change in *etr1-1* (Jinn *et al.*, 2000). This implies that floral organ abscission is regulated also via an ethylene independent development pathway.

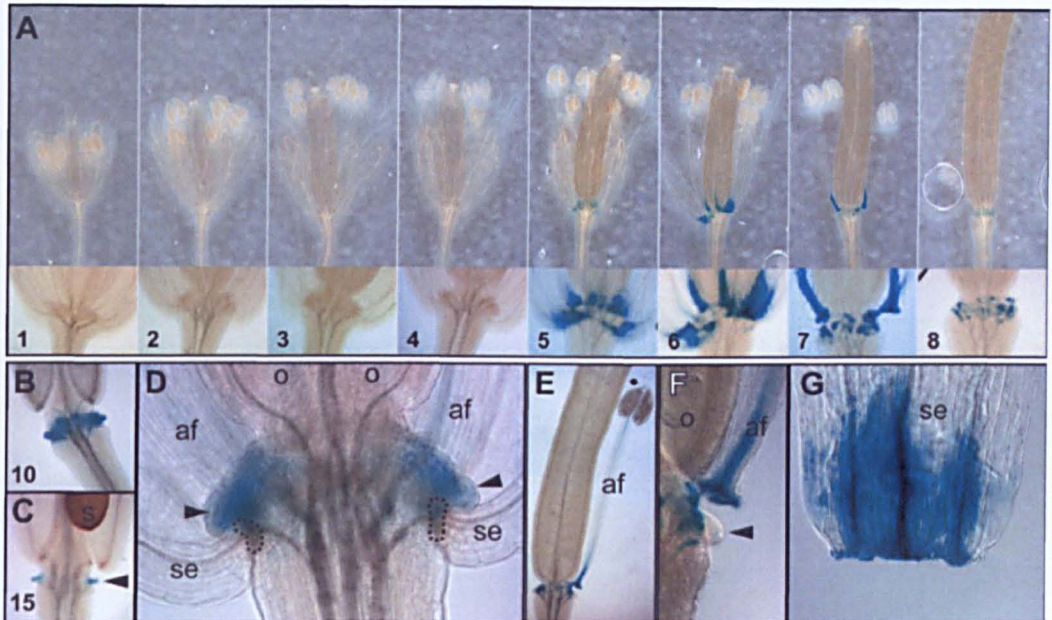


Figure 1.8 Different stages of development from *IDA:GUS* flowers. (A), (B) and (C) β -glucuronidase (GUS) expression of *IDA:GUS* flowers from flower positions 1-8. Flower position 8 showing clear GUS expression at the AZ where shedding of floral organs has occurred. (C) The arrowheads at flower position 15 is showing nectary outgrowth. (S, mature seed). (D) GUS expression in the nectarines (arrowheads) and AZ (lines) can be observed between the anther filaments (af) and the sepal bases (se). (O, ovule). (E) and (F) GUS expression at the AZs of the anther filament base and the plant body (arrowhead). (G) GUS expression shown at the sepal base. Illustration from Butenko *et al.* (2003).

1.5 Ubiquitin-mediated protein degradation

Various cellular events such as cell development, cell division, immune response, signal transduction, transcriptional regulation, receptor down-regulation, endocytosis and metabolism in eukaryotic organisms can be regulated by the ubiquitin-mediated protein degradation pathway. This pathway is important in controlling gene expression of plants and is a central regulatory mechanism in a diversity of cellular process (Hershko and Ciechanover, 1998). It consists of three enzymatic reactions known as (Uba1/E1), (Ubc/E2) and ubiquitin ligase (E3) (Figure 1.9) (Wang *et al.*, 2002). E1 is an ubiquitin activating enzyme which activates ubiquitin for conjugation to other proteins. E1 couples ATP to form a high-energy thioester bond

between the C-terminal residue of ubiquitin and specific Cys residue of E1. E1 linked ubiquitin moiety moves from E1 to the Cys residue of ubiquitin conjugating enzyme E2. Sequentially it will move to a Lys residue by the use of E3 (Varshavsky, 1997). The ubiquitin ligase (E3) is known to function in the same pathway as the ubiquitin-conjugating enzymes (E2) and ubiquitin-activating enzyme (E1) (Ni *et al.*, 2004). There is usually one E1 species, several E2 species and multiple families of E3 proteins. E3 is responsible for the selectivity of ubiquitin protein ligation and therefore of protein degradation, by binding specific protein substrates containing specific recognition signals. Transfer of ubiquitin to substrate proteins may be carried out by two different methods depending on the E3 type. In some E3 families, ubiquitin is transferred from an E2 to an E3 enzyme Cys residue. The resulting E3-ubiquitin thioester is the donor for amide (isopeptide) bond formation with the protein substrate. In other E3 families, this E3-ubiquitin thioester formation does not occur (Hershko *et al.*, 1983; David *et al.*, 2010). Ubiquitin is transferred directly from E2 to the protein substrate enabling the formation of a polyubiquitin chain, where the ubiquitins are linked to one another by their C-terminus and a particular Lys residue (usually Lys 48) (Hochstrasser, 1996; Deng *et al.*, 2000). The polyubiquitin chain is subsequently predestined to the 26s proteasome, where degradation of the target protein occurs. Some E2s have the ability to act with more than one E3 enzyme and some E3s are known to act with several E2s (Hershko And Ciechanover, 1998). The diversity of enzymes increases through the flow of ubiquitin transfer. There are four distinct classes of E3 ubiquitin ligase that are known. These include HECT, Vbrip, (Apc/c) and the SCF complex (Varshavsky, 1997; Craig and Tyers, 1999; Lorick *et al.*, 1999; Vierstra, 2003).

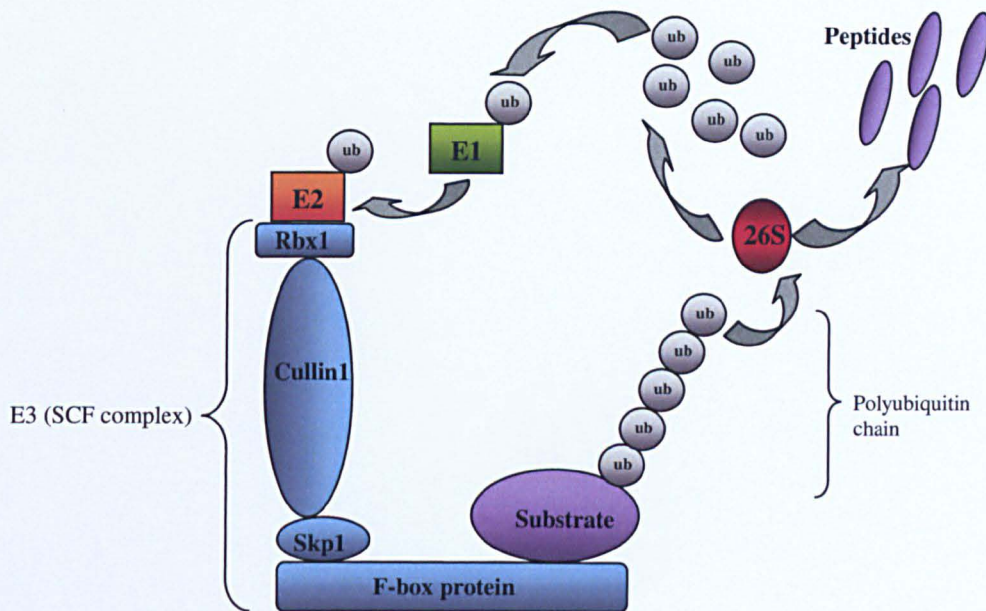


Figure 1.9 The process of ubiquitination involves the degradation of proteins carried out by three enzymatic reactions known as E1, E2 and E3 (SCF complex comprising of Rbx1, Cullin1, Skp1 and F-box proteins). E1 is involved in activating ubiquitin by its C-terminal Gly residue. The linked ubiquitin moiety moves from E1 to E2. E3 is responsible in the selectivity of ubiquitin protein ligation, by binding specific protein substrates containing specific recognition signals. This enables the formation of a polyubiquitin chain which is subsequently destined to 26S proteasome for degradation of the target protein producing free peptides. Furthermore 26S proteasomes subsequently produce free and reusable ubiquitin. Illustration modified from Welcker and Clurman (2008).

The SCF complex was first identified in yeast (Wang *et al.*, 2002). It is a major family of E3 ubiquitin protein ligases and it is composed of four subunits known as RBX1, SKP1, CUL1 and F-box proteins (Figure 1.9) (Patton *et al.*, 1998; Ni *et al.*, 2004). This complex aids protein ubiquitylation that is subsequently the subject for degradation (Ni *et al.*, 2004). Several hormone signalling SCF complexes have been characterized in *Arabidopsis* (Guo and Ecker, 2003; Potuschak *et al.*, 2003; Dharmasiri *et al.*, 2005; Kepinski and Leyser, 2005; Chini *et al.*, 2007, reviewed in Santner and Estelle, 2010). Plants use SCF complexes in order to control biological events. This is predicted by observing the large number of F-box genes in the *Arabidopsis* genome (Ni *et al.*, 2004). It has been suggested that flower development involves SCF complexes since genes encoding numerous protein components

are expressed in the inflorescence. *Arabidopsis* Skp-1 related proteins, ASK1 and ASK2 have the ability to interact with a number of F-box proteins and both *ASK1* and *ASK2* genes are expressed in all major tissues (Zhao *et al.* 2003). Thus it is possible that one of these genes is an element of several SCF complexes and is able to share redundant functions, such as development of flowers, during the plant life cycle. SCF complexes are able to control floral meristem identity, floral organ number and organ separation (Ni *et al.*, 2004).

The presence of F-box genes are widely distributed in eukaryotes such as nematodes, flies, flowering plants, yeast and humans (The Arabidopsis Genome Initiative, 2000). F-box, so called because of its basis of the presence of motif in cyclin F, is necessary for protein-protein interaction. Approximately 40 to 50 amino acid F-box motifs were initially identified in the N-terminal region cyclin F. The F-box protein, being part of the SCF complex, functions by interacting with substrate proteins. F-box proteins have a key role in floral organ formation, flowering, leaf senescence and auxin signal transduction. These are identified mostly in *Arabidopsis* and *Antirrhinum* (Wang *et al.*, 2002). F-box proteins participate in Skp1 interaction and this interaction normally found on the protein amino-terminal half. In *Arabidopsis*, 20 different F-box proteins were identified by the use of yeast (*Saccharomyces cerevisiae*) two-hybrid screen with the Skp1- related protein ASK1 (Del Pozo *et al.*, 2000). Some F-box proteins can interact with substrates like Grr1 showing that with the use of the core SCF complex, phosphorylated G1 cyclins are captured by Grr1 for ubiquitination (Wang *et al.*, 2002). F-box proteins have the capacity to regulate processes such as transcriptional regulation, signal transduction and cell cycle transition. This is achieved by interacting with SCF complexes and non-SCF complexes. It has been identified that approximately 600-700 genes encoding putative F-box proteins are present in the genome of *Arabidopsis thaliana* (Gagne *et al.*, 2002; Kuroda *et al.*, 2002). It was shown that only 2 F-box proteins consist of WD40 repeats, where as 29 F-box proteins contained leucine rich repeats (LLR) and 67 F-box proteins contained Kelch repeats (Kuroda *et al.*, 2002). These repeats are associated with protein-protein interactions (Kuroda *et al.*, 2002). The F-box proteins can be characterized by their protein-protein interaction domains, which are situated downstream of the

F-box domain. Most F-box proteins in *Arabidopsis* are not classified using the structure of their domain even though they contain WD40 repeats, LLRs or Kelch repeats (Kuroda *et al.*, 2002).

In *Arabidopsis*, the F-box proteins have been categorized into nineteen subgroups (Kuroda *et al.*, 2002) and nine F-box proteins have been identified in *Arabidopsis* via mutant plant analysis. These are recognized as UFO, which is involved in flower formation (Levin and Meyerowitz 1995); TIR1, containing LRRs, involved in auxin responses (Ruegger *et al.*, 1998, Dharmasiri *et al.*, 2005); COI1, containing LRRs, involved in regulating signal transduction of jasmonic acid (Xie *et al.* 1998; Chini *et al.*, 2007). F-box proteins, FLAVIN-BINDING, KELCH REPEAT, F-BOX 1 (FKF1), ZEITLUPE (ZTL) and (LOV KELCH PROTEIN 2) LKP2 consist of PAS/PAC domains that are engaged in circadian rhythm regulation (Somers *et al.*, 2000; Kuroda *et al.*, 2002). It was suggested that F-box protein EID1, containing a C-terminus leucine zipper motif, is crucial for light signal transduction, which is phytochrome A-specific. It has been shown that F-box protein ORE9 is involved in regulating leaf senescence and an identical protein to ORE9, known as MAX2, is engaged in repressing auxiliary shoot formation. It was also shown that SON1 regulated defense responses towards pathogens. These reports signify the importance of F-box proteins in biological processes of plant growth and development (Xiao and Jang 2000; Kuroda *et al.*, 2002).

There are several SCF-type E3 ubiquitin ligase F-box proteins and *UFO* is known to encode one of them. *UFO* may control inflorescence and floral meristem via an SCF^{UFO} complex which contains cullin AtCUL1. AtCUL1 has the ability to encode core components of several *Arabidopsis* SCF complexes. AtCUL1 also play a vital role throughout plant development. The SCF^{UFO} complex may be involved in controlling flower meristem identity (Ni *et al.*, 2004). *UFO* is capable of limiting cell division in the central region by interacting with ASK1 or ASK2. AtCUL1 as well as ASK1 and ASK2 may interact with *UFO* in order to regulate floral development. The *ask1-1* null mutant gives a weak floral phenotype compared to the strong phenotypes of *ufo* alleles. Both ASK1 and ASK2 are known to be important for development of

seedlings and of embryos (Ni *et al.*, 2004; Liu *et al.*, 2004). As mentioned previously in section 1.3, *HWS* also interacts with *ASK1* in an anther-specific yeast 2-hybrid library confirming regulatory similarities between *HWS* and *UFO* genes. It has been identified that *UFO* has the highest sequence similarity to the *HWS* amino acid pattern (Gonzalez-Carranza *et al.*, 2007).

The mechanism of protein degradation is known to be a key post-transcriptional regulatory process. It removes inefficient and mis-folded proteins and allows living organisms to adapt to environmental changes by supplying intracellular signals with fast and effective responses (Schumann *et al.*, 2011).

1.6 MicroRNAs in plants

The discovery of MicroRNAs (miRNAs), which direct several flower-expressed genes, has shed new light into the regulation of genes during flower development (Jones-Rhoades *et al.*, 2006). miRNAs are small RNAs (sRNAs) of about 20-24 nucleotides that are present in both animals and plants. Precursors of miRNAs have a stem-loop hairpin like structure with a low free energy. In plants, miRNAs are involved in plant development and play a key role in posttranscriptional regulation of eukaryotic gene expression (Bartel, 2004; Reinhart *et al.*, 2002). These fundamental molecules are found alongside 19-24 nucleotides long short-interfering RNAs (siRNAs) that mediate both transcriptional and posttranscriptional gene silencing (Zamore *et al.*, 2000; Elbashir *et al.*, 2001). Silencing of gene expression in plants is mediated by numerous sRNAs. In plants, the phenomenon of RNA-silencing involves double stranded RNA (dsRNA) induction, conversion of dsRNA into 18-25 nucleotide long sRNA, sRNA 3'-O- methylation and the integration of sRNAs into composites that correlate with fully or partially complementary target RNA or DNA (Chapman and Carrington, 2007).

Mature miRNAs are produced through a series of steps (Figure 1.10A) derived from long single stranded RNAs (ssRNAs) that form an imperfect

foldback structure. This involves the miRNA gene being transcribed by RNA polymerase II into polyadenylated and capped primary miRNA (pri-miRNA). The pri-miRNA is cleaved by an enzyme known as Dicer-like 1 enzyme (DCL1) to form precursor miRNA (pre-miRNA) (Bartel, 2004; Kurihara and Watanabe, 2004). The resulting pre-miRNA is cleaved into a miRNA/miRNA duplex by DCL1 and the dsRNA binding protein HYPONASTIC LEAVES1 (HYL1) which interacts with the C₂H₂ zinc-finger protein SERRATE (SE) in the nuclear processing centres known as D-bodies (Yang *et al.*, 2006; Kurihara *et al.*, 2006). Subsequently the 3' end of the miRNA/miRNA* duplex is methylated by the S-adenosylmethionine-dependent methyltransferase protein, HUA ENHANCER1 (HEN1) (Park *et al.*, 2002; Yu *et al.*, 2005). This enables the prevention of miRNA/miRNA duplex degradation and uridylation (Yang *et al.*, 2006). The duplex is translocated by a HASTY (HST), plant orthologue of the importin β -like nucleocytoplasmic transport receptors, exportin 5 in mammals, from the nucleus to the cytoplasm and transported by ARGONAUTE1 (AGO1), one of the 10 members of ARGONAUTE family in *Arabidopsis*. AGO1 is known to slice targets of miRNAs (Baumberger and Baulcombe, 2005) and is required for the suppression of miRNA translation (reviewed in Brodersen and Voinnet, 2006). The miRNAs are unwound into mature single stranded miRNAs and this leads to the miRNA guided cleavage of mature mRNAs (Vaucheret *et al.*, 2004; Park *et al.*, 2005). The *DCL1* gene is known to be crucial for the synthesis of mature miRNA and loss-of-function *dcl1* mutants lead to severe abnormalities in plant development (Figure 1.10B) (Park *et al.*, 2002; Bartel *et al.*, 2004; Reinhart *et al.*, 2002). Loss-of-function of the *HST* gene and *AGO1* gene also show reduced miRNA accumulation (Figure 1.10B) (Bollman *et al.*, 2003, Vaucheret *et al.* 2004). It has been demonstrated that the boundaries between adjacent sepals are broadened in mutants of *dcl1*, *hyl1* and *hen1* (Figure 1.11E, F, I, J, M and N) compared to wild type sepal boundaries (Figure 1.11A and B) (Jacobsen *et al.*, 1999; Kasschau *et al.*, 2003; Laufs *et al.*, 2004).

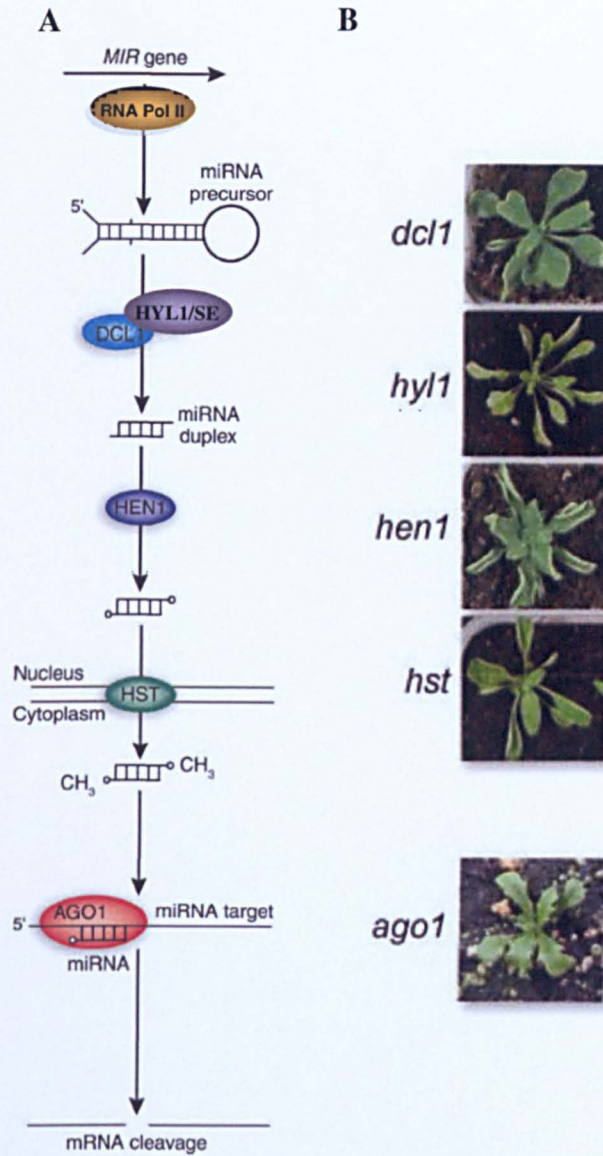


Figure 1.10 MicroRNA biogenesis. (A) microRNA biogenesis pathway modified from Mallory and Vaucheret (2006). (B) The phenotypic analysis of *dcl1*, *hyl1*, *hen1*, *hst* and *ago1* mutants showing upward and downward curling of leaves. Illustration from Garcia (2008).

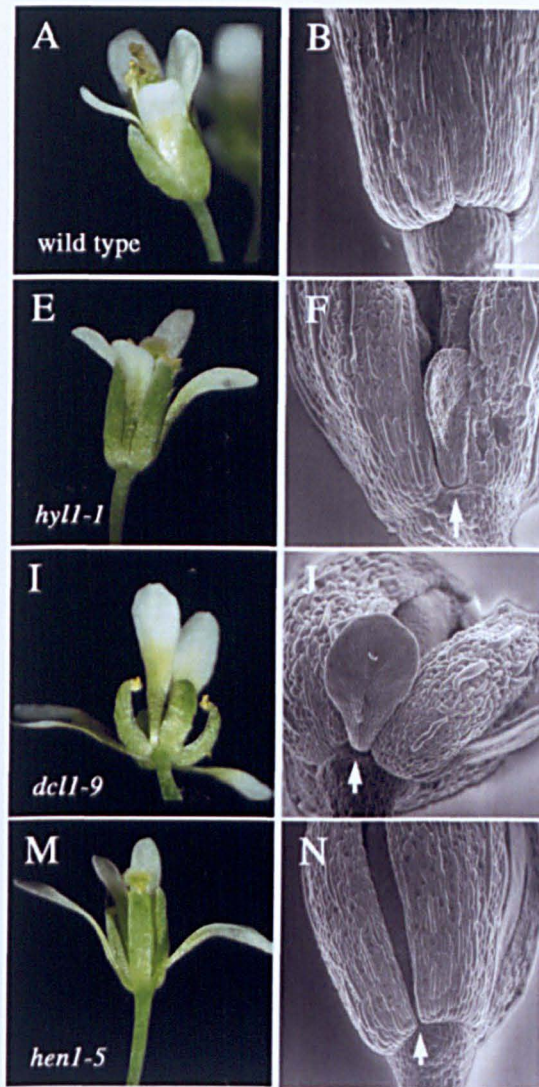


Figure 1.11 Flowers of miRNA pathway mutants. Loss-of-function *hyl1-1* (E, F arrow), *dcl1* (I, J arrow) and *hen1-5* (M, N arrow) mutants showing wider boundaries between sepals compared to the wild type flower (A, B). Illustration from Laufs *et al.* (2004).

It has been indicated that most miRNAs regulate plant development by controlling the level of transcription factors which affects development (Figure 1.12) (Rhoades *et al.*, 2002). This can be observed in *miR172* target gene *AP2*, which is a class A gene that plays a key role in floral morphology and flowering time (Figure 1.13a). Overexpression of *miR172* results in early flowering and an interruption of the floral organ identity specification by restraining the *AP2* gene translation. This regulates flowering time and floral organ identity in *Arabidopsis* (Aukerman and Sakai, 2003).

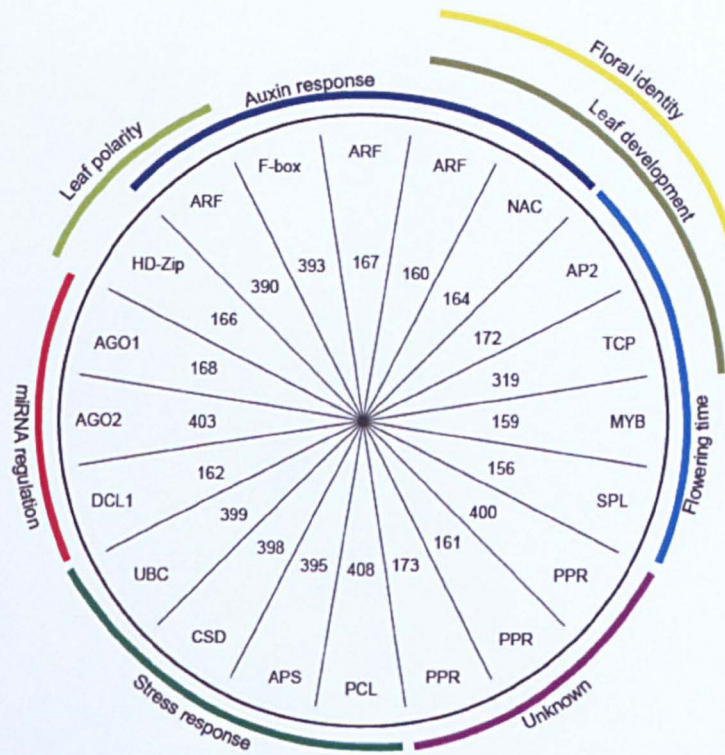


Figure 1.12 MicroRNAs gene regulation and their subsequent functions in different systems are shown in the above pie chart. The inner circle showing various miRNAs are arranged by their target genes that they regulate, shown by the outer circle. The coloured areas are showing the consequent roles of miRNAs in stress responses, miRNA pathway and in developmental stages Illustration from Mallory and Vaucheret (2006).

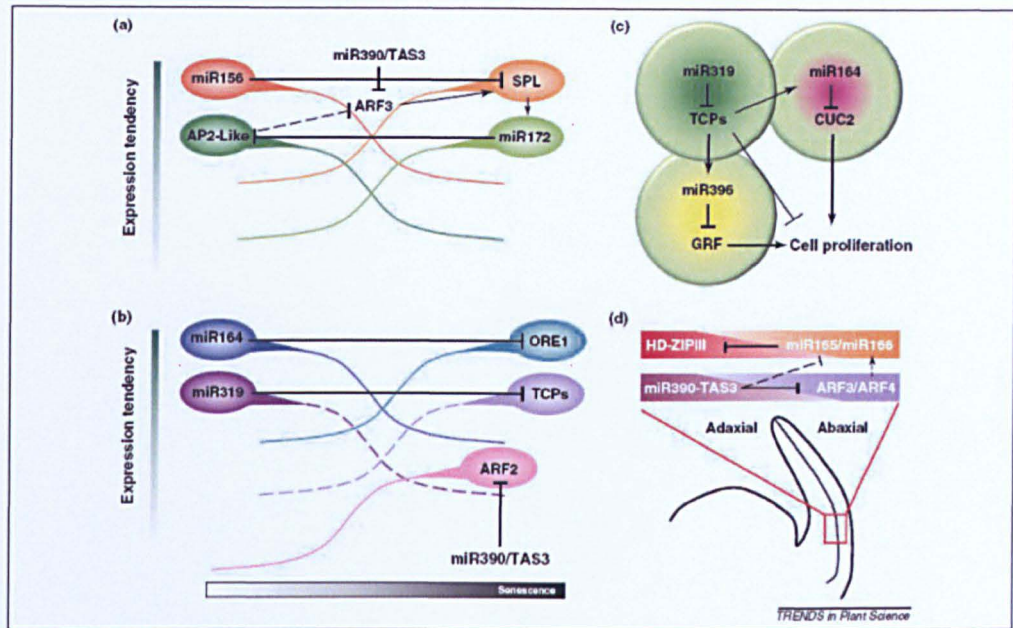


Figure 1.13 MiRNA gene regulations in leaf development. miRNA regulation of genes associated with (a) development phase transition, (b) leaf senescence, (c) cell proliferation and (d) adaxial-abaxial leaf polarity in *Arabidopsis*. Illustration from Rubio-Somoza and Weigel (2011).

Another miRNA, *miR319*, is involved in suppressing the onset of senescence by targeting the TEOSINTE BRANCHED1 CYCLOIDEA, PCF (TCP) transcription factor members (Figure 1.13b) and regulating LIPOXYGENASE2 (LOX2) activity which is a jasmonic acid (JA) biosynthesis enzyme. This leads to an up-regulation of JA levels which affects the timing of senescence. Overexpression of *miR319* results in plants that suppress the onset of senescence (Schommer *et al.*, 2008). Senescence is also controlled by *miR164*, where the expression of *miR164* decreases as the leaf ages leading to an increase in its targets NAC1 and ORE1 (AtNAC2) by use of an ethylene dependent approach (Figure 1.13b) (Kim *et al.*, 2009).

MicroRNAs are also known to affect shoot and root development. This can be observed on five members of the NAC-domain transcription factor family which includes *CUC1* and *CUC2* (Aida *et al.*, 1997). These are targets of *miR164* (Figure 1.13c) and an overexpression of *miR164* results in a decrease in lateral root emergence, unbalanced number of floral organs as well as

vegetative and floral organ fusion (Figure 1.14F). In contrast, loss-of-function of *miR164* results in an increase in the number of lateral root formations (Laufs *et al.*, 2004; Mallory *et al.*, 2004b). The overexpression of *miR164* leads to post-transcriptional downregulation of *CUC1* and *CUC2* mRNA levels and phenocopies the double mutant *cuc1/cuc2* (Figure 1.14 B-E) and *hws-1* mutant (Figure 1.14 G and H) (Laufs *et al.*, 2004; Gonzalez-Carranza *et al.*, 2007).

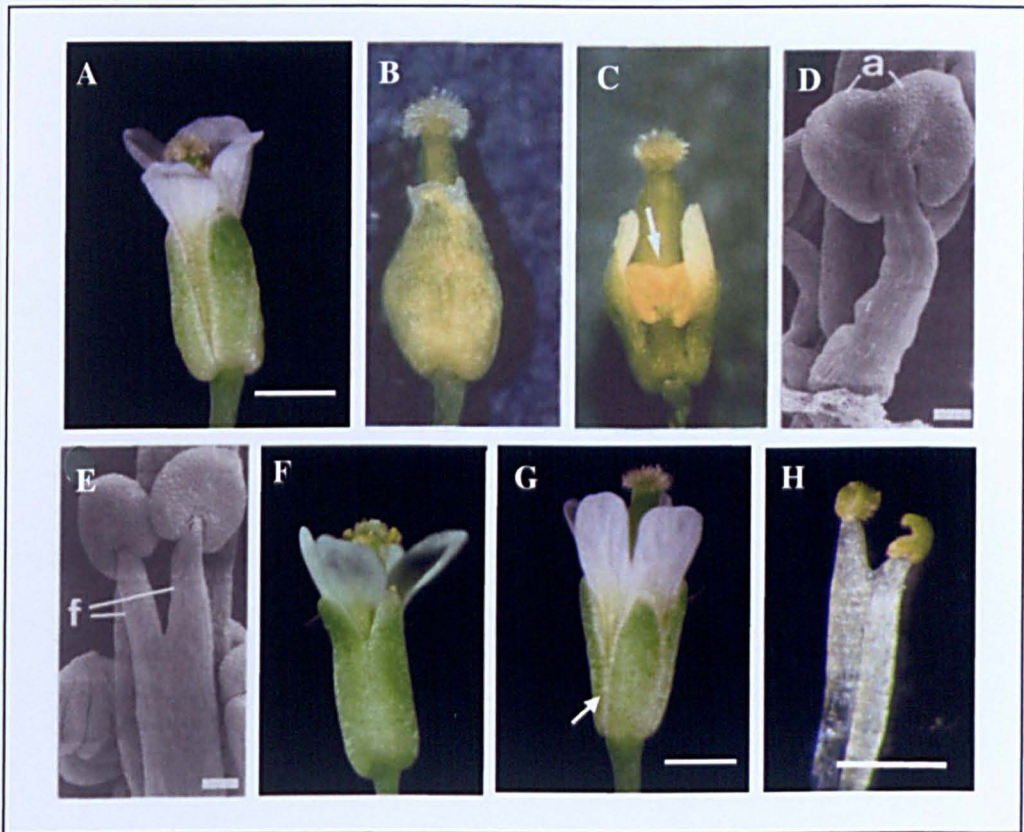


Figure 1.14 Col-0 wild type, *Cuc1cuc2* double mutant, ectopically expressing *miR164b* and *hws-1* mutant flower phenotype. (A) Col-0 wild type flower showing clear separation of sepal margins (B) *Cuc1cuc2* double mutant showing sepal fusion. (C) Sepal removed to show fusion of stamens (shown by arrow) on *cuc1cuc2* double mutant. (D and E) fusion of stamens on *cuc1cuc2* double mutant under scanning electron microscope (SEM). On (D), fusion can be seen up to the anthers (a) whereas on (E), fusion can be seen up to midway of the filaments (f). (F) Overexpressing *miR164b* flower showing fusion of sepal margins. Illustration modified from Aida *et al.* (1997) and Lauf *et al.* (2004). (G) *hws-1* mutant flower showing sepal fusion at basal margins (shown by arrow). (H) Fusion of *hws-1* mutant filaments. Bars (D and E) = 100 μ m, (A, G and H) = 1mm.

Genes such as *PHABULOSA* (*PHB*), *PHAVOLUTA* (*PHV*) and *REVOLUTA* (*REV*), which are members of the *Arabidopsis* HD-ZIP (class-III homeodomain leucine zipper) transcription factors are targets of *miR165* and *miR166* (Figure 1.13d). Dominant mutations in these transcription factor genes (*phb-d*, *phv-d* and *rev-d*) results in radialized leaves due to polarity defects. It was identified that the dominant mutation mapped to a complementary region of *miR165/166* caused a reduction in miRNA-directed cleavage effectiveness and developmental defects of the mutants (Mallory *et al.*, 2004a; McConnell *et al.*, 2001). A HD-ZIP protein family member, *ATHB15*, is a target of *miR166* and regulates plant vascular development (Kim *et al.*, 2005). An altered vascular system can be observed when *miR166a* is overexpressed resulting in reduction in levels of *ATHB15* mRNA (Kim *et al.*, 2005).

The *cuc1cuc2* mutant phenotype is similar to the sepal fusion of *hws-1* mutants and these sepal boundary defects are also phenocopied by ectopic expression of *miR164b*. It was discovered that floral buds of *hws-1* accumulated an increased level of *miR164* than Col-0 wild type plants and an overexpression of *HWS* results in a greater reduction in *miR164* accumulation (Zhang and Gonzalez-Carranza, unpublished data). These findings will be discussed in more detail in the following chapters.

1.7 Leaf formation and patterning in *Arabidopsis*

The success of a plant can be determined by its leaf shape and size. Leaf width and flatness decides the success of absorbing adequate light energy and its ability to facilitate gas exchange respectively. Mature leaf formation is determined by cell division and cell expansion. Cell division takes place at the early stages of leaf development (primary morphogenesis) and cell division halts when the leaf has attained its basic shape. Cell expansion aids in leaf growth and development throughout secondary morphogenesis (Donnelly *et al.*, 1999; Efroni *et al.*, 2008). Leaf primordia initiate from the periphery of the SAM and early leaf development and SAM signalling are tightly linked. The SAM size is maintained by a signalling pathway that is influenced by the *CLV*

loci, *CLV1* and *CLV3*, and the homeobox *WUSCHEL* (*WUS*) gene. Loss-of-function mutations in *CLV1* and *CLV3* result in accumulation of undifferentiated cells in the SAM (Clark *et al.*, 1996). Conversely *WUS* gene mutants fail to maintain SAM formation. *CLV* loci are involved in repressing *WUS* expression, however *WUS* is implicated in promoting *CLV3* function, producing a feedback loop system that regulate the size of the meristem (Figure 1.15A) (Schoof *et al.*, 2000). It has been tested through microsurgical studies that communication between the leaf primordia and SAM is essential for the leaf adaxial-abaxial polarity (Sussex, 1955). Subsequent leaf growth and asymmetric development is established by three primary axes of polarity known as proximal-distal, adaxial-abaxial and medial-lateral axes (Hudson, 1999). The leaf morphology is such that the adaxial side of the leaf differentiate into palisade mesophyll cells while the abaxial side of the leaf differentiate into spongy mesophyll cells (Lin *et al.*, 2003). Establishment of an adaxial-abaxial leaf polarity requires a SAM-derived signal since the interaction between leaf primordia and the SAM is significant for adaxial-abaxial leaf patterning.

Leaf form is divided into two categories known as simple leaf forms and compound leaf forms. Simple leaf forms, which include model plants such as *Antirrhinum majus*, *Zea mays* and *Arabidopsis*, display relative margin serration and the lamina is not subdivided into several units (leaflets). Conversely, Compound leaf form plants, such as rose and tomato, exhibit lamina that are subdivided into leaflets which is a consequence of frequent leaflet organogenesis on the primordium (Bharathan and Sinha, 2001). The variation between simple leaves and compound leaves is governed by the pattern of expression of a plant-specific homeobox gene family termed class 1 *KNOTTED*-like homeobox (*KNOX*) genes. *KNOX* genes play a key role in shoot meristem and axis development. These genes are transcribed in the SAM and ectopic expression of *KNOX* genes result in leaf lobing suggestive of ectopic *UFO* expression phenotype (Lee *et al.*, 1997). *KNOX* genes are down-regulated in simple leaf primordia, which is crucial for proper leaf development (Lincoln *et al.*, 1994; Bharathan *et al.*, 2002). Four members of class 1 *KNOX* gene have been identified in *Arabidopsis* as *SHOOT MERISTEMLESS* (*STM*),

BREVIPEDICELLUS (BP)/KNAT1, *KNAT2* and *KNAT6*. All four of these genes are expressed in the SAM, reminiscent of *CLV/WUS* signalling pathway, but not expressed in lateral organs (Lincoln *et al.*, 1994; Pautot *et al.*, 2001). *Arabidopsis* leaf form is governed by the expression of several genes such as *ASYMMETRIC LEAVES1 (AS1)* and *AS2*, which repress the expression of *BP* (also called *KNAT1*) (Figure 1.15B), and *KNAT2* and *BLADE-ON-PETIOLE1 (BOPI)*, which negatively regulate the expression of *BP*, *KNAT2* and *KNAT6* in developing leaf primordia (Byrne *et al.*, 2000; Semiarti *et al.*, 2001; Ha *et al.*, 2007). On the other hand gene expression of *STM*, represses the *AS1* and *AS2* function preventing improper development of leaves (Figure 1.15B) (Byrne *et al.*, 2002).

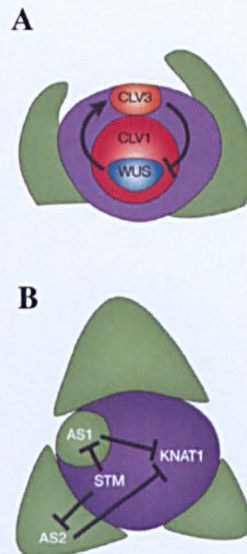


Figure 1.15 SAM and leaf primordia signalling pathway. (A) Longitudinal shoot apex showing the feedback loop system between *CLV* and *WUS* illustrating the *CLV3* activation by *WUS* expression and *WUS* repression by *CLV3* function. (B) Transverse shoot apex showing the suppression of *AS1* and *AS2* function by *STM* activity. Similarly *AS1* and *AS2* function is promoted by the downregulation of *STM*. Subsequently *AS1* and *AS2* suppress function of *KNOX* genes, *KNAT1*, *KNAT2* and *KNAT6* leading to functional development of SAM and leaf primordia. Illustration from Tsiantis and Hay (2003).

Auxin, a key plant growth hormone, is an essential element in leaf formation where by it is involved in regulating different stages of leaf development. Evidence has been shown that auxin is involved in promoting leaf lamina outgrowth and leaf margin development (Zgurski *et al.*, 2005). Auxin is transported from the epidermis to the young leaf primordia due to the subcellular localization of the *Arabidopsis* auxin efflux carrier, *PINFORMED1* (*PINI*) becoming apically polarized. *PINI* is basally polarized within the primordium and may contribute to the flow of auxin through the leaf centre delineating the position of the midvein (Reinhardt *et al.*, 2003; Heisler *et al.*, 2005). Loss-of-function *pin1* mutation leads to smooth leaf margins (Figure 1.16I) (Bilsborough *et al.*, 2011). Following establishment of auxin in the leaf primordia, auxin is transported back to the meristem for regulation of subsequent leaf formations. Auxin production in leaf primordia is emphasized by the regress of *PINI* polarity in the epidermis (Heisler *et al.*, 2005). This mechanism of auxin distribution via *PINI* polarization contributes to the maintenance of leaf phyllotaxis in *Arabidopsis* (Reinhardt *et al.*, 2003). Following auxin establishment in young leaf primordia, auxin is distributed symmetrically on both sides of the midvein from leaf margins (Aloni *et al.*, 2003; Benková *et al.*, 2003). Evidence that auxin promotes leaf lamina outgrowth was demonstrated by the *YUCCA* (*YUC*) genes. Members of this gene family encode flavin monooxygenases, which play a key role in biosynthesis of local auxin. Loss-of-function of at least four *YUC* genes (*YUC1*, *YUC2*, *YUC4* and *YUC6*) causes loss of leaf margin dispositions and narrow leaves (Zhao *et al.*, 2001; Cheng *et al.*, 2007).

The regulatory mechanism of serration at leaf margins in *Arabidopsis* development is important for correct special distribution as well as for accurate protrusion levels of these serrations (Figure 1.16C-H). There are feedback loop systems influencing this mechanism. First is the distribution of auxin via *PINI* polarization and the second is the promotion of *PINI*-dependent auxin induction by *CUC2* expression subsequently leading to *CUC2* repression by auxin activity (Figure 1.16A). The pinpoint repression of *CUC2* by auxin regulates the auxin maxima and *PINI* point of convergence position on the margin. The suppression of growth by *CUC2* activity indicates the location of

indentation. These mechanisms show that *CUC2* expression is required for indentation and protrusion positioning of leaf margin serrations (Figure 1.16K-M) (Bilsborough *et al.*, 2011).

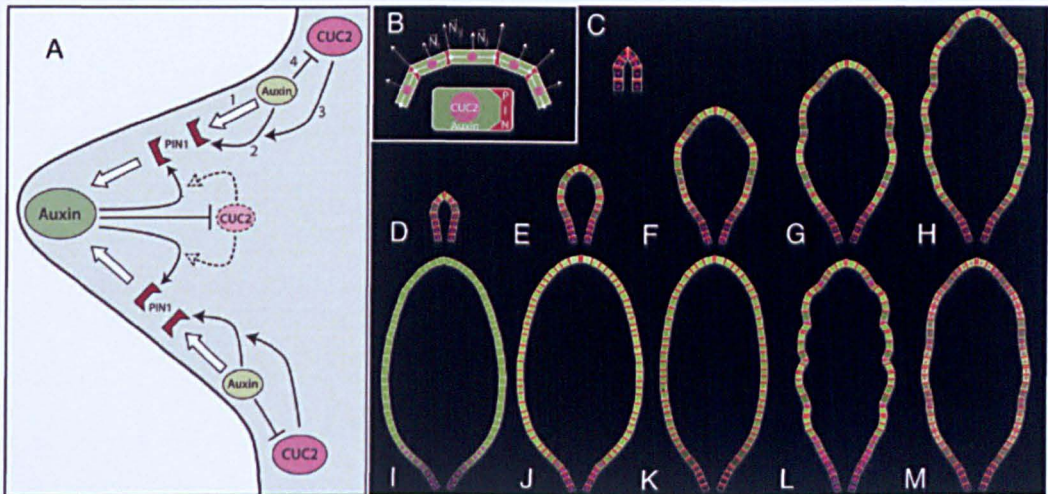


Figure 1.16 Theoretical model of interaction between *CUC2*, *PIN1* and auxin in the leaf margins. (A) Feedback loop system of auxin distribution by *PIN1* polarization and *PIN1*-dependent auxin induction by *CUC2* expression subsequently leading to *CUC2* repression by auxin activity. (B) Trapezium representation of a cell where decrease of auxin concentration is shown in black and augmentation is shown in bright green. Leaf margin propagation is affected by cell wall movement and readjustments of cell shapes. The average between normal directions N_i and N_j of adjacent cells governs the normal direction N_{ij} at a cell wall. (C-H) Wild type leaf development from primordium to mature stage. (I) *pin1* mutant phenotype, (J) auxin accumulation and (K) *cuc2* mutant phenotype showing a lack of serration at leaf margins. (L) Overexpression of *CUC2* resulting in increased serration. (M) standardized *CUC2* expression showing reduced serration of leaf margins. Illustration from Bilsborough *et al.* (2011).

1.8 Aims and objectives of project

The main aim of this project was to identify potential targets of *HWS* and to help identify the potential role of *HWS* in the miRNA pathway. This investigation was conducted by analysing suppressor lines from an EMS (ethyl methanesulfonate) mutagenized *hws-1* population. Two of the suppressor lines, 43.1 and 80.5, identified from the EMS *hws-1* populations were selected for analysis of this project.

Phenotypical comparison analyses were conducted between Col-0 wild type, *hws-1* and both mutants in Col-0 background and *hws-1* background on flowers, leaves and roots for characterisation of the genes involved.

A mapping population was constructed using F2 populations from a cross between the suppressor line and *ffo1*, an allele of *HWS* in the Landsberg ecotype. The DNA from the mutant was used for the mapping process which involves an InDel marker based genome-wide approach. Phenotypical comparisons are also made with previously identified analogous genes following the initial stage of mapping of the suppressor lines.

Once the gene(s) involved in the suppressor line was identified, further analyses were carried out to determine the correlation between these genes and *HWS*. These analyses will eventually support in understanding the role of *HWS* during flower development.

CHAPTER 2

Materials and methods

2.1 Plant materials and growth conditions

Arabidopsis thaliana ecotype Columbia (Col-0), *hasty*, *asymmetric leaves 2-1* (*as2-1*), *as2-4*, *as2-101*, *ufo-2*, and *ufo-6* mutants were obtained from the Nottingham Arabidopsis Stock Centre (NASC) for various crosses and mapping populations (Table 2.1). The *ffo1-1* (Landsberg *erecta* ecotype) mutant was kindly provided by the Meyerowitz group (California Institute of Technology) and the EMS mutagenized *hws-1* populations, *hws-1* and *35S_{pro}::HWS* seeds were kindly provided by Dr. Zinnia Gonzalez-Carranza (University of Nottingham).

Allele	Mutagen	Ecotype
<i>hst-1</i>	Diepoxybutane	Columbia
<i>as2-1</i>	X-ray	ER
<i>as2-4</i>	Unknown	En-2*
<i>as2-101</i>	EMS	Landsberg <i>erecta</i>
<i>ufo-2</i>	EMS	Landsberg <i>erecta</i>
<i>ufo-6</i>	EMS	Landsberg <i>erecta</i>

Table 2.1 Mutant alleles used in this project obtained from NASC. * En-2 background coincided with the Col-0 ecotype.

The EMS mutant seed populations were sown on 308 well trays containing Levington M3 (Scotts, UK Ltd): Vermiculite (2.0-5.0 mm, Sinclair) (3:1) (w/w) combined with 0.2 g L⁻¹ Intercept 70 WG (Scotts, Monro South) and transferred to the glasshouse at 22 °C ± 2 °C or the growth room at 22 °C ± 1 °C under 16 hours light and 8 hours dark photoperiod. Seeds were also sown in 9cm pots, 3 x 4 trays and 8 x 12 trays in Levington M3 treated with 0.2 g L⁻¹

Intercept 70 WG (Scotts, Monro South) for various crosses and phenotypic analysis.

Seedlings that were grown under sterile conditions were generated by sowing sterilised seeds on 4.3 g L⁻¹ Murashige and Skoog Basal salt mixture (Sigma) and 0.8% Bacto™ Agar. Seed sterilisation was carried out in a solution consisting of 50% (w/v) sodium hypochlorite. Sterilised seeds were then rinsed three times in a solution consisting of 0.01% (v/v) Triton X-100 followed by a rinse in 70% (v/v) ethanol and three rinses in sterile distilled water. The seeds were then placed onto the Murashige and Skoog agar Petri plates in a sterile hood using a pipette tip. The plates were sealed with micropore tape (3 M) and incubated at 4 °C for 48 hours to co-ordinate germination. The plates were subsequently transferred to a growth room at 23 °C ± 1 °C under 16h light and 8h dark photoperiod. Seeds were sown in Murashige and Skoog media for root measurements and for the selection of transformants, which in addition contained 50 µg.ml⁻¹ Kanamycin as described in section 2.10.7.

2.2 Phenotypic analysis and light microscopy

EMS *hws-1* mutant M2 populations were screened for suppressors which rescue the *hws-1* sepal fusion phenotype. A selfed EMS *hws-1* M2 population consists of 308 M3 plants where those that shed its floral organs were isolated as potential *hws-1* suppressors. Phenotypic comparisons were performed on seedlings and flowers of Col-0 wild type, *hws-1* and the *hws-1* suppressor lines as well as using other mutant lines described in chapters three and four. Rosette leaves were dissected from these genotypes and photographed using a Nikon CoolPix P6000 camera. Flowers and floral organs were photographed using a Kodak MDS290 digital camera mounted on a Stemi SV6 microscope. Objectives used include S1.0x, S2.5x and S0.63x. The identified suppressor lines were crossed with wild type Col-0 ecotype for segregation analysis and the F1 progeny was allowed to self. The suppressor lines of the same

population as well as those mutants from different populations that showed a similar phenotype were crossed with each other to perform allelism tests.

2.2.1 Tissue fixation and embedding

Stage 1.06, 6 rosette leaves >1mm in length, leaves were embedded in resin for analysis of cell size and number on dissected plant material. The plant material was immersed in fixation solution (0.2M sodium phosphate (pH 7.2); 10% (v/v) paraformaldehyde; 50% (v/v) glutaraldehyde; 20% (w/v) caffeine; 0.5% (v/v) tween 20) and vacuum infiltrated for 50 minutes. The samples were subsequently maintained at 4°C for 48 hours. Washes in, 50% (v/v) ethanol for 1 hour; 70% (v/v) ethanol overnight at 4°C; 70% (v/v) ethanol for 45 minutes; 90% (v/v) ethanol for 1 hour; 95% (v/v) ethanol for 1 hour; 100% (v/v) ethanol for 1 hour; 50/50% (v/v) ethanol/butanol for 24 hours at 4°C, were then performed. Consequently samples were immersed in 100% (v/v) butanol and vacuum infiltrated for 30 minutes prior to incubation at 4°C for 4-5 days. Plant material was then pre-impregnated in 50/50% (v/v) butanol/resin medium (Technovit 7100 resin (500ml; Kulzer, Wehrheim, Germany); Technovit 7100 accelerator (5g); glycol dimethacrylate (10ml) diluted 2 X in ethanol at 4°C for 2 hours; Technovit polyethylene glycol (PEG 400; 2ml) and vacuum infiltrated for 30 minutes. Samples were incubated at 4°C for 48 hours and embedded in 100% (v/v) resin in embedding moulds (Peel-A-Way® truncated T12, Polysciences, Inc). Tissue embedding was carried out in collaboration with Prof. Jean-Luc Verdeil, CIRAD, Montpellier.

2.2.2 Tissue sectioning

Resin embedded leaf material was sectioned using an ultra-microtome (Historange LBK) into 50-70 nm thick ribbons. Sections of tissue samples were placed on slides and covered with glass coverslips. Tissue sectioning was carried out in collaboration with Prof. Jean-Luc Verdeil, CIRAD, Montpellier.

2.2.3 Tissue staining

The sections were double stained with PAS (periodic acid-Schiff's reagent) and protein-specific NBB (Naphthol blue black) as described by Buffard-Morel *et al.* (1992). PAS stains polysaccharides red and NBB stains soluble and insoluble proteins blue (Fisher, 1968; Buffard-Morel *et al.*, 1992; Ribas *et al.*, 2011).

2.3 DNA extraction

Genomic DNA from leaf tissues was extracted according to the manufacturer's instructions provided by GenElute™ Plant Genomic DNA Miniprep Kit (Sigma) and The Extract-N-Amp Plant PCR (Sigma). For Extract-N-Amp Plant PCR, approximately 5mm leaf tissue samples were isolated, incubated in 25 µl extraction solution (Sigma), at 95 °C for 10 minutes and subsequently 25 µl dilution solution (Sigma) was added. The extracted DNA samples were stored at -20 °C until use. For GenElute™ Plant Genomic DNA Miniprep Kit, the tissues were disrupted by grinding using a mortar and pestle into a fine powder in liquid nitrogen. Up to a 100mg of material was obtained per sample tissue. To lyse the cells, 350 µl of lysis solution A and 50 µl of lysis solution B were added to the powdered material followed by a brief inversion and vortexing. The mixture was incubated at 65 °C for 10 minutes with occasional inversion. Prior to incubation a 35 µl of RNase A was added to the mixture to digest the RNA. In order to precipitate the debris, 130 µl of precipitation solution was added and mixed completely by inversion prior to incubating on ice for 5 minutes. The samples were then centrifuged at 13,000 x g for 5 minutes to pellet the cellular debris, polysaccharides and proteins. The supernatant was carefully pipetted onto a GenElute filtration column and centrifuged at 13,000 x g for 1 minute. The GenElute miniprep binding column was prepared by adding 500 µl of column preparation solution and centrifuging at 12,000 x g for 1 minute to maximise binding of DNA. Meanwhile 700 µl of binding solution was added directly to

the flow through liquid from the GenElute filtration column and mixed by inversion. This mixture was then loaded on to the prepared binding columns and centrifuged at 13,000 x g for 1 minute. This process was repeated until all the mixture was used. Subsequently 500 µl of Wash Solution, diluted with 100% (v/v) ethanol, was added to the binding column and centrifuged at 13,000 x g for 1 minute, followed by another addition of 500 µl of diluted wash solution and centrifuged at 13,000 x g for 3 minutes to dry the column. The DNA was eluted by adding 50 µl of elution solution pre-warmed at 65°C and centrifuged at 13,000 x g for 1 minute. DNA was stored at -20°C until use for PCR reaction.

2.4 RNA extraction

Total RNA was extracted from inflorescence and leaf tissues using manufacturer's instructions provided by Life Technologies with modifications for First-strand cDNA synthesis. The cells were disrupted by grinding plant tissue using a mortar and pestle into a fine powder in liquid nitrogen. Up to a 100mg of material was obtained per sample tissue. The samples were homogenised in 1ml of TRIzol reagent, mixed by inversion and placed on ice. Insoluble material was removed by centrifugation at 12,000 x g for 10 minutes at 4°C. The supernatant, containing the RNA, was transferred to a fresh Eppendorf tube and left at 25°C for 5 minutes to allow the total dissociation of nucleoprotein complexes. Subsequently 200 µl of chloroform was added to the sample, vigorously shaken for 15 seconds and incubated at 25°C for 3 minutes. The sample was then centrifuged at 12,000 x g for 15 minutes at 4°C. The aqueous phase, containing the RNA, was mixed with 10 µl of RQ1 RNase-Free DNase 10X Reaction Buffer and 10 µl of RQ1 RNase-Free DNase. This was subsequently incubated for 30 minutes at 37°C to purify the RNA from DNA contaminants. The RNA was precipitated from the aqueous phase by mixing the sample with 500 µl of 100% (v/v) isopropyl alcohol followed by incubation at 25°C for 10 minutes and centrifugation at 12,000 x g for 10 minutes at 4°C. The supernatant was removed and the RNA pellet washed with 1ml of 75% (v/v) ethanol followed by vortexing and centrifugation at 7,500 x g for 5

minutes at 4°C. The RNA pellet was dried for 5 to 10 minutes at room temperature and dissolved in 100 µl of RNase-free water.

Total RNA was purified using 1X Vol phenol: (100%) chloroform pH 4.5 in 1X Vol of total RNA and centrifuging at 10,000 x g for 5 minutes at 4°C. The solution separates into three phases, aqueous phase containing RNA, interphase containing DNA and organic phase containing proteins and lipids. The aqueous phase was extracted from the solution and transferred to a 1.5 ml Eppendorf tube with 1 µl of 10% (w/v) dextran. A 3X Vol 100% (v/v) ethanol was added to 1X Vol of solution and incubated overnight at -20°C. Subsequently, the pellet was dried at room temperature and re-suspended in 65 µl RNase-free water.

2.5 Nucleic acid concentration measurement

Quantification of DNA, total RNA and cDNA samples was conducted using NanoDrop® ND-1000 spectrophotometer. Measurements consisted of 1.5 µl control solution and 1.5 µl samples, which were recorded in units of ng µl⁻¹.

2.6 Image processing and statistical analysis

Images taken of MS media for root length measurements were analysed using ImageJ. Statistical analyses were conducted on Microsoft Excel 2007 and Genstat 15th edition for the standard error of the root growth graphs. Genstat was also used for standard deviation calculations and for P value analysis.

2.7 Polymerase Chain Reaction (PCR) amplification

2.7.1 PCR amplification via Taq DNA polymerase

The PCR reactions were performed using a GeneAmp® PCR system 9700 (Applied Biosystems, USA). PCR reactions consisted of 5 µl 5X PCR buffer (Bioline) (20mM Tris-HCl, pH 7.5, 100mM NaCl, 2mM DTT, 0.1mM EDTA, and 50% (v/v) Glycerol), 1 µl 50mM MgCl₂ (Bioline), 1.5 µl 5mM dNTPs (Promega, UK), 0.5 µl forward primer (100ng/µl), 0.5 µl reverse primer (100ng/µl), 0.15 µl (5 U/µl) Taq DNA Polymerase (Bioline), 1 µl (1-20 ng) DNA template and the volume was adjusted to 25 µl with sterile distilled water. The PCR reaction consisted of an activation step at 94°C for 3 minutes (hot start), 30-35 cycles of denaturation at 94°C for 30 sec, primer annealing at 50-70°C for 30 sec, primer extension at 72°C for 30-90 sec, followed by a final elongation step at 72°C for 7 minutes. Samples were chilled down to 4°C thereafter. The PCR programme varied according to the primer pairs used for different PCR reactions.

2.7.2 First-strand cDNA synthesis for reverse transcription-PCR

First-strand cDNA was synthesized from total RNA using SuperScript™II Reverse Transcriptase kit (Invitrogen) following manufacturer's instructions in a 20 µl reaction. This involved mixing 1 µg of total RNA with 1 µl of 500 µg ml⁻¹ oligo (dT)₁₂₋₁₈, 1 µl of dNTPs and 9 µl of sterile distilled water and incubating at 65°C for 5 minutes prior to a quick chill on ice. The mixture was then briefly centrifuged before adding 4 µl of 5X First-Strand Buffer and 2 µl of 0.1M DTT. The contents were gently mixed and incubated at 42°C for 2 minutes. Subsequently 1 µl (200 units) of SuperScript™II Reverse Transcriptase was added and mixed gently by pipetting. The mixture was then incubated at 42°C for 50 minutes, followed by incubation at 70°C for 15 minutes to inactivate the reaction. All the primer

sequences used in this project for PCR and RT-PCR are shown in the Appendix.

2.7.3 Gel electrophoresis

Amplification products were separated by gel electrophoresis in a 1-2% (w/v) gels consisting of 1-2g agarose, 50-100 ml 0.5 x TBE buffer (Tris-Borate-EDTA, Fisher BioReagents UK Ltd) and 1-2 μ l of 1% (w/v) ethidium bromide (Fisher Scientific, UK Ltd) depending on the gel percentage. Gels were immersed in 0.5 x TBE buffer and loaded with 5 μ l marker (100 bp and 1 Kb DNA ladder; Promega, UK Ltd) as well as 15 μ l of PCR product per well. The gel was run at 100 V for 20-30 minutes and visualized via UV light using a transilluminator (INGenius Bioimaging System, Syngene, Synoptics Ltd).

2.7.4 Purification of PCR product

PCR products were purified as shown on the manufacturer's instructions provided by QIAquick® PCR Purification (Qiagen). A 5X Vol of buffer PB (Qiagen) was added to 1X Vol of PCR product and mixed. Subsequently the sample was applied to a QIAquick column and centrifuged at 17,900 x g for 30 sec for DNA binding. The column was then washed with 750 μ l of buffer PE (Qiagen) and centrifuged at 17,900 x g for 30 sec. The column was yet again centrifuged at 17,900 x g for 1 minute and the DNA eluted by adding 50 μ l of buffer EB (10 mM Tris·Cl, pH 8.5) (Qiagen) to the centre of the column membrane. The column was incubated at room temperature for 1 minute before centrifuging at 17,900 x g for 1 minute.

2.8 Gel extraction for DNA recovery

Gel extraction was carried out on 1% (w/v) agarose gel samples using manufacturer's instructions according to GenElute™ Gel Extraction (Sigma).

The Gel band was extracted under UV light and weighed, prior to dissolving at 55°C for 10 minutes in three times the volume of solubilisation solution as the gel band. The solution was vortexed briefly every 2-3 minutes. Once the gel has dissolved, one gel volume of 100% (v/v) isopropanol was added to the gel solution and mixed until homogenous. This mixture was then loaded to on prepared GenElute Binding Column G (prepared using 500 µl Column Preparation Solution to the column and centrifuged at 13,000 x g for 1 minute) 700 µl at a time and centrifuged at 13,000 x g for 1 minute. This process was repeated until all the mixture was used. Subsequently 700 µl of Wash Solution, diluted with 100% (v/v) ethanol, was added to the binding column and centrifuged at 13,000 x g for 1 minute, followed by another centrifugation at 13,000 x g for 1 minute without adding any wash solution to dry the column. The DNA was eluted by adding 50 µl of Elution Solution pre-warmed at 65°C and centrifuged at 13,000 x g for 1 minute.

2.9 The *hws-1* suppressor line mapping

The mapping of *hws-1* suppressor line was performed by Dr. Janny Peters, University of Nijmegen, The Netherlands. The chosen *hws-1* suppressor lines were crossed with an allele of *HWS* in the *Lansberg* ecotype (*ffo1* (Levin *et al.*, 1998)) for gene mapping. DNA was extracted, as indicated in section 2.3, from the F2 progeny plants that display a phenotype similar to the suppressor lines that were sent to Dr. Janny Peters for gene mapping using InDel marker polymorphism. A brief description of the mechanism used for this mapping is indicated in section 2.9.1.

2.9.1 InDel (insertion, deletion) marker polymorphism.

The F2 population of the cross between *hws-1* suppressor line and *ffo1* was screened with two flanking InDel markers using the Cereon collection of InDel polymorphisms (Cereon, Cambridge, Mass, USA). For this PCR-based marker polymorphism, primers were developed to recognise the flanking marker in a co-dominant manner. For example, two InDel markers X and Y,

flanking the region of interest from above and below respectively where a larger fragment for Col-0 parent is shown compared to *Ler* parent in both InDel markers (Figure 2.1 A). PCR amplification from both X and Y InDel markers are simultaneously run on a polyacrylamide gel. A recombinant event within the region flanked by X and Y in the F2 population samples can be identified from the analysis of the polyacrylamide gel where three PCR fragments indicate recombinants, two PCR fragments indicate homozygous F2 non-recombinants and three PCR fragments indicate heterozygous non-recombinants (Figure 2.1 B). These recombinants can be used in further fine-mapping the region of gene of interest (Peters *et al.*, 2004).

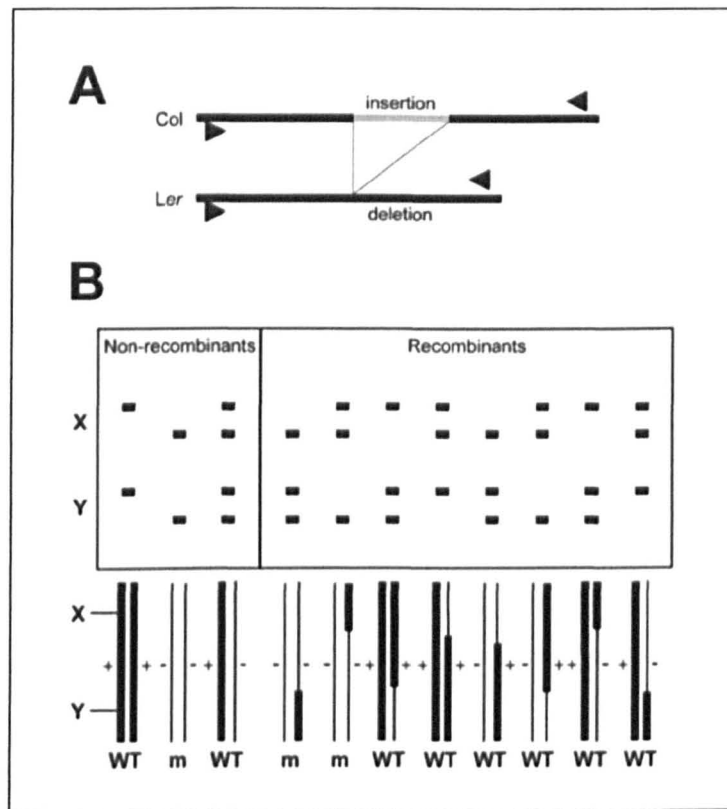


Figure 2.1 InDel marker polymorphism with two flanking InDel markers. (A) InDel markers flanking the region of interest amplified using specific primers with a larger fragment for Col (Columbia) parent compared to *Ler* (Landsberg) parent. (B) InDel marker examples X and Y, flanking the region of interest from above and below respectively. Homozygous F2 non-recombinants are shown with two PCR fragments and heterozygous non-recombinants indicated with three PCR fragments. WT: wild type phenotype and m: mutant phenotype. Illustration from Peters *et al.*, 2004.

2.10 Plasmid construction and transformation

2.10.1 *AS2_{pro}::AS2* line generation

Complementation analyses were carried out on the *hws-1* and *80.5/hws-1* mutants by amplifying a genomic fragment of *AS2* from Col-0 wild type DNA. The genomic fragment consisted of 3,564 bp of the promoter region, 557 bp of the 5'UTR, 664 bp of the introns, 600 bp of the ORF and 224 bp of the 3'UTR. The genomic fragment was amplified using the primers *AS2compFor* 5'**GCAATAAGCCTACATCAGATTTTA**3' and *AS2compRev* 5'**TCAATTAAGAGAGCAAGTCCATA**3' (Figure 2.2) via PhusionTM (Finnzymes) reaction. The reaction consisted of 10 µl of 5X Phusion HF buffer (Finnzymes), 1 µl of 10mM dNTPs, 1 µl of 100 ngµl⁻¹ forward and reverse primer, 50 ng of DNA template and 0.5 µl of Phusion DNA Polymerase (Finnzymes). The reaction was adjusted to 50 µl with sterile distilled water. The parameters used for the PCR reaction were 98°C for 30 sec, followed by 30 cycles of 98°C for 10 sec, 56°C for 30 sec and 72°C for 2.45 minutes, finally an elongation at 72°C for 7 minutes. By using this PCR product as a template, a second PCR reaction was carried out with forward and reverse primers containing restriction enzyme sites *Sall* and *Bam*HI, *AS2compSallFor* 5'**CGAGTCGACGCAATAAGCCTACATCAGATTTTA**3' and *AS2compBamHIRev* 5'**GTCGGATCCTCAATTAAGAGAGCAAGTCCATA**3' respectively, using PhusionTM (Finnzymes) reaction. The sites of the restriction enzymes are shown in bold. The same PCR parameters as shown above were used for amplification. The PCR product was PCR cleaned as shown in section 2.7.4.

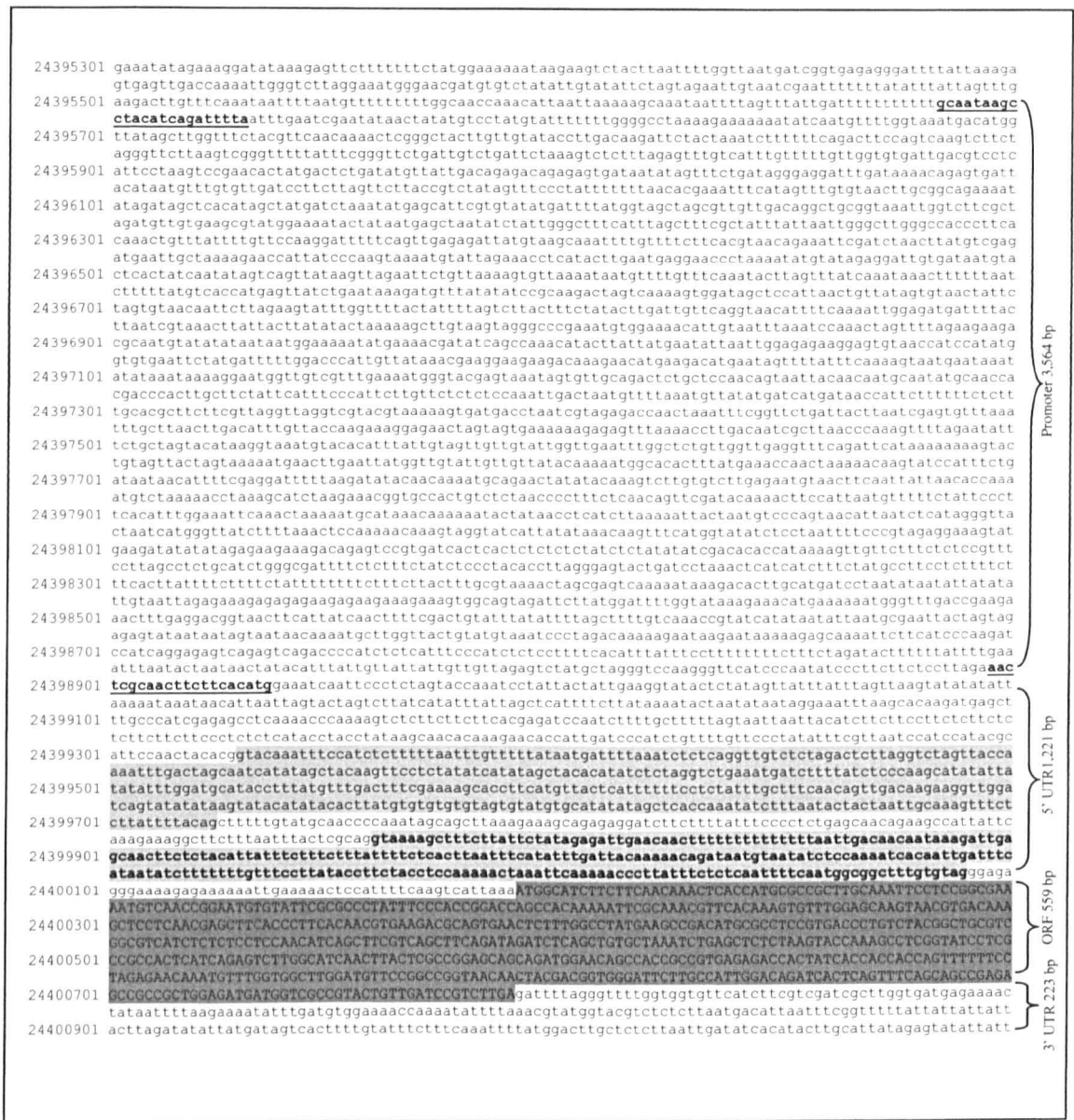


Figure 2.2 AS2 promoter and gene sequence. The gene contains 3,564 bp promoter region, 1,221bp of the 5'UTR, with two introns (intron 1 (390-788 bp) and intron 2 (905-1171 bp), 599 bp coding region, and 223 of 3'UTR. Exons are highlighted in light grey and the coding region is highlighted in dark grey. The primers AS2compFor and AS2compRev are underlined. Sequence obtained from TAIR.

2.10.2 *AS2_{pro}::GUS* line generation

GUS expression analyses were carried out on Col-0 wild type and *hws-1* mutant by amplifying a genomic fragment of *AS2* from Col-0 wild type DNA. The genomic fragment consisted of 3,564 bp of the promoter region and 557 bp of the 5'UTR. The forward primers (*AS2compFor* and *AS2compSallFor*) used for amplification were the same as for complementation test as indicated in section 2.10.1. However the reverse primers altered to *AS2compRevpro* 5'CATGTGAAGAAGTTGCGAGTT3' and *AS2compBamH1Rpro* 5'GTCGGATCCCATGTGAAGAAGTTGCGAGTT3'.

2.10.3 DNA digestion using restriction enzymes

Restriction enzymes used in this project are *Sall*, *BamHI* and *EcoRI*-HF (NEB). Each digestion consisted of 2 µl of 10X buffer (NEB), 0.2 µl of 100X BSA, 1 µl of restriction enzyme(s) and adjusted to 20 µl using sterile distilled water. The reaction was then incubated at 37°C for 2 hours.

2.10.4 *AS2* gene fragment and pBI101.2 vector ligation

The pBI101.2 vector (Figure 2.3) was digested using *Sall* and *BamHI* restriction enzymes prior to vector insert ligation. Ligation was carried out using a ratio of 3:1, insert:vector. The ligation reaction involved 1 X T4 DNA ligase buffer, 1 µl of pBI101.2 vector (50 ng.µl⁻¹), 3 µl of *AS2* insert (68 ng.µl⁻¹) and 1 unit of T4 DNA ligase. The reaction was adjusted to a final volume of 10 µl using sterile distilled water. A control ligation reaction was also made using pBI101.2 vector along with no added insert. The ligation reactions were incubated overnight at 4°C.

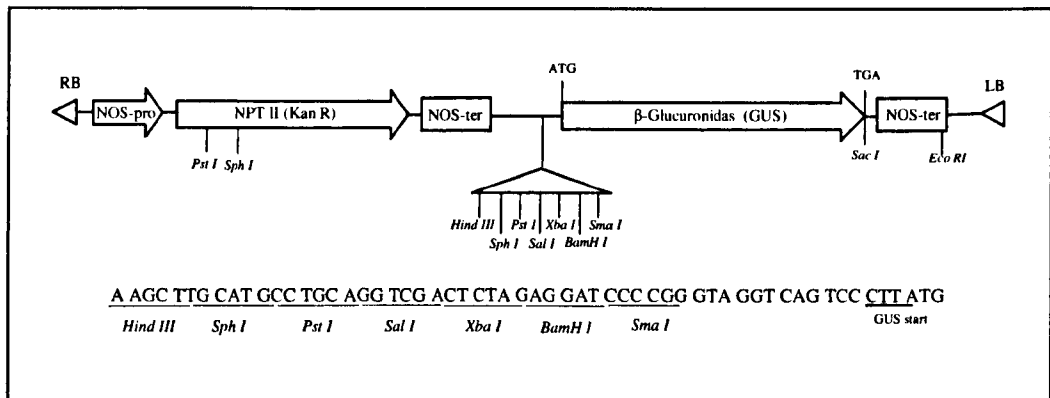


Figure 2.3 pBI101.2 T-DNA region. The polylinker cloning site is shown on the illustration up-stream of GUS. (NOS-ter, nopaline synthase polyadenylation). Illustration modified from Jefferson *et al.* (1987).

2.10.5 Bacterial transformation using DH5 α

Following ligation overnight, 50 μ l DH5 α competent cell suspension was added to the 10 μ l ligation reaction. The mixture was incubated on ice for 20 minutes, heat shocked for 45 seconds at 42 $^{\circ}$ C and immediately returned to ice for a further 2 minutes. A 450 μ l sample of pre-heated LB medium was added to the mixture and incubated at 37 $^{\circ}$ C for 2 hours with shaking at 200 rpm. A sample of 50 μ l and a sample of 100 μ l of the culture was plated onto LB agar medium containing 50 μ g.ml $^{-1}$ Kanamycin and incubated for 16-18 hours at 37 $^{\circ}$ C.

Colonies were tested using PCR with pBI101.2For 5'GAGTTAGC TCACTCATTAGG3' and AS2rev4 5'CAAGTAGCCCGAGTTTTGTT3' as well as AS2for4 5'GTCGATCGCTTGGTGATGAG3' and reverse primer GUSseq 5'TCACGGGTTGGGGTTTCTAC3'. Positive bacterial colonies were grown on LB agar medium containing 50 μ g.ml $^{-1}$ Kanamycin overnight at 37 $^{\circ}$ C. Cultures made overnight at 37 $^{\circ}$ C from the positive colonies were used for glycerol stock preparations and for DNA plasmid miniprep analysis.

2.10.6 *Agrobacterium* transformation using C58

A 5µl aliquot of the AS2::AS2 plasmid and a C58 competent cell aliquot of 50µl were mixed together by pipetting. This mixture was then transferred to an electroporation cuvette that was pre-cooled at -70°C for 10 minutes. An electric pulse of 2.2 kilovolts was applied for 6 milliseconds to the electroporation cuvette using a BioRad MicroPulser™ (Bio-Rad Lab Ltd). Immediately 1 ml of LB medium was added to the electroporation cuvette and incubated at 28°C for 3 hours before plating 50µl and 100µl of the incubated culture to LB agar medium consisting of 50 µg.ml⁻¹ Kanamycin and 25 µg.ml⁻¹ of Rifampicin. These plates were incubated at 28°C for 2 days. Positive colonies were selected by PCR using primers that were used for bacterial transformation analysis as described in section 2.10.5.

2.10.7 *Arabidopsis* transformation using floral dip

Arabidopsis transformation involved the use of the floral dip technique as described by Clough and Bent (1998). Col-0, *hws-1* and *80.5/hws-1* plants were grown in the growth room until they started to flower. The first bolt was excised to promote numerous secondary bolts. Four days after excising, an LB liquid medium (200ml) consisting of 50 µg.ml⁻¹ Kanamycin and 25 µg.ml⁻¹ of Rifampicin was inoculated with a positive colony that was identified by *Agrobacterium* transformation. The culture was incubated with shaking (200 rpm) at 28°C overnight and until the OD₆₀₀ measurement was equal to 0.8. This was then aliquoted to 50ml centrifuge tubes and centrifuged at 6,000 rpm for 5 minutes. The resulting pellet was resuspended in 5% (w/v) sucrose solution to OD₆₀₀ 0.8.

Prior to floral dipping, 0.05% of Silwet L-77 was added to the suspension. Above-ground areas of the plants were dipped, with gentle agitation, in the *Agrobacterium* solution for 10 sec before covering the dipped plants with plastic sleeves for 24 hours to sustain high humidity. The

transformed plants were placed in the growth room and watered as normal. Seeds were harvested once the plants had become dry.

2.10.8 Selecting for plant transformation

Harvested seeds were sterilized with distilled water containing 0.01% (w/v) Triton X-100 in 1.5ml Eppendorf tubes. The solution was decanted and sterilized with 50% (v/v) bleach prior to washing three times with the Triton and distilled water solution. All solutions were decanted and washed with 70% (v/v) Ethanol before being washed three times with SDW. All sterilized seeds were placed on filter paper to dry.

Dried seeds were spread on ½ MS media consisting of 50 µg.ml⁻¹ Kanamycin and incubated at 4°C for 2 days prior to transferring the plates to a growth room at 22.5°C with 24 hour daylight. The Kanamycin resistant seedlings were washed of any media and transplanted on Levington M3 soil with 0.2 g L⁻¹ Intercept 70 WG (Scotts, Monro South) and transferred to the glasshouse at 22 °C ± 2 °C. The phenotypes of the transgenic plants were analyzed.

2.10.9 Histochemical analysis of GUS activity

Two weeks old leaves, flower buds, flowers from positions 2 to 10 (stages 6.0 to 6.90 as shown on table 1.1, section 1.1) and incipient siliques from positions 10 to 16 of *AS2_{pro}::GUS* wild type and *AS2_{pro}::GUS hws-1* were immersed into GUS staining solution (0.1M sodium phosphate buffer (pH 7.0); 10mM EDTA; 0.1% (v/v) Triton X-100; 0.5% (w/v) 5-Bromo-4-chloro-3-indolyl β-D-glucuronide (X-Gluc) dissolved in 1ml of Dimethylformamide; 1mM potassium ferricyanide; 1mM potassium ferrocyanide (Sundaresan *et al.*, 1995)). Plant material immersed in GUS staining solution was incubated at 37°C overnight. GUS stained tissues were washed three times using 70% (v/v) ethanol with 30 minutes to 1 hour intervals between washes. GUS stained

tissue samples were photographed using a Kodak MDS290 digital camera mounted on a Zeiss Stemi SV6 Stereo microscope.

2.11 Bioinformatic analysis

BLAST (TAIR and NCBI) searches were carried out using sequences of *hws-1* suppressor mutants to identify potential orthologues of the genes. The sequences for primer designs were obtained from TAIR database. Nucleotide and protein alignments were carried out using Clustal W and nucleotide sequences were translated using ExPasy Translate tool. Gene expression levels in different tissues of a plant were analysed using the gene expression search engine, GENEVESTIGATOR.

CHAPTER 3

Characterisation of *43.1*

3.1 Introduction

3.1.1 Strategies to identify the substrate(s) of *HWS*

The *hws-1* mutant was generated by LEHLE SEEDS (Round Rock, TX., USA) using fast neutron bombardment at a dose of 55 Gy in the BARN (Biological Agriculture Reactor Netherlands) irradiation room. The mutagenesis was carried out on M1 *Arabidopsis* seeds in the Col-0 wild type background. These M1 plants were self-pollinated and the resulting approximately 1000 M2 families were screened. The *hws-1* mutant was identified among the M2 families due to its inability to shed its floral organs following silique desiccation.

HWS is an F-box protein and has been shown to interaction with the *Skp1*-like genes, *ASK1* and *ASK4* in an anther-specific yeast two-hybrid library (Gonzalez-Carranza et al, 2007). The HWS F-box domain is located in the region of 40-85 amino acids downstream of the N-terminus. *HWS* also exhibits a kelch-2 motif in its C-terminus. It has been identified in other F-box proteins that the kelch repeat motif is important in recognising the substrate involved in degradation (Jarillo *et al.*, 2001). It is also known that F-box proteins which contain C-terminal kelch repeats are multidomain proteins. In the SCF complex, the C-terminal domains may employ target proteins that are intended for degradation of proteasomes (Schumann *et al.*, 2011). Analyses are underway to identify the substrate(s) involved in the SCF complex where the F-box protein, *HWS* is a key player.

There are several approaches involved in identification of F-box protein substrates. These approaches commonly comprise the disruption of F-box protein expression using shRNA hairpins, ubiquitination target stabilization

using Cull-dominant negatives and the use of F-box protein collections as biochemical reagents in order to detect interacting proteins that maybe substrates. There are also strategies involved in the detection of F-box proteins that identify particular phosphodegrons (these are phosphorylated motifs that are formed from phosphorylation of ubiquitination target by pertinent kinases) via the use of immobilized phosphopeptides. A majority of these techniques depend on the prior knowledge of the turnover of a particular ubiquitylated protein and the establishment of specific identities of sites of phosphorylation, which are significant for turnover, within the protein (Jin *et al.*, 2005).

There are many challenges involved in the identification of F-box protein substrates. One of these challenges is the relatively weak and transitory detection of the F-box protein-substrate interaction. Even though current advances such as mass spectrometry have permitted the detection of these weak interactions, the analysis of such detections remains problematic due to the large number of proteins that need to undergo elimination binding non-specifically to a bait protein (Yumimoto *et al.*, 2012).

In an attempt to identify the substrate(s) associated with *HWS* for degradation, yeast-two-hybrid assays and proteomics approaches was developed. The yeast-two-hybrid system is a molecular genetic tool involving the detection of protein-protein interactions. This system can be used to identify prey proteins which interacts with the known bait protein or to understand the interaction between two proteins that are predicted to interact with each other (Young, 1998). If a protein interaction has been established, a reporter gene is transcriptionally activated. The yeast-two-hybrid system involves the expression of two chimeric proteins that interact and bring the separate activation domain (AD) and the binding domain (BD) into contact. This eventually drives the expression of a downstream reporter gene (Young, 1998). The yeast-two-hybrid assay did not identify the substrate(s) involved in *HWS* since the affinity of substrates for the required F-box protein is comparatively weak (Gonzalez-Carranza Z.H. and Zhang X., unpublished data).

For the isolation of HWS target proteins, a two dimensional (2D)-PAGE protein gel electrophoresis system was employed by comparing the proteomes of different plant genotypes. The 2D-PAGE gel electrophoresis technique was carried out on extracts of protein from *hws-1* and wild type tissue samples with the aim of identifying proteins that are present in *hws-1* but not in wild type. These techniques used to isolate target proteins for HWS have not yielded information that can move us closer to identifying the substrate(s) involved in the SCF_{HWS} complex (Gonzalez-Carranza Z.H. and Zhang X., unpublished data).

Due to the limited information on HWS substrate identification from yeast-two-hybrid and proteomics approaches, another approach was undertaken to isolate gene products that are interacting with HWS using a suppressor or enhancer analysis strategy. The first phase of this was achieved by mutation of *hws-1* using EMS mutagenesis.

EMS involves the chemical modification of nucleotides which leads to base mispairing. The principle behind EMS constitutes its capacity to alkylate a guanine base that is able to pair with thymine base resulting in mainly G/C to A/T substitution. This will eventually lead to an amino acid change or deletion (Maple and Møller, 2007). Most commonly EMS induces a base pair change from C-to-T directing to a C/G to A/T transition. EMS generates mutations that are randomly distributed throughout the *Arabidopsis* genome. This can subsequently lead to the understanding of the role of specific amino acid residues in protein function as well as producing loss- or gain-of-function mutants (Kim *et al.*, 2006). Unlike other mutagens which generally result in loss-of-function, EMS generates point mutations that frequently result in constitutive function, partially reduced function, qualitatively altered function as well as loss-of-function (Maple and Møller, 2007). The induction of multiple point mutations by EMS is such that mutant alleles of a specific locus are 1 in 2000-5000 M2 plants. This high rate in mutagenesis facilitates screening of plants to find mutants with the desired phenotype by making the screening process less laborious (Weigel and Glazebrook, 2002).

Screening of the M2 population for suppressors of the *hws-1* phenotype would enable the identification of specific proteins downstream of HWS that are targeted for degradation. A null mutation of the target encoding gene would result in *hws-1* phenotype rescue, leading to floral organ shedding. Approximately 560 M1 plants were used to develop roughly 112,000 M2 plants and these M2 plants were selfed to generate 112,000 M2 populations for screening of *hws-1* suppressor lines.

3.1.2 Interaction of *HWS* and microRNA genes

Similar phenotypic characteristics to the sepal fusion phenotype of *hws-1* mutant can also be seen in the ectopically expressed microRNA *miR164b* (Mallory et al., 2004b; Laufs et al., 2004). *MicroRNA164* is a target of both *CUC1* and *CUC2* gene expression. Overexpression of *miR164* (*2x35S:miR164*) demonstrates sepal fusion along their margins indicating that it phenocopies the *cuc1cuc2* double mutant. This is achieved by post-transcriptional downregulation of *CUC1* and *CUC2* levels of mRNA via *miR164*. The sepal fusion of *2x35S:miR164* is rescued by the expression of *CUC2* mRNA that is resistant to *miR164*-guided cleavage (*CUC2-m4*) (Laufs et al., 2004). *CUC2-m4* expression also leads to enlargement of the boundary domain resulting in an enhanced spacing between sepals indicating that the target degradation of *CUC1* and *CUC2* by miRNA restrict the enlargement of boundary domain (Laufs et al., 2004). Laufs et al. (2004) have also shown that the boundary domain expansion is constrained by *miR164*-dependent degradation of *CUC1* and *CUC2* transcripts due to boundary cell proliferation. These analyses demonstrated that *CUC1* and *CUC2* loss of function resulted in the sepal fusion flower phenotype observed on *miR164* overexpression. Furthermore the *cuc1cuc2* double mutant consists of fused cotyledons that are similar to the mutant phenotype of *miR319* and TCP regulation. *TCP* genes, targeted by *miR319*, are involved in regulation of leaf morphogenesis. *MiR319* targeted degradation of *TCP* results in crinkled larger leaves due to comprehensive leaf margin cell proliferation (Palatnik et al., 2003). Similar regulation of cell proliferation resulting in crinkled leaf phenotype was observed in ectopically

expressed *CUC2* (*2x35S::CUC2*) lines (Laufs *et al.*, 2004). *TCP3* binds to the promoter of *miR164a* and modulates its expression leading to *miR164a* targeted degradation of *CUC* genes (Koyama *et al.*, 2010). An EMS mutagenized *hws-1* suppressor, *prb-1*, which rescues the *hws-1* sepal fusion was isolated by Dr. Gonzalez-Carranza from the *hws-1* EMS populations. The nature of this mutation results in a single nucleotide change in *CUC1 miR164* binding site (Gonzalez-Carranza Z.H., unpublished data). These results may contribute to a relationship that shows a link between *HWS* and the miRNA regulation in plant development.

Further research carried out by Dr. Gonzalez-Carranza has shown that the *hws-1* phenotype is rescued when crossed with mutants of the microRNA pathway (Gonzalez-Carranza, unpublished data). This indicates that there may be a link between ubiquitination and the microRNA pathway. To further understand the role of the *HWS* gene in miRNA biogenesis, a number of EMS mutagenized *hws-1* suppressor lines were characterised.

3.1.3 Chapter aims and objectives

This Chapter involves the characterization of the EMS mutagenized *hws-1* suppressor line *43.1*. Phenotypic comparisons between Col-0 wild type, *hws-1* and *43.1* both in *hws-1* background and Col-0 wild type background were conducted on flowers, leaves and roots. This involved segregation of the *43.1/hws-1* double mutant into *43.1* single mutant.

Sequencing analyses were carried out to investigate the gene involved in the mutation and to identify the nature of the mutation. This also entailed crossing *43.1* with a mutant allele of the gene involved, for allelism tests. Furthermore the interaction between *HWS* and the gene involved in the *43.1* mutation was investigated.

3.2 Results

3.2.1 Morphological analysis of EMS populations

I have screened forty six (population shown on Table 3.1) EMS mutagenized *hws-1* M2 populations from 112,000 M2 populations. From the forty six EMS mutagenized *hws-1* M2 populations that were analysed, twenty suppressor lines were isolated by their ability to rescue the distinctive *hws-1* sepal fusion phenotype leading to the shedding of floral organs during senescence. Each suppressor line identified was first named after the EMS *hws-1* population number it was isolated from, then by its mutation number (i.e. 43.1 was the 43rd EMS *hws-1* population and 1st mutant selected from that same population) (Table 3.1). The EMS population numbers shown in Table 3.1 indicate to the populations that were screened for this project from 112,000 M2 EMS *hws-1* populations. All the suppressor lines were screened by PCR analysis, using *HWS* specific primers, SSLPHSfor and SSLPHSrev (band length 172 bp). Plants that amplified only Col-0 wild type (band length 200 bp) were discarded as wild type contaminants (Figure 3.1). A 28 bp difference was observed on the PCR analysis between wild type contaminants and suppressor lines. These results were confirmed by performing PCR analysis on the F1 generation of each suppressor line. Various phenotypic characteristics can be observed on each suppressor line aside from being able to rescue the *hws-1* phenotype.

Other mutations in the EMS *hws-1* populations were also observed that showed abnormal phenotypic characteristics (Figure 3.2) as well as rescuing of the *hws-1* sepal fusion mutation resulting in a pleiotropic effect. Some of these mutations rendered the majority of inflorescences flowerless (Figure 3.2 A and B) which made it difficult to determine whether the mutant plant was rescuing the *hws-1* phenotype. Another suppressor mutation observed was the lack of floral anthers and carpels, which were replaced by petals and sepals (Figure 3.2 D) giving the effect of a secondary flower formation on top of initial flowers. Other suppressor lines that showed abnormalities include mutations that lacked petals (Figure 3.2 F), mutations that produced additional inflorescences at the

proximal end of secondary inflorescence (Figure 3.2 E) and mutations that displayed abnormal phyllotaxis (Figure 3.2 C). Reciprocal crosses were made between suppressor lines obtained from the same EMS mutagenized populations were found to be allelic. This indicates that suppressor mutations identified from the same population are of the same gene hence providing only one mutation type per population analysed.

EMS population	Suppressor	EMS population	Suppressor
37		66	
38		67	
39		68	
40		69	
41		70	
42		71	
43	43.1	72	
44		73	
45	45.1,45.4	74	
46		75	
49		76	
50		77	77.1
53	53.4	78	78.1
54	54.6	79	79.1
55		80	80.1,80.2,80.4,80.5
56		81	
57		82	
58		83	
59		84	84.1,84.3,84.5,84.6,84.7,84.10,84.12
60		85	85.1
61		86	86.1
62		87	
65		88	

: populations and mutant lines that failed to rescue the *hws-1* phenotype
 : Identified suppressor lines

Table 3.1 Forty six M2 EMS mutagenized *hws-1* populations were analysed and twenty suppressor lines have been isolated (shown in white). Each suppressor line identified was first named after the EMS *hws-1* population number it was isolated from, then by its mutation number (i.e. 43.1 is 43rd EMS *hws-1* population and 1st mutant selected from that same population). EMS populations shown in grey are those that did not show suppressor lines. Those suppressor lines from the same population were tested for allelism by crossing to each other and were found to be allelic.

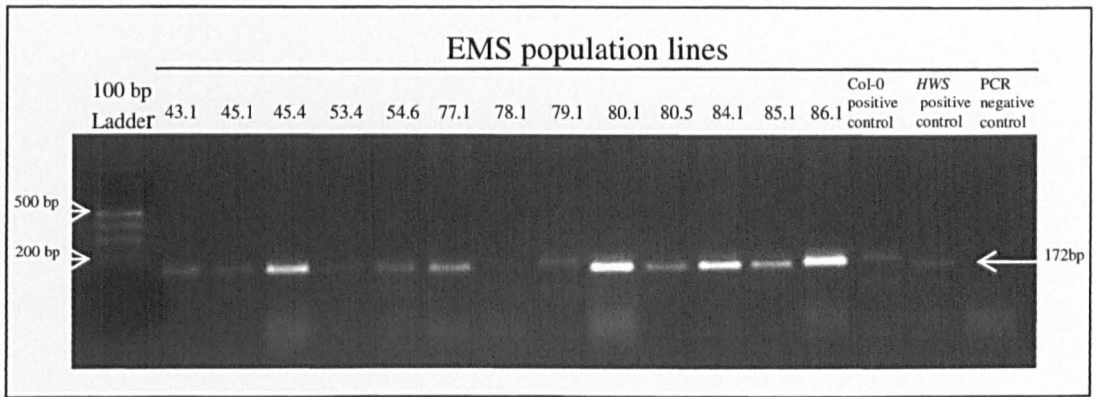


Figure 3.1 PCR analysis of some of the suppressor lines indicating the presence of the *HWS* gene with a 172 bp band. Line 79.1 is showing to be a contaminant as it amplifies a 200 bp fragment. These analyses aid to distinguish between true *hws-1* suppressor lines and wild type contaminants.

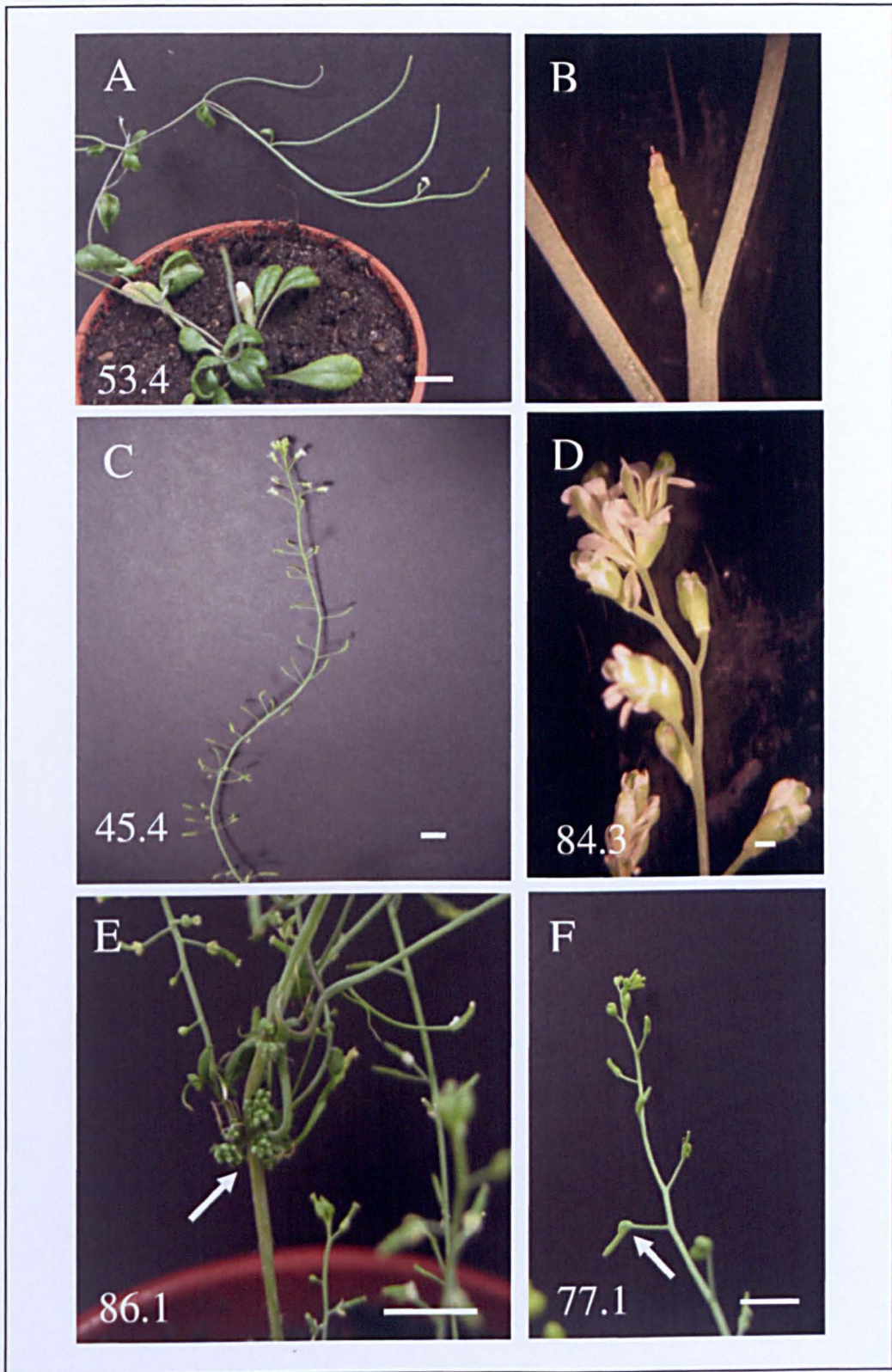


Figure 3.2 The different types of suppressor mutations, showing an effect on floral organ development. (A and B) Absence of floral organs in inflorescences. (C) Abnormal phyllotactic pattern. (D) Reproductive organs anthers and carpels, replaced by petals and sepals. (E) Presence of additional inflorescence at the proximal end of secondary inflorescence. (F) Absence of petals. Bars (A, C, E and F) = 1cm, Bars (B and D) = 1mm.

From the twenty suppressor lines isolated, two suppressor lines, *43.1* and *80.5* were identified for detailed analysis in this project. These suppressor lines rescue the distinctive sepal fusion phenotype of *hws-1* as well as displaying other phenotypic abnormalities. These abnormalities will be discussed in more detail in this chapter for *43.1* and in chapter four for *80.5*.

3.2.2 Phenotypic analysis of *43.1*

Besides the ability to rescue the *hws-1* phenotype (Figure 3.3 B) phenotypic analysis of *43.1/hws-1* show that the mutant had elongated leaves (Figure 3.3 A) as well as abnormal phyllotactic arrangement along the internodes (Figure 3.3 C) and additional petals in some of the flowers (Figure 3.3 D). Disrupted phyllotaxy can also be observed in *hasty* (*hst*) mutants (Bollman *et al.*, 2003). The loss of *HST* gene function also leads to mutants with similar elongated leaves as *43.1*. To further analyse the phenotypic similarities between *43.1* and *hst*, comparisons were made between different plant organs of the mutants.

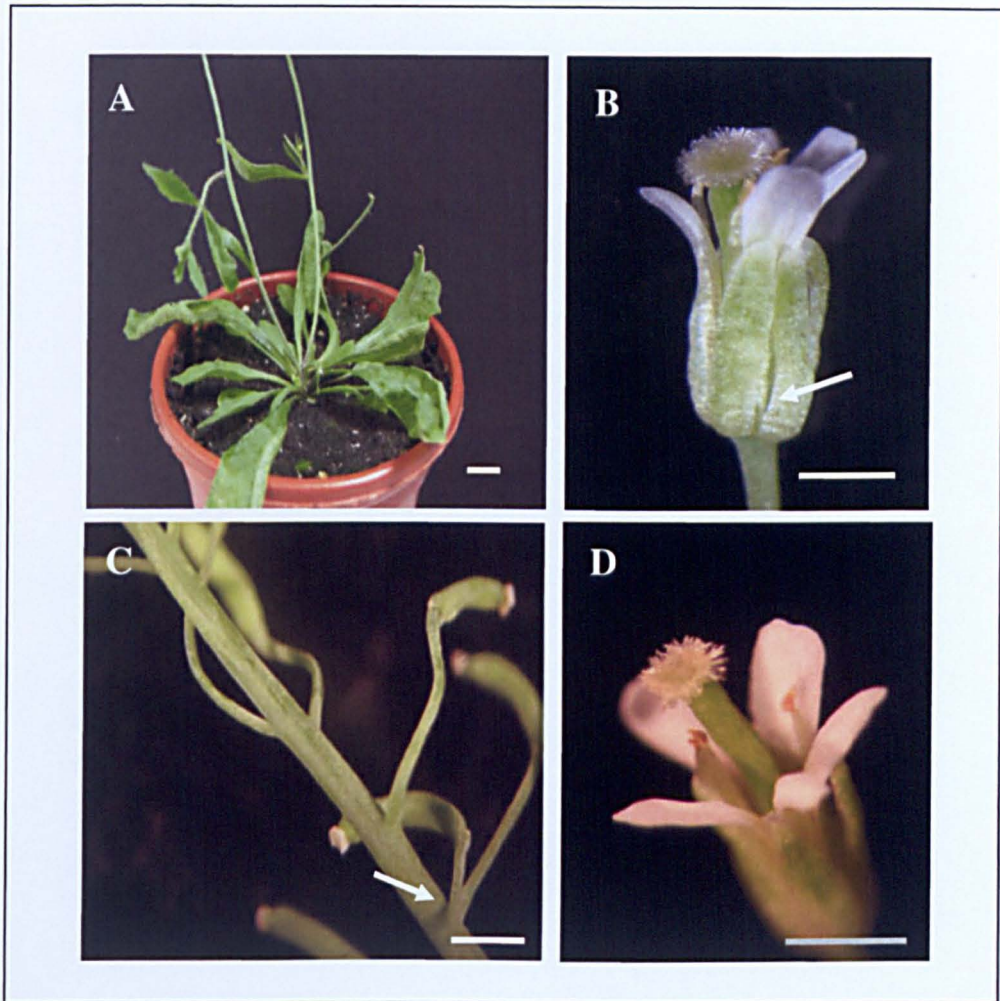


Figure 3.3 Various phenotypic characteristics of *43.1/hws-1*. (A) Elongated adaxialized rosette leaves. (B) Rescuing of the *hws-1* sepal fusion phenotype at the basal margins (arrow). (C) Siliques developing at the same region (arrow) resulting in disrupted phyllotaxis. (D) *43.1/hws-1* demonstrating extra petals (five) whereas a normal wild type *Arabidopsis* flower contains 4 petals. Bar (A) = 1cm, Bars (B-D) = 1mm.

To identify whether the mutant phenotype is due to dominant or recessive mutations and to analyse phenotypic characteristics of *43.1* as a single mutant, segregation analyses were carried out via a cross between *43.1/hws-1* double mutant and Col-0 wild type. The F1 progeny showed a wild type phenotype indicating that the mutation is nuclear and recessive. Ninety-six plants were grown for the F2 population of the cross between *43.1/hws-1* and Col-0 wild type. The F2 progeny displayed a segregation ratio of 3:1, Wild type:*43.1* phenotype. This confirms that *43.1* phenotype is caused by a single, recessive nuclear mutation. The plants that demonstrated a phenotype similar to *43.1*

were analysed by PCR using *HWS* specific primers (SSLPHSfor and SSLPHSrev) to segregate *43.1* away from *hws-1* background and to identify *43.1* single mutants. The analysis demonstrated that 26% of the segregation population was *43.1/colwt* (Figure 3.4). The suppressor line *43.1* in the Col-0 wild type background enables a phenotypic analysis of *43.1* in the absence of *hws-1*.

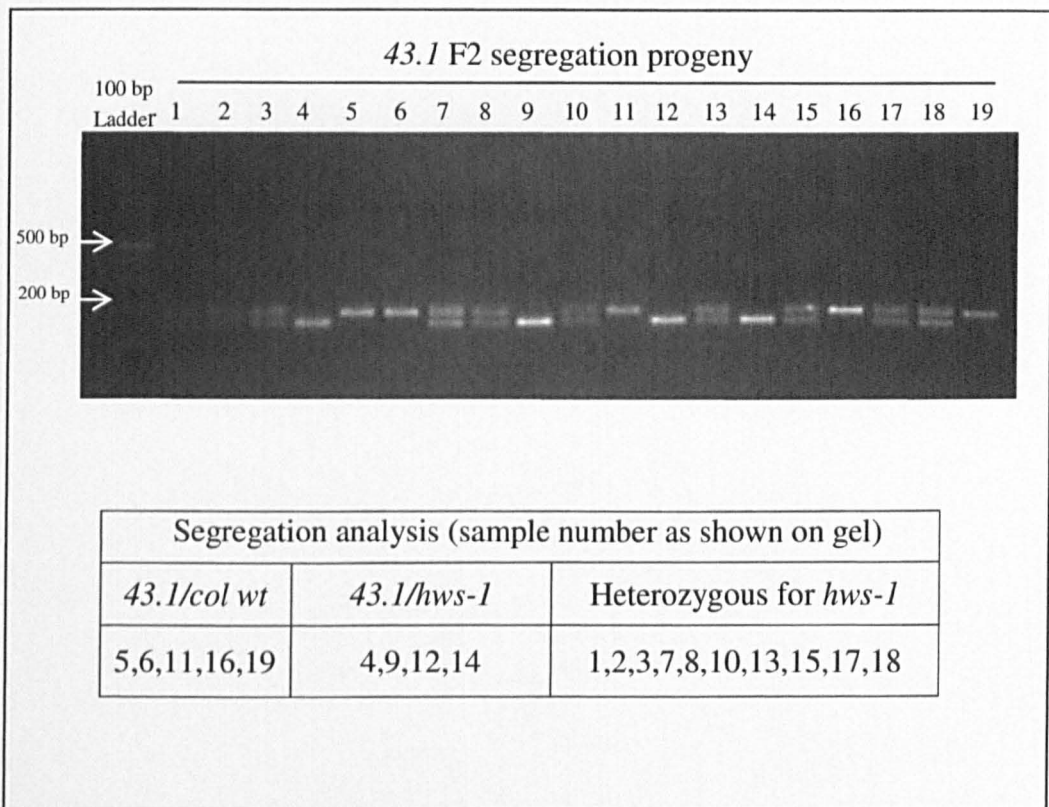


Figure 3.4 F2 progeny PCR amplification of the cross between Col-0 wild type and *43.1/hws-1*. The F2 progeny of the cross between Col-0 wild type and *43.1/hws-1* showed a total of nineteen plants out of ninety-six that displayed similar phenotypic characteristics as *43.1*. PCR amplification of these nineteen plants showed the segregation pattern of *43.1/col wt*, *43.1/hws-1* and heterozygous plants.

Flower comparisons between Col-0 wild type, *hws-1*, *43.1/hws-1* and *43.1/colwt* have shown that *43.1/hws-1* demonstrates an increased number of sepals and petals (Figure 3.5 C, G and M) compared to *43.1/col* (Figure 3.5 D and H) as well as *hws-1* (Figure 3.5 B and F), which is known to exhibit a standard number of floral organs comparable to Col-0 wild type (Figure 3.5 A and E). There is a reduction in petal and sepal sizes on both *43.1/hws-1* and *43.1/colwt* (Figure 3.5 N). The stigma of *43.1/hws-1* is also larger than that of Col-0 wild type and *hws-1*. The petal orientation within the *43.1/hws-1* flower is abnormal and there is an increase in the gap between adjacent petals of both *43.1/hws-1* (Figure 3.5 C) and *43.1/colwt* (Figure 3.5 D). These gaps may be due to the narrowing of petal bases and may also contribute to the slight opening of floral buds prematurely as seen on inflorescence of both *43.1/hws-1* (Figure 3.5 K) and *43.1/colwt* (Figure 3.5 L) compared to the closed buds observed on Col-0 wild type (Figure 3.5 I) and *hws-1* (Figure 3.5 J) inflorescence.

Analyses of petal and sepal numbers on the first twenty five flowers of six *43.1/hws-1* plants has revealed that an increase in these floral organs only occurs within the first ten flowers of each plant (Figure 3.6). The subsequent fifteen flowers of each plant demonstrated floral organ numbers comparable to wild type flowers. Approximately 58% of the flowers that showed an increase in petal and sepal number from the six plants displayed equal number of increase in both petals and sepals within a single flower. The highest number of sepals identified per flower is five sepals and the highest number of petals identified per flower is six petals. This increase in petal and sepal number is not observed consistently in flowers throughout plant development. These floral organ changes only arise in flowers that are established during the early phase of plant development

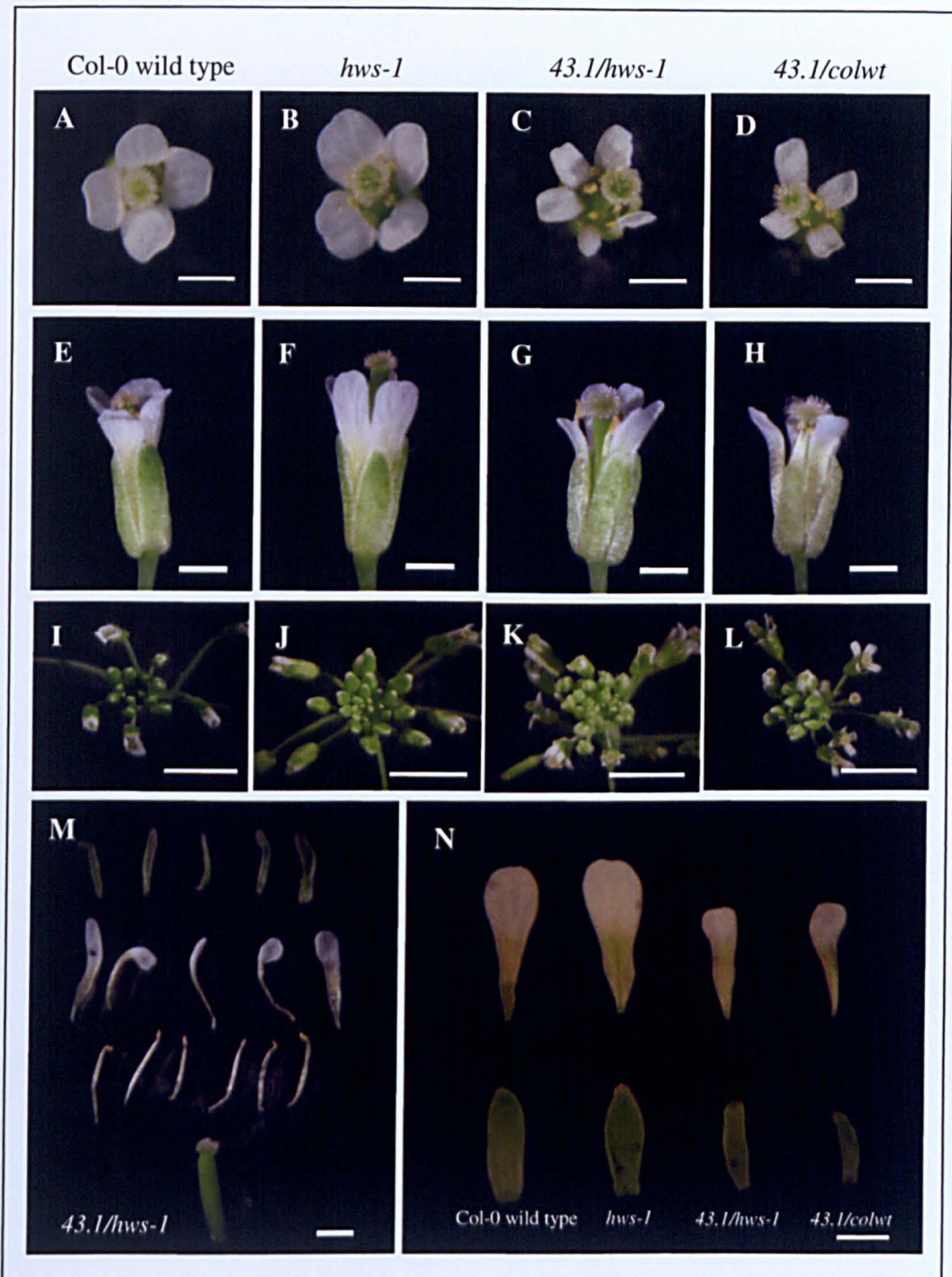


Figure 3.5 Phenotypic comparisons of flower at stage 6.90 (table 1.1, section 1.1) and inflorescence morphology of Col-0 wild type, *hws-1*, *43.1/hws-1* and *43.1/colwt*. (A, E and I) Col-0 wild type, (B, F and J) *hws-1*, (C, G and K) *43.1/hws-1* and (D, H and L) *43.1/colwt*. (M) Dissected flower of *43.1/hws-1* showing presence of extra sepals and petals; 5 sepals, 5 petals, 6 anther filaments and 2 fused carpel; compared to Col-0 wild type which contained 4 sepals, 4 petals, 6 anther filaments and 2 fused carpel. (N) Comparisons between petal and sepal morphology of Col-0 wild type, *hws-1*, *43.1/hws-1* and *43.1/colwt*. Bars = 1mm.

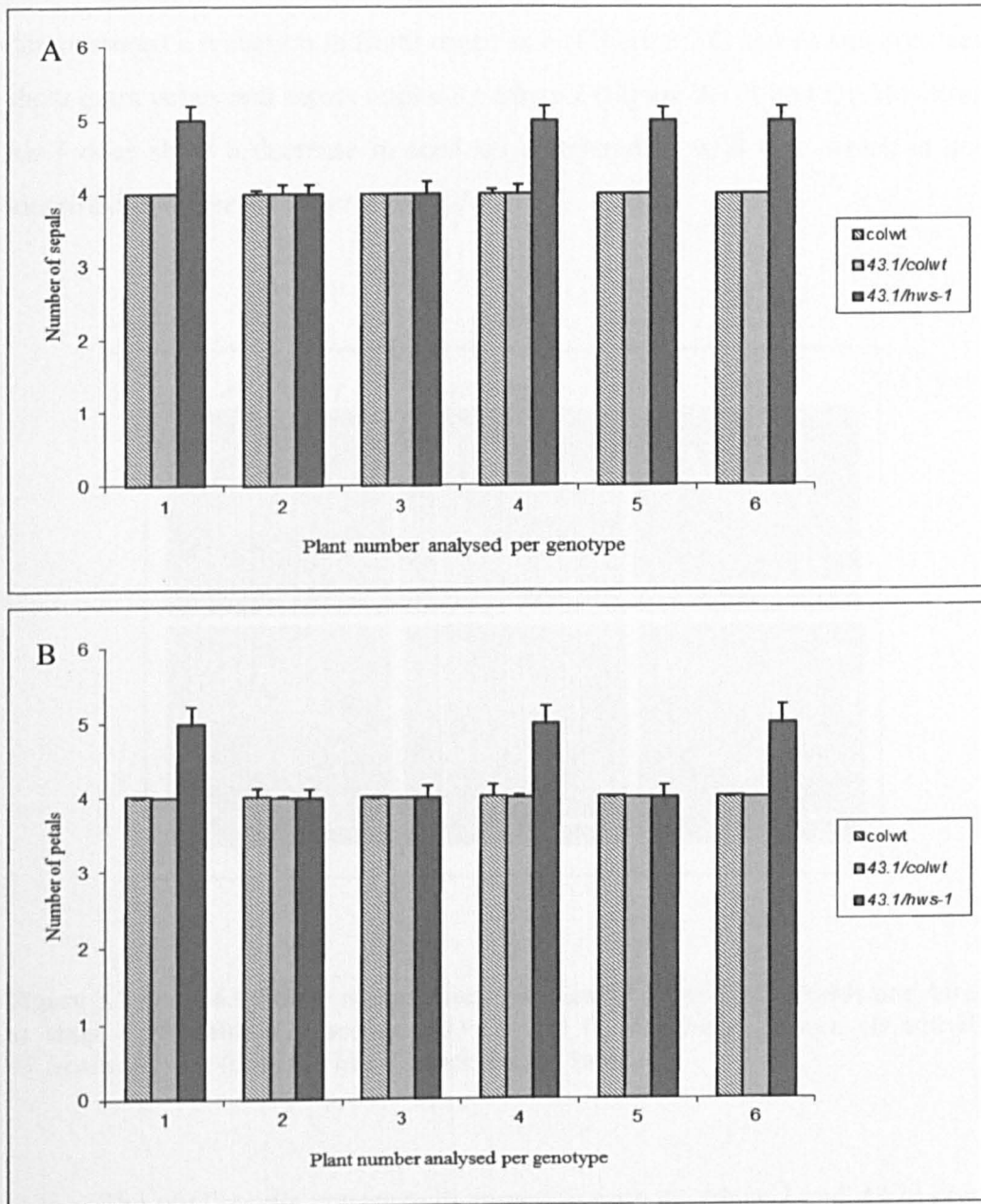


Figure 3.6 The average number of sepals and petals from the first ten flowers at stage 6.90 (table 1.1, stage 1.1) out of twenty five flowers analysed from six Col-0 wild type, *43.1/colwt* and *43.1/hws-1* plants. (A) Number of sepals per plant for each genotype $P=0.239$. (B) Number of petals per plant for each genotype $P=0.174$. Bars indicate standard errors, $n=48$.

Similar to *43.1/colwt* (Figure 3.7 B and E) flower morphology, *hst-1* demonstrates a reduction in floral organ size (Figure 3.7 C and F) and does not show extra petals and sepals unlike *43.1/hws-1* (Figure 3.7 A and D). However *hst-1* does show a decrease in seed set compared to wild type which is not identified in either *43.1/hws-1* or *43.1/colwt*.



Figure 3.7 Stage 6.5 flower comparisons between *43.1/hws-1*, *43.1/colwt* and *hst-1* at stage 6.90 (table 1.1, section 1.1) (A and D) *43.1/hws-1* flower. (B and E) *43.1/colwt* flower. (C and F) *hst-1* flower. Bars = 1mm

The phyllotactic pattern is disrupted in both *43.1/hws-1* and *43.1/colwt* compared to Col-0 wild type and *hws-1* (Figure 3.8 A). This is indicated by the clusters of siliques at certain regions of the stem which are separated by internode size and phyllotaxis similar to Col-0 wild type. Elongation of internodes within clusters of siliques is limited to little or no elongation. Another abnormality seen on *43.1/hws-1* and *43.1/colwt* is the reduction in growth of first few siliques that establishes during plant development. These changes in phyllotaxis are also observed in the *hst-1* mutant (Figure 3.8 B). However the reductions in growth of the first few siliques are not seen in *hst-1*.

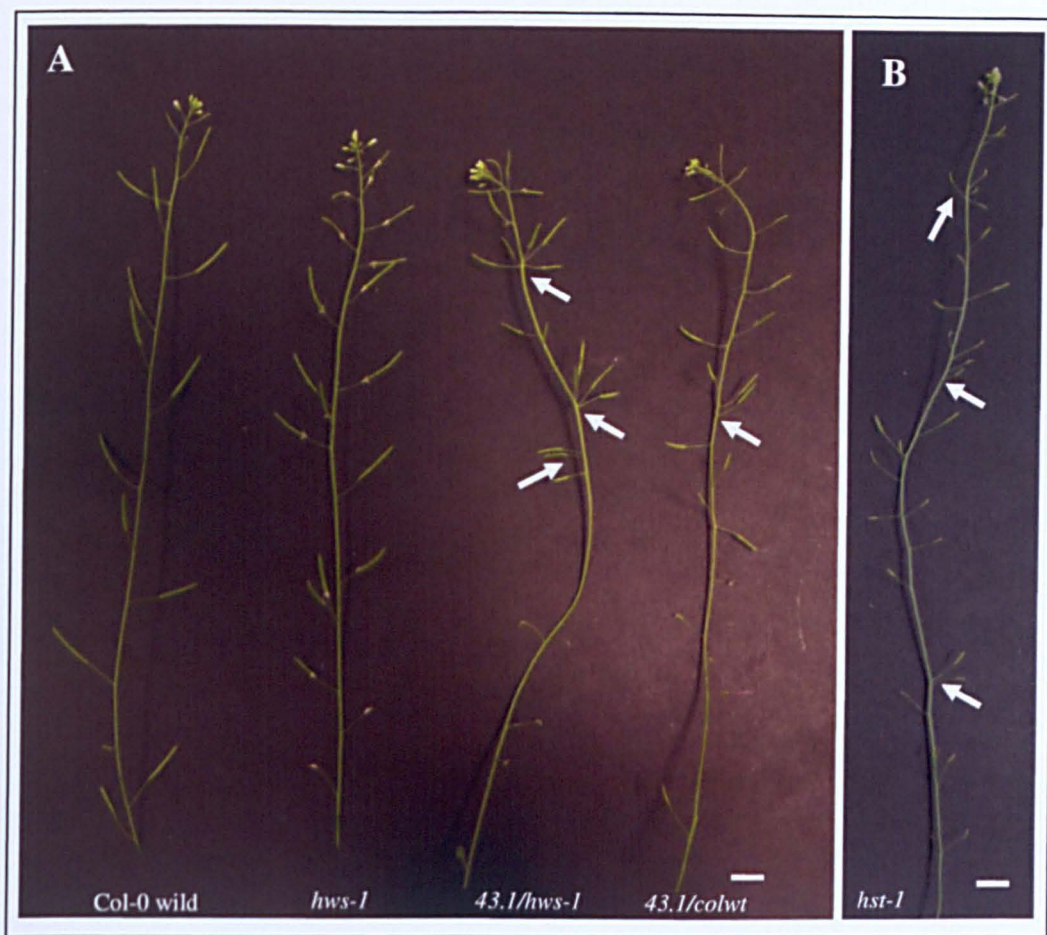


Figure 3.8. Abnormal phyllotaxis in *43.1/hws-1*, *43.1/colwt* and *hst-1* compared to Col-0 wild type and *hws-1*. (A) Comparisons between the phyllotactic pattern of Col-0 wild type, *hws-1*, *43.1/hws-1* and *43.1/colwt* demonstrate a disrupted phyllotaxis in both *43.1/hws-1* and *43.1/colwt* (shown by arrows). (B) Disrupted phyllotaxis (shown by arrows) is also seen in *hst-1*. Bars = 1cm

Comparisons between three week old plants of Col-0 wild type, *hws-1*, *43.1/hws-1* and *43.1/colwt* revealed that *43.1/hws-1* has elongated cauline leaves as well as rosettes with serrated margins (Figure 3.9 A and B). The overall size of *43.1/hws-1* seedlings are similar to that of wild type. The *43.1/hws-1* double mutant seedlings also demonstrated slightly adaxialized cauline leaves. This change in leaf phenotype can be observed from the fourth leaf onwards. The leaf morphology of *43.1/colwt* shows complete adaxialization of cauline leaves from the third leaf onwards. It also displays a reduction in seedling size compared to *43.1/hws-1*. Phenotypical analysis indicate there is a trend in reduction of the number of juvenile and adult leaves

in *43.1/colwt* compared to *43.1/hws-1* as well as Col-0 wild type and *hws-1*. Similar phenotypic characteristics to *43.1/colwt* can be observed on *hst-1* mutants where the cauline leaves are completely adaxialized and reduced number of juvenile and adult leaves compared to wild type (Figure 3.10 A and B). The adaxialization of *43.1/hws-1* leaves seems to be rescued to a certain degree by the *hws-1* mutation. The *hws-1* mutant may also restore the number and size of juvenile and adult leaves in *43.1/hws-1*, which is reduced in *43.1/colwt*.

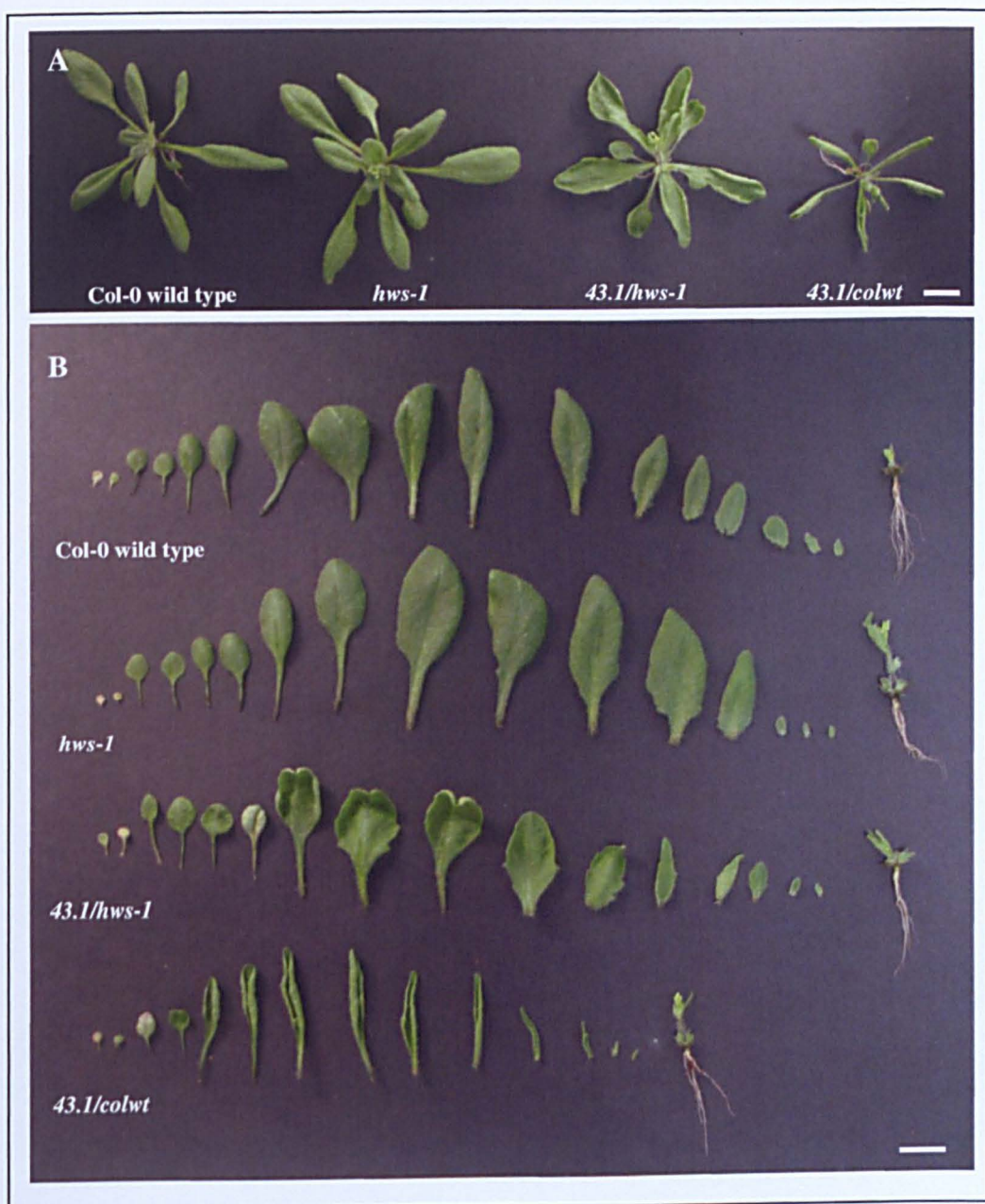


Figure 3.9 Comparison of the phenotypic characteristics between Col-0 wild type, *hws-1*, *43.1/hws-1* and *43.1/colwt*. (A) 22 days old seedlings. (B) Dissected leaves of seedlings from (A). Bars = 1cm

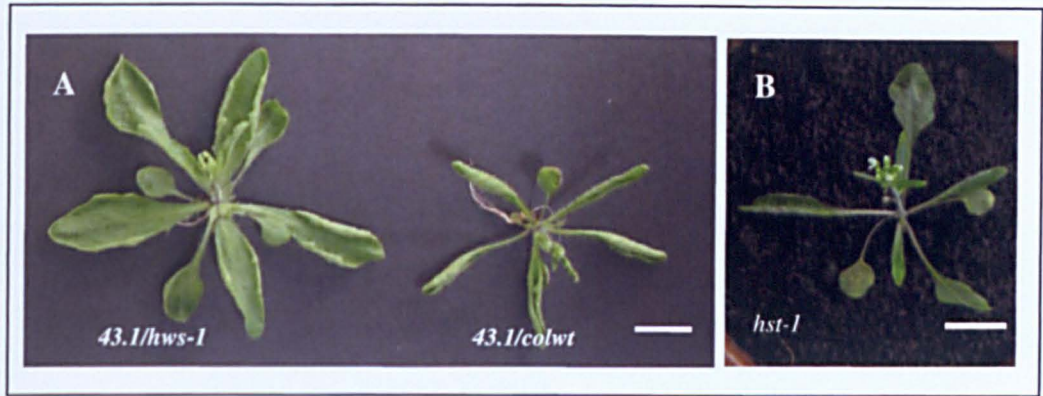


Figure 3.10 Seedling comparison between *43.1/hws-1*, *43.1/colwt* and *hst-1*. (A) 22 day old seedling of *43.1/hws-1* and *43.1/colwt*. (B) 22 day old *hst-1* mutant seedling showing adaxialization of rosette leaves. Bars = 1cm

Root comparisons between Col-0 wild type, *hws-1* and *43.1/hws-1* on six day old and twelve day old seedlings on MS media plates revealed that *43.1/hws-1* roots grow twice as fast as Col-0 wild type and *hws-1* (Figure 3.11 A and B). Comparisons between *43.1/colwt* and *hst-1* mutant alongside Col-0 wild type and *hws-1* showed that both the *43.1/colwt* and *hst-1* mutant roots grow at a similar rate (Figure 3.12). There are differences between *43.1/hws-1* and *hst-1* rate of root growth in that *43.1/hws-1* average root growth is more rapid than that of *hst-1* and *43.1/colwt*. The difference in significance between Col-0 wild type, *hws-1*, *43.1/hws-1*, *43.1/colwt* and *hst-1* was evaluated using the ANOVA test. There is a significant difference between the rate of root growth of the different genotypes on day 9 ($F_{(1,89)} = 16.82$, $P < 0.001$), 11 ($F_{(1,89)} = 13.42$, $P < 0.001$) and 15 ($F_{(1,89)} = 12.36$, $P < 0.001$). The average rate of root growth per day at its steepest for Col-0 wild type, *hws-1*, *43.1/hws-1*, *43.1/colwt* and *hst-1* is 3mm, 4mm, 3mm, 18mm and 3mm respectively.

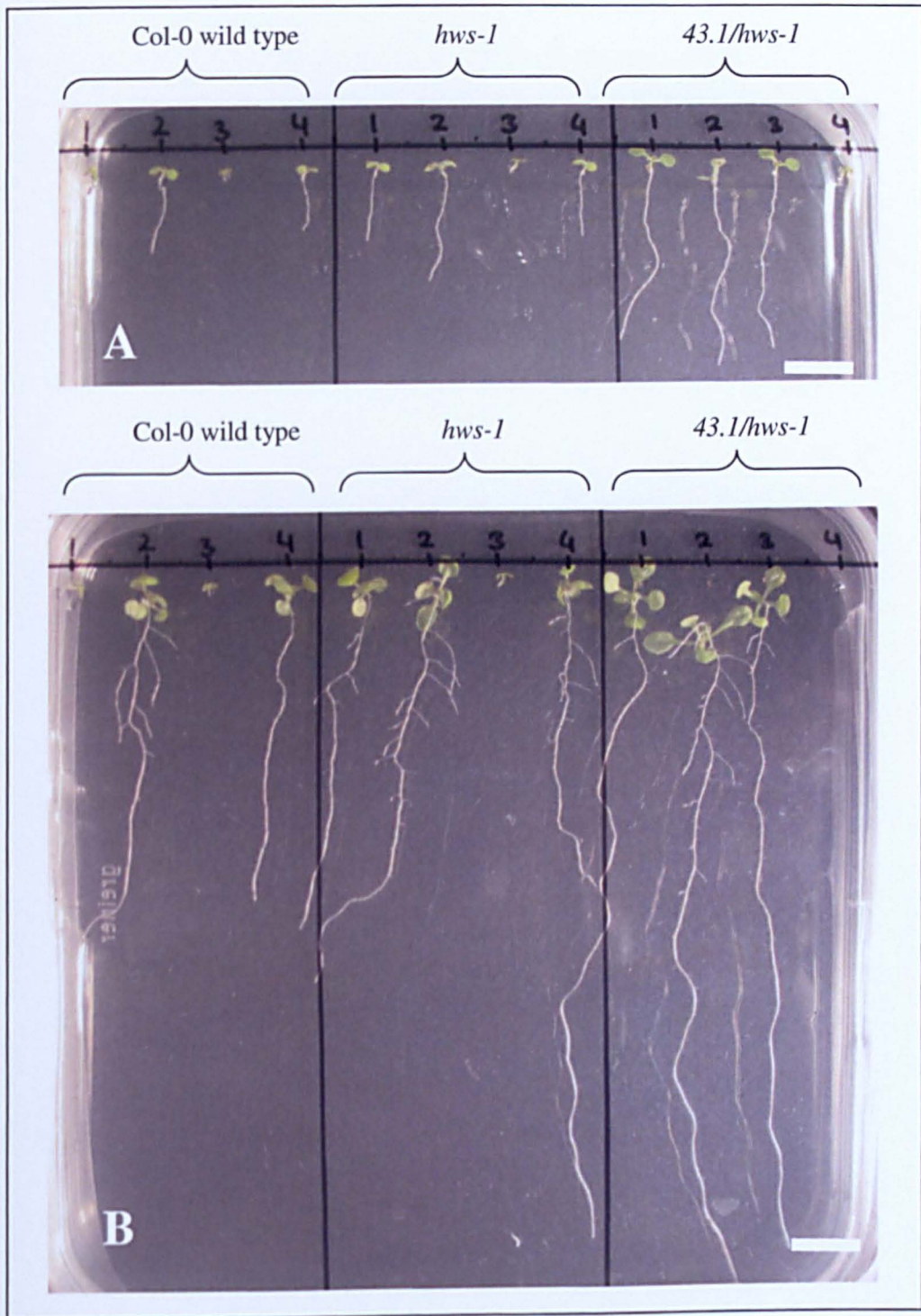


Figure 3.11 Comparison between Col-0 wild type, *hws-1* and *43.1/hws-1* seedling on MS media plates. This figure shows the comparisons of the three genotypes on one plate out of six plates that were studied. All the other five plates showed similar results. (A) Seedlings that are six days old. (B) Seedlings that are twelve days old. Growth of *43.1* roots are twice as fast as Col-0 wild type and *hws-1*. Those seedlings that did not fully develop (Col-0 wild type 3, *hws-1* 3 and *43.1/hws-1* 4) were excluded from this analysis. Bar = 1cm.

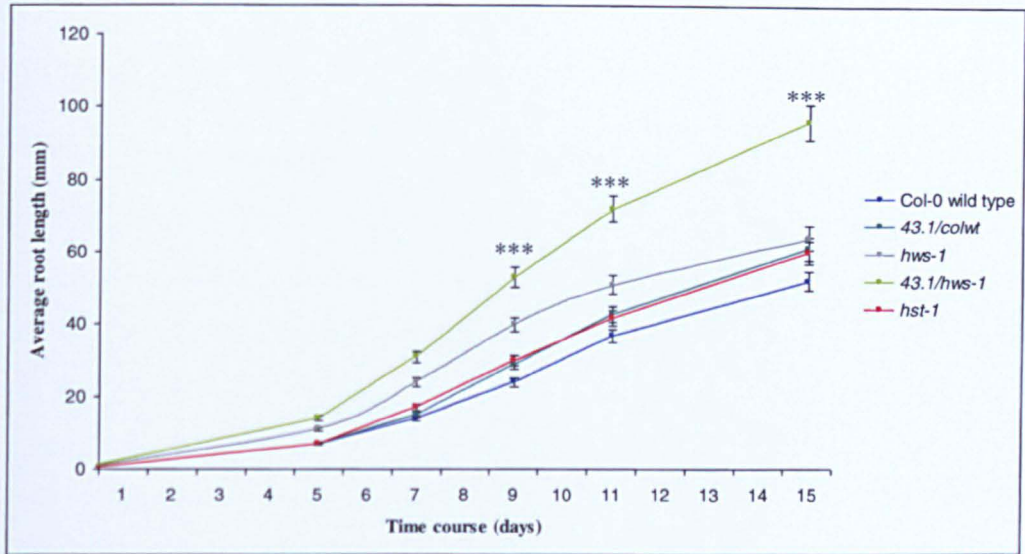


Figure 3.12 Root growth over a time course of 10 days of Col-0 wild type, *hws-1*, *43.1/hws-1* and *hst-1*. The analysis shows that both *43.1/hws-1* and *hst-1* root growth is faster than that of Col-0 wild type and *hws-1*. It appears that the root growth of *43.1/hws-1* is more rapid than that of *hst-1*. Bars indicate standard error and *** indicate significance at $P < 0.001$, $n = 90$.

3.2.3 Identifying the nature of *43.1* mutation

Reciprocal crosses were made between the suppressor line *43.1/hws-1* and some of the other suppressor lines (*45.1/hws-1*, *45.4/hws-1* and *54.6/hws-1*, *23.1/hws-1*), that were identified during the EMS mutant screening process, for allelism tests. The suppressor line *43.1* has undergone allelism tests to determine whether it is allelic to another suppressor line *23.1/hws-1*, identified by Dr. Zinnia Gonzalez-Carranza, that are phenotypically similar to one another. The allelism tests show that *43.1/hws-1* is allelic to *23.1/hws-1* indicating that they are of the same gene. The mapping analysis has shown the suppressor line *23.1* is an allele of the *HST* gene, an orthologue of exportin 5/*MSN5* of *Arabidopsis*, which is located on chromosome three between 1401Kb and 1408Kb (Gonzalez-Carranza Z.H., unpublished data). This led to the hypothesis that *43.1* may also be an allele of the *HST* gene. In order to confirm this, *43.1/hws-1* was crossed with *hst-1* mutant and the F1 population progressively showed they were allelic. To further evaluate this analysis, sequencing analysis of *43.1/hws-1* was carried out using cDNA and genomic DNA of *HST* to determine the nature of the genetic lesion via RT-PCR and PCR analysis. By employing the ClustalW programme, multiple sequence alignment was examined from *43.1* mutants compared to the *HST* DNA sequence (Figure 3.13). Sequencing of the *43.1* revealed that it contains a point mutation from G to A single base transition at exon two 172 bp downstream from the start of the open reading frame (ORF) translation. The point mutation introduces an amber codon instead of a tryptophan residue which would result in a premature termination of the gene and produce a truncated version of the predicted HST protein (Figure 3.14). This indicates that *43.1* is an allele of the *HST* gene.

```

CLUSTAL 2.1 multiple sequence alignment

Hasty      ATGGAAGATAGCAACTCCACGGCAAGTAATGTGGCTCGAGCGATTCTCGCCGTCGTCGAT 60
43.1      -----CGAGCGATTCTCGCCGTCGTCGAT 24
          *****

Hasty      TTCAGCTCCACGTCCGACACTCGCAAATCGGCGGTCCAATTCCTGGATTCTGTAAAATCT 120
43.1      TTCAGCTCCACGTCCGACACTCGCAAATCGGCGGTCCAATTCCTGGATTCTGTAAAATCT 84
          *****

Hasty      GGAGATGTCAGGGTTTTGGCAAAGACTTCTTTTCATCTTGTGAAAAAAGAGTGGTCTTCA 180
43.1      GGAGATGTCAGGGTTTTGGCAAAGACTTCTTTTCATCTTGTGAAAAAAGAGTGGTCTTCA 144
          *****

Hasty      GAAATTCGTCTCCATGCTTTTAAGATGCTACAGCATTGGTTAGACTACGATGGGACGAA 240
43.1      GAAATTCGTCTCCATGCTTTTAAGATGCTACAGCATTGGTTAGACTACGATGGGACGAA 204
          *****

Hasty      TTAAGTCTCCGGAGTGCAGGGGTCTTGTAAATCTTCTATCGAACTAATGTCAGAGGTT 300
43.1      TTAAGTCTCCGGAGTGCAGGGGTCTTGTAAATCTTCTATCGAACTAATGTCAGAGGTT 264
          *****

Hasty      GCTAATGCAAGCGAGAATTGGCCTCTTAAGAGTCAGTCTGCTGCCCTGTAGCTGAGATT 360
43.1      GCTAATGCAAGCGAGAATTGGCCTCTTAAGAGTCAGTCTGCTGCCCTGTAGCTGAGATT 305
          *****

Hasty      GTTAGAAGAGAAGGCCCTGATCGTTGGCAAGAGATATTTACTTTATTAACCTCATTGTCT 420
43.1      GTTAGAAGAGAAGGCCCTGATCGTTGGCAAGAGATATTTACTTTATTAACCTCATTGTCT 365
          *****

Hasty      GCTCAGGGCCCTTACAAGCTGAATTGGTATTGATGACTCTTAGATGGCTTCCTGAAGAT 480
43.1      GCTCAGGGCCCTTACAAGCTGAATTGGTATTGATGACTCTTAGATGGCTTCCTGAAGAT 425
          *****

Hasty      ATTACAATTTACAATGACGACTTGGAAAGGTGACAGGCGTAGGCTATTGTTGCGGGGACTT 540
43.1      ATTACAATTTACAATGACGACTTGGAAAGGTGACAGGCGTAGGCTATTGTTGCGGGGACTT 485
          *****

Hasty      ACTCAATCGTTGCCTGAGATTTTGCCTTTATTGTATAATCTTCTTGAGAGACACTTTGGA 600
43.1      ACTCAATCGTTGCCTGAGATTTTGCCTTTATTGTATAATCTTCTTGAGAGACACTTTGGA 545
          *****

Hasty      GCTGCAATGAGTGAAGCTGGTATGCAGCACTTTGACTTGGCAAACAGCATGCAGATGTA 660
43.1      GCTGCAATGAGTGAAGCTGGTATGCAGCACTTTGACTTGGCAAACAGCATGCAGATGTA 605
          *****

Hasty      GTTATAGCTTGCTTGAATGCCATCGTTGCATACACTGAGTGGGCTCCTGTTCCAGATCTT 720
43.1      GTTATAGCTTGCTTGAATGCCATCGTTGCATACACTGAGTGGGCTCCTGTTCCAGATCTT 635
          *****

Hasty      GCCAGATATGGAATCTTAGTGGGTGCAGCTTCTTACTTTCTTCTTCTGACTCCGTCTT 780
43.1      GCCAGATATGGAATCTTAGTGGGTGCAGCTTCTTACTTTCTTCTTCTGACTCCGTCTT 695
          *****

```

Figure 3.13 Part of the multiple sequence alignment of 43.1 and *HST* using ClustalW (EMBL-EBI) program. This sequence shows the premature termination of 43.1 mutant allele by an amber stop codon due to a point mutation of a single base transition from G to A highlighted in grey 172 bp from the *HST* ORF start codon. The start codon of the *HST* ORF, ATG is indicated in grey.

```

atggaagatagcaactccacggcaagtaatgtggctcgagcgattctcgccgctcgat
M E D S N S T A S N V A R A I L A V V D
ttcagctccacgtccgacactcgaaatcgggcgtccaattcctggattctgtaaaatct
F S S T S D T R K S A V Q F L D S V K S
ggagatgtcagggttttggcaagacttcttttcatcttgtaaaaaagagtagtcttca
G D V R V L A K T S F H L V K K E tagtcttca
gaaattcgtctccatgcttttaagatgctacagcatttggtagactacgatgggacgaa
E I R L H A F K M L Q H L V R L R W D E
ttaagtcctccggagtgcaggggtcttgtaaatctttctatcgaactaatgtcagaggt
L S P P E C R G L V N L S I E L M S E V
gctaatgcaagcgagaattggcctcttaagagtcagtctgctgcccttgtagctgagatt
A N A S E N W P L K S Q S A A L V A E I
gttagaagagaaggccctgatcgttggcaagagatatttactttattaacttcattgtct
V R R E G P D R W Q E I F T L L T S L S
gctcagggccccttacaagctgaattggtattgatgactcttagatggcttctctgaagat
A Q G P L Q A E L V L M T L R W L P E D
attacaatttacaatgacgacttggaaaggtgacagggcgtaggctattgttgcgggactt
I T I Y N D D L E G D R R R L L R G L
actcaatcgttgcctgagattttgcctttattgtataatcttcttgagagacactttgga
T Q S L P E I L P L L Y N L L E R H F G
gctgcaatgagtgaaagctggatgcagcactttgacttggcaaacagcatgcagatgta
A A M S E A G M Q H F D L A K Q H A D V
gttatagcttgcttgaatgccatcgttgcatacactgagtgggctcctgttccagatctt
V I A C L N A I V A Y T E W A P V P D L
gccagatatggaattccttagtgggtgcagcttcttactttcttcttctgacttccgtctt
A R Y G I L S G C S F L L S S S D F R L
catgcttgtgaggttttcaaactcgtctgctcaagaaaaagaccagtgatgcttctact
H A C E V F K L V C S R K R P S D A S T
gcagagttcgattctgcaattagcaatttgtttcagattctgacgaatgcctccagagaa
A E F D S A I S N L F Q I L T N A S R E
ttcttatgtagatcctcctcaagttctagcgttatagatgacaatgattatgattttgct
F L C R S S S S S V I D D N D Y D F A
gtatgcatgtgtgagagtatggcctctttaggctcaactaacttgcaaagcatctcttct
V C M C E S M A S L G S T N L Q S I S S
gatgggtggtgttatggctgtttatcttcagcagatgcttggctttttccaacactcaag
D G G V M A V Y L Q Q M L G F F Q H F K
ttgggccttcaacttcgagggcacttctcttttggctgtcactgatgggatttactcca
L G L H F E A L L F W L S L M R D L L P
aaacccaaggctgcgacttccaagtggtggggatcatcaactggcggatgatgatagt
K P K A A T Y P S G G G S S T G G D D S
tcaagccaggttgatagtgaaaagaaaaagactttaagtcttattaatgatgacatctcg
S S Q V D S E K K K T L S L I N D D I S
agcgctatactggacgtatctttccagcggatgctcaagaaagaaaaagttcctactgga
S A I L D V S F Q R M L K K E K V P T G
attgctctttcgcttgggcccctagaactctggagtgatgaatttgaaggggaagggagac
I A L S L G P L E L W S D E F E G K G D
tttggcccgtaccgatcaaagcttctagaattgatcaagcttactgcttctcacaagcct
F G P Y R S K L L E L I K L T A S H K P

```

Figure continues on page 78

Figure 3.14 Protein translation of HST coding region showing 43.1 stop codon. This sequence shows the premature termination of 43.1 mutant by an amber stop codon (tag) highlighted in grey. Courtesy of ExPASy Translate Tool, SIB Bioinformatics Resource Portal.


```

gaggaaaaactgttaagagatctaactcgggagattgcgactctcttttcaacaatggct
E E K L L R D L T R E I A T L F S T M A
tctcctggactaaacacaggagttccagttttggaacattcaggacatgttggtcgtg
S P G L N T G V P V L E H S G H V G R V
gacatgtccactctcaccgatttgcacggttcagatccaactctatggtgggtttcctc
D M S T L T D L H A F R S N S M V G F L
ttgaatcacaaaagcgtagctctaccagcactgcagatctgtttagaaaacttttacctgg
L N H K S V A L P A L Q I C L E T F T W
acagatggagaagcaccaccaaagtctgttacttttgggtgttggttcttcttagct
T D G E A T T K V C Y F C G V V V L L A
aaactaacaataacgtggagctccgagaatttgtttcaaaagatatgttctcggcagtc
K L T N N V E L R E F V S K D M F S A V
attcgtggcttgggcatggagtccaatgccattaacagccctgatttagttaatatatgc
I R G L G M E S N A I N S P D L V N I C
cgtgaaatatttatctatctctctgacagagaccagctcctcggcagggttttgccttcg
R E I F I Y L S D R D P A P R Q V L L S
ctcccgtgtctcactcccaacgacttgcacgcttttgaagaagctacagccaaaactagc
L P C L T P N D L H A F E E A T A K T S
agcccccagaacaaaagcagcttatgaggagcttgggtgttggctaggtactgggaacaac
S P K E Q K Q L M R S L L L L G T G N N
ttaaagcacttgctgctcaaaaaagtcagaatgttatcaccaatgtcacagcaagaacg
L K A L A A Q K S Q N V I T N V T A R T
cggctaccgcgaagcgtccagaaacaattggagcgggtgttttggggatgaagagttc
R L P A S A P E T I G A G V L W D E E F
gtacaatga
V Q -

```

Figure 3.14 (continuation) Protein translation of *HST* coding region. Courtesy of ExPASy Translate Tool, SIB Bioinformatics Resource Portal.

3.3 Chapter discussion

3.3.1 Flower morphology of *43.1*

The increase in petal and sepal number that is observed on *43.1/hws-1* mutant is absent in *43.1/colwt* and *hst-1* mutants. This extra petal and sepal phenotype arises within the first ten flowers of the *43.1/hws-1* mutant. These observations show that loss of *HWS* gene function on *43.1* leads to an increase in the number of both petals and sepals. The extra petal phenotype of *43.1/hws-1* resembles the petal morphology of *early extra petals1 (eep1)* mutant, which is a loss-of-function *MIR164c* allele (Baker *et al.*, 2005). Previous analysis of the *eep1/miR164b* double mutant demonstrated that petal number is controlled by *miR164c* in a non-redundant way by adjusting *CUC1* and *CUC2* transcript accumulation. This showed that miRNA members that are closely associated in targeting the same genes have various functions during development. *MIR164c* negatively regulates *CUC1* and *CUC2* to avert extra petal formation in incipient flowers of *Arabidopsis* (Baker *et al.*, 2005). Therefore the extra petal phenotype of *43.1/hws-1* is similar to the loss-of-function of *MIR164c*, which results in un-fused sepals whereas overexpression of *MIR164c* leads to sepal boundary fusion similar to *cuc1cuc2* double mutants and *hws-1* mutant. Aida *et al.* (1997) demonstrated that besides sepal boundary fusion, *cuc1cuc2* double mutants also had reduced number of petals and stamens. Although no missing petals and stamens were observed in *hws-1* mutants, the extra petal phenotype of early flowers in *43.1/hws-1* double mutant may result from a depletion of *MIR164* and an increase in *CUC1* and *CUC2* accumulation. The *43.1/hws-1* double mutant also displayed a slightly open incipient buds compared to Col-0 wild type and *hws-1*. This phenotype may be a result of an increase in width of boundary domain between adjacent sepals and petals as shown in *hst-1* mutant by Laufs *et al.* (2004). Loss of *HWS* gene function in *43.1/hws-1* may restrict *HST* expression to promote normal sepal separation leading to depletion in *MIR164* accumulation and an increase in expression of *CUC1* and *CUC2* boundary specific genes.

The phyllotactic pattern in the *43.1* mutant developing stem is abnormal compared to Col-0 wild type and *hws-1* pattern of mature inflorescence. The *43.1/hws-1* double mutant and *43.1/colwt* mutant also displayed semi-sterile incipient siliques. This aberrant phenotype is similar to that observed in *hst-1* mutants. Close examination of the mature inflorescence pattern on the stem between *43.1/hws-1* double mutant and *43.1* mutant indicates a slight difference in the phyllotactic pattern. Flowers of *43.1/hws-1* form clusters which are spaced with longer internodes than *43.1/colwt*. This clustering was observed to a greater extent in *miR164*-resistant *CUC2* (*CUC2g-m4*) gene expressing plants (Peaucelle *et al.*, 2007). It was demonstrated that aberrant phyllotaxy is established during stem development and growth and not at the meristem similar to that observed in *43.1* and *hst-1* (Peaucelle *et al.*, 2007). This supports further evidence that a depletion of *MIR164* may lead to the abnormal morphological characteristics seen on *43.1*.

3.3.2 Leaf phenotype of *43.1*

The supposed interaction between ubiquitination and the microRNA pathway is more apparent in this *hws-1* suppressor line since it is an *HST* allele, a gene involved in the microRNA pathway. One of the aspects involved in the phenotype of *43.1* is the loss of tissue polarity in the leaf blade mesophyll. The adaxialized phenotype of *43.1/colwt* starts from the third rosette leaf whereas in *43.1/hws-1* adaxialization starts from the fifth rosette leaf and to a lesser extent. This shows that loss of *HWS* function rescues adaxialization of *43.1* leaves and to a certain extent restores leaf polarity. This may indicate that *HWS* is involved in SAM-derived signalling as the interaction between leaf primordia and the SAM is important for adaxial-abaxial leaf patterning. This is also supported by the analysis that *HST* is necessary for SAM organization and growth (Bollman *et al.*, 2003). Bollman *et al.* (2003) demonstrated that a larger and rounder SAM, as well as reduced leaf 1 and 2 primordia, was observed in three day old *hst-1* seedlings compared to seedlings of wild type.

Loss of *HWS* function also restores the rosette leaf number as demonstrated by *43.1/hws-1* double mutant compared to the reduction in leaf number of *43.1/colwt* similar to *hst-1* mutant. Overexpression of *HWS* also results in decreased leaf size and number (Gonzalez-Carranza *et al.*, 2007) showing further evidence that loss of *HWS* gene function leads to repression of *HST*. There is a slight serration in *43.1* leaf margins compared to Col-0 wild type and *hws-1* mutant leaf margins. Similar serration of leaf margins are also observed on leaves of *miR164a* mutant seedlings. By contrast, overexpression of *miR164* developed smooth leaf margins. Furthermore enhanced expression of *miR164*-resistant *CUC2* results in serration of leaf margins and the degree of serration is determined by the balance between *CUC2* and *MIR164A* co-expression (Nikovics *et al.*, 2006). Leaf serration is also exhibited by mutants of *SE*, which interacts with *HYL1* to regulate miRNAs (Yang *et al.*, 2006). Early leaf serration and accelerated production of abaxial and adaxial trichomes starts from the third leaf on *hst-1* whereas in wild type plants the onset of leaf serration and increase in abaxial and adaxial trichome production starts from leaf five or six (Bollman *et al.*, 2003). This observation of early leaf serration from the third leaf can also be seen on *43.1/hws-1* mutant. The serration observed on leaf margins of *43.1* may be due to a reduction in *MIR164* accumulation as mentioned before.

There has been close correlation between the phenotype of *43.1/hws-1* and that of mutants with depleted *miR164* accumulation and upregulation of *CUC* genes. Similar morphological defects to *43.1* such as reduction in leaf number, serration of leaves, abnormal phyllotaxy and adaxialized leaves are also seen in *se* mutants, which are involved in miRNA biogenesis (Lobbes *et al.*, 2006). These observations show the importance of *HWS* gene expression in miRNA biogenesis.

3.3.3 Root growth of *43.1*

Root growth analyses of *43.1/hws-1* have shown that the rate of root elongation is much faster than that of Col-0 wild type and *hws-1*. Observations

on *hst-1* root growth is contrary to earlier findings by Bollman *et al.* (2003) which demonstrates a reduction in primary root growth in comparison to wild type root elongation. It has been shown that these reductions in root length of *hst-1* are not due to alterations in root cell identity as both cellular anatomy of wild type and *hst-1* were similar. It has also been demonstrated that sensitivity of *hst-1* to hormones such as abscisic acid, cytokinin and auxin, had no effect on root elongation (Bollman *et al.*, 2003). This may indicate that the results obtained on root growth of *hst-1* in this project and that of Bollman *et al.* (2003) may be due to differences in growth conditions. Bollman *et al.* (2003) used ½ x MS salts, 0.5 g/l MES and 5% sucrose for the preparation of MS media whereas this project consisted of 1 x MS salts and lacked MES and sucrose in the MS media preparation. Although the differences in root growth of Col-0 wild type and *hst-1* seen in this analysis are not significant there is a slight increase in root growth of *hst-1* compared to Col-0 wild type. This is further confirmed by the root growth pattern of *43.1/colwt*, which is comparable to the *hst-1* root growth. It is unclear as to what exactly is causing alterations in *hst-1* root elongation; however the growth conditions may be a factor contributing to these changes. The differences in results obtained from the root growth of *43.1* may be also due to other genes affected by EMS mutagenesis.

3.3.4 Isolation and mapping of the *43.1* locus

Sequencing of *43.1* showed that the mutation is caused by a single base pair change from G to A at exon two 172 bp from the *HST* coding region. This leads to a premature termination of the gene and produce a truncated version of the predicted HST protein. Other alleles of *HST* that have been identified previously are shown on Figure 3.15, alongside *43.1*. The nature of the mutation of *hst-1* allele causes a stop codon 31 bp following the intron-exon junction of intron 12, resulting in a splicing variant. It was identified by a Diepoxybutane-induced mutation on Columbia ecotype. The fast neutron induced *hst-3* has a 3 bp deletion on exon one and *hst-6* allele, caused by an EMS mutagenesis on Columbia, is the result of a G to A single base transition

resulting in a stop codon at position 107 of the predicted protein. It is also indicated that *hst-6* may be a null allele since the gene fragment occupying *hst-6* is only about 9% of the full-length protein. The *hst-7* allele, induced by X-ray on Columbia, is the result of a 7 bp deletion on exon 13 which initiates a stop codon in the ORF 12 bp downstream of the mutation. *hst-8*, resulting from a T-DNA insertion in Wasilewskija, is due to a 24 bp deletion in exon 9 and *hst-9*, an allele resulting from a fast neutron mutagenesis in Columbia, has a 300 kb inversion with breakpoints on intron 15 (Bollman *et al.*, 2003; Telfer and Poethig, 1998). The phenotypes of *hst-1*, *hst-2*, *hst-4*, *hst-6*, *hst-7*, *hst-8* and *hst-9* are comparable to one another in severity whereas *hst-3* is indicated to be less severe. *hst-1* mutants produce one to two juvenile leaves and variable number of adult leaves in the Columbia ecotype. However *hst-1* shoot morphology is more severely affected in the Landsberg ecotype, which generally produces a decreased number of juvenile and adult leaves than the Columbia ecotype. This change in phenotype indicates that *hst* alleles influence traits that also vary between ecotypes (Telfer and Poethig, 1998).

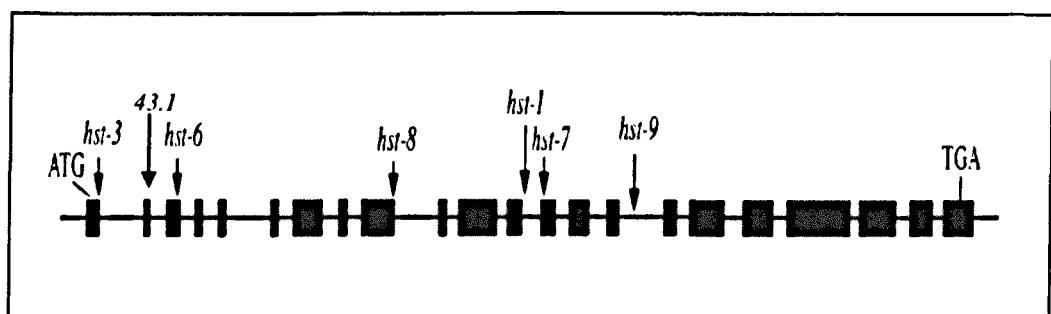


Figure 3.15 Genomic structure of *HST* showing the locations of various *hst* alleles. The exons are represented by the black boxes. The location of *43.1* is indicated in exon two. Illustration modified from Bollman *et al.* (2003).

3.3.5 Interaction between *HWS* and *HST*

The loss-of-*HST* gene function in *hws-1* results in rescuing of the *hws-1* sepal fusion phenotype and the loss-of-*HWS* function on *43.1*, which is a mutant allele of *hst*, results in rescuing of the decrease in seedling size, leaf number, adaxial curling of leaves. These results reveal that an interaction

between *HWS* and *HST* gene expression is taking place and indicate that *HWS* may function in sepal primordia to repress *HST* gene expression for normal development of sepal separation. The increase in petal number of *43.1/hws-1* double mutant suggests that there is a correlation between *HWS* gene function and miRNA biogenesis. The increase in petal number of incipient flowers may contribute to a depletion of *MIR164* and an increase in *CUC1* and *CUC2* accumulation. *HWS* may be also involved in SAM-derived signalling as the interaction between leaf primordia and the SAM is important for adaxial-abaxial leaf patterning. *HWS* is expressed throughout plant development in numerous plant tissues (Gonzalez-Carranza *et al.*, 2007) and may be involved in several signalling pathways other than ubiquitination and miRNA biogenesis.

CHAPTER 4

Characterisation of 80.5

4.1 Introduction

The EMS mutagenized *hws-1* suppressor line, 80.5, suppresses the *hws-1* sepal fusion phenotype as well as displaying other phenotypic abnormalities such as lobe-shaped leaves and asymmetry of the leaf lamina as presented in section 4.2. Several genes have been identified whose mutations lead to similar phenotypic changes.

4.1.1 The *LATERAL ORGAN BOUNDARIES DOMAIN (LBD)* gene family

The *Arabidopsis LATERAL ORGAN BOUNDARIES (LOB)* gene is expressed at the boundaries of all lateral organs during vegetative and reproductive development of plants as well as in the lateral root base (Shuai *et al.*, 2002). *LOB* encodes a protein that consists of a conserved plant-specific, N-terminal DNA-binding domain (LOB domain). The LOB domain is present in 43 *Arabidopsis* proteins known as *LOB DOMAIN (LBD)* genes, which are also termed *AS2-like (ASL)*. Loss of function of *LOB* does not provide an obvious phenotypic change (Husbands *et al.*, 2007). Currently there are two reasonably well characterised *LBD* genes, *LOB* being one of them and the other is *ASYMMETRIC LEAVES2 (AS2)*.

AS2 is involved in the repression of expression of class 1 *KNOTTED*-like homeobox (*KNOX*) genes and the establishment of leaf adaxial-abaxial polarity (Byrne *et al.*, 2000; Semiarti *et al.*, 2001). *AS2* is known to be involved in the development of a symmetric lamina and the formation of the venation system in leaves which includes the generation of a prominent mid vein. *AS2* represses

the abaxial-determinant genes, *ETTIN/ARF3*, *KANADI2 (KAN2)* and *YABBY5*. Characterisation of *AS2* has revealed that it encodes a cysteine repeat containing protein and a leucine-zipper-like primary sequence (Semiarti *et al.*, 2001; Kojima *et al.*, 2011). Analysis of *AS2* transcript levels reveal that it is expressed throughout plant development and that expression is at a high level in the shoot apices (Figure 4.1 A and B) (Iwakawa *et al.*, 2002). In the leaf, *AS2* expression occurs in the adaxial surface of the leaf primordia (Iwakawa *et al.*, 2007). *AS2* expression is down-regulated in the abaxial leaf domain by *KAN* protein via interactions with a *cis*-element in the *AS2* promoter region. Conversely overexpression of *AS2* results in a reduced level of *KAN* expression, indicating that *KAN* and *AS2* negatively regulate each other (Wu *et al.*, 2008).

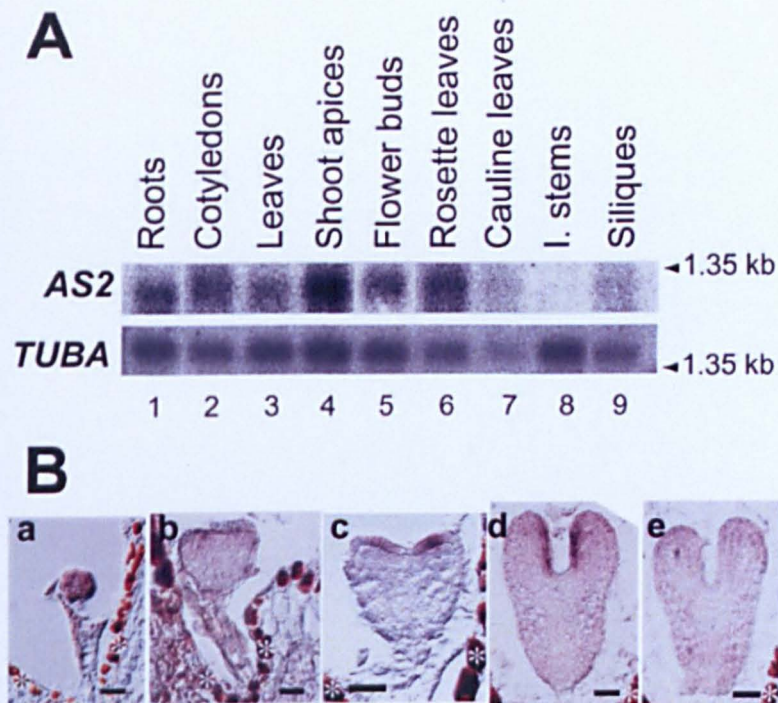


Figure 4.1 Expression of *AS2* various tissues of *Arabidopsis*. (A) Northern blot analysis of *AS2* expression of different tissues showing highest accumulation of expression in shoot apices followed by expression in rosette leaves. Enhanced amount of expression is also seen on flower buds. α -tubulin (*TUBA*) was used as a control and the marker RNA molecule size is indicated on the right as 1.35 Kb. (B) In situ hybridization analyses showing the expression of *AS2* in different stages; (a) Globular, (b) triangular, (c) heart-shaped, (d) torpedo. (e) shows sense control of (d). From Iwakawa *et al.*, 2002.

4.1.2 Adaxial-abaxial polarity

The establishment of adaxial-abaxial polarity is crucial for the development of lateral organs such as leaves and floral organs in plants (Husbands *et al.*, 2009). The mechanism of adaxial-abaxial patterning leads to dramatic alterations in the morphology of leaves and may act as an inducer for the creation of diverse leaf forms (Figure 4.2 A) (Gleissberg *et al.*, 2005). The MYB transcription factor encoding genes in *Arabidopsis*, *Antirrhinum majus* and maize, *ASI*, *PHANTASTICA (PHAN)* and *ROUGH SHEATH2 (RS2)* respectively, are involved in lateral organ abaxial-adaxial determination and in the early determination of proximal-distal axis. The relationship between lamina outgrowth and adaxial-abaxial leaf polarity was determined by the *phan* mutant, which demonstrated abaxial tissue patches on the adaxial side on weak *phan* mutants and fully abaxialized phenotype on strong *phan* mutants failing to laterally expand leading to radialized leaves (Figure 4.2 B). These studies show that *PHAN* is involved in promoting leaf adaxial cell fate (Waites and Hudson, 1995; Waites *et al.*, 1998). In *Arabidopsis*, adaxial cell fate is established by *HOMEODOMAIN-LEUCINE ZIPPER III (HD-ZIPIII)* genes, *PHB*, *PHV* and *REV*, thus regulating lateral organ polarity (Emery *et al.*, 2003; McConnell *et al.*, 2001). MicroRNA165 and/or microRNA166 negatively regulate the function of *HD-ZIPIII* genes by post-transcriptional gene regulation to act as an abaxial determinant (Emery *et al.*, 2003; Mallory *et al.*, 2004a). This microRNA binding process is disturbed by *PHB* and *PHV* gain-of-function mutations resulting in adaxialized leaves (McConnell *et al.*, 2001)

By contrast to adaxial cell fate establishment, members of the *YABBY* and *KANADI (KAN)* gene families are involved in the determination of abaxial cell fate (Emery *et al.*, 2003; Kerstetter *et al.*, 2001; Siegfried *et al.*, 1999). The *Arabidopsis* genome contains six *YABBY* genes where four (*FILAMENTOUS FLOWER (FIL)*, *YABBY2 (YAB2)*, *YAB3* and *YAB5*) are expressed in vegetative leaf primordia and two, *CRAB CLAW (CRC)* and *INNER NO OUTER (INO)*, are expressed in floral organs (Bowman and Smyth, 1999; Siegfried *et al.*, 1999; Villanueva *et al.*, 1999). *YABBY* genes are also involved in lamina

growth since gradual loss of *YABBY* function leads to conspicuous loss of lamina development (Siegfried *et al.*, 1999). Gene expression analysis carried out by Sarojam *et al.* (2010) using *Arabidopsis YABBY* quadruple mutants revealed initial establishment of adaxial-abaxial polarity but this polarity is not maintained. This shows that *YABBY* genes are required for polarity maintenance as well as for lamina outgrowth, but are not necessary for initial establishment of adaxial-abaxial polarity. *YABBY* gene function endorses lamina outgrowth by incorporating polarity signals (Eshed *et al.*, 2004). These genes are also involved in the repression of SAM genetic programs in developing leaves (Kumaran *et al.*, 2002; Sarojam *et al.*, 2010)

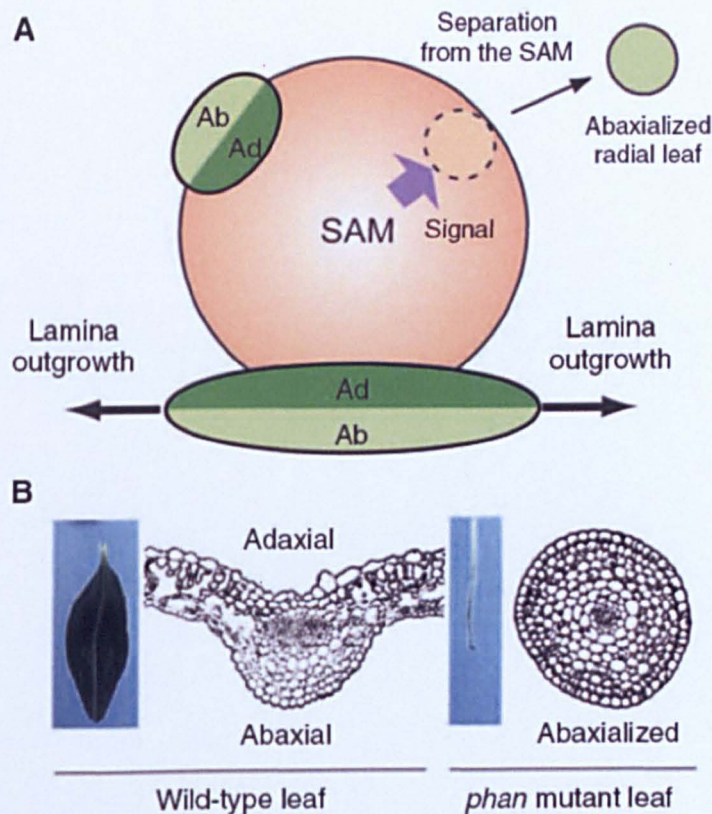


Figure 4.2 An illustration of Abaxial-adaxial polarity. (A) Transverse section of SAM showing the lamina outgrowth. Signalling from SAM directs adaxialization of early leaf primordium and leaf primordium separation from the SAM leads to abaxialized development of leaves. Junction between adaxial (Ad) and abaxial (Ab) domains promotes lamina outgrowth. (B) The *phan* mutant showing transverse section of abaxialized leaf in *Antirrhinum majus*. Illustration from Yamaguchi *et al.* (2012).

Abaxial identification also requires *AUXIN RESPONSE FACTOR3/ETTIN (ARF3/ETT)* and (*ARF4*) since combined loss of both *ARF3* and *ARF4* function leads to abaxialized leaves similar to leaves in *kan1kan2* double mutants. (Pekker *et al.*, 2005). Both of these abaxial determinants, *ARF3/ETT* and *ARF4*, are targeted by a trans-acting short interfering RNAs (ta-siRNA) class, ta-siR2141 and ta-siR2142, derived from non-coding *TAS3* precursor transcripts (Allen *et al.*, 2005). *TAS* transcripts are initially targeted by specific miRNAs for cleavage. Unlike regular miRNA directed cleavage, *TAS* is processed into dsRNAs via *SUPPRESSOR OF GENE SILENCING 3 (SGS3)* and *RNA-DEPENDENT RNA POLYMERASE 6 (RDR6)*. Subsequently these dsRNAs are converted into 21 bp long ta-siRNAs via *DICER-LIKE 4 (DCL4)*. As with miRNAs, these ta-siRNAs direct the cleavage of target mRNAs (Yoshikawa *et al.*, 2005). Synergic interaction between *as1* and *as2* mutants and ta-siRNA pathway mutants, *rdr6*, *dcl4* and *sgs3* show defects in leaf polarity, while these leaf polarity defects are absent in ta-siRNA pathway mutants alone. Another gene that functions in the ta-siRNA pathway is *AGO7* (also dubbed *ZIPPY (ZIP)*) and analysis of the double mutant *ago7/as2* consists of increased levels of *FIL* and miRNA165/166 as well as abnormal adaxial identity. This indicates that *AGO7* interacts with *AS2* to negatively regulate miR165/166 and *FIL* in leaf patterning. These observations suggest that adaxial-abaxial polarity may also be regulated by the ta-siRNA pathway (Figure 4.3) (Li *et al.*, 2005; Xu *et al.*, 2006).

MicroRNAs are known to regulate genes that are involved in directing critical steps in plant development. Evidence of such regulation is observed on miR165 and miR166, which targets *HD-ZIPIII* genes yielding defects in adaxial-abaxial patterning (Rhoades *et al.*, 2002). Further evidence of the repression of *HD-ZIPIII* gene expression by miR166 is apparent through the zinc finger protein *SE*, which is involved in the regulation of leaf polarity and meristem activity via the *HD-ZIPIII* genes (Grigg *et al.*, 2005). *SE* interacts with *HYL* in the regulation of miRNA levels by cleaving pre-miRNA into a miRNA/miRNA duplex along with *DCLI* (Yang *et al.*, 2006; Kurihara *et al.*, 2006). Loss-of-function in *HD-ZIPIII* suppresses defects in the *se* specific

mutant, *se-3*, which is consistent with the repression of *HD-ZIPIII* genes expression mediated by miR166 (Grigg *et al.*, 2005).

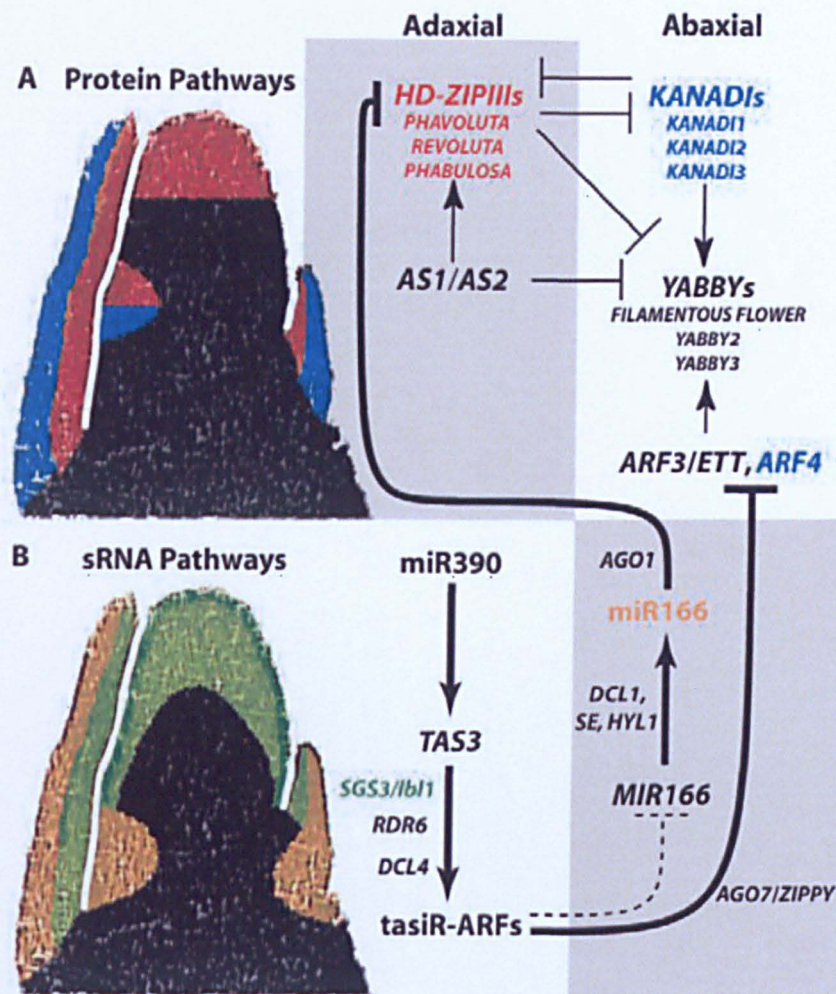


Figure 4.3 Adaxial-abaxial genetic network in leaves. Illustration showing the promoters and suppressors of adaxial and abaxial cell fate divided into regulators entailed in protein constituents (A) and those in the biogenesis of sRNAs (B). Illustration from Chitwood *et al.* (2007).

It has been established that loss of function in *YUC* genes, which encode flavin monooxygenases that are involved in biogenesis of local auxin, in leaf-abaxialized *as2/rev* and leaf-adaxialized *kan1/kan2* double mutants leads to a loss of ectopic lamina outgrowth. This demonstrates that the expression of *YUC* genes occurs in response to adaxial-abaxial juxtaposition and also suggests that auxin promotes lamina outgrowth by acting downstream of adaxial-abaxial polarity pathway (Wang *et al.*, 2011).

Floral organs are considered to be modified leaves which increase the likelihood of them sharing common developmental programs. One floral organ that is morphologically different to leaves is the stamen which consists of a proximal filament and a distal anther (Goldberg *et al.*, 1993). Toriba *et al.* (2010) has demonstrated in rice that the basic structure of the stamen is defined by the reorganization of the adaxial-abaxial polarity. It was demonstrated that the *OsPHB3* gene, an orthologue of *PHB*, is expressed in the adaxial domain and the *OsETTINI* gene, an orthologue of *ARF3/ETT*, is expressed in the abaxial domain during early stages of stamen establishment. Consequently during stamen development, *OsPHB3* is expressed in the lateral region of the anther primordium while losing its original adaxial expression and *OsETTINI* is expressed near the anther meristem along with its original abaxial expression. This recently formed polarity appears to be established in a novel development unit known as the theca primordium. Four outgrowths that consequently differentiate into pollen sacs are formed at the boundaries between the adaxial and the abaxial identities. Conversely, loss of expression in *OsPHB3* in the proximal filament results in abaxialized filament (Figure 4.4) (Toriba *et al.*, 2010). Thus identifying that adaxial-abaxial polarity establishment in the stamen is distinctly different from that of leaves.

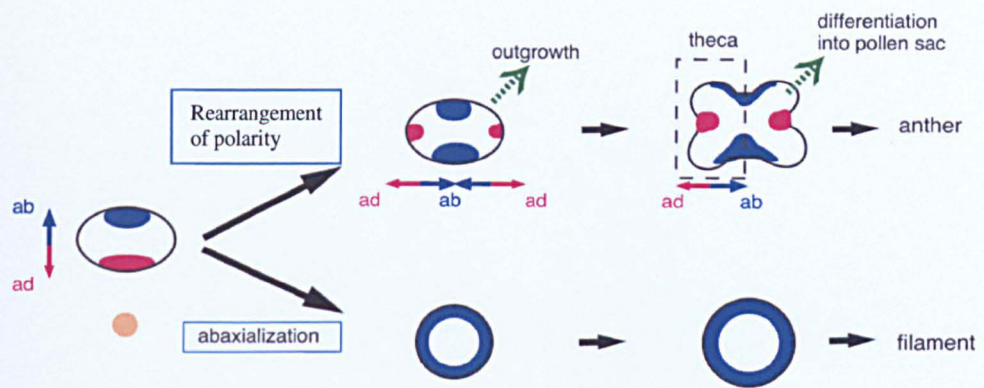


Figure 4.4 Adaxial-abaxial polarity in stamen development. Juxtaposition between adaxial-abaxial domains separate into pollen sacs. Abaxialization of the filament creates an organ that is radially symmetrical. Illustration from Toriba *et al.* (2011).

4.1.3 Chapter aims and objectives

This Chapter involves the characterization of the EMS mutagenized *hws-1* suppressor line *80.5*. Phenotypic comparisons between Col-0 wild type, *hws-1* and *80.5* both in *hws-1* background and Col-0 wild type background were conducted on flowers, leaves and roots. This involved segregation of the *80.5/hws-1* double mutant into *80.5* single mutant.

Homozygous *80.5/hws-1* mutant plants were crossed with *ffo1*, an allele of *HWS* in the *Landsberg* ecotype (Gonzalez-Carranza, unpublished data), to obtain a mapping population. The mapping was conducted using InDel (insertion/deletion) markers polymorphism by Dr. Janny Peters (Radboud University, Nijmegen). This work indicated on which chromosome *80.5* is located and the gene involved in causing the mutation observed in *80.5*. Sequencing analyses were then carried out to identify the nature of the mutation.

Complementation analyses were carried out to confirm that the gene involved was truly causing the phenotypic characteristics of the *80.5* mutant. Gene expression analysis was also conducted using *GUS* activity on Col-0 wild type and *hws-1* mutant as well as RT-PCR analysis on Col-0 wild type, *hws-1*, *80.5/hws-1*, *80.5/colwt*, *Pro35S::HWS* and *as2-1* using several genes involved in organ identity and boundary specificity.

Interaction between *80.5* with *UFO* and *Pro35S::HWS* was investigated using double mutants. Furthermore the interaction between *HWS* and the gene involved in the *80.5* mutation was explored.

4.2 Results

4.2.1 Phenotypic characteristics of 80.5

The second suppressor line analysed in this project that rescues the *hws-1* phenotype was the 80.5 suppressor line. One of the distinctive features of the 80.5/*hws-1* mutant phenotype is its abnormal leaf morphology. The leaf lamina shows a humped and dipped characteristic at its base demonstrating a near heart shaped and deep lobed leaf structures. The leaves on 80.5 produce an asymmetric lamina from the third rosette leaf compared to Col-0 wild type and *hws-1*. This indicates that the 80.5 mutant could play a role in the symmetry of leaves.

To analyse the phenotype of 80.5 in a wild type background, an F2 population of a cross between Col-0 wild type and 80.5/*hws-1* was performed to segregate 80.5 from *hws-1* background. This approach also determined whether the phenotype of 80.5 is caused by a dominant or recessive mutation. Ninety-six plants from the F2 population of the cross between Col-0 wild type and 80.5/*hws-1* were generated of which were 23 plants were phenotypically similar to the 80.5 mutant. The F1 population from the cross displayed a wild type phenotype and the analysis of the F2 progeny showed a 3:1; wild type: mutant segregation ratio demonstrating that the 80.5 was a single recessive nuclear mutation. The plants that demonstrated a phenotype similar to 80.5 were analysed by PCR using *HWS* specific primers (SSLPHSfor and SSLPHSrev) to segregate 80.5 away from *hws-1* background and to identify 80.5 single mutants. The analysis demonstrated that 35% of the segregation population was 80.5/*colwt* (Figure 4.5). Those that showed a band of 200 bp were 80.5 mutants in Col wild type background and those that showed a band of 172 bp were 80.5 mutants in *hws-1* background. The suppressor line 80.5 in the Col-0 wild type background enabled a phenotypic analysis of 80.5 to be determined in the absence of *hws-1*.

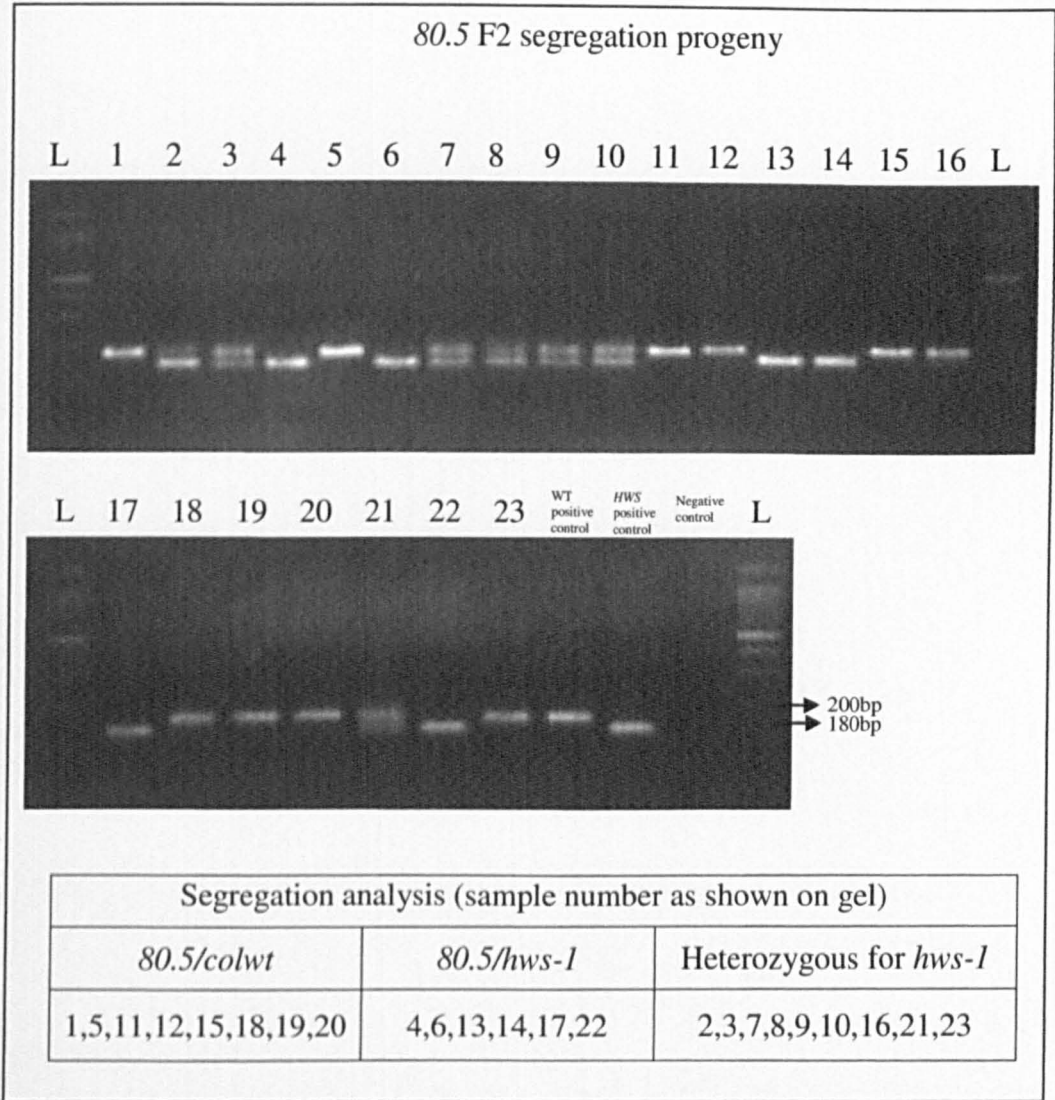


Figure 4.5 PCR amplifications of members of the F2 population from the cross between Col-0 wild type and *80.5/hws-1* using *HWS* specific primers. The F2 population revealed a total of twenty three plants out of ninety-six that displayed similar phenotypic characteristics to *80.5*. PCR amplification of these twenty three plants demonstrated that eight were homozygous for Col-0 wild type, six were homozygous for *hws* and nine were heterozygous. (L: 100 bp ladder)

Twenty day old seedling comparisons between *80.5/hws-1* and *80.5/colwt* indicated that the phenotype on *80.5/colwt* was more severe than that of *80.5/hws-1*. The *80.5/hws-1* (Figure 4.6 C) seedlings were distinctively smaller and had smaller rosette leaves compared to those of *80.5/colwt* (Figure 4.6 D), which is similar to Col-0 wild type (Figure 4.6 A) and *hws-1* leaf sizes (Figure 4.6 B). The *80.5/colwt* mutant produces short leaflet-like formations on the petioles and leaf-lobes on the base of the rosette leaves (Figure 4.6 E and F). Both *80.5/hws-1* and *80.5/colwt* have a crimped leaf surface that shows distinguishable deep venation (Figure 4.6 E and G). These leaflet-like structures starts from the third leaf upwards and are less distinct in the *80.5/hws-1* mutant plants (Figure 4.6 E). Leaf petioles of both *80.5/hws-1* and *80.5/colwt* are wider than that of Col-0 and *hws-1* and those petioles of *80.5/colwt* seem to be longer than that of *80.5/hws-1* (Figure 4.6 E). The crimped and humped leaf surface seen in *80.5* results in asymmetry of the leaf lamina. These *80.5* phenotypic characteristics such as leaflet-like structures, deep venation, humped leaf lamina base and deep lobes at the side of the leaves, can also be observed in *asymmetric leaves2 (as2)* mutants which are involved in adaxial-abaxial leaf polarity (Semiarti *et al.*, 2001).

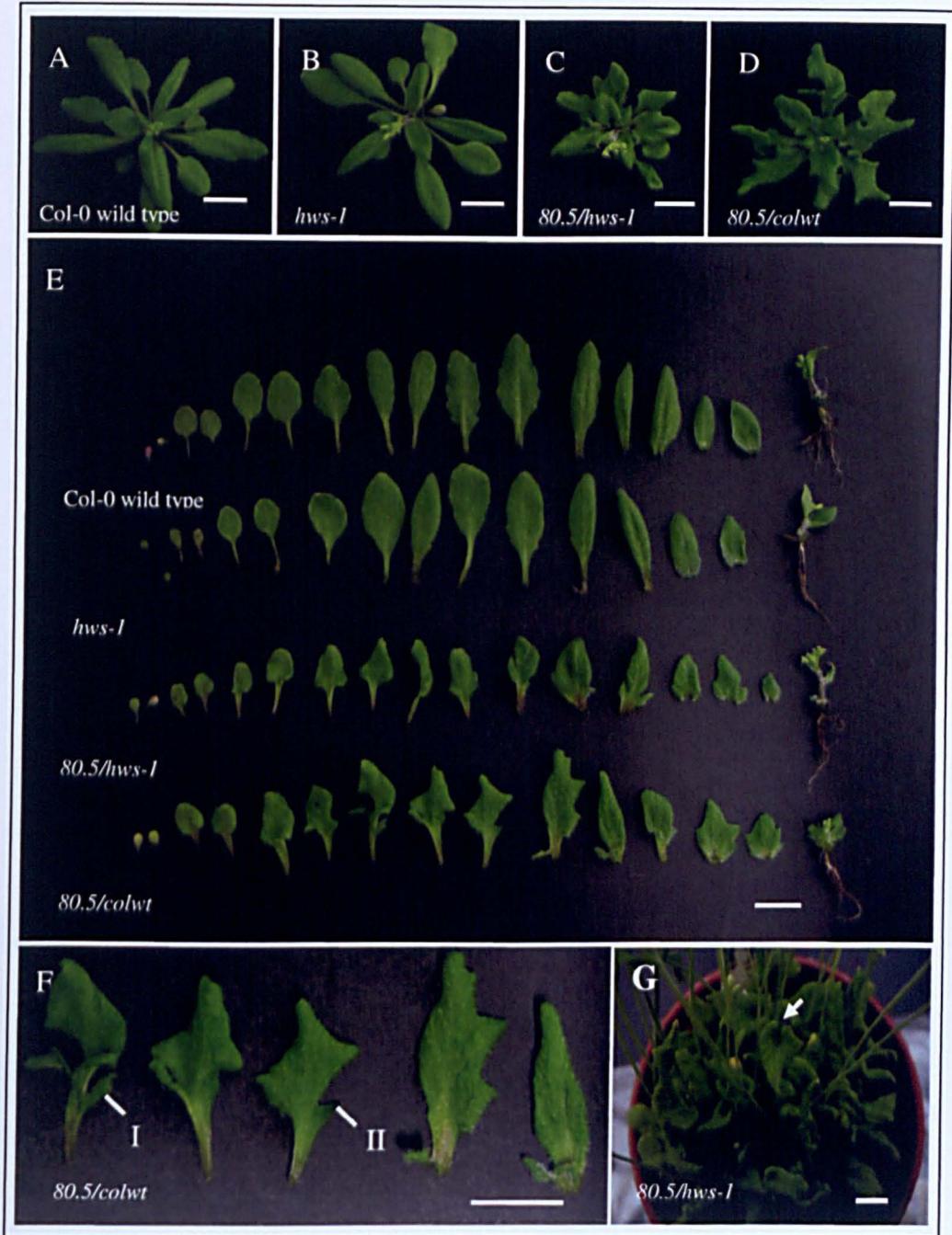


Figure 4.6 Comparisons between 20 day old seedlings of Col-0 wild type, *hws-1*, *80.5/hws-1* and *80.5/colwt*. (A) Col-0 wild type seedling. (B) *hws-1* seedling. (C) *80.5/hws-1* seedling. (D) *80.5/colwt* seedling. (E) Dissected leaves of all four genotypes. (F) Enhanced view of E *80.5/colwt* indicating the presence of leaflet-like structures (I) on the petiole and leaf lobes (II) on the base of the rosette leaf of *80.5/colwt* mutant. (G) Distinctive humped leaf lamina base (arrow) and deep leaf venation seen on *80.5/hws-1* mutants. Bars = 1cm

These distinctive morphological changes on leaves can be seen from the third rosette leaf on *as2*. Such traits are known to be more severe on the allele *as2-1* than on *as2-4* and *as2-101*, which are weak alleles of the *as2* mutant (Semiarti *et al.*, 2001). To establish comparisons between *80.5* and *as2* mutant plants, three mutant alleles identified as *as2-1*, *as2-4*, and *as2-101* were taken for analysis of leaf morphology. It was identified that *as2-1* (Figure 4.7 B) phenocopies the characteristic leaf morphology of *80.5* (Figure 4.7 A) whereas the rosette leaves of weak alleles *as2-4* and *as2-101* (Figure 4.7 B) are distinctly different to *80.5*. Seedling size of *as2-1*, *as2-4* and *as2-101* were all similar to *80.5/colwt*, however *80.5/hws-1* seedling size was much smaller in comparison to the other mutants including *80.5/colwt*.

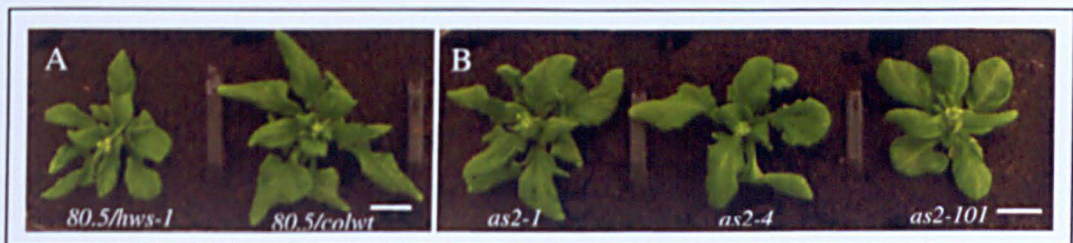


Figure 4.7 Comparisons between 24 day old seedlings of (A) *80.5/hws-1*, *80.5/colwt* and (B) *as2-1*, *as2-4*, *as2-101*. The leaf morphology of *80.5* photocopies that of *as2-1* compared to other alleles, *as2-4* and *as2-101*. Bars = 1cm

The floral architecture of *80.5/hws-1* (Figure 4.8 G) and *80.5/colwt* (Figure 4.8 H) shows that the width of the sepal and petal margin at the base is narrower compared to Col-0 wild type (Figure 4.8 E) and *hws-1* (Figure 4.8 F), consequently giving rise to a gap between adjacent petals and sepals (Figure 4.8 M). The inflorescence of *80.5/hws-1* (Figure 4.8 K, N and O) and *80.5/colwt* (Figure 4.8 L) demonstrates that the floral buds open earlier than the wild type (Figure 4.8 I) and *hws-1* (Figure 4.8 J) due to the outward curling of sepals and due to the increase in width of boundary domain between adjacent sepals. It has been reported that sepals and petals of *as2-101* were narrower than that of wild type thus leaving a gap between each organ similar to *80.5/hws-1*. The premature opening of floral buds in *80.5/hws-1* has also been documented on *as2-101* mutants (Xu *et al.*, 2008) whereas abaxialization of

80.5/hws-1 sepals has not been reported before. The orientation of petals within the flower of both *80.5/hws-1* and *80.5/colwt* is irregular compared to Col-0 wild type and *hws-1* petal orientation. The petals of *80.5/hws-1* (Figure 4.8 C) and *80.5/colwt* (Figure 4.8 D) tend to be concentrated to one side of the flower unlike petals of Col-0 (Figure 4.8 A) and *hws-1* (Figure 4.8 B) which are distributed symmetrically within the flower. The mis-orientation of petals in *80.5* is not due to twisting of petals within the flower. Therefore it may be due to asymmetry within the petal primordium. This confirms that *80.5* mutant is not only showing asymmetry in leaf morphology but also in petal orientation.



Figure 4.8 Comparable phenotypic analysis of flower at stage 6.90 (table 1.1, section 1.1) and inflorescence morphology of Col-0 wild type, *hws-1*, *80.5/hws-1* and *80.5/colwt*. (A, E and I) Col-0 wild type, (B, F and J) *hws-1*, (C, G and K) *80.5/hws-1* and (D, H and L) *80.5/colwt*. (M) Petal and sepal morphology comparisons of Col-0 wild type, *hws-1*, *80.5/hws-1* and *80.5/colwt*. (N) *80.5/hsw-1* inflorescence from the side. (O) a close up view of *80.5/hws-1* inflorescence from the top. Bars = 1mm.

Comparisons between floral architecture of *80.5/hws-1* and *80.5/colwt* with *as2* mutant alleles, *as2-1*, *as2-4* and *as2-101* shows similar abnormalities in petal orientation. The petal orientation in *as2-1* (Figure 4.9 A) is more similar to *80.5* than the other mutant alleles, *as2-4* (Figure 4.9 B) and *as2-101* (Figure 4.9 C). The morphology of the inflorescence is similar in all mutant alleles except for the *as2-101* (Figure 4.9 F) mutant allele since it is in the *Landsberg* ecotype whereas *as2-1* (Figure 4.9 D) and *as2-4* (Figure 4.9 E) are in the En-2 background which corresponds with the Col-0 ecotype.

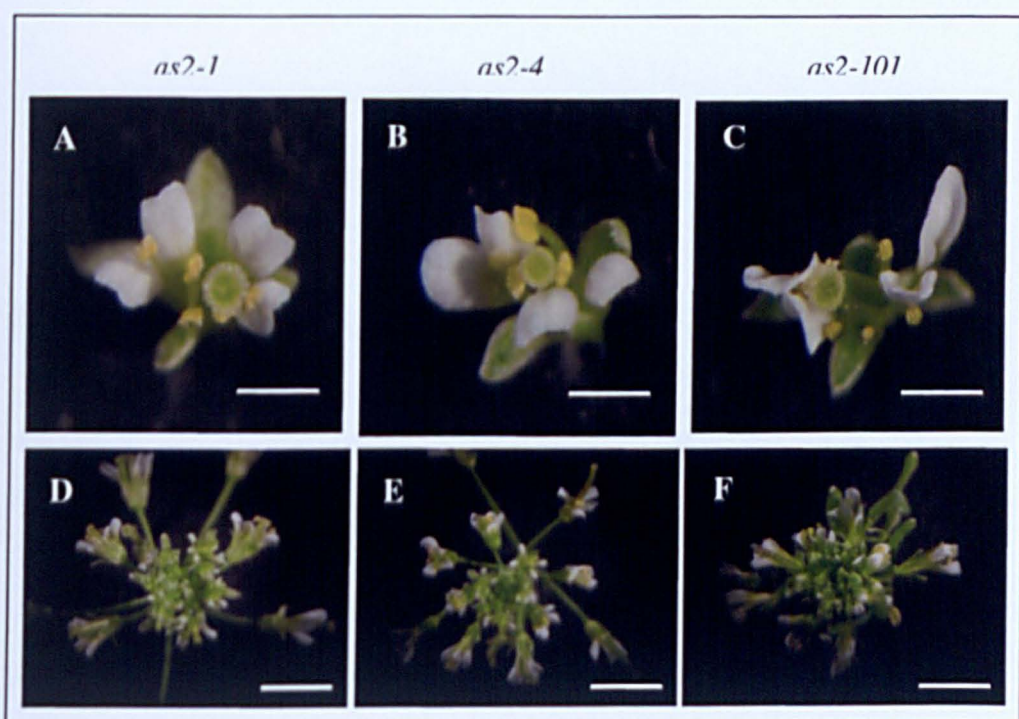


Figure 4.9 Flower at stage 6.90 (table 1.1, section 1.1) and inflorescence morphology of (A and D) *as2-1*, (B and E) *as2-4* and (C and F). *as2-101*. Bars = 1mm

Root analysis on MS media of Col-0 wild type, *hws-1*, *80.5/hws-1* and *80.5/colwt* have shown that *80.5* root growth is faster than that of both Col-0 wild type and *hws-1* (Figure 4.10). There are no significant differences between the root growth of *80.5/colwt* and *80.5/hws-1*. The difference in significance between Col-0 wild type, *hws-1*, *80.5/hws-1* and *80.5/colwt* was evaluated using the ANOVA test. There is a significant difference between the rate of root growth of the different genotypes on day 8 ($F_{(1,59)}= 13.24$, $P<0.001$), 11 ($F_{(1,59)}= 13.16$, $P<0.001$), 16 ($F_{(1,59)}= 12.67$, $P<0.001$) and 19 ($F_{(1,59)}= 13.65$, $P<0.001$). The average rate of root growth per day at its steepest for Col-0 wild type, *hws-1*, *80.5/hws-1* and *80.5/colwt* is 2mm, 3mm, 5mm and 5mm respectively. The average rate of root growth of the mutant is repressed in the *hws-1* background compared to the Col-0 wild type.

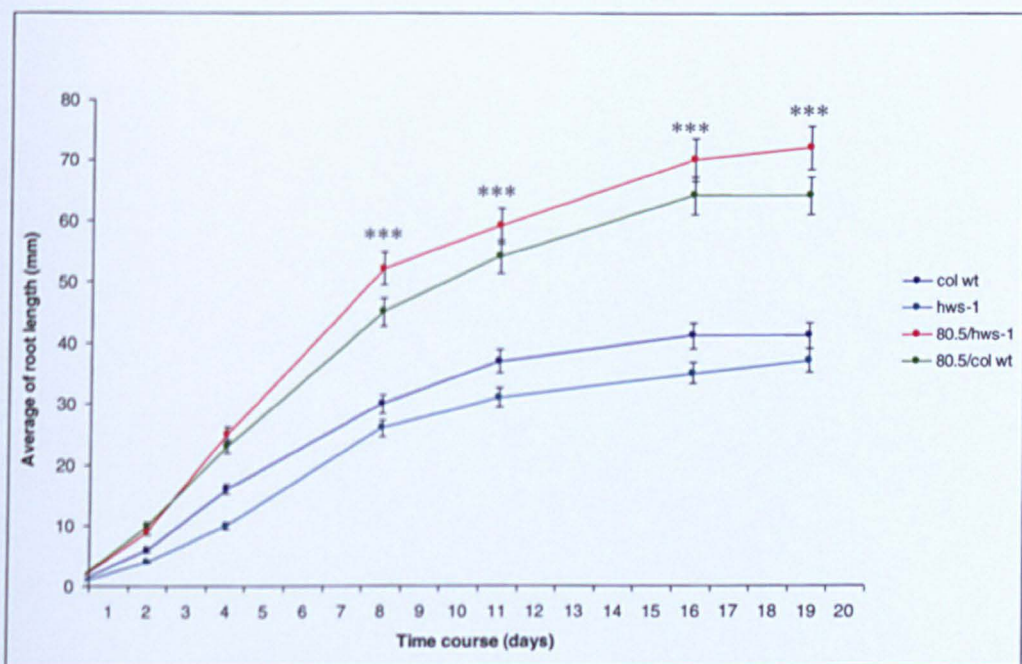


Figure 4.10 Root growth over a time course of 19 days of Col-0 wild type, *hws-1*, *80.5/hws-1* and *80.5/colwt*. The analysis shows that both *80.5/hws-1* and *80.5/colwt* root growth is faster than that of Col-0 wild type and *hws-1*. It appears that the root growth of *80.5/hws-1* is slightly more rapid than that of *80.5/colwt*. The difference in significance was analysed by ANOVA test. Bars indicate standard error and *** indicate significance at $P<0.001$, $n = 60$.

Vascular patterns of Col-0 wild type, *hws-1*, *80.5/hws-1* and *80.5/colwt* were analysed using transverse sections of 14 day old rosette leaves. Comparisons between transverse sections of leaf lamina showed that the central vascular bundle of *80.5/hws-1* (Figure 4.11 E) and *80.5/colwt* (Figure 4.11 G) were thinner than that of Col-0 wild type (Figure 4.11 A) and *hws-1* (Figure 4.11 C). It was also difficult to identify the central vascular bundle of *80.5/hws-1* and *80.5/colwt* since the adjacent vascular bundles to the central bundle were of the same thickness as that of the central vascular bundle. Xylem and phloem tissues in Col-0 wild type (Figure 4.11 B), *hws-1* (Figure 4.11 D), *80.5/hws-1* (Figure 4.11 F) and *80.5/colwt* (Figure 4.11 H) were situated respectively on the adaxial and abaxial sides of the vascular bundles. The leaf lamina cell sizes of all three varieties were of a similar size and did not show significant differences between them.

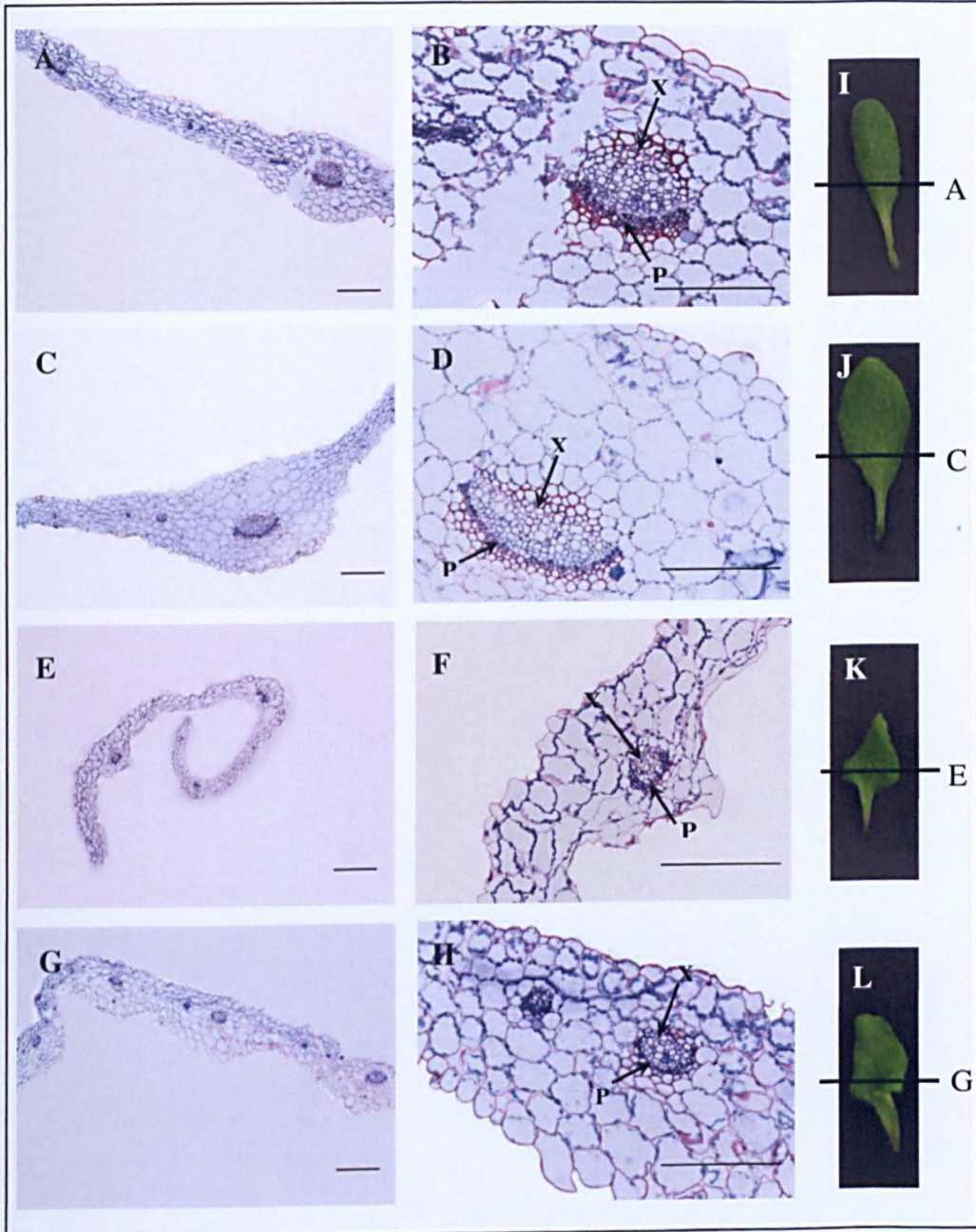


Figure 4.11 Anatomy of transverse sections stage 1.06 (table 1.1, section 1.1), 6 rosette leaves >1mm in length, Col-0 wild type, *hws-1*, *80.5/hws-1* and *80.5/colwt* rosette leaves. (A and B) Transverse section of Col-0 wild type leaf lamina. (C and D) Transverse section of *hws-1* leaf lamina. (E and F) Transverse section of *80.5/hws-1* leaf lamina. (G and H) Transverse section of *80.5/colwt* leaf lamina. (I-L) Position of leaf lamina transverse sections on Col-0 wild type, *hws-1*, *80.5/hws-1* and *80.5/colwt* respectively. X= xylem and P= phloem. Bars = 100 μ M

4.2.2 Mapping the gene responsible for the 80.5 phenotype

Homozygous *80.5/hws-1* mutant plants were crossed with *ffo1*, an allele of *HWS* in the *Landsberg* ecotype (Gonzalez-Carranza, unpublished data), to obtain a mapping population. The cross obtained with *ffo1* would ensure that the resulting F1 and F2 population background is of *hws-1* and is between Col-0 and *Landsberg*. This would make it possible to use ecotype specific markers. The F1 mapping population, from the cross between *ffo1* and the mutant, was selfed and the DNA of the resulting F2 population that exhibited a phenotype similar to *80.5* was extracted from 288 F2 plants (Figure 4.12). The DNA was used for mapping via InDel (insertion/deletion) markers by Dr. Janny Peters (Radboud University, Nijmegen). InDel polymorphisms are variations in DNA sequences that entail the insertion or deletion of one or more nucleotides. InDel markers can be obtained from Cereon *Arabidopsis* polymorphism collection. Primers can be developed for InDel polymorphism markers flanking the region of interest (Peters et al., 2004). The *80.5* mutant was mapped to a 4.2Mb region on chromosome 1 between markers *nga280* (20,877,364 bp) and *CER452443* (25,117,783 bp) using InDel markers (Figure 4.13). *AS2* is located between 24,398143bp and 24,400969bp on chromosome 1, thus making *AS2* a possible candidate gene for *80.5*.

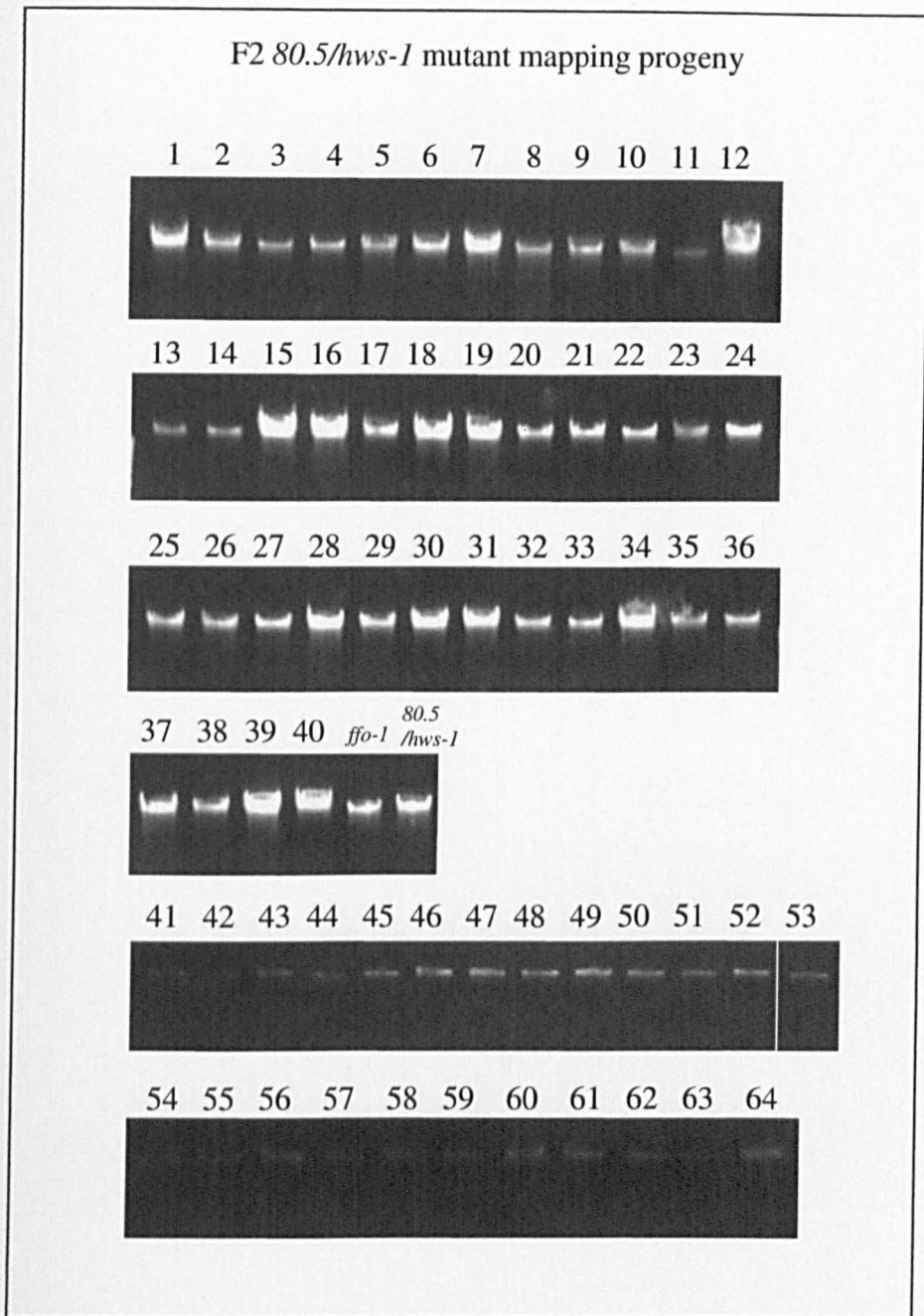


Figure 4.12 Genomic DNA of plant tissue extracted from 64 F2 plants out of 288 of the cross between *80.5/hws-1* (Columbia ecotype) and *ffo1* (Landsberg ecotype). These 64 F2 plants displayed a phenotype similar to that of *80.5*. The DNA samples were run on a 1.5% (w/v) agarose gel.

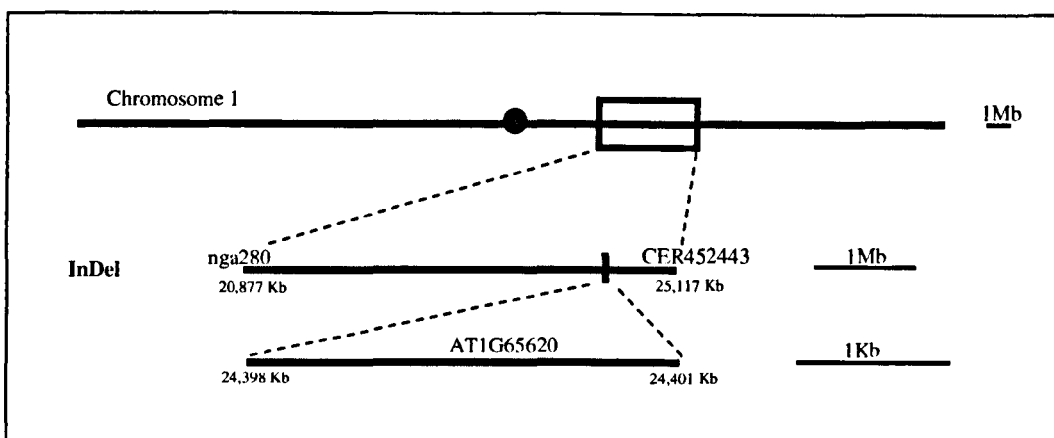


Figure 4.13 Mapping structure of 80.5. The illustration shows the mapping strategy of InDel marker polymorphism displaying markers nga280 and CER452443. AS2 locus *AT1G65620*.

As *AS2* was a likely candidate for *80.5*, the gene in the suppressor line was then sequenced. Sequencing of the *AS2* cDNA in *80.5* revealed a point mutation of a single base pair transition from C to T, 61 bp downstream from the start of the *AS2* ORF (Figure 4.14). This point mutation introduces an ochre stop codon resulting in a premature termination (Figure 4.15). The mutant *80.5* shows a truncated version of the predicted *AS2* protein and supports the hypothesis that *80.5* is an allele of the *AS2* gene. For further confirmation that *80.5* as an allele of *AS2*, complementation tests were conducted as described in section 4.2.3.

AS2	TATCTTTTTTTGTTTCCTTATACCTTCTACCTCCAAAACTAAATTCAAAAACCTTATT	1140
80.55'UTRrev	TATCTTTTTTTGTTTCCTTATACCTTCTACCTCCAAAACTAAATTCAAAAACCTTATT	216

AS2	TCCTCAATTTTCAATGGCGGCTTTGTGTAGGGAGAGGGAAAAGAGAAAAATGAAAA	1200
80.55'UTRrev	TCCTCAATTTTCAATGGCGGCTTTGTGTAGGGAGAGGGAAAAGAGAAAAATGAAAA	276

AS2	CTCCATTTTCAAGTCATTAATAATGGCATCTTCTTCAACAACTCACCATGCGCCGCTTGC	1260
80.55'UTRrev	CTCCATTTTCAAGTCATTAATAATGGCATCTTCTTCAACAACTCACCATGCGCCGCTTGC	336

AS2	AAATTCCTCCGGCGAAAATGTC AACCGGAATGTGTATTTCGCGCCTATTTCACCACGGAC	1320
80.5ORFfor	AAATTCCTCCGGCGAAAATGTC AACCGGAATGTGTATTTCGCGCCTATTTCACCACGGAC	78

AS2	CAGCCACAAAAATTCGCAACCGTTCACAAAGTGTGGAGCAAGTAACGTGACAAAGCTC	1380
80.5ORFfor	CAGCCACAAAAATTCGCAACCGTTCACAAAGTGTGGAGCAAGTAACGTGACAAAGCTC	138

AS2	CTCAACGAGCTTCACCCCTCACAACGTGAAGACGCAGTGAACCTTTGGCCTATGAAGCC	1440
80.5ORFfor	CTCAACGAGCTTCACCCCTCACAACGTGAAGACGCAGTGAACCTTTGGCCTATGAAGCC	198

AS2	GACATGCGCCTCCGTGACCTGTCTACGGCTGCGTCGGCGTCATCTCTCTCCTCCAACAT	1500
80.5ORFfor	GACATGCGCCTCCGTGACCTGTCTACGGCTGCGTCGGCGTCATCTCTCTCCTCCAACAT	258

AS2	CAGCTTCGTGAGCTTCAGATAGATCTCAGCTGTGCTAAATCTGAGCTCTCTAAGTACCAA	1560
80.5ORFfor	CAGCTTCGTGAGCTTCAGATAGATCTCAGCTGTGCTAAATCTGAGCTCTCTAAGTACCAA	318

AS2	AGCCTCGGTATCCTCGCCGCCACTCATCAGAGTCTTGGCATCAACTTACTCGCCGGAGCA	1620
80.5ORFfor	AGCCTCGGTATCCTCGCCGCCACTCATCAGAGTCTTGGCATCAACTTACTCGCCGGAGCA	378

AS2	GCAGATGGAACAGCCACCGCCGTGAGAGACCACTATCACCACCACAGTTTTTCTCTAGA	1680
80.5ORFfor	GCAGATGGAACAGCCACCGCCGTGAGAGACCACTATCACCACCACAGTTTTTCTCTAGA	438

AS2	GAACAAATGTTTGGTGGCTTGGATGTTCCGGCCGGTAACAACACGACGGTGGGATTCCT	1740
80.5ORFfor	GAACAAATGTTTGGTGGCTTGGATGTTCCGGCCGGTAACAACACGACGGTGGGATTCCT	498

AS2	GCCATTGGACAGATCACTCAGTTTCAGCAGCCGAGAGCCGCCGCTGGAGATGATGGTCGC	1800
80.5ORFfor	GCCATTGGACAGATCACTCAGTTTCAGCAGCCGAGAGCCGCCGCTGGAGATGATGGTCGC	558

AS2	CGTACTGTTGATCCGTCTTGAGATTTTAGGGTTTGGTGGTGTTCATCTTCGTCGATCGC	1860
80.5ORFfor	CGTACTGTTGATCCGTCTTGAGATTTTAGGGTTTGGTGGTGTTCATCTTCGTCGATCGC	618

AS2	TTGGTGATGAGAAAACTATAATTTAAGAAAATTTTGGATGTGAAAACCAAATATTTT	1920
80.5ORFfor	TTGGTGATGAGAAAACTATAATTTAAGAAAATTTTGGATGTGAAAACCAAATATTTT	678

AS2	AAACGTATGGTACGTCTCTCTTAATGACATTAATTCGGTTTTTATTATTATTACTT	1980
80.5ORFfor	AAACGTATGGTACGTCTCTCTTAATGACATTAATTCGGTTTTTATTATTATTACTT	738

AS2	AGATATATTATGATAGTCACTTTTGTATTCTTTCAAATTTTATGGACTTGCTCTCTTAA	2040
80.5ORFfor	AGATATATTATGATAGTCACTTTTGTATTCTTTCAAATTTTATGGACTTGCTCTCTTAA	798

Figure 4.14 Multiple sequence alignment of AS2 and 80.5 5'UTR and ORF using ClustalW (EMBL-EBI) program. This sequence alignment shows the premature termination of 80.5 mutant allele by an ochre stop codon due to a point mutation of a single base pair transition from C to T highlighted in grey 61 bp from the start of AS2 coding region, ATG (also indicated in grey).

AS2 protein sequence

```
MASSSTNSPCAACKFLRRKCQPECVFAPYFPPDQPQKFANVHKVFGASNVTKLLNELHPS  
QREDAVNSLAYEADMRLRDPVYGCVGVISLLQHQLRQLQIDLSCAKSELSKYQSLGILAA  
THQSLGINLLAGAADGTATAVRDHYHHHQFFPREQMFGGLDVPAGNNYDGGILAIGQITQ  
FQQPRAAAGDDGRRTVDPS-
```

80.5 protein sequence

```
MASSSTNSPCAACKFLRRKCQPECVFAPYFPPDQPQKFANVHKVFGASNVTKLLNELHPS  
QREDAVNSLAYEADMRLRDPVYGCVGVISLLQHQLRQLQIDLSCAKSELSKYQSLGILAA  
THQSLGINLLAGAADGTATAVRDHYHHHQFFPREQMFGGLDVPAGNNYDGGILAIGQITQ  
FQQPRAAAGDDGRRTVDPS-
```

Figure 4.15 Protein translations of AS2 and 80.5. This sequence shows the premature termination of 80.5 mutant 20 amino acids downstream of the start of AS2 coding region introducing an amino acid transition from Glutamine to an ochre stop codon highlighted in grey. Courtesy of ClustalW (EMBL-EBI) program and ExPASy Translate Tool, SIB Bioinformatics Resource Portal.

Other alleles of AS2 that have been identified previously including *as2-1*, *as2-4* and *as2-10*, which are described phenotypically in section 4.3.1, are shown on (Figure 4.16). The nature of the mutation of *as2-1* and *as2-4* causes 13 bp and 1 bp deletion respectively which results in a frame-shift mutation (Iwakawa *et al.*, 2002). The *as2-101*, *as2-102*, *as2-103* and *as2-5* alleles causes a single base pair change from G to T, C to T, C to T and G to A respectively resulting in an amino acid change from arginine to leucine at position 17, serine to phenylalanine at position 68, arginine to tryptophan at position 17 and glycine to glutamate at position 46 respectively (Xu *et al.*, 2002; Iwakawa *et al.*, 2002).

```

                                     (as2-103) TT (as2-101)
ATGGCATCTTCTTCAACAAACTCACCATGCGCCGCTTGCAAATTCCTCCGGCGAAAATGT
M A S S S T N S P C A A C K F L R R K C

T (80.5)
CAACCGGAATGTGTATTTCGCGCCCTATTTCCACCGGACCAGCCACAAAATTTCGCAAAC
Q P E C V F A P Y F P P D Q P Q K F A N

                                     A (as2-5) ----- (as2-1)
GTTCAAAAGTGTGTTGGAGCAAGTAACGTGACAAAGCTCCTCAACGAGCTTACCCTTCA
V H K V F G A S N V T K L L N E L H P S

                                     T (as2-102)
CAACGTGAAGACGCAGTGAACCTTTTGGCCTATGAAGCCGACATGCGCCTCCGTGACCCT
Q R E D A V N S L A Y E A D M R L R D P

GCTTACGGCTGCGTCGGCGTCATCTCTCTCTCCAACATCAGCTTCGTCAGCTTCAGATA
V Y G C V G V I S L L Q H Q L R Q L Q I

GATCTCAGCTGTGCTAAATCTGAGCTCTCTAAGTACCAAAGCCTCGGTATCCTCGCCGCC
D L S C A K S E L S K Y Q S L G I L A A

ACTCATCAGAGTCTTGGCATCAACTTACTCGCCGGAGCAGCAGATGGAACAGCCACCGCC
T H Q S L G I N L L A G A A D G T A T A

                                     - (as2-4)
GTGAGAGACCACTATCACCACCACAGTTTTTTTCTTAGAGAACAAATGTTTGGTGGCTTG
V R D H Y H H H Q F F P R E Q M F G G L

GATGTTCCGGCCGGTAACAACACTACGACGGTGGGATTCTTGCCATTGGACAGATCACTCAG
D V P A G N N Y D G G I L A I G Q I T Q

TTTCAGCAGCCGAGAGCCCGCTGGAGATGATGGTCGCCGTAAGTTGATCCGTCTTGA
F Q Q P R A A A G D D G R R T V D P S -

```

Figure 4.16 Protein translation of AS2. This sequence shows the single base pair change from C to T which results in the premature termination of 80.5 mutant allele by an ochre stop codon (taa). It also shows other mutant alleles of AS2. The mutant alleles *as2-101* (C to T transition causing amino acid change from arginine to leucine), *as2-102* (C to T transition causing amino acid change from serine to phenylalanine), *as2-103* (G to T transition causing amino acid change from argentine to tryptophan), *as2-5* (G to A transition causing amino acid change from glycine to glutamate). The position of nucleotide deletions of *as2-1* and *as2-4* are indicated by -. Courtesy of ExPASy Translate Tool, SIB Bioinformatics Resource Portal

4.2.3 Complementation analysis of 80.5

4.2.3.1 Plasmid construction

There are several methods that could be adapted to confirm that *AS2* is responsible for the phenotypic characteristics of the 80.5 mutant. One way is to cross the T-DNA insertion of the gene with *hws-1* and observe that the phenotype acquired is that of the 80.5 mutant. The most definitive method is to complement the mutation by creating a construct consisting of the *AS2* promoter region and *AS2* coding region and transform it into 80.5/*hws-1*, which would lead to a T1 population with *hws-1* phenotype.

For the purpose of complementation analysis of 80.5, the second method was employed. The construct (*AS2_{pro}::AS2*) consisted of 3,333 bp of *AS2* promoter region, 1,221 bp of 5'UTR with two introns (intron 1 (398 bp) and intron 2 (266 bp)), 599 bp of ORF and 223 bp of 3'UTR (Figure 4.17). The *AS2_{pro}::AS2* construct was transformed into 80.5/*hws-1* mutant plants, using *Agrobacterium tumefaciens*, as well as into *hws-1* and Col-0 wild type plants which were used as controls. The *AS2* fragment consisting of the 5387 bp fragment along with *SalI* and *BamHI* restriction enzymes was amplified from wild type DNA by PCR using the primer set *AS2compSalIFor* and *As2compBamHIRev* (Figure 4.18). The PCR product was purified and digested to produce sticky ends for ligation onto the digested and dephosphorylated pBI101.2 vector (Figure 4.19 A). The construct was subsequently transformed into DH5 α cells and these were plated on to LB medium containing 50 $\mu\text{g}\cdot\text{ml}^{-1}$ Kanamycin. The positive colonies obtained were amplified by PCR using a forward primer located 315 bp from the start codon of the pBI101.2 vector (*pBI101.2for*) and a reverse primer located at the promoter region of *AS2*, 3,202 bp upstream from the start of the 5'UTR (*AS2rev4*) (Figure 4.19 C). The positive colonies were pooled in the first instance into 10 colonies per pool for PCR amplification. Individual colonies of those pools that amplified an expected band of 315 bp were amplified by PCR (Figure 4.19 B).

```

1 AATCCCTCT AGTACCAAAT CCTATFACTA TTGAAGGTAT ACTCTATAGT
51 TATTTATTTA GTTAAGTATA TATATTAATA ATAAATAACA TTAATTAGTA
101 CTAGTCTTAT CATATTTATT AGCTCATTTT CTTATAAAA ACTAATATAA
151 TAGGAAATTT AAGCACAAGA TGAGCTTTGC CCATCGAGAG CCTCAAACC
201 CAAAAGTCTC TTCTTCTTCA CGAGATCCAA TCTTTTGCTT TTAGTAATT
251 AATTACATCT TCTTCTTCT CTTCTCTCTT CTTCTTCCCT CTCTCATACC
301 TACCTATAAG CAACACAAAG AACACCATTG ATCCCATCTG TTTTGTGCC
351 TATATTTTCG TAATCCATCC ATACGCATTC CAACTACACG GTACAAATTT
401 CCATCTCTTT TTAATTTGTT TTTATAATGA TTTTAAATCT CTCAGGTTGT
451 CTCTAGACTC TTAGGTCTAG TTACCAAAT TTGACTAGCA ATCATATAGC
501 TACAAGTTCC TCTATATCAT ATAGCTACAC ATATCTCTAG GTCTGAAATG
551 ATCTTTTATC TCCAAGCAT ATATTATATA TTTGGATGCA TACCTTTATG
601 TTTGACTTTC GAAAAGCACC TTCATGTTAC TCATTTTTTC CTCTATTTGC
651 TTTCAACAGT TGACAAGAAG GTTGGATCAG TATATATAAG TATACATATA
701 CACTTATGTG TGTGTGTAGT GTATGTGCAT ATATAGCTCA CCAAATATCT
751 TTAATACTAC TAATTGCAA GTTTCTCTTA TTTTACAGCT TTTTGTATGC
801 AACCCCAAAT AGCAGCTTAA AGAAAGCAGA GAGGATCTTC TTTTATTCC
851 CCTCTGAGCA ACAGAAGCCA TTATTCAAAG AAAGGCTTCT TTAATTTACT
901 CGCAGGTAAA AGCTTTCTTA TTCTATAGAG ATTGAACAAC TTTTTTTTTT
951 TTTTAATTGA CAACAATAAA GATTGAGCAA CTTCTCTACA TTATTTCTTT
1001 CTTTATTTTC TCACTTAATT TCATATTTGA TTACAAAAAC AGATAATGTA
1051 ATATCTCCAA AATCACAATT GATTTCTATA TATCTTTTTT TGTTTCCTTA
1101 TACCTTCTAC CTCCAAAAAC TAAATTCAAA AACCTTATT TCTCTCAATT
1151 TTCAATGGCG GCTTTGTGTA GGGAGAGGGA AAAGAGAAA AATTGAAAA
1201 CTCCATTTT AAGTCATTAA AATGGCATCT TCTTCAACAA ACTCACCATG
1251 CGCCGCTTGC AAATTCCTCC GCGGAAAATG TCAACCGGAA TGTGTATTGC
1301 CGCCCTATTT CCCACCGGAC CAGCCACAAA AATTCGCAA CGTTCACAAA
1351 GTGTTTGGAG CAAGTAACGT GACAAAGCTC CTCAACGAGC TTCACCCTC
1401 ACAACGTGAA GACGCAGTGA ACTCTTTGGC CTATGAAGCC GACATGCGCC
1451 TCCGTGACCC TGTCTACGGC TCGTTCGGCG TCATCTCTCT CCTCCAACAT
1501 CAGCTTCGTC AGCTTCAGAT AGATCTCAGC TGTGCTAAAT CTGAGCTCTC
1551 TAAGTACCAA AGCCTCGGTA TCCTCGCCGC CACTCATCAG AGCTTTGGCA
1601 TCAACTTACT CGCCGGAGCA GCAGATGGAA CAGCCACCGC CGTGAGAGAC
1651 CACTATCACC ACCACCAGTT TTTTCTFAGA GAACAAATGT TTGGTGGCTT
1701 GGATGTCCG GCCGGTAACA ACTACGACGG TGGGATCTT GCCATTGGAC
1751 AGATCACTCA GTTTCAGCAG CCGAGAGCCG CCGCTGGAGA TGATGGTCCG
1801 CGTACTGTTG ATCCGCTTG AGATTTTAGG GTTTTGGTGG TGTTTCTCTT
1851 CGTCGATCGC TTGGTGATGA GAAACTATA ATTTAAGAA AATATTTGAT
1901 GTGAAAACC AAAATATTTT AAACGTATGG TACGTCTCTC TTAATGACAT
1951 TAATTTCCGG TTTTATTATT ATTATTACTT AGATATATTA TGATAGTCAC
2001 TTTTGTATTT CTTTCAAATT TTATGGACTT GCTCTCTTAA TTGAT

```

ORF	1222-1821 bp
5'UTR	1-390 bp
5'UTR	789-905 bp
5'UTR	1172-1221 bp
Coding_region	1222-1821 bp
Exon	1-390 bp
Intron	391-788 bp
Exon	789-905 bp
Intron	906-1171 bp
Exon	1172-2045 bp
3'UTR	1822-2045 bp

Figure 4.17 AS2 gene sequence. The gene contains 1,221bp of the 5'UTR, with two introns (intron 1 (390-788 bp) and intron 2 (905-1171 bp), 599 bp coding region, and 223 of 3'UTR. Exons are shown in bold and the coding region is highlighted in grey.

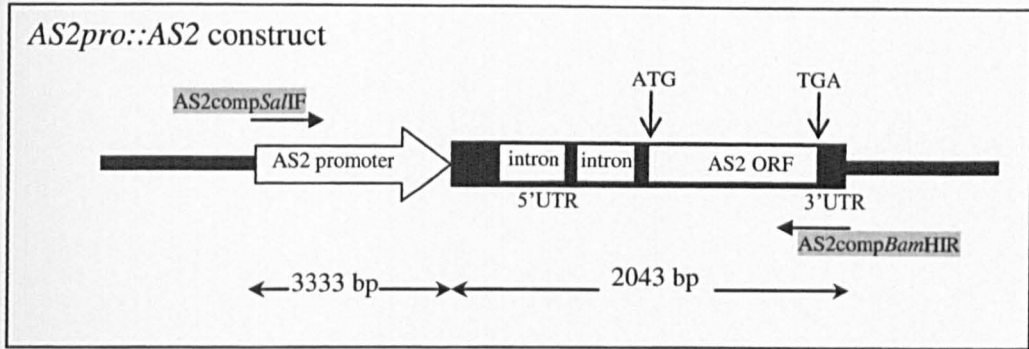


Figure 4.18 The structure of the *AS2pro::AS2* construct for complementation analysis in *80.5/hws-1* including Col-0 wild type and *hws-1* as controls. The construct included 3,333 bp of the promoter region of *AS2* and 2,043 bp of the coding region including the 5'UTR and 3'UTR. The primers used for the construct (highlighted in grey) consisting of the restriction enzymes *SalI* and *BamHI* were used for the amplification of *AS2pro::AS2* from wild type DNA by PCR.

The chosen positive plasmid colony number 3 was digested and sequenced following purification to determine whether the expected gene fragment was present and in the correct orientation in the pBI101.2 vector. The purified colony was digested with *EcoRI* restriction enzyme. The restriction enzyme *EcoRI* has two cutting sites located within the *AS2pro::AS2* line and one cutting site located within the pBI101.2 vector. The pattern of digestion shows bands at 474bp (fragment between the two *EcoRI* cutting sites on the *AS2pro::AS2* line), 6,122 bp (fragment between one cutting site on the *AS2pro::AS2* line and the cutting site on pBI101.2 vector) and 10,574 bp (fragment between the second cutting site on the *AS2pro::AS2* line and the cutting site on pBI101.2 vector) indicating that the gene fragment was in the correct orientation (Figure 4.20). To further confirm that the *AS2pro::AS2* gene fragment was inserted in the correct orientation in to the pBI101.2 vector, sequencing analysis was carried out. The purified colony was sequenced with primers pBI101.2for and AS2rev4. This set of primers determined the orientation of the *AS2pro::AS2* insert in the pBI101.2 vector as shown in Figure 4.20. The sequencing of *AS2pro::AS2::pBI101.2* plasmid also identified the site of digestion with *SalI* restriction enzyme where the *AS2pro::AS2* insert is ligated to the pBI101.2 vector (Figure 4.21).

4.2.3.2 *Agrobacterium* and *Arabidopsis* transformation

Following the determination of the presence of $AS2_{pro}::AS2$ line fragment in the pBI101.2 vector, the $AS2_{pro}::AS2::pBI101.2$ plasmids were transformed into *Agrobacterium tumefaciens* C58 cells and plated onto LB medium containing $50\mu\text{g.ml}^{-1}$ Kanamycin and $25\mu\text{g.ml}^{-1}$ Rifampicin. Some of the resulting positive colonies analysed by PCR using the same primers that were used to amplify the $AS2_{pro}::AS2::pBI101.2$ plasmids in DH5 α cells. From the positive clones that showed an expected band of 315 bp, positive clone 1 (Figure 4.22) was used for transformation via floral dip (Clough and Bent, 1998) into Col-0 wild type, *hws-1* and *80.5/hws-1*.

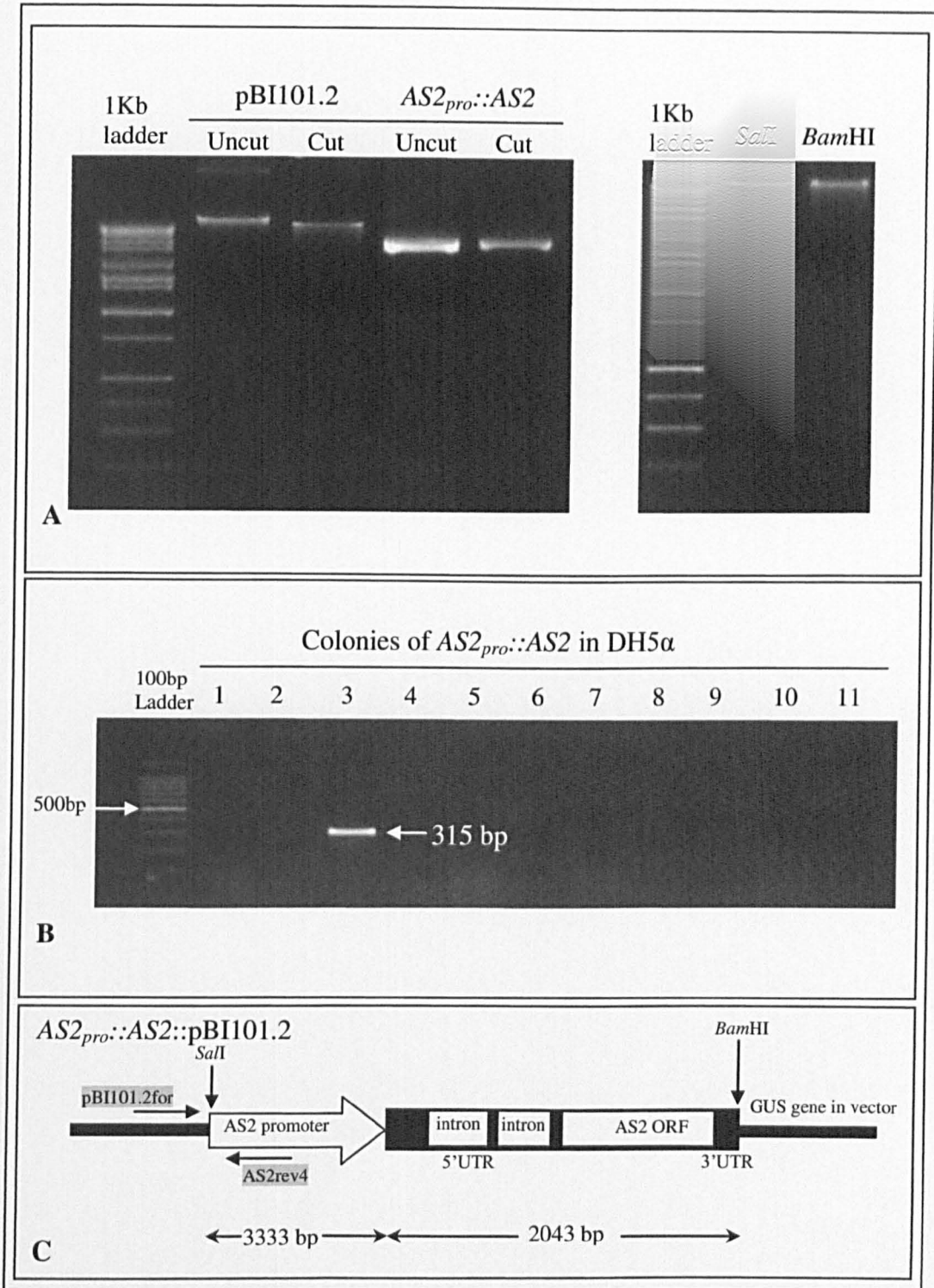


Figure 4.19 Ligation and transformation of the *AS2_{pro}::AS2::pBI101.2* construct. (A) Restriction enzyme (*SalI* and *BamHI*) digestion of the *pBI101.2* vector and the *AS2_{pro}::AS2* insert. (B) Individual colonies obtained from DH5 α cell transformation showing the PCR amplification positive colony 3 using primers *pBI101.2for* and *AS2rev4*. (C) The *AS2_{pro}::AS2::pBI101.2* construct showing the ligation between *AS2_{pro}::AS2* insert and *pBI101.2* vector by restriction enzymes *SalI* and *BamHI*. The positive colonies obtained from the DH5 α cell transformation were amplified by PCR using primers *pBI101.2for* and *AS2rev4* (shown in grey).

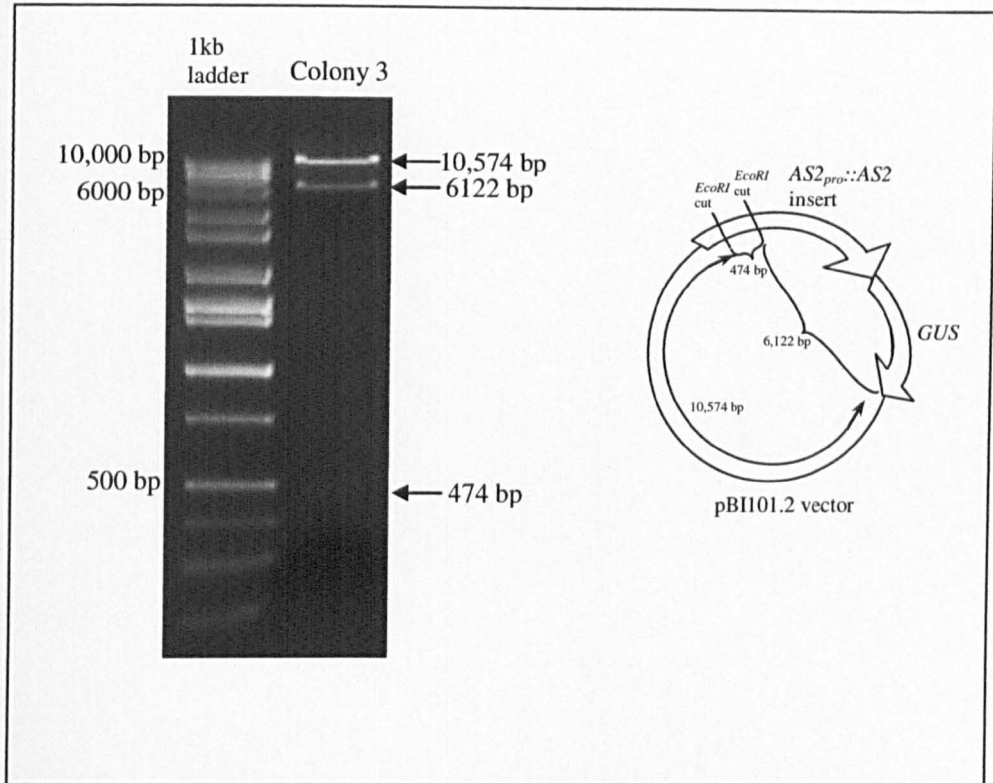


Figure 4.20 The pattern of $AS2_{pro}::AS2::pBI101.2$ construct (positive colony 3) digestion. The digestion shows bands at 474bp (fragment between the two *EcoRI* cutting sites on the $AS2_{pro}::AS2$ line), 6,122 bp (fragment between one cutting site on the $AS2_{pro}::AS2$ line and the cutting site on pBI101.2 vector) and 10,574 bp (fragment between the second cutting site on the $AS2_{pro}::AS2$ line and the cutting site on pBI101.2 vector) indicating that the gene fragment is in the correct orientation.

PBI101.2_AS2 AS2rev4	CCAAATGGCTCAAGTCGGTGACGGTGATAATTCACCTTTAATGAATAATTTCCGTCAATA 2220 -----
PBI101.2_AS2 AS2rev4	TTTACCTTCCCTCCCTCAATCGGTTGAATGTCGCCCTTTTGTCTTTGGCCCAATACGCCAA 2280 -----
PBI101.2_AS2 AS2rev4	ACCGCCTCTCCCCGCGGTTGGCCGATTCAATTAATGCAGCTGGCAGCAGGTTTCCCGA 2340 -----
PBI101.2_AS2 AS2rev4	CTGGAAGCGGGCAGTGAGCGCAACGCAATTAATGTGAGTTAGCTCACTCATTAGGCACC 2400 -----
PBI101.2_AS2 AS2rev4	CCAGGCTTTACACTTTATGCTTCCGGCTCGTATGTTGTGTGGAATTGTGAGCGGATAACA 2460 -----GCTTCCGGCTCGTATGTTGTGTGGAATTGTGAGCGGATAACA 42 *****
PBI101.2_AS2 AS2rev4	ATTCACACAGGAAACAGCTATGACCATGATTACGCCAAGCTTGCATGCCTGCAGG---- 2516 ATTCACACAGGAAACAGCTATGACCATGATTACGCCAAGCTTGCATGCCTGCAGGTCGA 102 *****
PBI101.2_AS2 AS2rev4	--CAATAAGCCTACATCAGATTTTAATTTGAATCGAATATAACTATATGTCCTATGTATT 2574 CGCAATAAGCCTACATCAGATTTTAATTTGAATCGAATATAACTATATGTCCTATGTATT 162 *****
PBI101.2_AS2 AS2rev4	TTTTTGGGGCCTAAAAGAAAAAATCAATGTTTGGTAAATGACATGGTTATAGCTTG 2634 TTTTTGGGGCCTAAAAGAAAAAATCAATGTTTGGTAAATGACATGGTTATAGCTTG 222 *****
PBI101.2_AS2 AS2rev4	GTTTCTACGTTCAACAAAACTCGGGCTACTTGTGTATACCTTGACAAGATTCTACTAAA 2694 GTTTCTACGTTCAACAAAACTCGGGCTACTT-----AAA 256 *****
PBI101.2_AS2 AS2rev4	TCTTTTTTTCAGACTTCCAGTCAAGTCTTCTAGGGTCTTAAGTCGGGTTTTTATTTCCGG 2754 TTTC----- 260 * *
PBI101.2_AS2 AS2rev4	TTCTGATTGCTGATTCTAAAGTCTCTTTAGAGTTTGTTCATTTGTTTTGTTGGTGTGAT 2814 -----
PBI101.2_AS2 AS2rev4	TGACGTCCTCATTCCCTAAGTCCGAACACTATGACTCTGATATGTTATTGACAGAGACAGA 2874 -----
PBI101.2_AS2 AS2rev4	GAGTGATAATATAGTTTCTGATAGGGAGGATTTGATAAACAGAGTGATTACATAATGTT 2934 -----
PBI101.2_AS2 AS2rev4	TGTGTTGATCCTTCTTAGTCTTACCGTCTATAGTTCCCTATTTTTTAACACGAAATT 2994 -----
PBI101.2_AS2 AS2rev4	TCATAGTTTGTGTAACCTGCGGCAGAAAAATAGATAGCTCACATAGCTATGATCTAAAT 3054 -----
PBI101.2_AS2 AS2rev4	ATGAGCATTCGTGTATATGATTTTATGGTAGCTAGCGTTGTTGACAGGCTGCGGTAAATT 3114 -----

Figure 4.21 Sequence alignment of AS2_{pro}::AS2::pBI101.2 construct with the primers used for PCR amplification of purified positive colony 3. The primers pBI101.2for and As2rev4 are underlined and the site of *SalI* restriction enzyme digestion is shown in grey. The conserved region on the sequence alignment shows that the AS2_{pro}::AS2::pBI101.2 construct is in the correct orientation. Courtesy of ClustalW (EMBL-EBI) program.

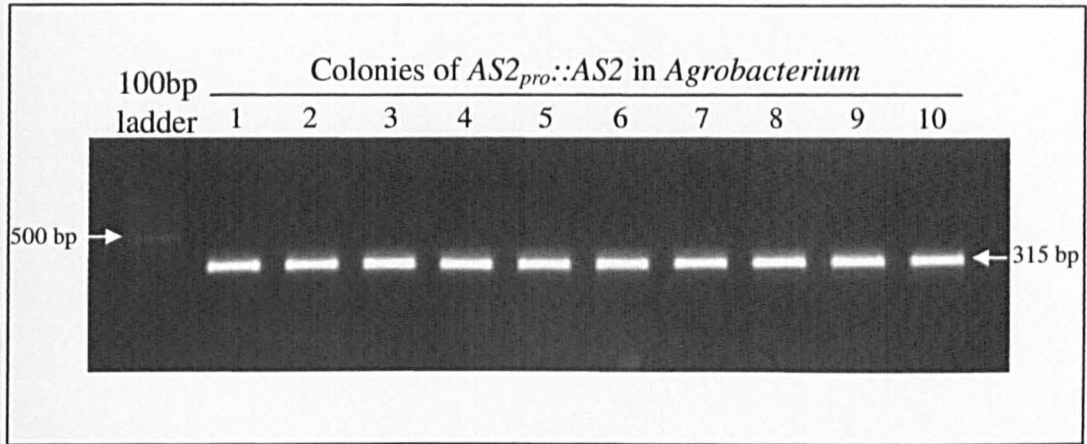


Figure 4.22 PCR amplification of the positive colonies from the *AS2_{pro}::AS2::pBI101.2* plasmid transformation via *Agrobacterium tumefaciens* C58. Primers used for the PCR amplification were pBI101.2for and As2rev4. From the positive clones that showed an expected band of 315 bp, positive clone 1 was used for transformation via floral dip into Col-0 wild type, *hws-1* and *80.5/hws-1*.

4.2.3.3 Screening for plant transformants

Following floral dip transformation, sterilized seeds of *AS2_{pro}::AS2* from the transformation were grown on ½ MS media containing 50µg.ml⁻¹ Kanamycin. The Kanamycin resistant seedlings were transferred to the growth room following the development of at least 4 rosette leaves. The *hws-1* and the *80.5/hws-1* transformed plants both exhibited a *hws-1* phenotype and the Col-0 wild type transformed plants, which were used as a control, demonstrated a wild type phenotype in the T1 population. To confirm the success of the transformation, genomic DNA was isolated from the transformed T1 population and amplified by PCR using *AS2_{pro}::AS2::pBI101.2* plasmid primers (pBI101.2for and AS2rev4) (Figure 4.23 A), *HWS* primers (SSLPHSfor and SSLPHSrev) ((Figure 4.23 B), and specific primers designed to amplify wild type (WTfor and MISMATCHrev) ((Figure 4.23 C) and *80.5* mutant (MUTANTfor and MISMATCHrev) ((Figure 4.23 D). The four PCR reactions amplified bands of 315 bp, 200 bp and 172 bp and 564 bp respectively. The analysis of the PCR amplifications showed that the *AS2_{pro}::AS2* plasmid construct was present in all the transgenics, confirming that the floral dip transformation was successful. *HWS* specific primers

confirmed that the transformants were of the correct genotype (ie: 200 bp band length for *AS2_{pro}::AS2* plasmid transformation into Col-0 wild type and 172 bp band length for *AS2_{pro}::AS2* plasmid transformation into *hws-1* and *80.5/hws-1*). *AS2_{pro}::AS2/Colwt* and *AS2_{pro}::AS2/hws-1* transformants recognises wild type and the transgene whereas *AS2_{pro}::AS2/80.5/hws-1* transformants recognises only the transgene. T2 population analysis of *AS2_{pro}::AS2* transformation into *80.5/hws-1* showed a segregation ratio of 3:1, *hws-1*:*80.5* phenotype, which confirms that the transformation has worked. This experiment provides further evidence that *80.5* is an allele of the *AS2* gene.

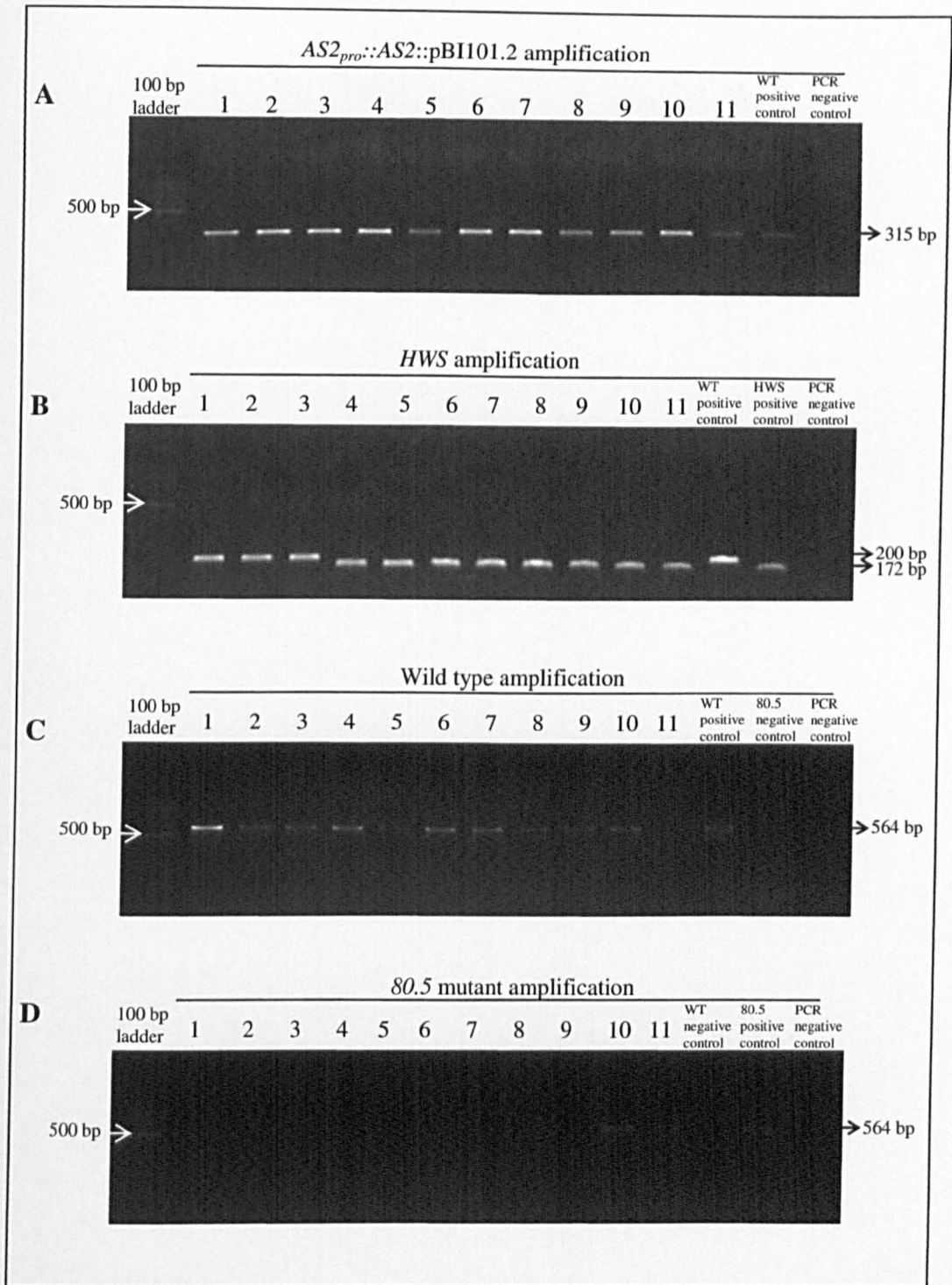


Figure 4.23 PCR amplification of the T1 transformants. Primers used for PCR amplification include (A) *AS2_{pro}::AS2::pBI101.2* plasmid primers (pBI101.2for and AS2rev4), (B) *HWS* primers (SSLPHSfor and SSLPHSrev), (C) specific primers designed to amplify wild type (WTfor and MISMATCHrev) and (D) *80.5* mutant (MUTANTfor and MISMATCHrev). PCR products 1-3 represent *AS2_{pro}::AS2* transformed into colwt, 4-9 represent *AS2_{pro}::AS2* transformed into *hws-1* and 10 and 11 represent *AS2_{pro}::AS2* transformed into *80.5/hws-1*.

4.2.4 Expression analysis of *AS2_{pro}::GUS* transgenic lines

Since the *hws-1* phenotype is rescued in *80.5/hws-1*, the expression pattern of *AS2* in the *hws-1* mutant was examined. Expression analysis of the *GUS* reporter gene fused to *AS2* promoter was undertaken in both Col-0 wild type and *hws-1* plants. The same strategy for plasmid construction and transformation were used as previously indicated in section 4.2.3. The plasmid construct for *GUS* reporter gene fusion consisted of 3,333 bp of the *AS2* promoter and 1,221 bp of the 5'UTR. This DNA fragment was amplified from wild type DNA using PCR with primers *AS2compSalIFor* and *AS2compBamHIRpro* which consisted of restriction enzymes *SalI* and *BamHI* respectively (Figure 4.24 A). The PCR product was purified and digested to produce sticky ends for ligation onto the digested and dephosphorylated pBI101.2 vector. The construct was subsequently transformed into DH5 α cells and these were plated onto LB medium containing 50 $\mu\text{g.ml}^{-1}$ Kanamycin. The positive colonies obtained were amplified by PCR using a forward primer located 315 bp from the start codon of the pBI101.2 vector (*pBI101.2for*) and a reverse primer located at the promoter region of *AS2*, 3,202 bp upstream from the start of the 5'UTR (*AS2rev4*). Positive colonies were pooled in the first instance into 10 colonies per pool for PCR amplification (Figure 4.24 B). Individual colonies of the pool (colonies 21-30) that amplified an expected band of 315 bp were amplified again by PCR and colony 22 was found to be a positive colony (Figure 4.24 C). Sequencing of purified colony 22 revealed that the plasmid construct was ligated in the correct orientation (Figure 4.25). The *AS2pro::GUS* construct was transformed into *Agrobacterium tumefaciens* C58 cells and plated onto LB medium containing 50 $\mu\text{g.ml}^{-1}$ Kanamycin and 25 $\mu\text{g.ml}^{-1}$ Rifampicin. The resulting positive colonies were confirmed by PCR amplification (Figure 4.26). Positive colony 4 was used for transformation via floral dip (Clough and Bent, 1998) into Col-0 wild type and *hws-1*. PCR amplification using primers *pBI101.2for* and *AS2rev4* was used to confirm the presence of the transgene in the T1 population of Col-0 wild type transformants (Figure 4.27 A) and *hws-1* transformants (Figure 4.27 B).

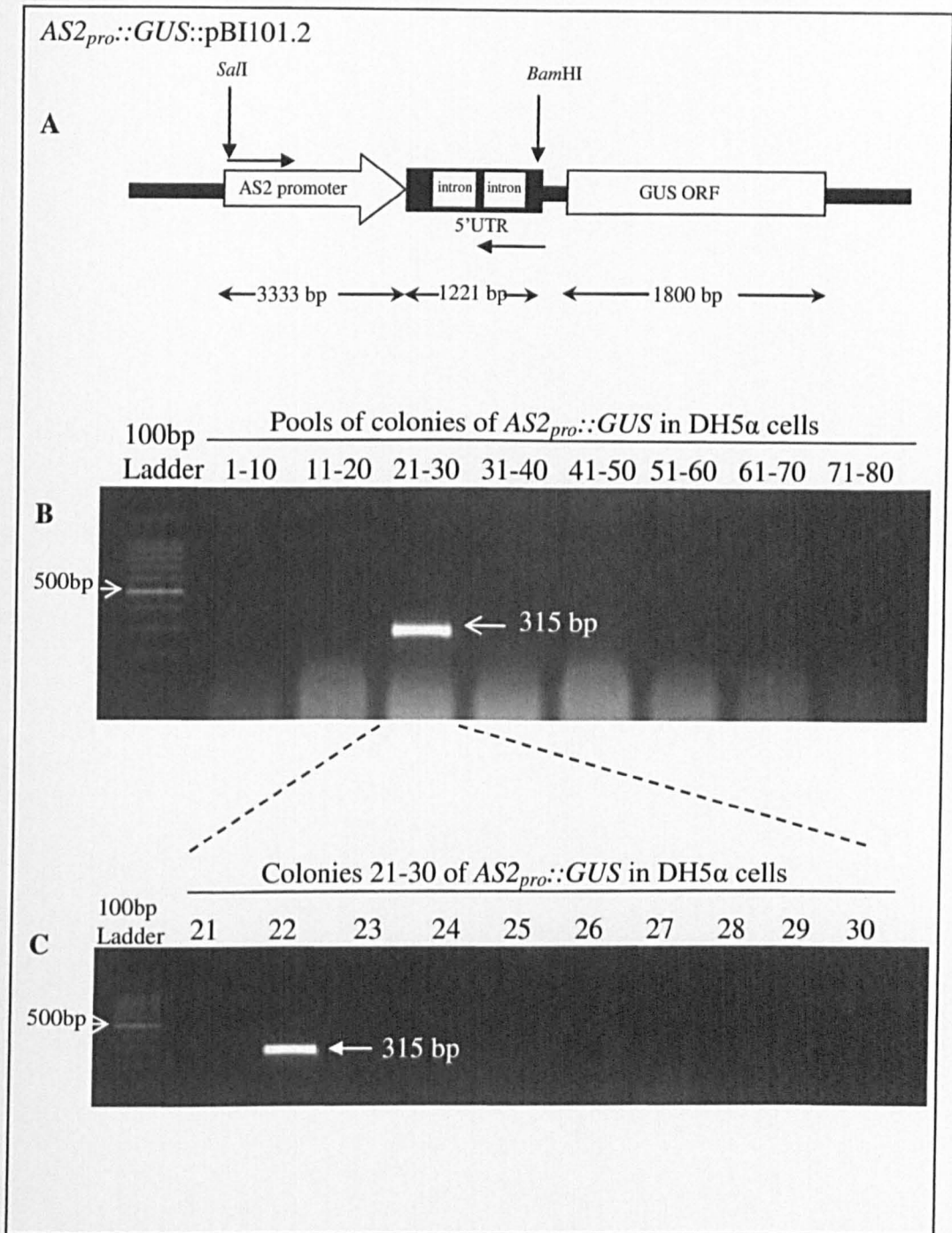


Figure 4.24 The structure of the *AS2_{pro}::GUS* construct and PCR amplification of the DH5α cell transformation. (A) The *AS2_{pro}::GUS* construct structure indicating *SalI* and *BamHI* restriction enzyme digestion site. The construct consists of 3,333 bp of AS2 promoter region, 1,221 bp of 5'UTR along with 1,800 bp of *GUS* coding region. (B) DH5α cell transformation colony pools. The PCR amplification consisted of 10 individual colonies per pool sample and colony pool 21-30 amplified a 315 bp band. (C) Individual colonies from the pool 21-30 were amplified for positive colonies.

pBI101.2 Gusseq AS2for5	AAACATGAAAAATGGGTTTGACCGAAGAACTTTGAGGACGGTAACTTCATTATCAACT 2940 ----- -----
pBI101.2 Gusseq AS2for5	TTTCGACTGTATTTATATTTTAGCTTTTGTCAAACCGTATCATATAATATTAATGCGAAT 3000 ----- -----
pBI101.2 Gusseq AS2for5	TACTAGTAGAGAGTATAATAATAGTAATAACAAAATGCTTGGTTACTGTATGTAAATCCC 3060 ----- -----
pBI101.2 Gusseq AS2for5	TAGACAAAAGAATAAGAATAAAAAGACAAAATCTTCATCCCAAGATCCATCAGGAGA 3120 ----- -----CTTTAGGAGA 10 ----- ----- *****
pBI101.2 Gusseq AS2for5	GTCAGAGTCAGACCCCATCTCTCATTGCCATCTCTCCTTTTCACATTTATTCCTTTT 3180 GTCAGAGTCAGACCCCATCTCTCATTGCCATCTCTCCTTTTCACATTTATTCCTTTT 70 ----- -----CTTTTC-CATTATTCCTTTT 22 *****
pBI101.2 Gusseq AS2for5	TTTCTTTCTAGATACTTTTTTATTTTGAATTTAATACTAATAACTATACATTTATTGTT 3240 TTTCTTTCTAGATACTTTTTTATTTTGAATTTAATACTAATAAC-ATACATTTATTGTT 129 TTTCTTTCTAGATACTTTTTTATTTTGAATTTAATACTAATAACTATACATTTATTGTT 82 *****
pBI101.2 Gusseq AS2for5	ATTATTGTTGTTAGAGTCTATGCTAGGGTCCAAGGGTTCATCCCAATATCCCTTCTTCTC 3300 ATTATTGTTGTTAGAGTCTATGCTAGGGTCCAAGGGTTCATCCCAATATCCCTTCTTCTC 189 ATTATTGTTGTTAGAGTCTATGCTAGGGTCCAAGGGTTCATCCCAATATCCCTTCTTCTC 142 *****
pBI101.2 Gusseq AS2for5	CTTAGAAACTCGCAACTTCTTCACATGGAATCGATCCCGGGTAGGTCAGTCCCTTATG 3360 CTTAGAAACTCGCAACTTCTTCACATGG-----GATCCCGGGTAGGTC----- 233 CTTAGAAACTCGCAACTTCTTCACATGG-----GATCCCGGGTAGGTCAGTCCCTTATG 197 *****
pBI101.2 Gusseq AS2for5	TTACGTCTGTAGAAACCCCAACCCGTGAAATCAAAAACGACGGCCTGTGGGCATTC 3420 ----- TTACGTCTGTAGAAACCCCAACCCGTGAAATTTGGCT----- 237 *****
pBI101.2 Gusseq AS2for5	AGTCTGGATCGGAAAACGTGGAATTGATCAGCGTTGGTGGGAAAGCGGTTACAAGAA 3480 ----- -----
pBI101.2 Gusseq AS2for5	AGCCGGGCAATTGCTGTGCCAGGCAGTTTTAACGATCAGTTCGCCGATGAGATATTCTG 3540 ----- -----
pBI101.2 Gusseq AS2for5	AATTATGCGGGCAACGTCTGGTATCAGCGCAAGTCTTTATACCGAAAGGTTGGGCAGGC 3600 ----- -----
pBI101.2 Gusseq AS2for5	CAGCGTATCGTGCTGCGTTTCGATGCGGTCCTACTATTACGGCAAAGTGTGGGTCAATAAT 3660 ----- -----

Figure 4.25 Sequence alignment of *AS2_{pro}::GUS* construct with the primers used for PCR amplification of purified positive colony 22 using ClustalW (EMBL-EBI) program. The primers used for the PCR amplification, AS2for4 and GUSsequencing, are underlined and the site of *Bam*HI restriction enzyme digestion is shown in grey. The conserved region on the sequence alignment shows that the *AS2_{pro}::GUS* construct is in the correct orientation.

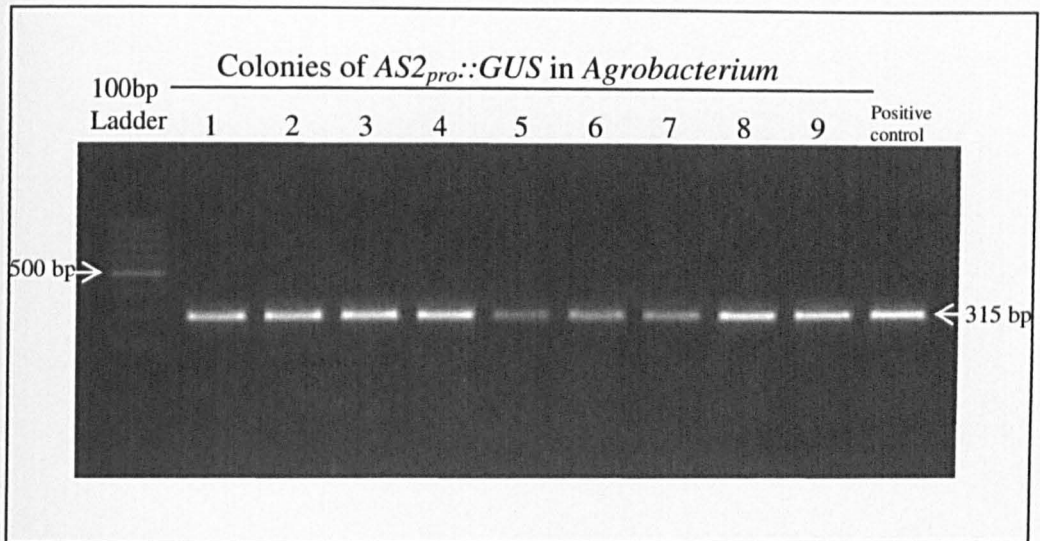


Figure 4.26 PCR amplification of the positive colonies from the *AS2_{pro}::GUS* plasmid transformation via *Agrobacterium tumefaciens* C58. Primers used for the PCR amplification were pBI101.2for and As2rev4. From the positive clones that showed an expected band of 315 bp, positive clone 4 was used for transformation via floral dip into Col-0 wild type, *hws-1*.

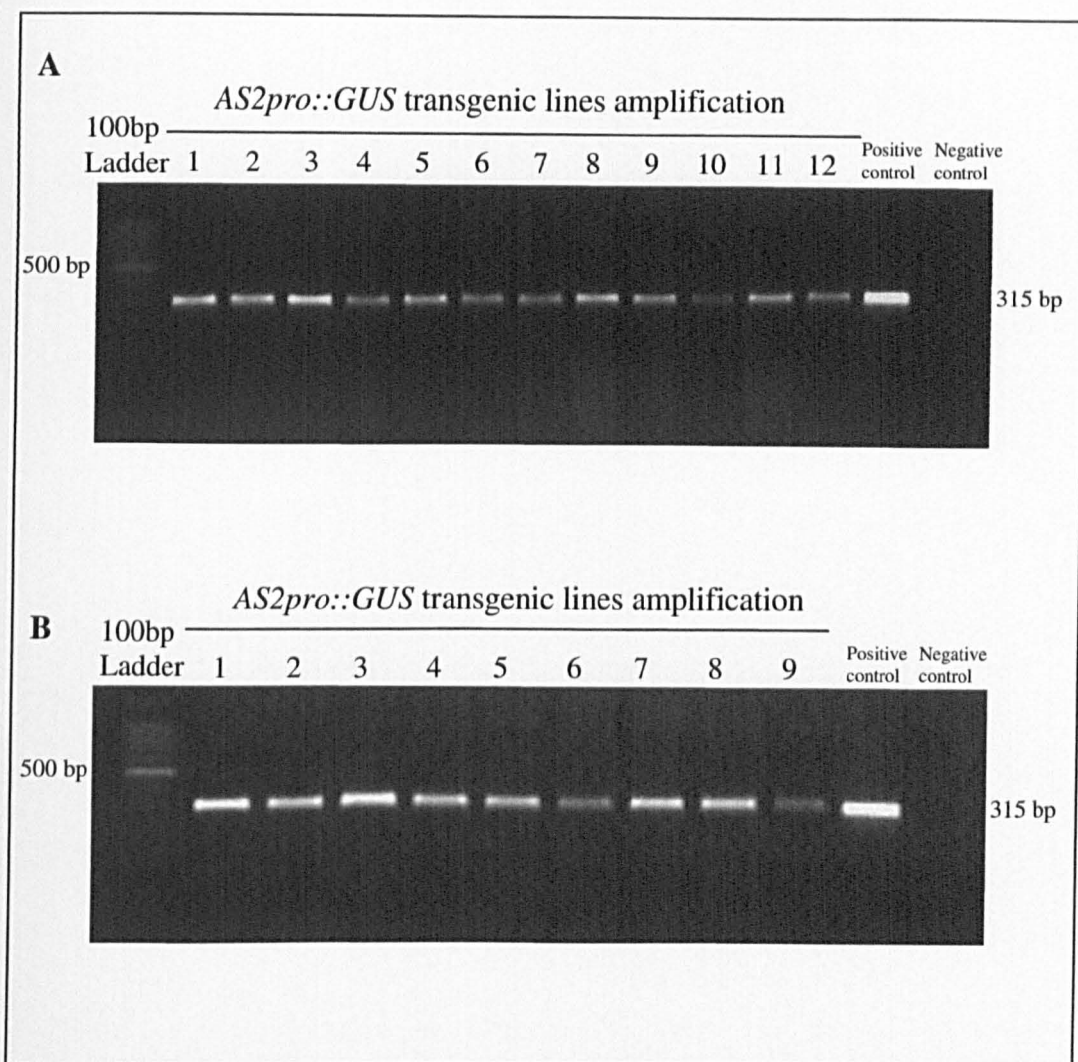


Figure 4.27 PCR amplification of the T1 transformants. Primers used for transgene amplification include pBI101.2for and AS2rev4, (A) Amplification of transgene in T1 progeny of the *hws-1* transformed plants. (B) Amplification of transgene in T1 progeny of the Col-0 wild type transformed plants. The T1 progeny has yielded 12 *hws-1* positively transformed plants and 9 Col-0 wild type positively transformed plants.

Fourteen day old *AS2pro::GUS* transformed Col-0 wild type and *hws-1* young buds and flowers (position 2-6, 9, 11, 16 (where position 1 is the first flower when petals are visible)) were GUS stained and the pattern of expression was identified after 24 h incubation at 37°C in *GUS* substrate. Analysis of the expression of *GUS* reporter gene fused to *AS2* promoter revealed that *AS2pro::GUS* expression is detected in the anther filaments and at the base of floral organs of young buds of Col-0 wild type (Figure 4.28). At flower

positions 2-6 and 9, expression is detected not only in the filaments and floral organ base, but also in petal venation. *GUS* expression is observed along the floral pedicels and more strongly in the axils of the pedicels. Flower positions 12 and 16 show strong *GUS* expression at the abscission zone and the flower pedicel. Expression is also detected in the silique valve margins at positions 12 and 16. *AS2pro::GUS* expression is detected in both flowers and leaves of *hws-1*. In young buds of *hws-1*, *AS2pro::GUS* expression is observed in anther filaments and the floral organ base (Figure 4.29). Flower positions 2-6 show expression at the filaments and strong expression the base of floral organs. Expression is also seen in the axils of floral pedicels. At position 9, the expression level at the filament was diminished and more specifically expressed at the abscission zone of floral organs. This expression in the abscission zone is more visible at positions 12 and 16. These observations show that *AS2* expression in the floral pedicels and the petals is not detected in *hws-1*. As the flower matures, the expression of *AS2* in *hws-1* is limited to the floral abscission zone.

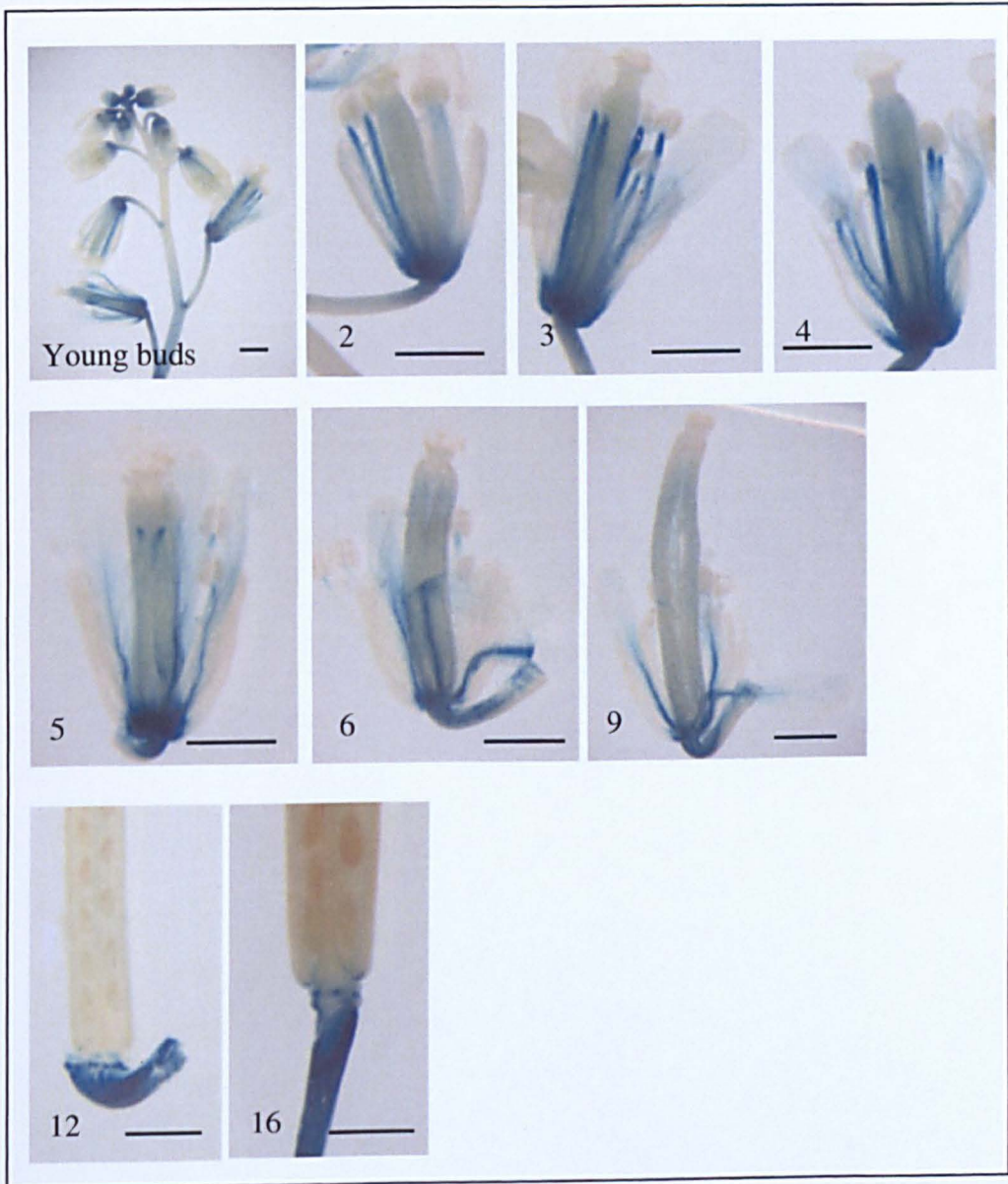


Figure 4.28 Expression analysis of *AS2_{pro}::GUS* transformed Col-0 wild type T1 progeny. *GUS* expression pattern on young buds and at flower position 2-6, 9, 12 and 16, where position 1 is the first flower when petals are visible. Bars = 1mm.

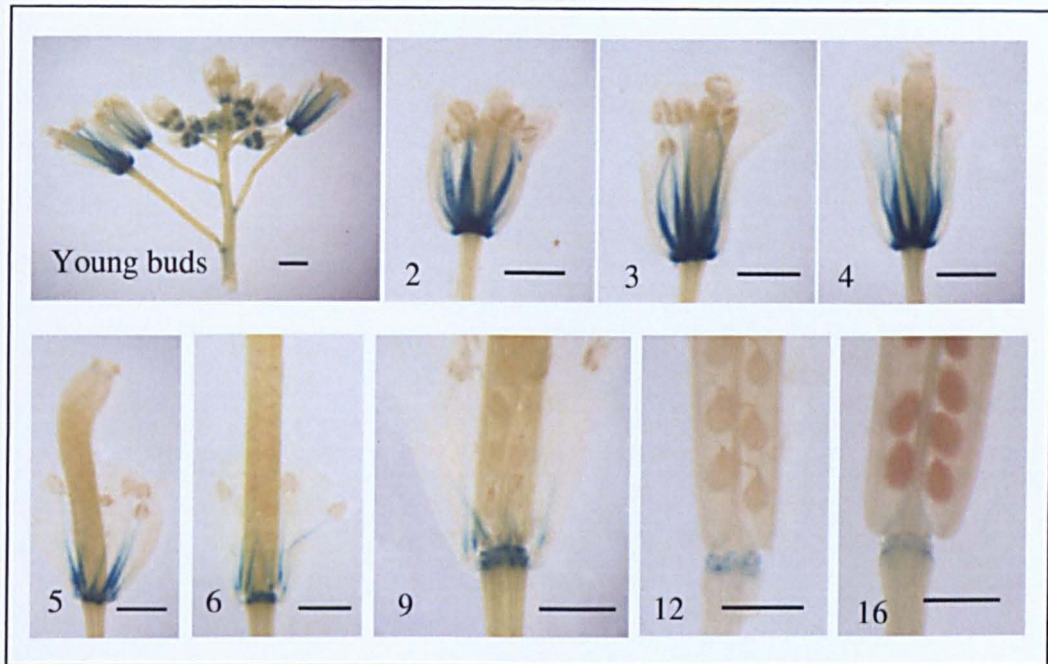


Figure 4.29 Expression analysis of $AS2_{pro}::GUS$ transformed *hws-1* T1 progeny. *GUS* expression pattern on young buds and at flower position 2-6, 9, 12 and 16, where position 1 is the first flower when petals are visible. Bars = 1mm.

GUS expression was also analysed in $AS2_{pro}::GUS$ transformed Col-0 wild type and *hws-1* two week old seedlings. The analysis has shown that *AS2* is expressed in leaf meristem and in the petioles of young leaves in both Col-0 wild type (Figure 4.30 A and B) and *hws-1* (Figure 4.30 C and D). *GUS* expression is stronger in Col-0 wild type incipient leaves compared to *hws-1* incipient leaves where expression was more restricted to the leaf petioles and veins. Expression was also observed on the seedling stem in Col-0 wild type and was absent in *hws-1* seedling stem. The *GUS* expression analysis shows that in the absence of *HWS*, $AS2::GUS$ expression level is much more discrete.

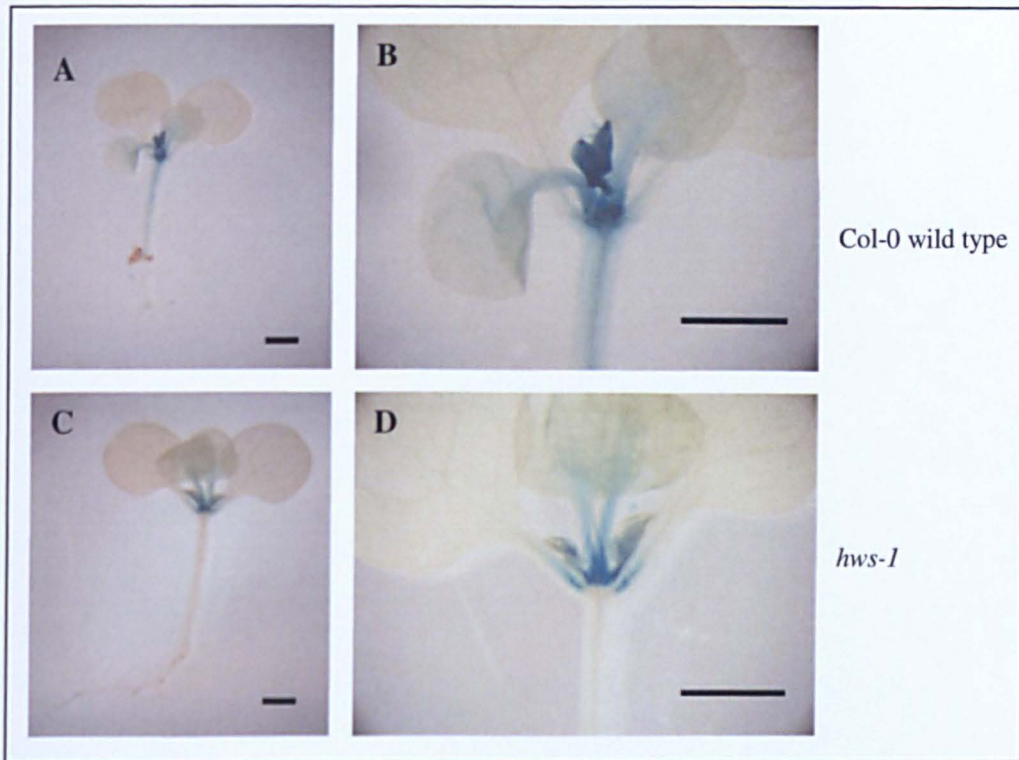


Figure 4.30 *GUS* expression in two week old seedlings of *AS2_{pro}::GUS* transformed Col-0 wild type and *hws-1*. (A and B) *AS2_{pro}::GUS* expression on Col-0 wild type. (C and D) *AS2_{pro}::GUS* expression on *hws-1*.

4.2.5 Gene expression analysis of 80.5

Gene expression analysis of several genes in Col-0 wild type, *hws-1*, *Pro_{35S}::HWS*, *80.5/hws-1*, *80.5/colwt* and *as2-1* were investigated using RT-PCR analysis. cDNA was obtained from leaf and inflorescence tissue samples and amplified using RT-PCR with specific primer of *HWS*, *AS1*, *AS2*, *CUC1*, *CUC2*, *LFY*, *API* and *PTL*. CBP (cap-binding protein) was used as a positive control for the gene expression analysis (Figure 4.31). Expression of *HWS*, *AS1* and *AS2* is detected in all the genotypes both in inflorescence and in leaves. Expression level of *HWS* is greatly increased in *Pro_{35S}::HWS* due to the *HWS* gene overexpression. The expression level of *CUC1* and *CUC2* is reduced in *80.5/hws-1* and up-regulated in *Pro_{35S}::HWS* inflorescence compared to the others. *CUC1* and *CUC2* are not expressed in the leaves of these plants. *LFY* is also expressed in the inflorescence of all the genotypes, but expression is not

detected in the leaves except for *80.5/hws-1*. The loss of gene function of either *hws-1* or *80.5* did not yield any *LFY* expression in the leaves. However the loss of gene function of both *hws-1* and *80.5* has resulted in the expression of *LFY*. Gene expression of *API* is detected in inflorescence of all varieties however expression is absent in the leaves. Weak expression of *PTL* can be observed in the inflorescence of *Pro_{35S}::HWS* and *80.5/hws-1* as well as in the leaves of *hws-1* and *80.5/hws-1*.

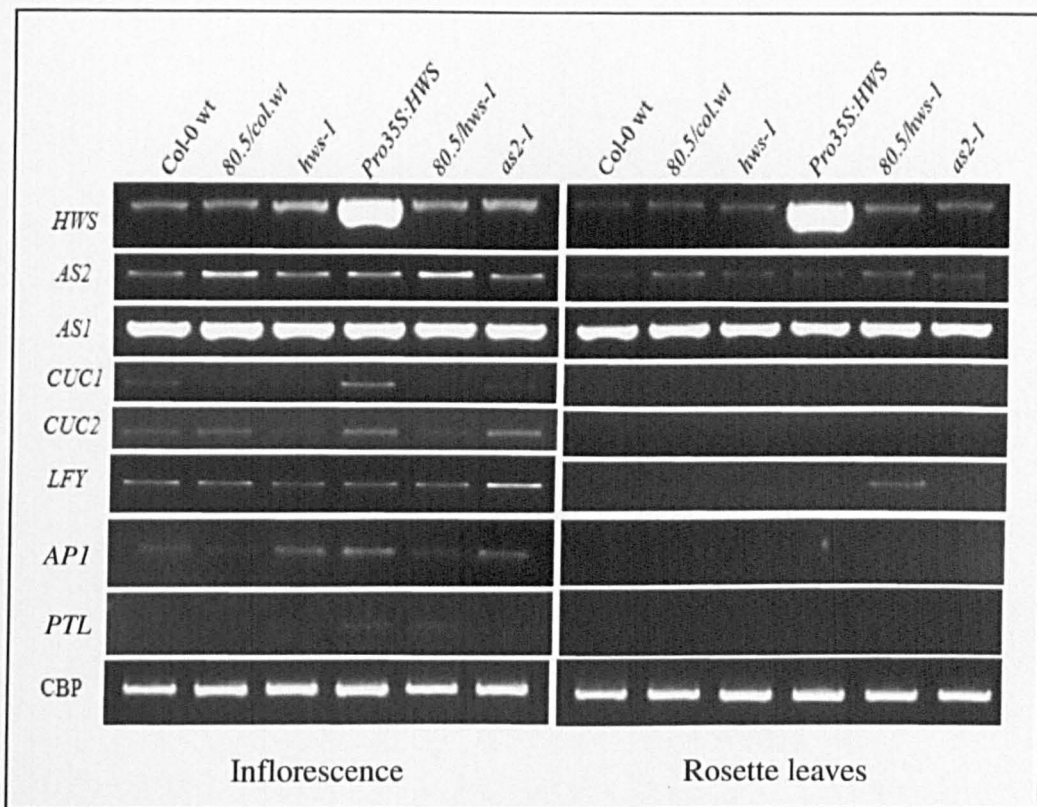


Figure 4.31 Gene expression analysis of inflorescence and leaves of Col-0 wild type, *hws-1*, *Pro_{35S}::HWS*, *80.5/hws-1*, *80.5/colwt* and *as2-1* cDNA using RT-PCR analysis. CBP is used as a positive control.

4.2.6 Genetic interactions of *80.5* and *Pro_{35S}::HWS*

A cross between *80.5/colwt* and *Pro_{35S}::HWS* was conducted to identify *80.5/Pro_{35S}::HWS* double mutant phenotype. A population of 24 F₂ plants were analysed for the identification of the double mutant. The F₂ progeny demonstrated a segregation ratio of 3:1, *Pro_{35S}::HWS*:*80.5*. This was expected since the *Pro_{35S}::HWS* was dominant and *80.5* is a recessive mutation.

Genomic DNA from the 24 F2 progeny plants was obtained for PCR amplification using *Pro_{35S}::HWS* specific primers (Figure 4.32 A). Those that displayed a double mutant phenotype (4, 6, 8, 9, 15 and 23) were amplified using *80.5* specific primers, MUTANTfor and MISMATCHrev (Figure 4.32 B). These primer sets identify *Pro_{35S}::HWS:80.5* homozygous plants and *80.5* homozygous plants. The PCR amplification shows that plants 4, 8 and 15 demonstrates a phenotype characteristic of *80.5/Pro_{35S}::HWS* double mutant.

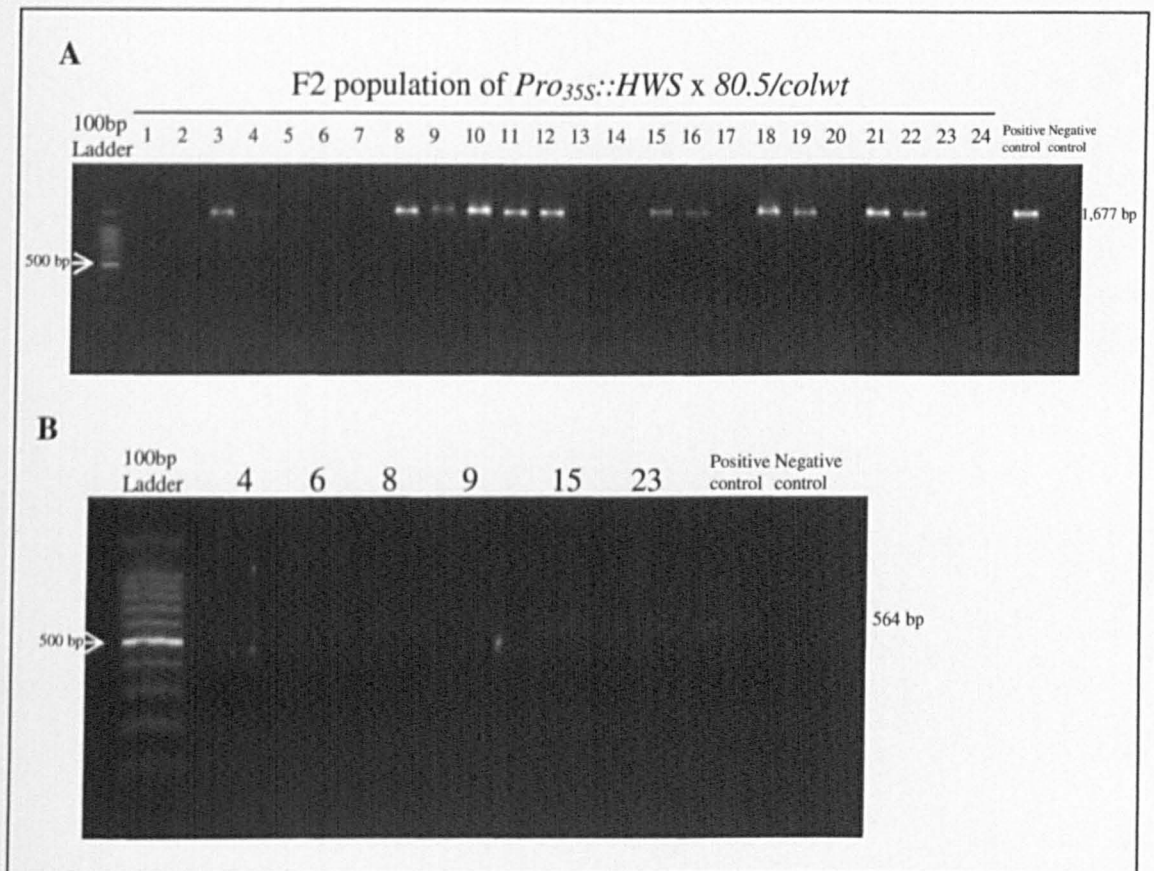


Figure 4.32 PCR amplification for the selection of *80.5/Pro_{35S}::HWS* double mutant. (A) The genomic DNA of a population of 24 F2 progeny plants as amplified by PCR using *Pro_{35S}::HWS* specific primers. (B) *80.5* specific primers used to amplify plants 4, 6, 8, 9, 15 and 23 which showed a phenotype that could of on double mutant.

Phenotypic analysis of the *80.5/Pro_{35S}::HWS* double mutant demonstrated an overall phenotype similar to *80.5*. The *80.5/Pro_{35S}::HWS* double mutant also showed a greater and a more distinctive width between boundary domains of adjacent sepals and petals than *80.5* (Figure 4.33 E) as well as *Pro_{35S}::HWS* (Figure 4.33 D) due to increased narrowing of the sepal and petal base margins (Figure 4.33 F). The double mutant has a disrupted petal orientation ((Figure 4.33 C) equivalent to *80.5* (Figure 4.33 B) unlike *Pro_{35S}::HWS* (Figure 4.33 A). However the petals of the double mutant are smaller in size compared to *Pro_{35S}::HWS* and *80.5* resulting in increased width between petal boundaries. The leaf morphology of *80.5/Pro_{35S}::HWS* double mutant is similar to *80.5* (Figure 4.33 H) compared to *Pro_{35S}::HWS* (Figure 4.33 G), but the rosette leaves are more serrated (Figure 4.33 I) and it has an increase in leaflet-like structure (Figure 4.33 J). The overall phyllotactic pattern of *80.5/Pro_{35S}::HWS* (Figure 4.33 K) double mutant is normal.



Figure 4.33 Phenotypic characteristics of *Pro_{35S}::HWS*, *80.5/colwt* and *80.5/Pro_{35S}::HWS* double mutant. (A, D and G) Flower and seedling phenotype of *Pro_{35S}::HWS*. (B, E and H) Flower and seedling phenotype of *80.5/colwt*. (C, F and I) Flower and seedling phenotype of *80.5/Pro_{35S}::HWS* double mutant. (J) 22 day old leaf morphology of *80.5/Pro_{35S}::HWS* double mutant showing the leaflet-like structure (arrow). (K) six weeks old *80.5/Pro_{35S}::HWS* double mutant plant showing a phenotype similar to *80.5*. Bars (A-F) = 1mm, Bars (G-K) = 1cm

4.2.7 Genetic interactions of *80.5* and *UFO*

A cross between *80.5/colwt* and *ufo-2* was conducted to identify *80.5/ufo-2* double mutant phenotype. This was carried out since *UFO* is the closest F-box gene to *HWS* and to see whether the floral organ phenotype is affected by a double mutation leading to correlation between floral meristem identity and adaxial-abaxial identity. Previous analysis on the *hws/ufo* double mutant showed a flowerless filamentous phenotype (Zhang *et al.*, unpublished data). The *ufo-2* mutant was used since it is stronger allele of *UFO* than other *UFO* alleles. A population of 24 F₂ plants were analysed for the identification of the double mutant. Genomic DNA from the 24 F₂ progeny plants was obtained for PCR amplification using *UFO-2* specific primers, (Figure 4.34 A), *80.5* specific primers (Figure 4.34 B) and specific primers design to detect wild type (Figure 4.34 C). These primer sets identify *ufo-2* homozygous plants and *80.5* homozygous plants. The PCR amplification shows that plants 4 and 13 demonstrate a genotype characteristic of *80.5/ufo-2* double mutant.

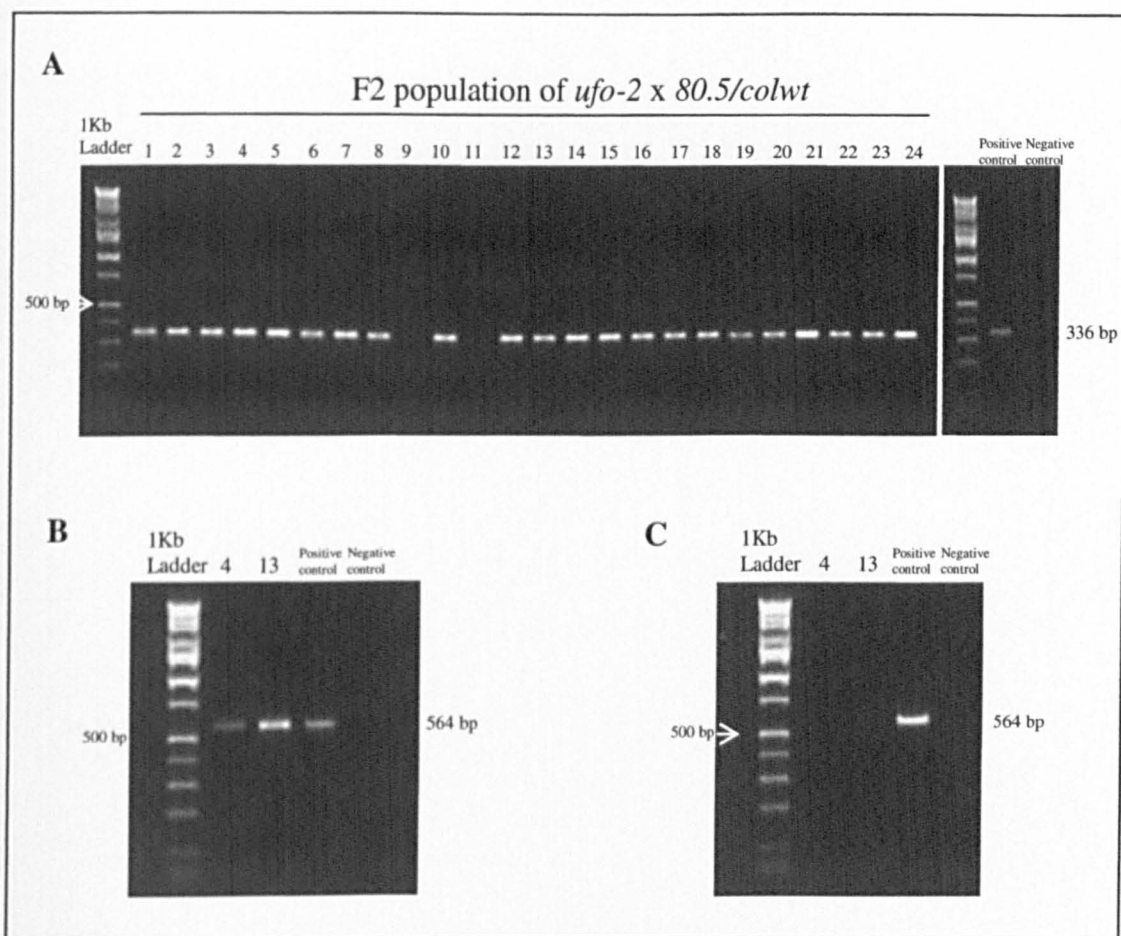


Figure 4.34 PCR amplification for the selection of *80.5/ufo-2* double mutant. (A) PCR amplification of the 24 F2 progeny plant tissue with *UFO-2* specific primers. (B) PCR amplification of plants 4 and 13, which displayed a double mutant phenotype, using *80.5* specific primers. (C) Amplification of wild type genomic DNA using specific primers designed to detect wild type of *80.5* mutant.

In Comparison to *ufo-2*, which lacks flower petals (Figure 4.35 D), and *80.5* (Figure 4.35 A), *80.5/ufo-2* double mutant display flowerless filamentous phenotype at the primary and secondary inflorescences (Figure 4.35 E and F). Approximately 95% of the *80.5/ufo2* double mutant flowers displayed flowerless inflorescences. Therefore the double mutant did not produce any viable seeds. The leaf morphology of *80.5/ufo-2* double mutant was similar to wild type (Figure 4.35 E) whereas *80.5/colwt* show abaxialized rosette leaves (Figure 4.35 B) and *ufo-2* show rounder and slightly adaxialized leaves (Figure 4.35 C). The *80.5/ufo2* double mutant rescue the distinctive abaxialization of *80.5* single mutant leaves.

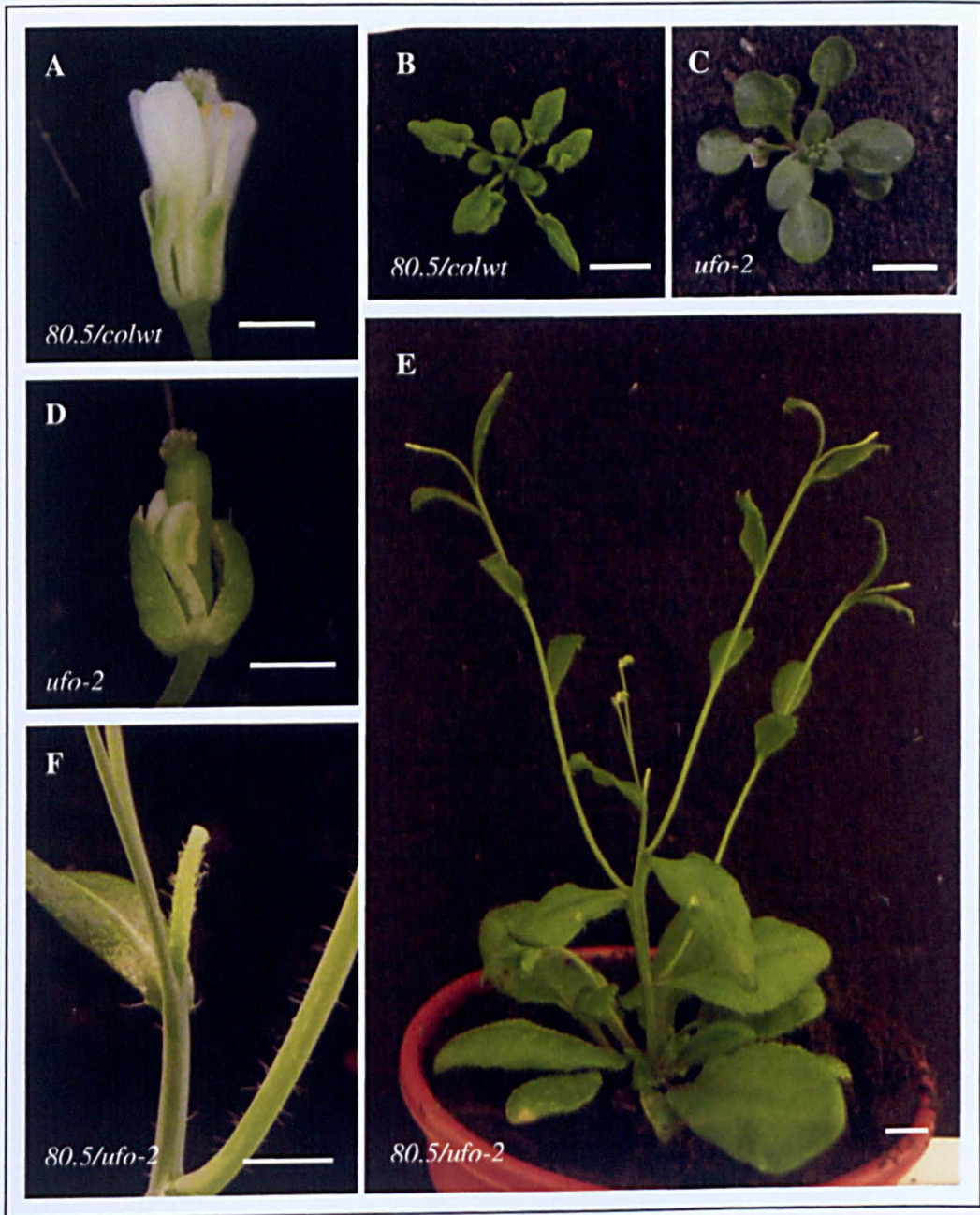


Figure 4.35 Phenotypic characteristics of *80.5/colwt*, *ufo-2* and *80.5/ufo-2* double mutant. (A and B) Flower and seedling morphology of *80.5/colwt*. (C and D) Flower and seedling morphology of *ufo-2*. (E) *80.5/ufo-2* double mutant demonstrating a flowerless and filamentous structure at the inflorescence. (F) A closer view of the filamentous inflorescence of *80.5/ufo-2* double mutant. Bars (A) and (D) = 1mm, Bars (B), (C), (E) = 1cm, Bar (F) = 5mm

4.3 Chapter discussion

4.3.1 Phenotype of the *80.5* mutant

The *80.5* mutant was isolated from an EMS mutagenized population of *hws-1*, due to its ability to rescue the *hws-1* mutant phenotype. The *80.5* mutant phenotype also displays asymmetric leaf morphology and floral organ orientation. The downward curling of *80.5* leaf lamina indicates that the leaves are abaxialized and the asymmetric leaf shape of *80.5* compared to Col-0 wild type and *hws-1* demonstrates that it may be involved in establishing leaf symmetry. Several rosette leaves of *80.5* also demonstrate the lack of a distinct midvein and asymmetric leaf venations compared to Col-0 and *hws-1* rosettes. Similar characteristics in leaf phenotype can be observed in *as2* mutants. Loss of function of the *AS2* gene induces abaxial domain growth indicating that *AS2* is involved in adaxial domain suppression (Semiarti *et al.*, 2001). The phenotype of *80.5* in Col-0 wild type background is more severe than that of *80.5* in *hws-1* background. Leaf phenotype of *80.5/colwt* displays more leaflet-like structures on the petiole and leaf lobes than that of *80.5/hws-1*. The leaf lobes are only visible from the eighth leaf in *80.5/hws-1*, whereas leaf lobes can be identified from the third rosette leaf in *80.5/colwt*. The general rosette leaf size of *80.5/hws-1* is smaller from the cotyledons onwards with shorter petioles than that of *80.5/colwt*. *80.5/hws-1* leaf morphology exhibit traits that are less distinct than *80.5/colwt*. It has been shown that ectopic expression of class-1 *KNOX* genes in *as2* mutants can result from a decrease in leaf size due to a repression of the gibberellin (GA) pathway in *as2* mutants (Ikezaki *et al.*, 2010). Loss of *HWS* gene function may be repressing the expression of *AS2* gene, since the *hws-1* sepal fusion phenotype is rescued in the *80.5/hws-1* double mutant. The repression of *AS2* may lead to a further increase in expression of class-1 *KNOX* genes, therefore resulting in increased reduction in *80.5/hws-1* leaf size compared to *80.5/colwt*. *HWS* gene loss-of-function may also control the effect of leaf lobes and leaflet-like structures in *80.5/hws-1* double mutant. However this may be an indirect process since the effect of leaf lobes and leaflet-like structures are not completely eliminated in *80.5/hws-1*.

The leaf morphology of *80.5/colwt* is characteristically similar to the *as2-1* leaf phenotype, which is a strong allele of *as2* that consists of a 13 bp deletion resulting in frame shift leading to a premature termination of the protein (Iwakawa *et al.*, 2002). Comparisons between *80.5* and weak *as2* alleles, *as2-4* and *as2-101*, seedlings show that the leaf phenotype is distinctly different indicating that *80.5* may be a strong allele of *as2*. The difference between seedling size of *80.5/hws-1* and *80.5/colwt* may be a factor influenced by the loss of the *HWS* gene function. The differences in seedling sizes are contributed by the differences in leaf size as mentioned before.

Floral organs of *80.5* demonstrated several defects in sepal and petal phenotype. Both sepals and petals of *80.5* showed narrowed sizes resulting in open spaces between flanking sepals and petals. Unlike the *hws-1* mutant sepals, *80.5* did not show any fusion of adjacent sepals and petals confirming the rescue of the *hws-1* mutant phenotype. Floral architecture of *80.5* also demonstrated abnormal orientation of the petals within mutant flowers similar to the *as2* floral morphology (Xu *et al.*, 2008). The inward facing concave adaxial pattern of Col-0 wild type and *hws-1* mutant petals was not observed in the *80.5* petals causing mis-orientation of petal primordium. Compared to Col-0 wild type and *hws-1*, the inflorescence of *80.5* generates floral buds that experience premature opening. Similar characteristics in floral architecture of *80.5* can be observed in *as2* mutant flowers. The petal orientation of *80.5* is comparable to *as2-1* unlike *as2-4* and *as2-101*. It has been reported using in situ hybridisation that *AS2* conveys a pattern of polar expression in floral organs and that *AS2* function is spatially and temporally regulated throughout floral development (Xu *et al.*, 2008). One distinctive trait between *80.5/hws-1* and *80.5/colwt* is the partially abaxialized *80.5/hws-1* sepal phenotype that is absent in *80.5/colwt*. This downward bending of sepals may be a factor contributed by the loss of *HWS* function resulting in further abaxialization of *80.5* mutants compared to *as2* mutants. This indicates that *HWS* may be directly or indirectly involved in the adaxial-abaxial pathway.

Primary root measurements of *80.5/hws-1* and *80.5/colwt* with Col-0 wild type and *hws-1* have shown that a significant increase in root growth is

observed in both *80.5/hws-1* and *80.5/colwt* compared to Col-0 wild type and *hws-1*. Root measurements have not been analysed previously in *as2* mutants. This increase in root growth in *80.5* may be due to enhanced auxin response factors as *AS2* is involved in repression of *ETT/ARF3*, which plays a role in abaxial identification (Ishibash *et al.*, 2012).

4.3.2 Isolation and mapping of the *80.5* locus

In order to obtain a mapping population, *80.5/hws-1* was crossed with *ffo1*, an allele of *HWS* in the *Landsberg* ecotype (Gonzalez-Carranza, unpublished data). DNA of 64 plants from 288 F2 progeny plants that exhibited *80.5/hws-1* phenotype were analysed using InDel marker polymorphism by Dr. Janny Peters (Radboud University, Nijmegen) (Peters *et al.*, 2004). The *80.5* mutant was mapped to a region of 4.2 Mb on chromosome 1 between *nga280* (20,877,364 bp) and *CER452443* (25,117,783 bp) using InDel marker polymorphism. Research on publicly available databases such as TAIR for candidate genes showed that the gene *AS2* has also been mapped to this region in chromosome 1, making *AS2* a feasible candidate for *80.5* mutant identification. The *80.5* mutant was sequenced to identify the nature of the mutation using *AS2* primers. Sequence analysis demonstrated a point mutation of a single base pair transition from C to T, 61 bp downstream of the start of the *AS2* coding region introducing an amino acid transition from Glutamine to an ochre stop codon, resulting in a premature termination of the protein. The mutant *80.5* shows a truncated version of the predicted *AS2* protein and indicates that *80.5* is an allele of the *AS2* gene. This may explain the severe leaf phenotype of *80.5* similar to the *as2-1* mutant, which also results in a premature termination of *AS2*, confirming that *80.5* is a strong allele of *as2*.

Segregation of the *80.5/colwt* mutant was obtained from an F2 population of a cross between *80.5/hws-1* and Col-0 wild type. The analysis of the F2 progeny showed a 3:1 Wild type: mutant segregation ratio demonstrating that *80.5* is caused by a single, recessive nuclear mutation. Complementation test between *80.5/colwt* and *as2-1* was conducted for

functional allelism. The F1 progeny demonstrated *as2* mutant phenotype indicating that *80.5/colwt* and *as2-1* are allelic. The progeny analyses show that *80.5* and *as2-1* mutations are alleles of the same gene.

Furthermore complementation analyses were carried out to prove that *80.5* is encoded by the *AS2* gene. This was achieved by creating a construct consisting of the *AS2* promoter region and the *AS2* coding region and transforming it into *80.5/hws-1*, which leads to a T1 population with *hws-1* phenotype. This confirmed that *80.5* encodes *AS2* and further confirmation of the complementation analysis was achieved by segregating the T2 population which showed a 3:1 ratio of *hws-1*: *80.5* phenotype respectively. These analyses correlated with the phenotypic characteristics of *80.5/colwt* and *as2-1* mutants in terms of adaxialized leaf morphology, leaf lobes and leaflet-like structures, disrupted petal orientation and premature opening of incipient buds.

4.3.3 Expression analysis of *80.5*

To analyse the genetic consequences of the expression of different genes, RT-PCR analysis on *80.5*, *hws-1* mutants were carried out to shed some light on the expression pattern of these organ identity genes. The sepal fusion phenotype of *hws-1* mutant plants phenocopies the *cuc1cuc2* double mutant and the ectopic expression of *miR164* (Laufs *et al.*, 2004; Mallory *et al.*, 2004b). Furthermore the *hws-1* sepal fusion phenotype is rescued by *80.5*, which is an allele of *as2*. These phenotypic observations are supported by genetic analysis of *CUC1* and *CUC2* expression in *hws-1* and *as2* mutants. An upregulation of *CUC1* and *CUC2* expression is observed in the inflorescence of *Pro_{35S}::HWS* and *as2* mutant. A downregulation of *CUC1* and *CUC2* expression is observed in *hws-1* mutant inflorescences. These results are supported by earlier findings that show *AS2* function partially suppresses the *CUC1* overexpression (*35S::CUC1*) phenotype (Hibara *et al.*, 2003). It was also demonstrated that *35S::CUC1* phenotype is genetically enhanced by mutation on *AS2* due to the similarity in *35S::CUC1/as2* phenotype with that of affected *35S::CUC1* phenotype. The double mutant, *cuc1cuc2* is partially

rescued by the loss of function mutation *as1*, where *AS1* is regulated in the same pathway as *AS2* (Hibara *et al.*, 2003). The expression levels of *CUC1* and *CUC2* are downregulated in the *80.5/hws-1* double mutant indicating that *AS2* loss-of-function alone may not be involved in the regulation of *CUC1* and *CUC2* expression and that *HWS* activity is required for this up-regulation of *CUC1* and *CUC2* expression. Increased expression of *CUC1* and *CUC2* in *as2-1* and *80.5/colwt* may be due to *HWS* gene expression. This shows that *HWS* is regulated upstream of *AS2* gene function. *CUC1* and *CUC2* expression may also be downregulated in the *80.5/hws-1* double mutant by post-transcriptional downregulation of *CUC1* and *CUC2* via *MIR164* accumulation.

Previous studies have shown that the function of *AS2* along with *AS1* and the C₂H₄ transcription factor gene, *JAG*, in sepal and petal primordia represses boundary specifying genes *CUC1*, *CUC2* and *PTL* to promote normal floral organ development (Xu *et al.*, 2008). *JAG* is involved in promoting morphogenesis in various lateral organs in *Arabidopsis* (Dinneny *et al.*, 2004). An increased level of *PTL* expression is observed in *Pro35S::HWS* and *80.5/hws-1* double mutant. This shows that *PTL* expression is up-regulated by loss of *AS2* and *HWS* gene function. Loss-of-function *hws-1* mutant is involved in repressing *AS2* function which in turn leads to an increase in *PTL* expression. These results demonstrate that *AS2* and *HWS* interact to co-regulate the boundary specific genes, *CUC1*, *CUC2* and *PTL*. The increase in *PTL* expression in *Pro35S::HWS* inflorescence correlates with enhanced expression of other boundary specific gene, *CUC1* and *CUC2* in *Pro35S::HWS*.

LFY is known to be involved in decreased cell elongation at the adaxial domain of the pedicel base. Loss-of-function *lfy* mutant phenotype leads to abaxialized pedicels which have a reduction in adaxial cortical cells. Steroid activated gain-of-function of *LFY* results in enhanced ectopic expression of *AS2* and *REV* and conditional *35S::LFY* pedicel architecture is similar to that of *bp* mutants (Yamaguchi *et al.*, 2012). The *as2* mutant partly suppresses the pedicel orientation and length phenotypic defects of *35S::LFY*. This shows that *LFY* activity determines adaxial cell fate in the pedicel and regulates proper length and orientation of the pedicel by promoting *AS2* expression which

subsequently leads to *BP* suppression (Yamaguchi *et al.*, 2012). *LFY* expression in leaves of *as2* mutant is reduced, however loss-of-function of both *as2* and *hws* lead to an enhanced expression of *LFY* as seen from the RT-PCR analysis (Figure 4.31). *GUS* expression analyses have shown that *LFY* is expressed in newly emerging leaf primordia, but expression is deficient in older leaves (Blázquez *et al.*, 1997). This indicates that *HWS* and *AS2* interact to negatively regulate *LFY* expression in older leaves. A change in *LFY* expression was not observed in the inflorescence of single and double mutants.

GUS expression analysis of *AS2* in Col-0 wild type and *hws-1* has shown that the expression of *AS2* is restricted to stamen filaments and the base of floral organ meristem in *hws-1* whereas expression is observed along the pedicels, filaments and petal venation in Col-0 wild type. This shows that loss of *HWS* gene function leads to repression of *AS2* expression in flower pedicels. *GUS* activity is observed in Col-0 wild type and *hws-1* SAM as well as petioles of young leaves. Expression is also seen in the petiole base of Col-0 wild type and *hws-1* cotyledons. *GUS* expression is observed in the stem and strongly expressed in incipient leaves as well as their trichomes of Col-0 wild type. Expression is not observed in the stem of *hws-1* and only expressed on the petiole and venation of incipient leaves. This is further evidence that loss of *HWS* gene function leads to a repression of *AS2* expression in seedling stem and tissues and trichomes of incipient leaves.

4.3.4 Genetic Crosses between *80.5* and selected *Arabidopsis* mutants

Genetic crosses between *80.5* and *Pro_{35S}::HWS* have shown that *80.5/Pro_{35S}::HWS* double mutant display a phenotype similar to *80.5* single mutants. This may be due to the repression of *AS2* expression in leaves by enhanced *HWS* gene function which results in a phenotype similar to that of *as2* loss-of-function mutant. The *80.5/Pro_{35S}::HWS* double mutant however did display more aberrant differences to *80.5* single mutant in that the width of the boundary domain between sepals and petals was increased as well as more

serrated leaves with elongated petioles. The failure of *Pro_{35S}::HWS* to rescue *80.5* mutant leaf phenotype is consistent with the unchanged expression levels of *HWS* in *80.5* mutants.

Genetic crosses between *80.5* and *ufo-2* resulted in double mutants with the majority of flowers substituted by flowerless inflorescences producing filaments. Previous analyses on *hws/ufo* double mutants showed a similar phenotype to that of *80.5/ufo* showing a correlation between floral meristem identity genes and adaxial-abaxial identity (Zhang *et al.*, unpublished data). Flowerless pedicels were also observed in *fil/lfy* double mutants (Sawa *et al.*, 1999). *UFO* is known to act as a transcription co-factor of *LFY* resulting in *LFY* promoting *AP3* expression (Chae *et al.*, 2008). The *80.5/ufo-2* double mutant has shown that both *AS2* and *UFO* are important in floral meristem formation. This is a novel function since *AS2* has not previously been described as a regulator of floral meristem organisation.

CHAPTER 5

General discussion

In an attempt to identify the substrate(s) associated with *HWS* for degradation, an EMS mutagenesis of the *hws-1* mutant was undertaken, which isolates gene products that are interacting with HWS using a suppressor analysis strategy. This project focuses on two of the *hws-1* suppressors identified from the EMS mutagenesis *hws-1* populations. Characterization of the suppressor lines *43.1* and *80.5* has revealed that they are alleles of *HST* gene, which is involved in miRNA biogenesis, and the *AS2* gene, which is involved in adaxial-abaxial polarity, respectively.

5.1 The role of the *HWS* gene in miRNA biogenesis

Phenotypic analysis of *hws-1* has shown that it phenocopies ectopic expression of *miR164b* and *cuc1cuc2* double mutant phenotype. The *hws-1* mutant has been crossed to miRNA pathway genes which rescues the *hws-1* sepal fusion phenotype (Gonzalez-Carranza, unpublished data). This analysis has led to the hypothesis that *hws-1* may interact with miRNA biogenesis. Characterization of the *hws-1* suppressor line *43.1* has revealed that it is an allele of *HST* gene, which is involved in the miRNA biogenesis. The *43.1/hws-1* double mutant rescues the distinctive sepal fusion phenotype of *hws-1*. Other phenotypic changes observed in this double mutant include increase in petal number in incipient flowers, increase in width of boundary domain between adjacent sepals, abnormal phyllotaxis between internodes and reduction in petiole size of rosette leaves. Similar phenotypic characteristics can also be seen in *miR164c*, which shows extra petals in early occurring flowers; *miR164*-resistant *CUC2*, which shows abnormal phyllotaxis, increase in width of sepal boundary domain; and *miR164*-resistant *CUC1*, which shows a reduction in petiole size of rosette leaves (Laufs *et al.*, 2004; Mallory *et al.*, 2004b; Baker *et al.*, 2005). The increase in boundary domain of adjacent sepals is also observed

on mutants involved in miRNA biogenesis, *dcl1*, *hyl1* and *hen1* (Laufs *et al.*, 2004) as well as *hst-1*. It has been demonstrated that accumulation of mature miRNA164 transcript is enhanced in *hws-1* mutant (Gonzalez-Carranza Z.H. and Zang X., unpublished data). These results suggest that loss of function mutation of *HST* may show reduced levels of *miR164* expression. The *43.1/hws-1* double mutant rescues the sepal fusion phenotype of *hws-1*. The extra petal phenotype in *miR164c* is due to an increase in *CUC1* and *CUC2* mRNA levels, which are targets of *miR164* for degradation (Baker *et al.*, 2005). This suggests that the *hst-1* mutant may show an increase in *CUC1* and *CUC2* expression and since *HWS* is known to repress the *HST* gene expression (Figure 5.1), overexpression of *HWS* would also show an increase in expression of *CUC1* and *CUC2* genes. This is confirmed by the *CUC1* and *CUC2* expression analysis in *hws-1* (Figure 4.31) which shows an increase in accumulation of both *CUC1* and *CUC2* in *Pro_{35S}::HWS* and a decrease in *hws-1* inflorescence. This also supports the phenotypic similarities in sepal fusion of the *hws-1* and *cuc1cuc2* double mutant.

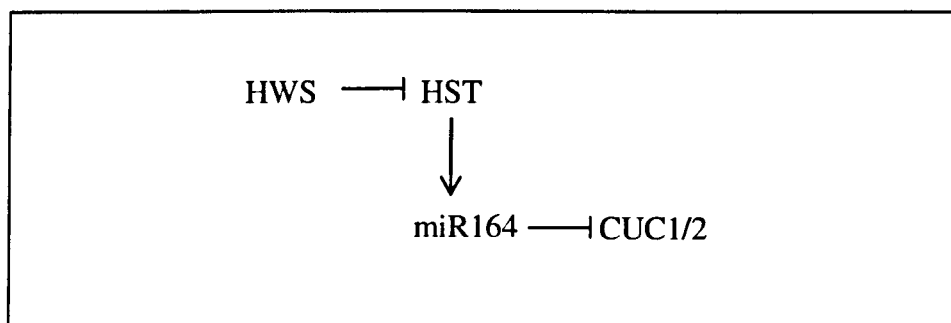


Figure 5.1 *HWS* and *HST* gene interactions. The diagram shows the repression of *HST* by *HWS* gene function which may lead to an upregulation of *CUC1* and *CUC2* gene. Loss of function of *HWS* lead to posttranscriptional downregulation of *CUC1* and *CUC2* by miR164.

The level of *miR165/166* in *hst-1* mutant was reduced compared to wild type (Park *et al.*, 2005). This reduction in *miR165/166* was also seen in overexpressed AS2 protein nuclear localization where a decrease in mature *miR165/166* was observed. As mentioned in section 4.1.2, *miR165/166* is involved in negatively regulating adaxial determinant genes *PHB*, *PHV* and *REV* function. Loss-of-function mutations in *HST* results in a decrease in

miRNA accumulation leading to an increase in *miR165/166* targets, *PHB*, *PHV* and *REV* transcripts (Ueno *et al.*, 2007). Other adaxial determinant genes such as *AS1* and *AS2* are also involved in downregulating *miR165/166* accumulation leading to stabilization of *PHB*, *PHV* and *REV* transcripts (Li *et al.*, 2005; Fu *et al.*, 2007). Characterization of the *80.5* mutant has identified that *HWS* represses the expression of *AS2* since *80.5/hws-1* double mutant rescues the sepal fusion phenotype of *hws-1*. The interaction between *AS2* and *HWS* may lead to negative regulation of *miRNA165/166* accumulation. These findings indicate that *HWS* regulate *miR165/166* levels independently with *HST* and *AS2*. It has been identified that the repression of *miR165/166* accumulation is an indirect process which occurs at a posttranscriptional level (Ueno *et al.*, 2007). These results show that *HWS* is a key player in regulating *miRNA* accumulation in combination with other regulatory genes involved in *miRNA* biogenesis.

CUC1 and *CUC2* are targets for *miR164* expression. Overexpression of *miR164* (*2x35S:miR164*) demonstrates sepal fusion along their margins indicating that it phenocopies the *cuc1cuc2* double mutant. This is achieved by post-transcriptional downregulation of *CUC1* and *CUC2* levels of mRNA via *miR164*. The sepal fusion of *2x35S:miR164* is rescued by the expression of *CUC2* mRNA that is resistant to *miR164*-guided cleavage (*CUC2-m4*) (Laufs *et al.*, 2004). This demonstrates that *CUC1* and *CUC2* loss of function accredited to the flower phenotype observed on *miR164* overexpression. *CUC2-m4* expression also leads to the enlargement of boundary domain resulting in an enhanced spacing between sepals indicating that the target degradation of *CUC1* and *CUC2* by *miRNA* restricts the enlargement of boundary domain (Laufs *et al.*, 2004). The overexpression of *miR164* also generated abnormalities such as fusion of stem and leaves, decrease in rosette leaf petiole size and broadened shape of rosette leaves. These phenotypic abnormalities show that *miR164* is a widespread regulatory element in controlling different developmental organ separation and the accurate localization and dosage of *miR164* is required for proper floral, vegetative and embryonic organ separation (Mallory *et al.*, 2004b). The sepal margin fusion

phenotype is also seen in the *hws-1* mutant, which is rescued by loss-of-function mutants *43.1* and *80.5*.

The double mutants, *as1/jag* and *as2/jag* results in severely under developed sepals and petals with enhanced *CUC1*, *CUC2* and *PTL* expression levels inhibiting sepal primordia cell division. Loss of function of *CUC1*, *CUC2* and *PTL* expression in *as2/jag* rescues the abnormal sepal and petal phenotype indicating that the phenotypic changes are due to the ectopic expression of these three boundary specific genes. In *as2/jag* mutant, ectopic expression of *PTL* and *CUC1* were shown to be present in adaxial region of the sepal and expression of *CUC2* was detected throughout the sepal (Xu *et al.*, 2008). These results demonstrate that *AS2* and *HWS* interact to co-regulate the boundary specific genes, *CUC1*, *CUC2* and *PTL* (Figure 5.2). Petal size is also affected in *43.1/hws-1*, which suggests that there is an association between miRNA biogenesis and boundary specific genes and *HWS* is a key player in this process.

5.2 The role of the *HWS* gene in adaxial-abaxial polarity

Another possibility is that *HWS* is involved in other mechanisms such as the ta-siRNA pathway, which regulates adaxial-abaxial leaf polarity, for the regulation of miRNA accumulation. This hypothesis was developed due to the interaction of *HWS* with *AS2*, which also interacts with *AGO7* (a gene that functions in the ta-siRNA pathway) to negatively regulate miR165/166 accumulation (Li *et al.*, 2005; Xu *et al.*, 2006). These results further show that *HWS* is involved in posttranscriptional gene regulation. The link between *AS2* and *HWS* gene function maybe operate through an indirect pathway. *HWS* may also be involved in SAM-derived signalling as the interaction between leaf primordia and the SAM is important for adaxial-abaxial leaf patterning (Bollman *et al.*, 2003) since *hws-1* partially rescues the adaxialization of *hst-1* leaf phenotype.

5.3 *HWS* and meristem-to-organ boundary

The transcriptional activators of leaf formation, *BOP1* and *BOP2*, which are members of the BTB/ZIP domain proteins, promote *AS2* activation in the leaf proximal and adaxial region near the leaf primordia and SAM boundary. It has been demonstrated that *STM* indirectly or directly represses *BOP1* and *BOP2* expression which leads to the formation of a functional embryonic SAM and the repression of *KNOX* gene function at the leaf base due to induction of *AS2* transcription activity by *BOP1* and *BOP2* is indispensable for the regulation of leaf morphogenesis along the proximodistal and adaxial-abaxial axes. The *BOP* genes in addition to *AS1* and *AS2* are also involved in negatively regulating embryonic *BP* (Jun *et al.*, 2010). In SAM, *STM* is activated by *CUC* gene function during embryogenesis and *CUC* gene expression is then downregulated by *STM* (Rast and Simon, 2008). The expression of *AS2* is downregulated indirectly by *STM* gene function. This is shown by the ectopic expression of *AS2* on *stm-11* embryo subsequent to the *stm* phenotype being apparent (Byrne *et al.*, 2002; Jun *et al.*, 2010). Both *AS2* and *BOP* genes are involved in superimposing genetic pathways (Ha *et al.*, 2007; Jun *et al.*, 2010) (Figure 5.2). Ectopic expression of *HWS* leads to increased accumulation of *CUC1* and *CUC2* genes. This would lead to an activation of *STM* gene function which will indirectly lead to a downregulation of *AS2* expression. This shows further evidence that *HWS* may be involved in SAM-derived signalling.

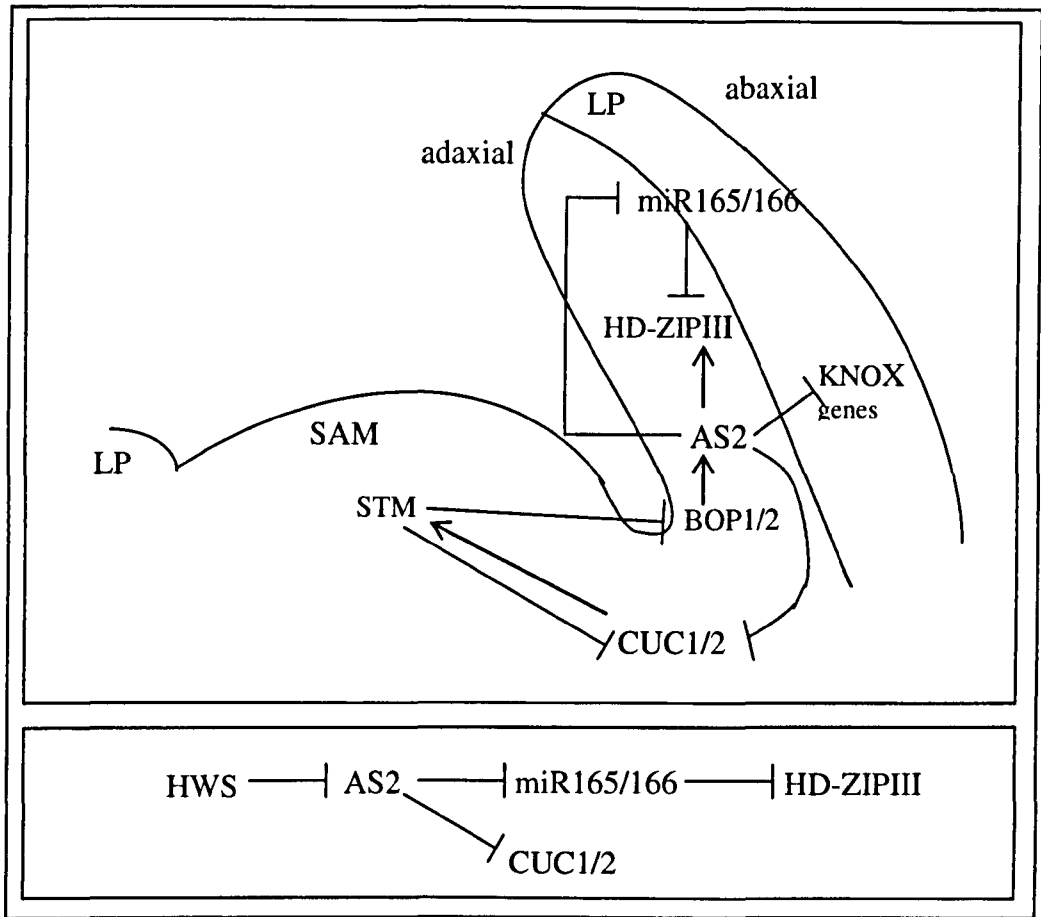


Figure 5.2 *HWS* and adaxial-abaxial gene interactions. *HWS* downregulates *AS2* expression leading to an upregulation of *CUC1* and *CUC2* genes. SAM: shoot apical meristem. LP: leaf primordial.

5.4 Conclusion

EMS mutagenesis of *hws-1* has identified several suppressor lines, two of which were characterized in this project. These suppressor lines, *43.1* and *80.5* rescue the distinctive sepal fusion phenotype of *hws-1* resulting in floral organ shedding during senescence. Characterization of the suppressor lines has identified that *43.1* is an allele of *HST* gene, which is involved in miRNA biogenesis, and *80.5* is an allele of *AS2* gene, which is an adaxial cell fate determinant. Expression analyses have revealed that loss of *HWS* gene function leads to the repression of both *43.1* and *80.5*. Genetic analyses have also confirmed that loss of *HWS* gene function results in an upregulation of *CUC1*

and *CUC2* gene expression. The results obtained in this project have shown that *HWS* is involved in miRNA, adaxial-abaxial and organ boundary signalling, concluding that *HWS* may have a wider function in different signalling pathways than previously proposed.

5.5 Future work

- 5.5.1 The screening of EMS *hws-1* mutant populations in this project has identified 20 suppressor lines from 46 populations, however 14 suppressors were found to be allelic following allelism tests (see appendix). Allelism tests should be carried out on all suppressors that phenocopy each other from a single population as well as between populations. Allelism tests should also be carried out on suppressors from population screenings conducted prior to this project as suppressor lines *231* and *43.1* were found to be allelic.
- 5.5.2 The *43.1/hws-1* double mutant rescues the *hws-1* sepal fusion phenotype. Loss of *HWS* gene function in *43.1/hws-1* may restrict *HST* expression to promote normal sepal separation leading to increase in expression of *CUC1* and *CUC2* boundary specific genes. Expression analysis of *CUC1* and *CUC2* may be conducted using RT-PCR analysis on flower and leaf tissues of *43.1/hws-1* and *43.1/colwt*.
- 5.5.3 In both Col-0 wild type and *hws-1* transformants, *GUS* activity was detected at the floral meristem base. *GFP* expression analysis of *AS2* on *hws-1* and Col-0 wild type at a more cellular level via light and electron microscopy using tissue samples fixed in formaldehyde and embedded in paraffin may determine whether *GFP* activity is expressed at the floral meristem base or restricted to floral organ boundaries.
- 5.5.4 The RT-PCR analysis of the expression of *HWS*, *AS2* and *LFY* have identified that there is no change in expression level between Col-0

wild type *80.5/colwt*, *hws-1*, *Pro_{35S}::HWS*, *80.5/hws-1* and *as2-1* both in inflorescence tissue and leaf tissue. Quantitative RT-PCR analysis of *AS2* and *HWS* expression in Col-0 wild type *80.5/colwt*, *hws-1*, *Pro_{35S}::HWS*, *80.5/hws-1* and *as2-1* would be able to determine quantitatively the differences of these genes in each variety. The *AS2* gene downregulates abaxial determinate *KNOX* (*BP*, *KNAT2* and *KNAT6*) genes. RT-PCR analysis of *KNOX* gene expression on *80.5/colwt*, *hws-1*, *Pro_{35S}::HWS*, *80.5/hws-1* and *as2-1* mutants would determine whether repression of *KNOX* genes by *AS2* is overcome in *hws-1* mutants.

- 5.5.5 It has been previously demonstrated that *as2-1/hst-1* double mutant result in virtually flat leaves whereas *as2-1* single mutant produce abaxialized leaves and *hst-1* produce adaxialized leaves (Ueno et al., 2007). Analysing the interaction between *43.1*, *80.5* and *hws-1* by constructing a triple mutant may give us more information about the role *hws* plays in the phenotype of the triple mutant. The *hws-1* single mutant does not show any abnormalities in leaf phenotype but the interaction between these mutants may lead to a change.
- 5.5.6 Protein analysis from meristematic, flower and leaf tissue using western blot with specific antibodies may determine *HWS* proteins expression which may lead to identification of proteins expressed in specific tissues that may be involved in protein-protein interactions.
- 5.5.7 Ectopic expression of *HWS* leads to increased accumulation of *CUC1* and *CUC2* genes. This would lead to an activation of *STM* gene function which will indirectly lead to a downregulation of *AS2* expression. This shows evidence that *HWS* may be involved in SAM-derived signalling. Microarray analysis may be used to analyse gene expression at meristematic and primordial tissue.

References

- Abramoff M.D., Magelhaes P.J., Ram S.J.** (2004) Image processing with ImageJ. *J. Biophotonics Int.* 11: 36–42.
- Addicott F.T.** (1982) *Abscission*. (University of California Press, Berkeley).
- Aida M., Ishida T., Fukaki H., Fujishawa H., Tasaka M.** (1997) Genes involved in organ separation in *Arabidopsis*: an analysis of the *cup-shaped cotyledon* mutant. *Plant Cell* 9: 841–857.
- Aida M., Tasaka M.** (2006a) Genetic control of shoot organ boundaries. *Curr. Opin. Plant Biol.* 9: 72–77.
- Aida M., Tasaka M.** (2006b) Morphogenesis and patterning at the organ boundaries in the higher plant shoot apex. *Plant Mol. Biol.* 60: 915–928.
- Allen E., Xie Z., Gustafson A.M., Carrington J.C.** (2005) microRNA-directed phasing during trans-acting siRNA biogenesis in plants. *Cell* 121: 207–221.
- Aloni R., Schwalm K., Langhans M., Ullrich C.I.** (2003) Gradual shifts in sites of free-auxin production during leaf-primordium development and their role in vascular differentiation and leaf morphogenesis in *Arabidopsis*. *Planta*. 216: 841–853.
- Alonso J.M., Stepanova A.N., Leisse T.J., Kim C.J. et al.** (2003) Genome-wide insertional mutagenesis of *Arabidopsis thaliana*. *Science*. 301: 653–7.
- Alonso J.M., Ecker J.R.** (2006) Moving forward in reverse: genetic technologies to enable genome-wide phenomic screens in *Arabidopsis*. *Nature Reviews Genetics*. 7: 524–536.
- Alvarez-Buylla E.R., Benítez M., Corvera-Poiré A., Chaos Cador A., de Folter S., de Buen G., Garay-Arroyo A., García-Ponce B., Jaimes-Miranda F., Pérez-Ruiz R.V., Piñeyro-Nelson A., Sánchez-Corrales Y.E.** (2010) Flower development. *Arabidopsis Book* 8: e0127.
- Aukerman M.J., Sakai H.** (2003) Regulation of flowering time and floral organ identity by a MicroRNA and its *APETALA2-like* target genes. *Plant Cell* 15: 2730–2741.
- Baker C.C., Sieber P., Wellmer F. and Meyerowitz E.M.** (2005) The *early extra petals1* mutant uncovers a role for microRNA miR164c in regulating petal number in *Arabidopsis*. *Curr. Biol.* 15: 303–315.
- Bartel D.P.** (2004) MicroRNAs: genomics, biogenesis, mechanism, and function. *Cell* 116: 281–297.

Baumberger N., Baulcombe D.C. (2005) *Arabidopsis* ARGONAUTE1 is an RNA slicer that selectively recruits microRNAs and short interfering RNAs. *Proc Natl Acad Sci USA* 102: 11928–11933.

Benjamins R., Quint A., Weijers D., Hooykaas P., and Offringa R. (2001) The *PINOID* protein kinase regulates organ development in *Arabidopsis* by enhancing polar auxin transport. *Development* 128: 4057-4067.

Benková E., Michniewicz M., Sauer M., Teichmann T., Seifertová D., Jürgens G., Friml J. (2003) Local, efflux-dependent auxin gradients as a common module for plant organ formation. *Cell*. 115: 591–602.

Bharathan G., Sinha N. (2001) The regulation of compound leaf development. *Plant Physiology*. 127: 1533-1538

Bharathan G., Goliber T.E., Moore C., Kessler S., Pham T., Sinha N.R. (2002) Homologies in leaf form inferred from *KNOXI* gene expression during development. *Science*. 296: 1858–1860.

Bilsborough G.D., Runions A., Barkoulas M., Jenkins H.W., Hasson A., Galinha C., Laufs P., Hay A., Prusinkiewicz P., Tsiantis M. (2011) Model for the regulation of *Arabidopsis thaliana* leaf margin development. *Proc Natl Acad Sci*. 108: 3424-9.

Blazquez M., Soowal L., Lee I., Weigel D. (1997) *LEAFY* expression and flower initiation in *Arabidopsis*. *Development* 124: 3835-3844.

Bleecker A., Patterson S.E., (1997) Last exit: Senescence, abscission, and meristem arrest in *Arabidopsis*. *Plant Cell*. 9: 1169–1179.

Bollman K.M., Aukerman M.J., Park M.-Y., Hunter C., Berardini T.Z., Poethig R.S. (2003). *HASTY*, the *Arabidopsis* ortholog of exportin 5/*MSN5*, regulates phase change and morphogenesis. *Development* 130: 1493–1504.

Bonghi C., Rascio N., Ramina A., Casadoro G. (1992) Cellulase and polygalacturonase involvement in the abscission of leaf and fruit explants of peach. *Plant Mol Biol*. 20: 839–848.

Borghi L., Bureau M., Simon R. (2007) *Arabidopsis* *JAGGED LATERAL ORGANS* is expressed in boundaries and coordinates *KNOX* and *PIN* activity. *Plant Cell* 19: 1795–1808.

Bowman J.L., Smyth D.R., Meyerowitz E.M. (1989) Genes directing flower development in *Arabidopsis*. *Plant Cell* 1: 37-52.

Bowman J.L., Alvarez J., Weigel D., Meyerowitz E.M., Smyth D.R. (1993) Control of flower development in *Arabidopsis thaliana* by *APETALA1* and interacting genes. *Development* 119: 721–743.

Bowman J.L., Smyth D.R. (1999) *CRABS CLAW*, a gene that regulates carpel and nectary development in *Arabidopsis*, encodes a novel protein with zinc finger and helix-loop-helix domains. *Development* 126: 2387-2396.

Boyes D.C., Zayed A.M., Ascenzi R., McCaskill A.J., Hoffman N.E., Davis K.R., Görlach J. (2001) Growth stage-based phenotypic analysis of *Arabidopsis*: a model for high throughput functional genomics in plants. *Plant Cell* 13: 1499-510.

Brewer P., Howles P., Dorian K., Griffith M., Ishida T., Kaplan-Levy R., Kilinc A., Smyth D. (2004) *Petal loss*, a trihelix transcription factor gene, regulates perianth architecture in the *Arabidopsis* flower. *Development* 131: 4035–4045.

Brown K.M. (1997) Ethylene and abscission. *Physiol Plant.* 100:567–576.

Breuil-Broyer S., Morel P., de Almeida-Engler J., Coustham V., Negrutiu I., Trehin C. (2004) High-resolution boundary analysis during *Arabidopsis thaliana* flower development. *Plant Journal* 38: 182–192.

Brodersen P., Voinnet O. (2006) The diversity of RNA silencing pathways in plants. *Trends in Genetics.* 22: 268-280.

Brown K.M. (1997) Ethylene and abscission. *Physiol Plant.* 100: 567–576.

Buffard-Morel J., Verdeil J.L., Pannetier C. (1992) Embryogenèse du cocotier (*Cocos nucifera* L.) à partir de tissus foliaires: études histologiques. *Canadian Journal of Botany* 70: 735-741.

Butenko M.A., Patterson S.E., Grinia P.E., Stenvika G.E., Amundsen S.S., Mandalc A., Aalen R.B. (2003) INFLORESCENCE DEFICIENT IN ABSCISSION Controls Floral Organ Abscission in *Arabidopsis* and Identifies a Novel Family of Putative Ligands in Plants. *The Plant Cell*, 15: 2296-2307.

Byrne M.E., Barley R., Curtis M., Arroyo J.M., Dunham M., Hudson A., Martlenssen R.A. (2000) *ASYMMETRIC LEAVES1* mediates leaf patterning and stem cell function in *Arabidopsis*. *Nature.* 4088: 967–971.

Byrne M.E., Simorowski J., Martiensen R.A. (2002) *ASYMMETRIC LEAVES1* reveals knox gene redundancy in *Arabidopsis*. *Development.* 1298: 1957–1965.

Chae E., Tan Q.K., Hill T.A., Irish V.F. (2008) An *Arabidopsis* F-box protein acts as a transcriptional co-factor to regulate floral development. *Development* 135: 1235–1245.

Chapman E.J., Carrington J.C. (2007) Specialization and evolution of endogenous small RNA pathways. *Nat. Rev. Genet.* 8: 884–896

Cheng Y., Dai X., Zhao Y. (2007) Auxin synthesized by the YUCCA flavin monooxygenases is essential for embryogenesis and leaf formation in *Arabidopsis*. *The Plant Cell*. 19:2430–2439.

Chini A., Fonseca S., Fernandez G., Adie B., Chico J.M., Lorenzo O., García-Casado G., López-Vidriero I., Lozano F.M., Ponce M.R., Micol J.L., Solano R. (2007) The JAZ family of repressors is the missing link in jasmonate signalling. *Nature*. 448: 666–671.

Chitwood D.H., Guo M., Nogueira F.T.S., Timmermans M.C.P. (2007) Establishing leaf polarity: the role of small RNAs and positional signals in the shoot apex. *Development*. 134: 813-823.

Cho H-T., Cosgrove D.J. (2000) Altered expression of expansin modulates leaf growth and pedicel abscission in *Arabidopsis thaliana*. *Proc Natl Acad Sci USA*. 97:9783–9788.

Chuang, C. F., Running, M. P., Williams, R. W. and Meyerowitz, E. M. (1999) The *PERIANTHIA* gene encodes a bZIP protein involved in the determination of floral organ number in *Arabidopsis thaliana*. *Genes Dev*. 13: 334 -344.

Clarke A.E., Gleeson P.A. (1981) Molecular aspects of recognition and response in pollen-stigma interactions. *Rec Adv Phytochem*. 15: 161–211.

Clark S.E., Running, M.P., Meyerowitz E.M. (1993) *CLAVATA1*, a regulator of meristem and flower development in *Arabidopsis*. *Development* 119: 397-418.

Clark S.E., Running, M.P., Meyerowitz E.M. (1995) *CLAVATA3* is a specific regulator of shoot and floral meristem development affecting the same processes as *CLAVATA1*. *Development* 121: 2057-2067.

Clark S.E., Jacobsen S.E., Levin J.Z., Meyerowitz E.M. (1996) The *CLAVATA* and *SHOOT MERISTEMLESS* loci competitively regulate meristem activity in *Arabidopsis*. *Development*. 122: 1567-1575.

Clough S.J., Bent A. (1998) Floral dip: A simplified method for *Agrobacterium*-mediated transformation of *Arabidopsis thaliana*. *Plant J*. 16:735–743.

Coen E.S., Meyerowitz E.M. (1991) The war of the whorls: genetic interactions controlling flower development. *Nature* 353: 31-37.

Cosgrove D.J. (1998) Cell wall loosening by expansins. *Plant Physiol*. 118: 333–339.

Cosgrove D.J. (2000) Loosening of plant cell walls by expansins. *Nature*. 407: 321–326.

Chini A., Fonseca S., Fernandez G., Adie B., Chico J.M., Lorenzo O., García-Casado G., López-Vidriero I., Lozano F.M., Ponce M.R., Micol J.L., Solano R. (2007) The JAZ family of repressors is the missing link in jasmonate signalling. *Nature*. 448: 666–671.

Christensen S.K., Dagenais N., Chory J., and Weigel D. (2000) Regulation of auxin response by the protein kinase *PINOID*. *Cell* 100: 469-478.

Craig K.L., Tyers M. (1999) The F-box: a new motif for ubiquitin dependent proteolysis in cell cycle regulation and signal transduction. *Prog. Biophys. Mol. Biol.* 72: 299–328.

Crawford B.C.W., Yanofsky M.F. (2011) *HALF FILLED* promotes reproductive tract development and fertilization efficiency in *Arabidopsis thaliana*. *Development* 138: 2999-3009.

David Y., Ziv T., Admon A., Navon A. (2010) The E2 Ubiquitin-conjugating Enzymes Direct Polyubiquitination to Preferred Lysines. *The Journal of Biological Chemistry*. 285: 8595–8604.

Del Campillo E. (1999) Multiple endo-1,4-β-D-glucanase (cellulase) genes in *Arabidopsis*. *Curr Top Dev Biol.* 46:39–61.

Del Pozo J. C., Estelle M. (2000) F-box proteins and protein degradation: An emerging theme in cellular regulation, *Plant Mol. Biol.* 44: 123.

Deng L., Wang C., Spencer E., Yang L.Y., Braun A., You J.X., Slaughter C., Pickart C., Chen Z.J. (2000) Activation of the I kappa B kinase complex by TRAF6 requires a dimeric ubiquitin-conjugating enzyme complex and a unique polyubiquitin chain. *Cell* 103: 351–361.

Dharmasiri N., Dharmasiri S., Estelle M. (2005) The F-box protein TIR1 is an auxin receptor. *Nature* 435: 441–445

Dinneny J.R., Yadegari R., Fischer R.L., Yanofsky M.F., Weigel D. (2004) The role of JAGGED in shaping lateral organs. *Development* 131: 1101–1110

Ditta G., Pinyopich A., Robles P., Pelaz S., Yanofsky M.F. (2004) The *SEP4* Gene of *Arabidopsis thaliana* Functions in Floral Organ and Meristem Identity. *Current Biology*. 14: 1935-1940.

Donnelly P.M., Bonetta D., Tsukaya H., Dengler R.E., Dengler N.G. (1999) Cell cycling and cell enlargement in developing leaves of *Arabidopsis*. *Dev Biol* 215: 407–419.

Drews G.N., Bowman J.L., Meyerowitz E.M. (1991) Negative regulation of the *Arabidopsis* homeotic gene *AGAMOUS* by the *APETALA2* product. *Cell* 65: 991–1002.

Durfee T., Roe J.L., Sessions R.A., Inouye C., Serikawa K., Feldmann K.A., Weigel D., Zambryski P.C. (2003) The F-box-containing protein UFO and AGAMOUS participate in antagonistic pathways governing early petal development in *Arabidopsis*. *Proc Natl Acad Sci U S A.* 100: 8571-8576.

Elbashir S.M., Lendeckel W., and Tuschl T. (2001) RNA interference is mediated by 21 and 22 nt RNAs. *Genes Dev.* 15: 188–200.

Efroni I., Blum E., Goldshmidt A., Eshed Y. (2008) A protracted and dynamic maturation schedule underlies *Arabidopsis* leaf development. *Plant Cell.* 20: 2293–2306.

Emery J.F., Floyd S.K., Alvarez J., Eshed Y., Hawker N.P., Izhaki A., Baum S.F., Bowman J.L. (2003) Radial patterning of *Arabidopsis* shoots by Class III HD-ZIP and *KANADI* genes. *Curr. Biol.* 13: 1768-1774.

Eshed Y., Izhaki A., Baum S.F., Floyd S.K., Bowman J.L. (2004) Asymmetric leaf development and blade expansion in *Arabidopsis* are mediated by *KANADI* and *YABBY* activities. *Development* 131: 2997–3006.

Fisher D.B. (1968) Protein staining of ribboned epon sections for light microscopy. *Histochemie* 16: 92-96.

Fisher R.L., Bennett A.B. (1991) Role of cell wall hydrolases in fruit ripening. *Ann Rev Plant Physiol.* 42: 675–703.

Garcia D. (2008) A miRacle in plant development: Role of microRNAs in cell differentiation and patterning. *Seminars in Cell & Developmental Biology.* 19: 586–595.

Fu Y., Xu L., Xu B., Yang L., Ling Q., Wang H., Huang H. (2007) Genetic interactions between leaf polarity-controlling genes and *ASYMMETRIC LEAVES1* and 2 in *Arabidopsis* leaf patterning. *Plant Cell Physiol.* 48: 724-735.

Gagne J.M., Downes B.P., Shiu S.H., Durski A.M., Vierstra R.D. (2002). The F-box subunit of the SCF E3 complex is encoded by a diverse superfamily of genes in *Arabidopsis*. *Proc. Natl. Acad. Sci. USA* 99: 11519–11524.

Gagne J.M., Smalle J., Gingerich D.J., Walker J.M., Yoo S.D., Yanagisawa S., Vierstra R.D. (2004) *Arabidopsis* EIN3-binding F-box 1 and 2 form ubiquitin-protein ligases that repress ethylene action and promote growth by directing EIN3 degradation. *Proc Natl Acad Sci USA* 101: 6803–6808.

Gilchrist E., Haughn G. (2010) Reverse genetics techniques: engineering loss and gain of gene function in plants. *Briefing in Functional Genomics.* 9: 103-110.

- Gleissberg S., Groot E.P., Schmalz M., Eichert M., Kolsch A., Hutter S.** (2005) Developmental events leading to peltate leaf structure in *Tropaeolum majus* (Tropaeolaceae) are associated with expression domain changes of a *YABBY* gene. *Dev. Genes Evol.* 215: 313–319.
- Goldberg R.B., Beals T.P., Sanders P.M.** (1993) Anther development: basic principles and practical applications. *Plant Cell* 5: 1217–1229.
- Gonzalez-Carranza Z.H., Rompa U., Peters J.L., Bhatt A.M., Wagstaff C., Stead A.D., Roberts J.A.** (2007) *HAWAIIAN SKIRT*: an F-box gene that regulates organ fusion and growth in *Arabidopsis*. *Plant physiology.* 144: 1370-1382.
- Griffith M. E., da Silva Conceição A., Smyth D. R.,** (1999) *PETAL LOSS* gene regulates initiation and orientation of second whorl organs in the *Arabidopsis* flower. *Development.* 126; 5635 -5644.
- Grigg S.P., Canales C., Hay A., Tsiantis M.** (2005) *SERRATE* coordinates shoot meristem function and leaf axial patterning in *Arabidopsis*. *Nature* 437: 1022-1026.
- Guo H., Ecker J.R.** (2003) Plant responses to ethylene gas are mediated by SCF(EBF1/EBF2)-dependent proteolysis of EIN3 transcription factor. *Cell* 115: 667–677
- Ha C.M., Jun J.H., Nam H.G., Fletcher J.C.** (2007) *BLADE-ON-PETIOLE1* and 2 control *Arabidopsis* lateral organ fate through regulation of LOB domain and adaxial-abaxial polarity genes. *Plant Cell.* 19: 1809–1825.
- Heisler M.G., Ohno C., Das P., Sieber P., Reddy G.V., Long J.A., Meyerowitz E.M.** (2005) Patterns of auxin transport and gene expression during primordium development revealed by live imaging of the *Arabidopsis* inflorescence meristem. *Curr Biol.* 15: 1899–1911.
- Hershko A., Heller H., Elias S., Ciechanover A.** (1983) Components of ubiquitin-protein ligase system. Resolution, affinity purification, and role in protein breakdown. *J. Biol. Chem.* 258: 8206–8214.
- Hershko A., Ciechanover, A.** (1998) The ubiquitin system. *Annu. Rev. Biochem.* 6: 425.
- Hibara K., Takada S., Tasaka M.** (2003) *CUC1* gene activates the expression of SAM-related genes to induce adventitious shoot formation. *Plant J* 36: 687–696
- Hill J.P., and Lord E.M.** (1989) Floral development in *Arabidopsis thaliana*: Comparison of wild-type and the homeotic *pistillata* mutant. *Can. J. Bot.* 67: 2922-2936.

- Hochstrasser M.** (1996) Ubiquitin-dependent protein degradation. *Annu. Rev. Genet.* 30: 405–439.
- Hudson A.** (1999) Axioms and axes in leaf formation. *Curr Opin Plant Biol* 2: 56–60.
- Husbands A., Bell E.M., Shuai B., Smith H.M.S., Springer P.S.** (2007) LATERAL ORGAN BOUNDARIES defines a new family of DNA-binding transcription factors and can interact with specific bHLH proteins. *Nucleic Acids Research* 35: 6663–6671.
- Husbands A.Y., Chitwood D.H., Plavskin Y., Timmermans M.C.** (2009) Signals and prepatterns: New insights into organ polarity in plants. *Genes Dev.* 23: 1986–1997.
- Ikezaki M., Kojima M., Sakakibara H., Kojima S., Ueno Y., Machida C., Machida Y.** (2010) Genetic networks regulated by *ASYMMETRIC LEAVES1* (*AS1*) and *AS2* in leaf development in *Arabidopsis thaliana*: *KNOX* genes control five morphological events. *Plant J.* 61, 70–82.
- Irish V.F.** (2010) The flowering of *Arabidopsis* flower development. *Plant Journal.* 61: 1014–1028.
- Ishibashi N., Kanamaru K., Ueno Y., Kojima S., Kobayashi T., Machida C., Machida Y.** (2012) *ASYMMETRIC-LEAVES2* and an ortholog of eukaryotic NudC domain proteins repress expression of AUXIN-RESPONSE-FACTOR and class 1 *KNOX* homeobox genes for development of flat symmetric leaves in *Arabidopsis*. *Biology Open* 000: 1–11.
- Iwakawa H., Ueno Y., Semiarti E., Onouchi H., Kojima S., Tsukaya H., Hasebe M., Soma T., Ikezaki M., Machida C., Machida Y.** (2002) The *ASYMMETRIC LEAVES2* gene of *Arabidopsis thaliana*, required for formation of a symmetric flat leaf lamina, encodes a member of a novel family of proteins characterized by cysteine repeats and a leucine zipper. *Plant and Cell Physiology* 43: 467–478.
- Iwakawa H., Iwasaki M., Kojima S., Ueno Y., Soma T., Tanaka H., Semiarti E., Machida Y., Machida C.** (2007) Expression of the *ASYMMETRIC LEAVES2* gene in the adaxial domain of *Arabidopsis* leaves represses cell proliferation in this domain and is critical for the development of properly expanded leaves. *The Plant Journal* 51: 173–184.
- Jack T., Brockman L.L., Meyerowitz E.M.** (1992) The homeotic gene *APETALA3* of *Arabidopsis thaliana* encodes a MADS box and is expressed in petals and stamens. *Cell* 68: 683–697.
- Jacobsen S.E., Running M.P., Meyerowitz E.M.** (1999) Disruption of an RNA helicase/RNase III gene in *Arabidopsis* causes unregulated cell division in floral meristems. *Development.* 126: 5231 -5243.

- Jarillo J.A., Capel J., Tang R.H., Yang H.Q., Alonso J.M., Ecker J.R., Cashmore A.R.** (2001) An *Arabidopsis* circadian clock component interacts with both *CRY1* and *phyB*. *Nature*. 410: 487-490.
- Jefferson R.A., Kavanagh T.A., Bevan M.W.** (1987) GUS fusions: beta-glucuronidase as a sensitive and versatile gene fusion marker in higher plants. *EMBO J* 6: 3901–3907.
- Jenkins E.S., Paul W., Craze M. et al.** (1999) Dehiscence-related expression of an *Arabidopsis thaliana* gene encoding a poly-galacturonase in transgenic plants of *Brassica napus*. *Plant Cell and Environment* 22: 159–167.
- Jin S., Zhuo Y., Guo W., Field J.** (2005) PAK1-dependent phosphorylation of RAF-1 regulates its mitochondrial localization, phosphorylation of BAD, and BCL-2 association. *J Biol Chem*. 280: 24698–24705.
- Jinn T-L., Stone J.M., Walker J.C.** (2000) HAESA, an *Arabidopsis* leucine-rich repeat receptor kinase controls floral organ abscission. *Genes Devel* 14:108–117.
- Jones-Rhoades M.W., Bartel D.P., Bartel B.** (2006) MicroRNAs and their regulatory roles in plants. *Annual Review of Plant Biology*. 57: 19–53.
- Jun J.H., Ha C.M., Fletcher J.C.** (2010) BLADE-ON-PETIOLE1 Coordinates Organ Determinacy and Axial Polarity in *Arabidopsis* by Directly Activating *ASYMMETRIC LEAVES2*. *The Plant Cell*. 22: 62-76.
- Kalaitzis P., Koehler S.M., Tucker M.L.** (1995) Cloning of a tomato polygalacturonase expressed in abscission. *Plant Mol Biol*. 28: 647–656.
- Kasschau K.D., Xie Z., Allen E., Llave C., Chapman E.J., Krizan K.A., Carrington J.C.** (2003) P1/HC-Pro, a viral suppressor of RNA silencing, interferes with *Arabidopsis* development and miRNA function. *Dev. Cell*. 4: 205-217.
- Kepinski S., Leyser O.** (2005) The *Arabidopsis* F-box protein TIR1 is an auxin receptor. *Nature*. 435: 446–451.
- Kerstetter R.A., Bollma K., Taylor R.A., Bomblies K., Poethig R.S.** (2001) *KANADI* regulates organ polarity in *Arabidopsis*. *Nature* 411: 706-709.
- Kim J., Jung J.H., Reyes J.L., Kim Y.S., Kim S.Y., Chung K.S., Kim J.A., Lee M., Lee Y., Kim V.N., Chua N.H., Park C.M.** (2005) MicroRNA directed cleavage of *ATHB15* mRNA regulates vascular development in *Arabidopsis* inflorescence stems. *Plant J*. 42: 84–94.
- Kim Y., Schumaker K.S., Zhu J.K.** (2006) EMS mutagenesis of *Arabidopsis*. *Methods Mol Biol*. 323: 101-103.

Kim J.H., Woo H.R., Kim J., Lim P.O., Lee I.C., Choi S.H., Hwang D., Nam H.G. (2009) Trifurcate feed-forward regulation of age-dependent cell death involving miR164 in *Arabidopsis*. *Science* 323: 1053-1057.

Kojima S., Iwasaki M., Takahashi H., Imai T., Matsumura Y., Fleury D., Lijsebettens M.K., Machida Y., Machida C. (2011) *ASYMMETRIC LEAVES2* and elongator, a histone acetyltransferase complex, mediate the establishment of polarity in leaves of *Arabidopsis thaliana*. *Plant Cell Physiol.* 52: 1259-1273.

Koyama T., Mitsuda N., Seki M., Shinozaki K., Ohme-Takagi M. (2010) TCP transcription factors regulate the activities of *ASYMMETRIC LEAVES1* and miR164, as well as the auxin response, during differentiation of leaves in *Arabidopsis*. *Plant Cell.* 22: 3574-3588.

Krizek B.A., Fletcher J.C. (2005) Molecular mechanisms of flower development: an armchair guide. *Nature Reviews Genetics* 6: 688-698.

Krizek B.A., Lewis M.W., Fletcher J.C. (2006) RABBIT EARS is a second-world repressor of AGAMOUS that maintains spatial boundaries in *Arabidopsis* flowers. *Plant J.* 45: 369-383.

Krizek B.A. (2009) *Arabidopsis*: Flower Development and Patterning. *Encyclopedia of Life Sciences*. John Wiley & Sons. Ltd: Chichester.

Kumaran M.K., Bowman J.L., Sundaresan V. (2002) *YABBY* polarity genes mediate the repression of *KNOX* homeobox genes in *Arabidopsis*. *Plant Cell* 14: 2761-2770.

Kunst L., Klenz J.E., Martinez-Zapater J., and Haughn G.W. (1989) *AP2* gene determines the identity of perianth organs in flowers of *Arabidopsis thaliana*. *Plant Cell* 1: 1195-1208.

Kurihara Y., Watanabe Y. (2004) *Arabidopsis* microRNA biogenesis through Dicer-like 1 protein functions. *Proc. Natl. Acad. Sci. USA* 101: 12753-12758.

Kurihara Y., Takashi Y., Watanabe Y. (2006) The interaction between DCL1 and HYL1 is important for efficient and precise processing of pri-miRNA in plant microRNA biogenesis. *RNA* 12: 206-212.

Kuroda H., Takahashi N., Shimada N., Seki M., Shinozaki K., Matsui M. (2002) Classification and expression analysis of *Arabidopsis* F-box containing protein genes. *Plant Cell Physiology.* 43: 1073-1085.

Lampugnani E.R., Kilinc A., Smyth D.R. (2012) *PETAL LOSS* is a boundary gene that inhibits growth between developing sepals in *Arabidopsis thaliana*. *Plant Journal* 71: 724-735.

- Lashbrook C.C., Gonzalez B.C., Bennett A.B.** (1994) Two divergent endo- β -1,4-glucanase genes exhibit overlapping expression in ripening fruits and abscising flowers. *Plant Cell*. 6: 1485–1493.
- Laufs P., Coen E., Kronenberger J., Traas J., Doonan J.** (2003) Separable roles of *UFO* during floral development revealed by conditional restoration of gene function. *Development* 130: 785–796.
- Laufs P., Peaucelle A., Morin H., Traas J.** (2004) MicroRNA regulation of the *CUC* genes is required for boundary size control in *Arabidopsis* meristems. *Development* 131: 4311–4322.
- Lee I., Wolfe D.S., Nilsson O., Weigel D.** (1997). A *LEAFY* co-regulator encoded by *UNUSUAL FLORAL ORGANS*. *Curr. Biol.* 7: 95–104.
- Levin J., Fletcher J., Chen X., Meyerowitz E.** (1998) A genetic screen for modifiers of *UFO* meristem activity identifies three novel fused floral organs genes required for early flower development in *Arabidopsis*. *Genetics* 149: 579–595
- Levin J.Z., Meyerowitz E.M.** (1995) *UFO*: an *Arabidopsis* gene involved in both floral meristem and floral organ development. *Plant Cell* 7: 529–548.
- Li H., Xu L., Wang H., Yuan Z., Cao X., Yang Z., Zhang D., Xu Y., Huang H.** (2005) The Putative RNA-dependent RNA polymerase RDR6 acts synergistically with *ASYMMETRIC LEAVES1* and 2 to repress *BREVIPEDICELLUS* and MicroRNA165/166 in *Arabidopsis* leaf development. *Plant Cell* 17: 2157-2171.
- Liljegren S.J., Gustafson-Brown C., Pinyopich A., Ditta G.S., Yanofsky M.F.** (1999) Interactions among *APETALA1*, *LEAFY*, and *TERMINAL FLOWER1* specify meristem fate. *Plant Cell* 11: 1007–1018.
- Lin W.C., Shuai B., Springer P.S.** (2003) The *Arabidopsis* *LATERAL ORGAN BOUNDARIES*-domain gene *ASYMMETRIC LEAVES2* functions in the repression of *KNOX* gene expression and in adaxial-abaxial patterning. *Plant Cell* 15: 2241–2252.
- Lincoln C., Long J., Yamaguchi J., Serikawa K., Hake S.** (1994) A knotted1-like homeobox gene in *Arabidopsis* is expressed in the vegetative meristem and dramatically alters leaf morphology when overexpressed in transgenic plants. *Plant Cell*. 6: 1859–1876.
- Liu F., Ni W., Griffith M.E., Huang Z., Chang C., Peng W., Ma H., Xie D.** (2004) The *ASK1* and *ASK2* genes are essential for *Arabidopsis* early development. *Plant Cell* 16: 5–20.
- Lobbes D., Rallapalli G., Schmidt D.D., Martin C., Clarke J.** (2006) *SERRATE*: a new player on the plant microRNA scene. *EMBO Rep.* 7: 1052–1058.

Lorick K.L., Jensen J.P., Fang S., Ong A.M., Hatakeyama S., Weissman A.M. (1999) RING fingers mediate ubiquitin-conjugating enzyme (E2)-dependent ubiquitination. *Proc Natl Acad Sci USA*. 96: 11364–11369.

Mallory A.C., Reinhart B.J., Jones-Rhoades M.W., Tang G., Zamore P.D., Barton M.K., Bartel D.P. (2004a) MicroRNA control of *PHABULOSA* in leaf development: importance of pairing to the microRNA 5' region. *EMBO J*. 23: 3356–3364.

Mallory A.C., Dugas D.V., Bartel D.P., Bartel B., (2004b) MicroRNA regulation of NAC-domain targets is required for proper formation and separation of adjacent embryonic, vegetative, and floral organs. *Curr. Biol*. 14: 1035–1046.

Mallory A.C., Vaucheret H. (2006) Functions of microRNAs and related small RNAs in plants. *Nat Genet*. 38: 31–36.

Maple J., Møller S.G. (2007) Mutagenesis in *Arabidopsis*. In *Methods in Circadian Biology*. *Methods in Molecular Biology series*. (Humana press). 362: 197–206.

Mandel M.A., Gustafson-Brown C., Savidge B., Yanofsky M.F. (1992) Molecular characterization of the *Arabidopsis* floral homeotic gene *APETALA1*. *Nature* 360: 273–277.

Matsumoto N., Okada K. (2001) A homeobox gene, *PRESSED FLOWER*, regulates lateral axis-dependent development of *Arabidopsis* flowers. *Genes & Development*. 15: 3355–3364.

McConnell J.R., Emery J., Eshed Y., Bao N., Bowman J., Barton M.K., (2001) Role of *PHABULOSA* and *PHAVOLUTA* in determining radial patterning in shoots. *Nature* 411: 709–713.

Meakin P., Roberts J. (1990) Dehiscence of fruit in oilseed rape. I. Anatomy of pod dehiscence. *Journal of Experimental Botany* 41: 995–1002.

Meinke D.W., Cherry J.M., Dean C., Rounsley S.D., Koornneef M. (1998) *Arabidopsis thaliana*: A Model Plant for Genome Analysis. *Science* 282: 662–682.

Meinke D.W., Meinke L.K., Showalter T.C., Schissel A.M., Mueller L.A., Tzafrir I. (2003) A sequence-based map of *Arabidopsis* genes with mutant phenotypes. *Plant Physiol*. 131:409–18.

Ni W., Xie D., Hobbie L., Feng B., Zhao D., Akkara J., Ma H. (2004) Regulation of flower development in *Arabidopsis* by SCF complexes. *Plant Physiol*. 134: 1574–1585.

- Nikovics K., Blein T., Peaucelle A., Ishida T., Morin H., Aida M., Laufs P.** (2006) The balance between the *MIR164A* and *CUC2* genes controls leaf margin serration in *Arabidopsis*. *Plant Cell* 18: 2929–2945.
- Osborne D.J.** (1989) Abscission. *Critical Reviews in Plant Sciences* 8: 103–129.
- Østergaard L., Yanofsky M.F.** (2004) Establishing gene function by mutagenesis in *Arabidopsis thaliana*. *The Plant Journal*. 39: 682–696.
- Palatnik J.F., Allen E., Wu X., Schommer C., Schwab R., Carrington J.C., Weigel D.** (2003) Control of leaf morphogenesis by microRNAs. *Nature*. 425: 257–263.
- Park W., Li J., Song R., Messing J., Chen X.** (2002) CARPEL FACTORY, a Dicer homolog, and *HEN1*, a novel protein, act in microRNA metabolism in *Arabidopsis thaliana*. *Curr. Biol.* 12: 1484–1495.
- Park M.Y., Wu G., Gonzalez-Sulser A., Vaucheret H., Poethig R.S.** (2005) Nuclear processing and export of microRNAs in *Arabidopsis*. *Proc. Natl. Acad. Sci. USA* 102: 3691–3696.
- Patterson S.E.** (2001) Cutting loose. Abscission and dehiscence in *Arabidopsis*. *Plant Physiol.* 126: 494–500.
- Patton E.E., Willems A.R., Tyers M.** (1998) Combinatorial control in ubiquitin-dependent proteolysis: Don't Skp the F-box hypothesis. *Trends Genet.* 14: 236–243.
- Pautot V., Dockx J., Hamant O., Kronenberger J., Grandjean O., Jublot D., Traas J.** (2001) KNAT2: Evidence for a link between knotted-like genes and carpel development. *Plant Cell*. 138: 1719–1734.
- Peaucelle A., Morin H., Traas J., Laufs P.** (2007) Plants expressing a *miR164*-resistant *CUC2* gene reveal the importance of post-meristematic maintenance of phyllotaxy in *Arabidopsis*. *Development* 134: 1045–1050.
- Pekker,I., Alvarez J.P., Eshed Y.** (2005). Auxin response factors mediate *Arabidopsis* organ asymmetry via modulation of KANADI activity. *Plant Cell* 17: 2899–2910.
- Pelaz S., Ditta G.S., Baumann E., Wisman E., Yanofsky M.F.** (2000) B and C floral organ identity functions require *SEPALLATA* MADSbox genes. *Nature* 405: 200–203.
- Peretto R., Favaron F., Bettini V., De Lorenzo G., Marini S., Alghisi P., Cervone F., Bonfante P.** (1992) Expression and localization of polygalacturonase during the outgrowth of lateral roots in *Allium porrum* L. *Planta*. 188: 164–172.

Peters J.L., Cnops G., Neyt P., Zethof J., Cornelis K., Van Lijsebettens M., Gerats T. (2004) An AFLP-based genome-wide mapping strategy. *Theor. Appl. Genet.* 108: 321–327.

Potuschak T., Lechner E., Parmentier Y., Yanagisawa S., Grava S., Koncz C., Genschik P. (2003) EIN3-dependent regulation of plant ethylene hormone signaling by two *Arabidopsis* F box proteins: EBF1 and EBF2. *Cell.* 15: 679–689.

Rast M.I., Simon R. (2008) The meristem-to-organ boundary: more than an extremity of anything. *Curr. Opin. Genet. Dev.* 18: 287–294.

Reinhart B.J., Weinstein E.G., Rhoades M.W., Bartel B., Bartel D.P. (2002) MicroRNAs in plants. *Genes Dev.* 16: 1616–1626.

Reinhardt D., Pesce E.R., Stieger P., Mandel T., Baltensperger K., Bennett M., Traas J., Friml J., Kuhlemeier C. (2003) Regulation of phyllotaxis by polar auxin transport. *Nature* 426: 255-260.

Ribas A.F., Dechamp E., Champion A., Bertrand B., Combes M.C., Verdeil J.L., Lapeyre F., Lashermes P., Etienne H. (2011) *Agrobacterium*-mediated genetic transformation of *Coffea arabica* (L.) is greatly enhanced by using established embryogenic callus cultures. *BMC Plant Biol.* 11: 92.

Rhoades M.W., Reinhart B.J., Lim L.P., Burge C.B., Bartel B., Bartel D.P. (2002) Prediction of plant microRNA targets. *Cell.* 110: 513-20.

Riechmann J.L., Meyerowitz E.M., (1997) Determination of floral organ identity by *Arabidopsis* MADS domain homeotic proteins *API*, *AP3*, *PI*, and *AG* is independent of their DNA-binding specificity. *Molec. Biol. Cell* 8: 1243-1259.

Roberts J.A., Gonzalez-Carranza Z.H. (2013) *Abscission*. eLS. John Wiley & Sons. 2 :1-11.

Rubio-Somoza I., Weigel D. (2011) MicroRNA networks and developmental plasticity in plants. *Trends in Plant Science.* 16: 258-264.

Ruegger, M., Dewey, E., Gray, W.M., Hobbie, L., Turner, J. and Estelle, M. (1998) The TIR1 protein of *Arabidopsis* functions in auxin response and is related to human SKP2 and yeast grr1p. *Genes Dev.* 12: 198–207.

Running, M. P. and Meyerowitz, E. M. (1996) Mutations in the *PERIANTHIA* gene of *Arabidopsis* specifically alter floral organ number and initiation pattern. *Development.* 122: 261 -1269.

Sakai H., Medrano L.J., Meyerowitz, E.M. (1995) Role of *SUPERMAN* in maintaining *Arabidopsis* floral whorl boundaries. *Nature* 378: 199-203.

- Samach A., Klenz J.E., Kohalmi S.E., Risseuw E., Haughn G.W., Crosby W.L.** (1999) The UNUSUAL FLORAL ORGANS gene of *Arabidopsis thaliana* is an F-box protein required for normal patterning and growth in the floral meristem. *Plant J.* 20: 433–445.
- Sarojam R., Sappl P.G., Goldshmidt A., Efroni I., Floyd S.K., Eshed Y., Bowman J.L.** (2010) Differentiating *Arabidopsis* shoots from leaves by combined YABBY activities. *Plant Cell* 22: 2113–2130.
- Santner A., Estelle M.** (2010) The ubiquitin-proteasome system regulates plant hormone signalling. *Plant J.* 61: 1029–1040.
- Sawa S., Watanabe K., Goto K., Kanaya E., Morita E.H., Okada K.** (1999) *FILAMENTOUS FLOWER*, a meristem and organidentity gene of *Arabidopsis*, encodes a protein with a zinc finger and HMG-related domains. *Genes Dev* 13:1079–1088
- Schommer C., Palatnik J.F., Aggarwal P., Chételat A., Cubas P., Farmer E.E., Nath U., Weigel D.** (2008) Control of Jasmonate Biosynthesis and Senescence by miR319 Targets. *PLoS Biol* 6: e230.
- Schoof H., Lenhard M., Haecker A., Mayer K.F., Jurgens G., Laux T.** (2000) The stem cell population of *Arabidopsis* shoot meristems is maintained by a regulatory loop between the *CLAVATA* and *WUSCHEL* genes. *Cell.* 100: 635-644.
- Schumann N., Navarro-Quezada A., Ullrich K., Kuhl C., Quint M.** (2011) Molecular Evolution and Selection Patterns of Plant F-Box Proteins with C-Terminal Kelch Repeats. *Plant Physiology.* 155: 835-850.
- Siegfried K.R., Eshed Y., Baum S.F., Otsuga D., Drews G.N., Bowman J.L.** (1999) Members of the *YABBY* gene family specify abaxial cell fate in *Arabidopsis*. *Development* 126: 4117-4128.
- Semiarti E., Ueno Y., Tsukaya H., Iwakawa H., Machida C., Machida Y.** (2001) The *ASYMMETRIC LEAVES2* gene of *Arabidopsis thaliana* regulates formation of a symmetric lamina, establishment of venation and repression of meristem-related homeobox genes in leaves. *Development* 128: 1771-1783.
- Shuai B., Reynaga-Peña C.G., Springer P.S.** (2002) The *LATERAL ORGAN BOUNDARIES* gene defines a novel, plant-specific gene family. *Plant Physiol.* 129: 747–761.
- Sitrit Y., Hadfield K.A., Bennett A.B., Bradford K.J., Downie A.B.** (1999) Expression of a polygalacturonase associated with tomato seed germination. *Plant Physiol.* 121: 419–428.
- Somers D.E., Schultz T.F., Milnamow M., Kay S.A.** (2000) *ZEITLUPE* encodes a novel clock-associated PAS protein from *Arabidopsis*. *Cell* 101: 319–329.

- Stenvik G.E., Butenko M.A., Urbanowicz B.R., Rose J.K., Aalen R.B.** (2006) Overexpression of *INFLORESCENCE DEFICIENT IN ABSCISSION* activates cell separation in vestigial abscission zones in *Arabidopsis*. *Plant Cell*. 18: 1467–1476.
- Sundaresan V., Springer P., Volpe T., Haward S., Jones J.D.G., Dean C., Ma H., Martienssen R.** (1995) Patterns of gene action in plant development revealed by enhancer trap and gene trap transposable elements. *Genes Dev* 9: 1797–1810.
- Sussex I.M.** (1955) Morphogenesis in *Solanum tuberosum* L: experiment investigation of leaf dorsoventrality and orientation in the juvenile shoot. *Phytomorphology*. 5: 286–300.
- Takada S., Hibara K., Ishida T., Tasaka M.** (2001) The *CUP-SHAPED COTYLEDON1* gene of *Arabidopsis thaliana* regulates shoot apical meristem formation. *Development* 128: 1127–1135.
- Takahashi N., Kuroda H., Kuromori T., Hirayama T., Seki M., Shinozaki K., Shimada H., Matsui M.** (2004) Expression and interaction analysis of *Arabidopsis* Skp1-related genes. *Plant Cell Physiol* 45: 83–9.
- Takeda S., Matsumoto N., Okada K.** (2004) *RABBIT EARS*, encoding a SUPERMAN-like zinc finger protein, regulates petal development in *Arabidopsis thaliana*. *Development* 131: 425–434.
- Taylor J.E., Webb T.S., Coupe S.A., Tucker G.A., Roberts J.A.** (1993) Changes in polygalacturonase activity and solubility of polyuronides during ethylene-stimulated leaf abscission in *Sambucus nigra*. *J Exp Bot*. 44: 93–98.
- Telfer A., Poethig R.S.** (1998) *HASTY*: a gene that regulates the timing of shoot maturation in *Arabidopsis thaliana*. *Development* 125: 1889–1898.
- Toriba T., Suzaki T., Yamaguchi T., Ohmori Y., Tsukaya H., Hirano H.Y.** (2010) Distinct regulation of adaxial-abaxial polarity in anther patterning in rice. *Plant Cell* 22: 1452–1462.
- Torki M., Mandaron P., Mache R., Falconet D.** (2000) Characterization of a ubiquitous expressed gene family encoding polygalacturonase in *Arabidopsis thaliana*. *Gene* 242: 42–436.
- The Arabidopsis Genome Initiative.** (2000) Analysis of the genome sequence of the flowering plant *Arabidopsis thaliana*. *Nature*. 408: 796–815.
- Tsiantis M., Hay A.** (2003) Comparative plant development: the time of the leaf? *Nature Reviews Genetics*. 4: 169–180.
- Ueno Y., Ishikawaa T., Watanabe K., Terakura S., Iwakawa H., Okada K., Machida C., Machida Y.** (2007) Histone Deacetylases and

- ASYMMETRIC LEAVES2** Are Involved in the Establishment of Polarity in Leaves of *Arabidopsis*. *The Plant Cell* 19:445-457.
- van Nocker S.** (2009) Development of the abscission zone. *Stewart Postharvest Rev.* 5: 1–6.
- Vaucheret H., Vazquez F., Crété P., Bartel D.P.** (2004) The action of *ARGONAUTE1* in the miRNA pathway and its regulation by the miRNA pathway are crucial for plant development. *Genes Dev.* 18: 1187–1197.
- Varshavsky A.**, (1997) The ubiquitin system. *Trends Biochem. Sci.*, 22: 383.
- Vierstra R.D.** (2003) The ubiquitin/26S proteasome pathway, the complex last chapter in the life of many plant proteins. *Trends Plant Sci.* 8: 135–142
- Villanueva J. M., Broadhvest J., Hauser B.A., Meister R.J., Schneitz K., Gasser C.S.** (1999) INNER NO OUTER regulates abaxial-adaxial patterning in *Arabidopsis* ovules. *Genes Dev.* 13: 3160-3169.
- Waites R., Hudson A.** (1995) phantastica: A gene required for dorsoventrality of leaves in *Antirrhinum majus*. *Development* 121: 2143–2154.
- Waites R., Selvadurai H.R., Oliver I.R., Hudson A.** (1998) The *PHANTASTICA* gene encodes a MYB transcription factor involved in growth and dorsoventrality of lateral organs in *Antirrhinum*. *Cell* 93: 779–789.
- Wang H., Huang J., Zhao L., Xue Y.** (2002) F-box proteins in flowering plants. *Chinese Science Bulletin*, 47: 1497-1501.
- Wang W., Xu B., Wang H., Li J., Huang H., Xu L.** (2011) *YUCCA* genes are expressed in response to leaf adaxial-abaxial juxtaposition and are required for leaf margin development. *Plant Physiol.* 157: 1805–1819.
- Weigel, D., Alvarez, J., Smyth, D. R., Yanofsky, M. F. and Meyerowitz E.M.** (1992) *LEAFY* controls floral meristem identity in *Arabidopsis*. *Cell* 69: 843-859.
- Weigel D., Glazebrook J.** (2002) *Arabidopsis: A Laboratory Manual*. (Cold Spring Harbor, NY: Cold Spring Harbor Laboratory Press).
- Welcker M., Clurman B.E.** (2008) FBW7 ubiquitin ligase: a tumour suppressor at the crossroads of cell division, growth and differentiation. *Nat Rev Cancer.* 8: 83-93.
- Wu G., Lin W.C., Huang T., Poethig R.S., Springer P.S., Kerstetter R.A.** (2008) KANADII regulates adaxial–abaxial polarity in *Arabidopsis* by directly repressing the transcription of *ASYMMETRIC LEAVES2*. *Proceedings of the National Academy of Sciences. USA* 105: 16392–16397.

- Xiao W. and Jang J.C.,** (2000) F-BOX proteins in *Arabidopsis*. Trends Plant Sci. 5: 454–457.
- Xie, D.X., Feys, B.F., James, S., Nieto-Rostro, M. and Turner, J.G.** (1998) COI1: an *Arabidopsis* gene required for jasmonate-regulated defense and fertility. Science 280: 1091–1094.
- Xu Y., Sun Y., Liang W., Huang H.** (2002) The *Arabidopsis* AS2 gene encoding a leucine-zipper protein is required for the polarity formation in leaves. Acta Botanica Sinica. 44(10): 1194-1202
- Xu L., Yang L., Pi L., Liu Q., Ling Q., Wang H., Poethig R.S., Huang H.** (2006) Genetic interaction between the AS1-AS2 and RDR6-SGS3-AGO7 pathways for leaf morphogenesis. Plant Cell Physiol. 47: 853-863.
- Xu B., Li Z., Zhu Y., Wang H., Ma H., Dong A., Huang H.** (2008) *Arabidopsis* genes AS1, AS2, and JAG negatively regulate boundary-specifying genes to promote sepal and petal development. Plant Physiol. 146: 566–575.
- Yamaguchi T., Nukazuka A., Tsukaya H.** (2012) Leaf adaxial-abaxial polarity specification and lamina outgrowth: evolution and development. Plant Cell Physiol. 53: 1180-94.
- Yang L., Liu Z., Lu F., Dong A., Huang H.** (2006) SERRATE is a novel nuclear regulator in primary microRNA processing in *Arabidopsis*. The Plant Journal 47: 841–850.
- Yanofsky M.F., Ma H., Bowman J.L., Drews G.N., Feldmann K.A., Meyerowitz E.M.** (1990) The protein encoded by the *Arabidopsis* homeotic gene *agamous* resembles transcription factors. Nature 346: 35-39.
- Yoshikawa M., Peragine A., Park M.Y., Poethig R.S.** (2005) A pathway for the biogenesis of trans-acting siRNAs in *Arabidopsis*. Genes Dev. 19: 2164-2175
- Young K.H.** (1998) Yeast Two-Hybrid: so many interactions, (in) so little time, Biology of Reproduction 58, p-302-311.
- Yu B., Li J., Minakhina S., Yang M., Padgett R.W., Steward R., Chen X.** (2005) Methylation as a crucial step in plant microRNA biogenesis. Science 307: 932–935.
- Yu H., Ito T., Wellmer F., Meyerowitz E.M.** (2004) Repression of *AGAMOUS-LIKE 24* is a crucial step in promoting flower development. Nat. Genet. 36: 157-161.
- Yumimoto K., Matsumoto M., Oyamada K., Moroishi T., Nakayama K.I.** (2012) Comprehensive identification of substrates for F-box proteins by differential proteomics analysis. J. Proteome Res.

Zamore P.D., Tuschl T., Sharp P.A., and Bartel D.P. (2000) RNAi: Double-stranded RNA directs the ATP-dependent cleavage of mRNA at 21 to 23 nucleotide intervals. *Cell* 101: 25–33.

Zgurski J.M., Sharma R., Bolokoski D.A., Schultz E.A. (2005) Asymmetric auxin response precedes asymmetric growth and differentiation of *asymmetric leaf1* and *asymmetric leaf2* *Arabidopsis* leaves. *Plant Cell*. 17: 77–91.

Zhao Y., Christensen S.K., Fankhauser C., Cashman J.R., Cohen J.D., Weigel D., Chory J. (2001) A role for flavin monooxygenase-like enzymes in auxin biosynthesis. *Science*. 291: 306–309.

Zhao D., Ni W., Feng B., Han T., Petrusek M.G., Ma H. (2003) Members of the *ASK* gene family exhibit a variety of expression patterns and may play diverse roles in *Arabidopsis*. *Plant Physiology*. 133: 203–217.

Zhao Y., Medrano L., Ohasho K., Fletcher J.C., Yu H., Sakai H., Meyerowitz E.M. (2004) HANABA TARANU is a GATA transcription factor that regulates shoot apical meristem and flower development in *Arabidopsis*. *Plant Cell* 16: 2586–2600.

Appendix

List of primers used in this project

Name	bp	Oligo sequence	Intended purpose
SSLPHSfor	24	GAGAGAGGCTTGTGATTGTCGGAG	<i>HWS</i> specific primers
SSLPHSrev	24	GTGCCACTACTCGCGAAAACCTCG	
HST1for	26	ATGGAAGATAGCAACTCCACGGCAAG	For sequencing of the <i>43.1/hws-1</i> using <i>HST</i> to determine the nature of the genetic lesion
HST1rev	25	CTCAGCTACAAGGGCAGCAGACTG	
HST2for	25	CATTTGGTTAGACTACGATGGGACG	
HST2rev	24	CACGTAATGCATAATGAACTTCAG	
HST3for	25	GATGACATCTCGAGCGCTATACTGG	
HST3rev	24	GGTGCAGAAGCACTCCCAGCCATG	
HST4for	25	GAACTAAGGAAGGACAAGCCGAGGC	
HST4rev	26	CCAATTGACCGATTGTTTAAATACTG	
AS2for1	24	ATCAATTCCTCTAGTACCAAATC	For sequencing of the <i>80.5/hws-1</i> using <i>AS2</i> to determine the nature of the genetic lesion
AS2rev1	24	GAACGTTTGCGAATTTTGTGGCT	
AS2for2	24	CTCCATTTTCAAGTCATTAATAATG	
AS2rev2	24	TGATATCAATTAAGAGAGCAAGTC	
AS2compFor	24	GCAATAAGCCTACATCAGATTTTA	<i>AS2_{pro}::AS2</i> and <i>AS2_{pro}::GUS</i> line generation
AS2compRev	24	TCAATTAAGAGAGCAAGTCCATAA	<i>AS2_{pro}::AS2</i> line generation
AS2compSalIFor	33	CGAGTCGACGCAATAAGCCTACATCA GATTTTA	<i>AS2_{pro}::AS2</i> and <i>AS2_{pro}::GUS</i> line generation
AS2compBamHIRev	33	GTCGGATCCTCAATTAAGAGAGCAAG TCCATAA	<i>AS2_{pro}::AS2</i> line generation
AS2compRevpro	21	CATGTGAAGAAGTTGCGAGTT GTCGGATCCCATGTGAAGAAGTTGCG	<i>AS2_{pro}::GUS</i> line generation
AS2compBamHIRpro	30	AGTT	
AS2for4*	20	GTCGATCGCTTGGTGATGAG	Bacterial (DH5 α) transformed colonies tested for positive colonies
GUSseq	20	TCACGGGTTGGGGTTTCTAC	
pBI101.2For	20	GAGTTAGCTCACTCATTAGG	For amplification of T1 <i>AS2_{pro}::AS2</i> and <i>AS2_{pro}::GUS</i> transformants
AS2rev4*	20	CAAGTAGCCCGAGTTTTGTT	
WTfor	24	GCAAATTCCTCCGGCGAAAATATC	Mismatch primers design to amplify wild type and <i>80.5</i> mutant
MUTANTfor	24	GCAAATTCCTCCGGCGAAAATATT	
MISMATCHrev	20	CTCAAGACGGATCAACAGTACG	
AS1for	24	CAAGTCTTGTTTAGAGAGATGGAA	For gene expression analysis
AS1rev	24	AGGCGATAATGTCAAAGTTACCGA	
CUC1for	24	GTGCCGACAATGGATGTTGATGTG	
CUC1rev	24	GCATGGCGATCAGAGAGTAAACGG	
CUC2for	24	ATGGCGGAGACAGCCAATATCTTC	
CUC2rev	24	GATAGTTTCTTGAGATTGTTGAGG	
LFYfor	20	CTGAAGGTTTCACGAGTGGC	
LFYrev	20	TCCGGTACAGCTAATACCGC	
AP2for	20	CTCTTCGAATACTCCACTGA	
AP2rev	20	GCGTCAAGTATCTTCTCCA	
PTLfor	20	GAGGAACAACGGATGATGAA	
PTLrev	20	TGAATCAACTTCGCTGCGAT	

Name	bp	Oligo sequence	Intended purpose
pKT735Sprom	20	GAGGAGCATCGTGGAAAAAG	For genetic cross between 80.5 and 35S::HWS (amplify 35S::HWS)
At3g61590Rev	24	CAGACCCATTTGCTTCTTCATTGC	
UFOforMutant	20	TGGTAAGATGGTTTACGGGT	For genetic cross between 80.5 and <i>ufo-2</i> (amplify <i>UFO</i>)
UFOmismatchRev	20	TCTTGATTCCGACACTC	

Allelism tests between *hws-1* suppressor lines from the EMS *hws-1* populations.

Allelism tests				
	Carpel (♀)	Cross	Pollen (♂)	Results
1	43.1	X	45.1	allelic
2	45.1	X	43.1	Partially allelic*
3	43.1	X	54.6	Non-allelic
4	54.6	X	43.1	Non-allelic
5	45.4	X	45.1	Allelic
6	45.1	X	45.4	Allelic
7	45.1	X	54.6	Non-allelic
8	54.6	X	45.1	Non-allelic
9	23.1	X	45.1	Allelic
10	45.1	X	23.1	Allelic
11	23.1	X	45.4	Allelic
12	43.1	X	23.1	Allelic
13	23.1	X	43.1	Allelic
14	80.1	X	80.2	Allelic
15	80.4	X	80.5	Allelic
16	80.5	X	80.4	Allelic
17	80.5	X	80.2	Allelic
18	84.3	X	84.1	Partially allelic
19	84.6	X	84.3	Allelic
20	84.6	X	84.5	Allelic
21	84.7	X	84.3	Allelic
22	84.10	X	84.12	Allelic

*: more than 50% of the flowers per plant are shedding their floral organs, thus resulting in an allelic phenotype.

Observed and expected phenotype ratios of different crosses in the F2 populations and transformations in the T2 populations

Cross	Observed		Expected		Theoretical ratio (WT:m)	Chi-square (χ^2)	Probability	
	n.							
	WT	m	WT	m				
Col-0 wild type X <i>43.1/hws-1</i> F2	96	77	19	72	24	3:1	1.389	0.239
Col-0 wild type X <i>80.5/hws-1</i> F2	96	73	23	72	24	3:1	0.056	0.813
<i>ffo1</i> X <i>80.5/hws-1</i> F2	288	224	64	216	72	3:1	1.185	0.276
<i>Pro35S::HWS</i> X <i>80.5/Colwt</i> F2	24	19*	5	18*	6	3:1	0.222	0.638
Transformation								
<i>AS2pro::AS2/80.5/hws-1</i> T2	24	20**	4	18**	6	3:1	0.889	0.346

WT: wild type. M: mutant. *: *Pro35S::HWS* as the dominant phenotype. **: *hws-1* as the dominant phenotype. n.: total number of plants.

During my doctoral research at the University of Nottingham, I was also involved in a project that was based on the Alliance: Franco-British research partnership programme which generated a publication. The research took place in collaboration with Dr. Timothy Tranbarger, IDR, Montpellier and the project was titled functional diversity underlying cell separation processes: comparison of *arabidopsis* floral organ and *Eaeais guineensis* (oil palm) fruit shedding. The objectives of the project included comparisons between two key cell separation processes, abscission and fruit ripening, of *Arabidopsis* and *Elaeis guineensis* at a cellular and molecular level. The research at the University of Nottingham involved RT-PCR analysis using degenerate primers from genes which included *polygalacturonases* (PGs), *IDA*, *HAESA* and Cellulases on cDNA samples from fruit oil palm abscission zone at several time courses of abscission in the presence and absence of ethylene.



Temporal and spatial expression of polygalacturonase gene family members reveals divergent regulation during fleshy fruit ripening and abscission in the monocot species oil palm

Roongsattham *et al.*

RESEARCH ARTICLE

Open Access

Temporal and spatial expression of polygalacturonase gene family members reveals divergent regulation during fleshy fruit ripening and abscission in the monocot species oil palm

Peerapat Roongsattham¹, Fabienne Morcillo², Chatchawan Jantasuriyarat³, Maxime Pizot¹, Steven Moussu², Dasuni Jayaweera⁴, Myriam Collin¹, Zinnia H Gonzalez-Carranza⁴, Philippe Amblard⁵, James W Tregear¹, Somvong Tragoonrung⁶, Jean-Luc Verdeil⁷ and Timothy J Tranbarger^{1*}

Abstract

Background: Cell separation that occurs during fleshy fruit abscission and dry fruit dehiscence facilitates seed dispersal, the final stage of plant reproductive development. While our understanding of the evolutionary context of cell separation is limited mainly to the eudicot model systems tomato and *Arabidopsis*, less is known about the mechanisms underlying fruit abscission in crop species, monocots in particular. The polygalacturonase (PG) multigene family encodes enzymes involved in the depolymerisation of pectin homogalacturonan within the primary cell wall and middle lamella. PG activity is commonly found in the separation layers during organ abscission and dehiscence, however, little is known about how this gene family has diverged since the separation of monocot and eudicots and the consequence of this divergence on the abscission process.

Results: The objective of the current study was to identify PGs responsible for the high activity previously observed in the abscission zone (AZ) during fruit shedding of the tropical monocot oil palm, and to analyze PG gene expression during oil palm fruit ripening and abscission. We identified 14 transcripts that encode PGs, all of which are expressed in the base of the oil palm fruit. The accumulation of five PG transcripts increase, four decrease and five do not change during ethylene treatments that induce cell separation. One PG transcript (*EgPG4*) is the most highly induced in the fruit base, with a 700–5000 fold increase during the ethylene treatment. *In situ* hybridization experiments indicate that the *EgPG4* transcript increases preferentially in the AZ cell layers in the base of the fruit in response to ethylene prior to cell separation.

Conclusions: The expression pattern of *EgPG4* is consistent with the temporal and spatial requirements for cell separation to occur during oil palm fruit shedding. The sequence diversity of PGs and the complexity of their expression in the oil palm fruit tissues contrast with data from tomato, suggesting functional divergence underlying the ripening and abscission processes has occurred between these two fruit species. Furthermore, phylogenetic analysis of *EgPG4* with PGs from other species suggests some conservation, but also diversification has occurred between monocots and eudicots, in particular between dry and fleshy fruit species.

Keywords: Abscission, Fruit development, *Elaeis guineensis*, Polygalacturonase, Ethylene, Cell separation

* Correspondence: timothy.tranbarger@ird.fr

¹Institut de Recherche pour le Développement, IRD Centre de Montpellier, IRD/CIRAD Palm Development Group, DIADE 911 avenue agropolis BP 64501, 34394 Montpellier cedex 5, France

Full list of author information is available at the end of the article

Background

The shedding of plant organs is a highly coordinated developmentally regulated event that can occur in different contexts throughout the plant life cycle [1-4]. Organ shedding is important for both plant vegetative and reproductive development, including abscission of leaves, branches, whole flowers, floral parts, seeds and immaturely aborted or ripe fruit. In particular, cell separation that occurs during fleshy fruit abscission and dry fruit dehiscence facilitates seed dispersal, the final stage of reproductive development, and therefore governs important characters in many crop species. For fruit to be shed, cell separation must occur in a precise location timed to optimize dispersal under the most favourable conditions. For crop species, if fruit are shed too early or late, economic consequences can be significant. Whereas our understanding of the evolutionary context for this phenomenon is mainly limited to model systems such as tomato and *Arabidopsis*, less is known about the mechanisms underlying fruit abscission in non-model crop species in general and, monocot species in particular.

Oil palm is a tropical perennial monocotyledonous species in the family Arecaceae with an extraordinarily oil rich fleshy mesocarp, which is the number one source of edible vegetable oil worldwide. In addition, potential use of palm oil as a biofuel is predicted to cause constraints on the worldwide supply of edible palm oil and increase the pressure for higher yields and an expansion of cultivatable areas. While conventional breeding schemes have allowed increases in yield of palm oil up to 1% per year, non-synchronized ripening and subsequent shedding of the ripest fruit before harvest limit yield gains [5,6]. In addition, the difficulty to schedule regular harvests due to non-synchronized fruit shedding results in a labour intensive logistics that increases overall production costs. Furthermore, several original characters of oil palm fruit shedding warrant further detailed investigations. In particular, the two-stage process involving primary and adjacent abscission zones (AZs), plus the extraordinary low amount of methylated pectin and high levels of polygalacturonase (PG) activity, collectively suggest that divergent mechanisms may underlie the cell separation process that leads to fruit shedding in this monocotyledonous species [7-9]. Finally, the only organ observed to shed in this palm species is the ripe fruit. Flowers and immature fruitlets from many species are naturally thinned by organ abscission in response to nutritional status to optimized reproductive success, whereas this phenomenon is not observed to any extent in oil palm. Indeed, the oil palm maintains all fruit on a bunch until ripening related signalling takes place to induce ripe fruit abscission.

While examples of organ shedding in plants are diverse, the common model proposed is mainly based on

studies with eudicotyledons [2,3]. Firstly, the development of the abscission zone (AZ) takes place at the base of subtending organ to be shed. Secondly, as the AZ develops, it must become competent for cell separation events required for organ abscission. Indeed, once the AZ develops, it responds differently from adjacent tissues to the signals that induce cell separation [10]. After the AZ becomes competent for separation to be induced, cellular activity, in particular the expansion of the golgi vesicles and activation of the endomembrane system with the release of hydrolytic enzymes to the apoplast leads to the degradation of the middle lamella and cell separation [11,12]. An important feature of the model is the induction of the genes encoding cell wall hydrolytic enzymes targeted to modify and degrade cell wall components for separation to occur. The expression of these genes is often induced by ethylene and inhibited by auxin, characteristics that correlate with the positive and negative effects of these hormones on the abscission process respectively [1-3]. Despite the central importance of the mechanisms that allow changes in adhesion of adjacent cells to take place with such temporal and spatial precision, our understanding of these events even in model organisms is limited.

PG gene expression and activity are common features of organ abscission, observed in bean, tomato, peach and *Sambucus nigra* [13-16]. PG activity depolymerises the homogalacturonan backbone of pectin and while PG transcripts and activity increase in various species during the abscission process, they can also be induced by ethylene or inhibited by auxin [14,15,17-22]. In tomato, there is a single PG transcript (*pTOM6*, also known as *TFPG*) expressed during fruit ripening, while up to four other PGs (*TAPG1*, *TAPG2*, *TAPG4* and *TAPG5*) are expressed in the flower/fruit pedicel AZ associated with abscission [20,21,23-27]. Interestingly, the down-regulation or knockout of *TFPG* results in a decrease in pectin depolymerisation, but surprisingly no change in fruit softening which suggests other components are involved [25,27-29]. Furthermore, down-regulation of fruit *TFPG* has no effect on the timing or rate of leaf abscission, indicating a specific function of this enzyme during fruit ripening but not organ abscission [22]. In contrast, silencing of the abscission *TAPG1* expression delays abscission and increases break strength of the AZ [30]. Overall, these experiments suggest that while PGs are important for processes during both ripening and abscission, the same genes may not be responsible and there are other factors involved in abscission. Indeed, there are up to 69 and 59 PG genes in *Arabidopsis* and rice respectively, many with overlapping expression domains [31,32]. At least four of the *Arabidopsis* genes have expression profiles correlated to cell wall loosening and cell wall dissolution events during floral organ abscission

[32]. Furthermore, *ADPG1*, *ADPG2* and *QRT2* have been shown to have overlapping functions during different cell separation processes. *ADPG1* and *ADPG2* are essential for silique dehiscence, while *ADPG2* and *QRT2* contribute to floral organ abscission, and all three genes contribute to anther dehiscence, suggesting precise combinations of PG activities may be necessary during the cell separation events underlying these different processes [33].

A previous study revealed a large increase in PG activity in the oil palm AZ in the base of the fruit during cell separation events that lead to fruit abscission [7]. Our main objective in the present study was to identify PG genes that could be responsible for this activity observed during fruit shedding. We have performed a detailed expression analysis of 14 genes that encode PGs in the base of the oil palm fruit. PG sequence diversity in the fruit tissues and their profiles of expression during fruit ripening and during ethylene induced abscission contrasts with that observed in tomato, suggesting some functional divergence underlying these processes in this monocotyledonous fruit species. The results of a phylogenetic analysis of EgPG4 with PGs with known functions and/or expression profiles from various species will also be discussed in relation to divergence that may have occurred between eudicots and monocots, in particular between fleshy and dry fruit species.

Results

Ethylene induced oil palm fruit shedding experimental system

Previous studies published on oil palm fruit shedding were done with material transported by airfreight from plantations in Malaysia to a laboratory in the United Kingdom where the experiments were performed [7-9]. In order to determine precisely the timing of events that occur during abscission, our first objective was to set up an experimental system that could be used in a local field setting to eliminate problems that could arise due to the time and conditions required for storage and long distance shipment of the fruit. Based on the results of earlier studies with oil palm, ethylene was implicated as the main signal that induces cell separation in the primary AZ of the oil palm fruit [9]. Therefore, to synchronize fruit shedding, we treated spikelet explants with ethylene in airtight boxes (see Material and Methods for details; Figure 1A). The first experiment examined the ethylene dose effect on the induction of cell separation in the primary AZ of ripe fruit (150 days after pollination, DAP) treated for 12 h (Figure 1B). An increase in the number of fruit shed (13%) was observed in spikelets treated with $0.1 \mu\text{l l}^{-1}$ ethylene, while at $10 \mu\text{l l}^{-1}$, 100% of the fruit underwent cell separation in the primary AZ. This experiment confirmed the use of $10 \mu\text{l l}^{-1}$ as

an effective concentration for our studies as used previously [9]. In addition, the experiment also confirmed the two-stage separation process (data not shown) during which separation first occurs within the predetermined primary AZ, followed later by separation events in adjacent AZs [8,9]. The concentration of $10 \mu\text{l l}^{-1}$ was used in further experiments to compare fruit separation at different stages of development (Figure 1C). Spikelets of fruit at 30, 120 and 180 DAP were treated and shedding was quantified at time intervals up to 24 h after treatment. No fruit were observed to shed at 3 and 6 h. Fruit at 30 DAP were only observed to shed after 24 hours of treatment, while 120 DAP fruit and 180 DAP fruit began to separate after 12 h and 9 h of treatment respectively. In air controls, only the 180 DAP fruit were observed to shed at 12 h (1%) and 24 h (100%). These experiments define the time frame during which cell separation must occur for oil palm fruit shedding to take place, and suggests an importance of developmental factors that influence the response to ethylene.

Polygalacturonase gene family expression in the oil palm fruit tissues and the identification of the EgPG4 transcript induced in the AZ prior to fruit shedding

A 35-fold increase in polygalacturonase (PG) activity was reported to occur in the AZ during fruit shedding [7]. Furthermore, PGs are implicated in cell separation underlying organ separation in many species. In this context, our next objective was to identify PG candidate genes responsible for this large PG activity observed during cell separation events in the AZ. Briefly, our approach involved searches of available databases for sequences similar to known PGs, including locally derived 454 pyrosequencing transcriptome data, followed by designing of specific primers for each sequence identified to test, along with degenerate primers, to amplify from a mixture of cDNAs derived from fruit tissues treated or not treated with ethylene, or from genomic DNA (see Materials and Methods for details). Overall, our searches resulted in the identification of 35 putative non-redundant PG sequences, 28 of which contained either a partial or complete glycoside hydrolase family 28 (GH28) PG signature domain and were retained for further studies (see Additional file 1 for nucleotide sequences). From the 28 sequences, RT-PCR analysis revealed that 14 non-redundant PG transcripts were expressed in the AZ of oil palm fruit and a detailed analysis of their expression in fruit tissues during ethylene induced abscission was performed. The 14 transcripts are *EgPG1*, *EgPG3*, *EgPG4*, *EgPG7*, *EgPG8*, *EgPG9*, *EgPG10*, *EgPG11*, *EgPG16*, *EgPG17*, *EgPG18*, *EgPG19*, *EgPG22* and *EgPG26*.

To analyze expression, qPCR analysis was performed with tissue samples from the ethylene experiments

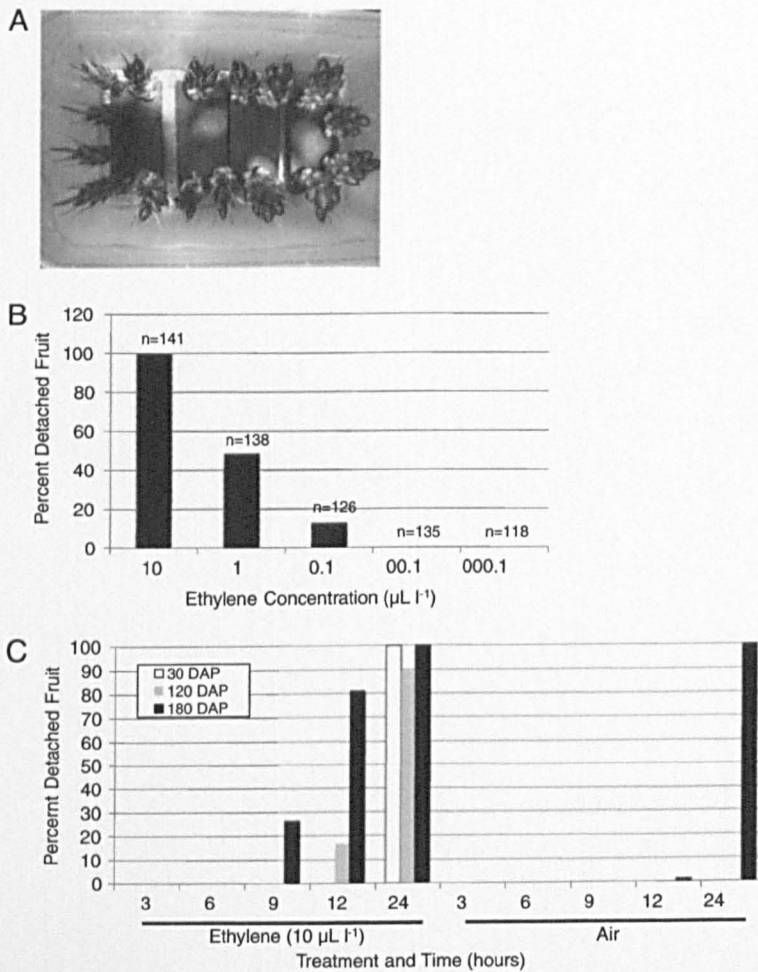


Figure 1 (A) Experimental system used for ethylene-induced fruit shedding experiments. (B) Dose response of ripening fruit (150 days after pollination, DAP) treated with a selected concentration range of ethylene for 12 h. (C) Ethylene time course treatment of oil palm fruit spikelets at contrasting stages of development (DAP 30, 120, and 180). To test for separation, fruits were subjected to light pressure and separation in the primary zone was recorded. For 30 DAP samples, $n > 200$, for 120 DAP samples $n > 90$ and for 180 DAP samples $n > 80$ per time point/treatment respectively. Experiments were performed twice during 2010 and once during 2011 for three biological repetitions with comparable results. The data from one representative experiment are shown.

described above (Figure 1C). The results confirmed the RT-PCR analysis in that each of the 14 primer pairs successfully amplified a PG sequence from the oil palm fruit AZ, but also from the adjacent pedicel or mesocarp tissues before and after ethylene treatment (Figure 2A-N). The profiles of transcript abundance accumulation in the AZ can be grouped into the following three main categories: I) five transcripts increase significantly (more than 2 fold; Figure 2A-E), II) four transcripts decrease significantly (more than 0.5 fold; Figure 2F-I) and, III) five transcripts have no significant change in abundance in the AZ during ethylene treatments (Figure 2J-N) respectively. By far the most abundant PG transcript detected with the most dramatic increase in abundance in the AZ is that of *EgPG4* (Figure 2B). *EgPG4* transcript increases approximately 700, 2000, 4000 and 5000 fold in the AZ after 3, 6, 9 and 12 h of ethylene treatment

respectively. In contrast, *EgPG4* is also highly expressed in the mesocarp sampled from the upper portion below the apex of the untreated fruit, but only increases 10, 5, 36 and 13 fold after 3, 6, 9 and 12 h of ethylene treatment respectively (Figure 2B). Finally, *EgPG4* is faintly detectable in pedicel tissue before ethylene treatment, and increases at a lower magnitude during the ethylene treatments compared to that observed in the AZ.

An overview of PG gene expression reveals that the three adjacent fruit tissues respond differently to the ethylene treatments (Figure 3 and Figure 1 and Additional file 2). In the mesocarp below the apex of 180 DAP fruit, the *EgPG4* transcript represents 95% of the total PG transcript before ethylene treatment, then increases to 99% after 6 h of ethylene treatment (Figure 3). In contrast, in the AZ of fruit prior to ethylene treatment, *EgPG11* is the most abundant (43%) followed by *EgPG10* (15%) and

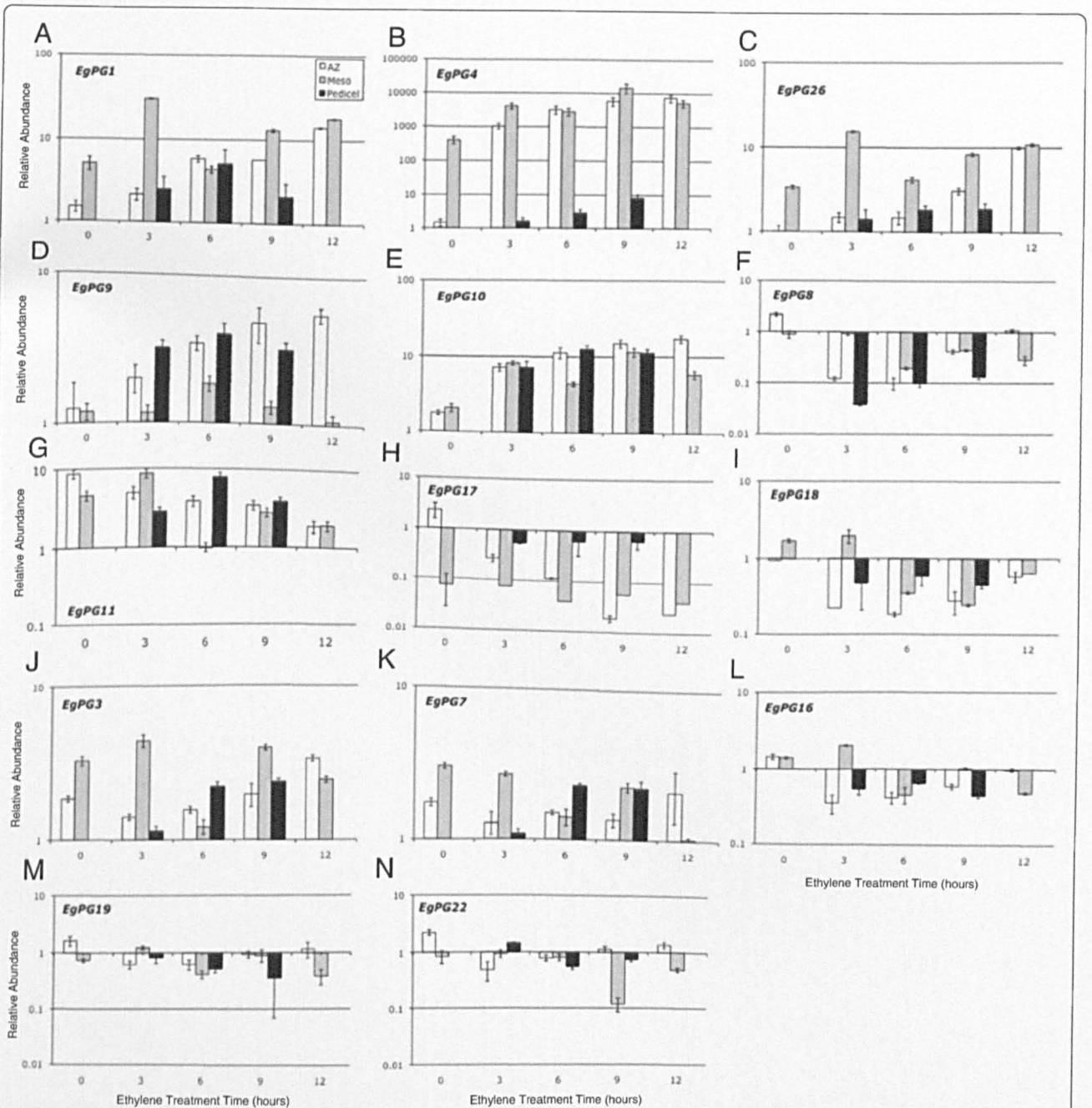


Figure 2 qPCR analysis of PG transcript abundance in oil palm fruit tissues and during ethylene treatment time course. (A-E) PG transcripts that increase during ethylene treatment in one or all tissues examined; (F-I) PG transcripts that decrease during ethylene treatment in one or all tissues examined; (J-N) PG transcripts with no significant change and/or with low abundance. Standard deviation (error bars) was calculated from three experiments. The y-axes are expressed in logarithmic scale. No data for the 12 h ethylene treated pedicel were collected.

EgPG8 (10%) and *EgPG18* (10%), whereas *EgPG4*, represented only 4% of the total PG transcript detected. By contrast, *EgPG4* accounts for 99% of the PG transcript in the AZ after 6 h of ethylene treatment. In the pedicel, *EgPG10* (62%) and *EgPG11* (19%) are the most abundant PG transcripts after 6 h ethylene treatment, while the *EgPG4* transcript accounts for only 7% and 4% total transcript in untreated and ethylene treated fruit respectively. Our

findings indicate that *EgPG4*, the most abundant PG transcript detected, is spatially and temporally differentially regulated in the three adjacent fruit tissues examined. Indeed, *EgPG4* accounts for the majority of the total PG transcript detected in the mesocarp, and more notably undergoes a dramatic increase in abundance preferentially in the AZ prior to the onset of separation observed after 9 h of ethylene treatment (Figure 1C).

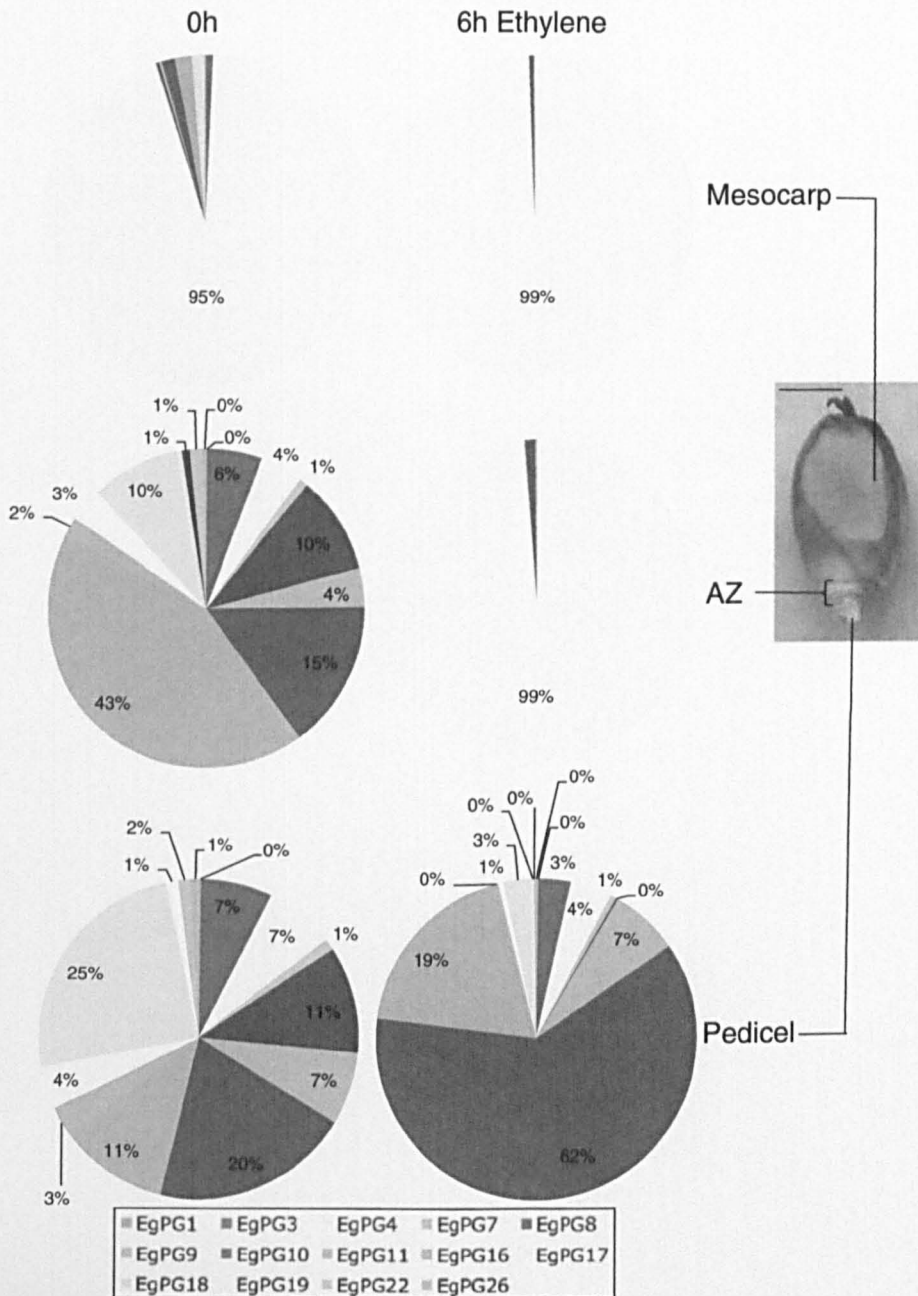
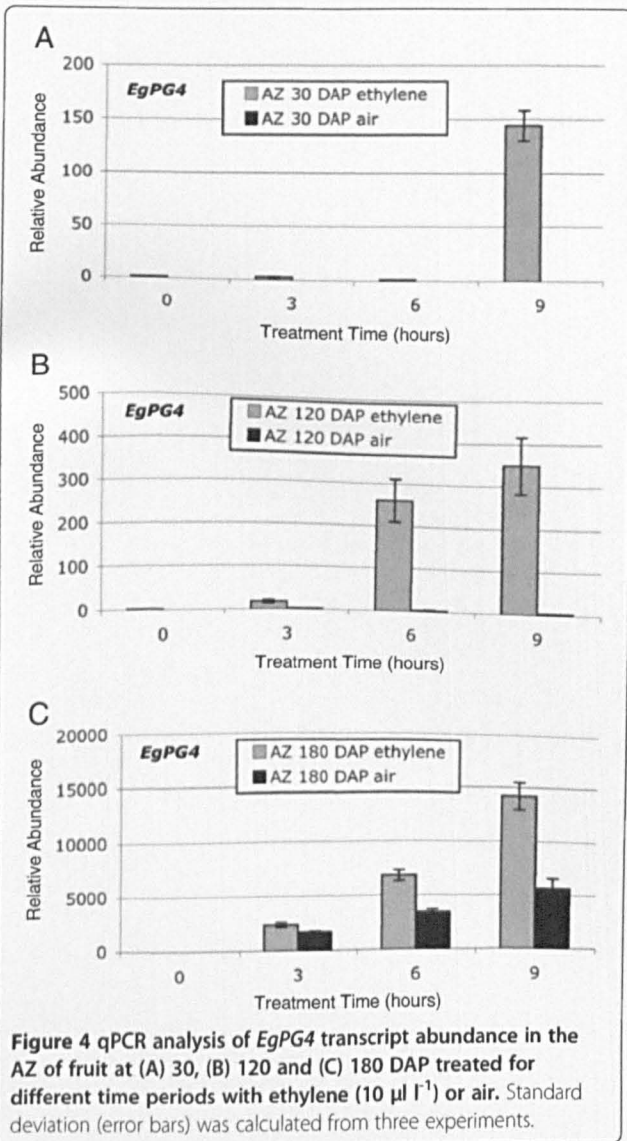


Figure 3 The percentage contribution of individual PG family members to total expression in the abscission zone, mesocarp and pedicel of the oil palm fruit in untreated and 6 h ethylene treated fruit, prior to cell separation. Data were calculated from the expression values shown in Figure 2. Standard error is in Additional file 2. Scale bar 1 cm.

During our ethylene experiments, we observed that 30 and 120 DAP fruit do not separate without treatment with ethylene (control treatments in air in the presence of ethylene absorbing material), while in the presence of ethylene they first separate after 12 h and 24 h respectively, and only after 24 h of ethylene treatment are the majority of the fruit shed (Figure 1C). By contrast, the 180 DAP fruit treated with air in the presence of ethylene absorbing material (control treatments) will begin to

undergo cell separation after 12 h and will completely separate after 24 h (Figure 1C). To determine whether *EgPG4* transcript accumulation coincides with these observations, we examined the expression of *EgPG4* in 30, 120 and 180 DAP fruit in the presence or absence of ethylene (Figure 4A-C and Figure 1C). The results reveal a close correlation of the accumulation of the *EgPG4* mRNA with the timing of shedding of 30, 120 and 180 DAP fruit. Indeed, *EgPG4* has very low relative



expression in untreated 30 and 120 DAP fruit compared to 180 DAP, and after 3 h of ethylene treatment, the increase is 2,400 fold in the 180 DAP fruit compared to only 2.5 fold and 17 fold in the 30 and 120 DAP fruit respectively (Figure 4A-C). After 6 h, *EgPG4* transcript increases 0.70, 260 and 6,803 fold in 30, 120 and 180 DAP fruit respectively, while after 9 h of ethylene treatment, the *EgPG4* transcript is increased 143, 350 and 14,200 fold in 30, 120 and 180 DAP fruit respectively.

In situ analysis of the spatial and temporal expression of *EgPG4* during ethylene induced fruit shedding

Whereas the qPCR analysis of *EgPG4* transcript accumulation correlates well with the timing of cell separation events that occur in the base of the oil palm fruit, the AZ samples that were used for the expression analysis include a mixture of all three tissues including the AZ and the

margins of the adjacent pedicel and mesocarp tissues (Figure 5). To examine whether both the temporal and spatial expression of *EgPG4* correlates with the cell separation events in the AZ that lead to fruit shedding, *in situ* hybridization analysis was performed. Firstly, we used a combination of bright field, polarized light and epifluorescence microscopy to clearly distinguish the localization of the *EgPG4* transcript within the AZ cells, compared to the adjacent mesocarp and pedicel tissues (Figure 5A-J). With polarized light, the AZ cell layers are well defined in addition to the lignified vasculature in all the tissues (Figure 5E-G). In contrast, epifluorescence microscopy mainly detected the lignified vasculature, predominantly in the pedicel and the mesocarp (Figure 5H-J). In the base of ripe fruit before ethylene treatment, the *EgPG4* transcript was neither detected in the AZ, nor in the lower margin of the mesocarp or upper margin of the pedicel tissues (Figure 5A,E,H). By 6 h after ethylene treatment, the *EgPG4* transcript increased in abundance preferentially in the AZ cell layers, including the parenchyma cells and the undifferentiated xylem cells of the vascular bundles (Figure 5B,F,I). By contrast, no *EgPG4* transcript was detected or was only present in relatively lower amounts in the adjacent pedicel and mesocarp tissues. At higher magnification of the boundary region between the pedicel and the AZ, the *EgPG4* transcript clearly accumulates in the AZ cells while it remains at very low or undetectable amounts in the adjacent pedicel cells (Figure 5C,G,I). In contrast, the control hybridizations with ribosomal RNA (rRNA) sense and antisense probes revealed a more even distribution of rRNA throughout the pedicel, AZ and mesocarp tissues when compared to *EgPG4* (Figure 5B and D; Additional file 3). Furthermore, the sense strand control with *EgPG4* also had a less intense signal than the antisense (Additional file 3). As a comparison, *in situ* hybridization experiments were also performed with *EgPG10* and *EgPG8*, the former of which is shown by qPCR analysis to increase to similar amounts in all three tissues, while the later decreases during the ethylene treatments (Figure 2E and F). For *EgPG10*, the results showed an even distribution of transcript present in the three tissues after ethylene treatment, while *EgPG8* was not detected (data not shown). Together, these results corroborate the correlation between the spatial and temporal expression profile of the *EgPG4* transcript in relation to ethylene and cell separation observed by qPCR, and provides further evidence for an important function for this transcript during fruit abscission.

Phylogenetic analysis of *EgPG4* in relation to PGs with known functions or expression profiles

To examine the relationship of *EgPG4* with other plant PGs, a phylogenetic comparison of its amino acid sequence with those predicted from DNA/RNA sequences

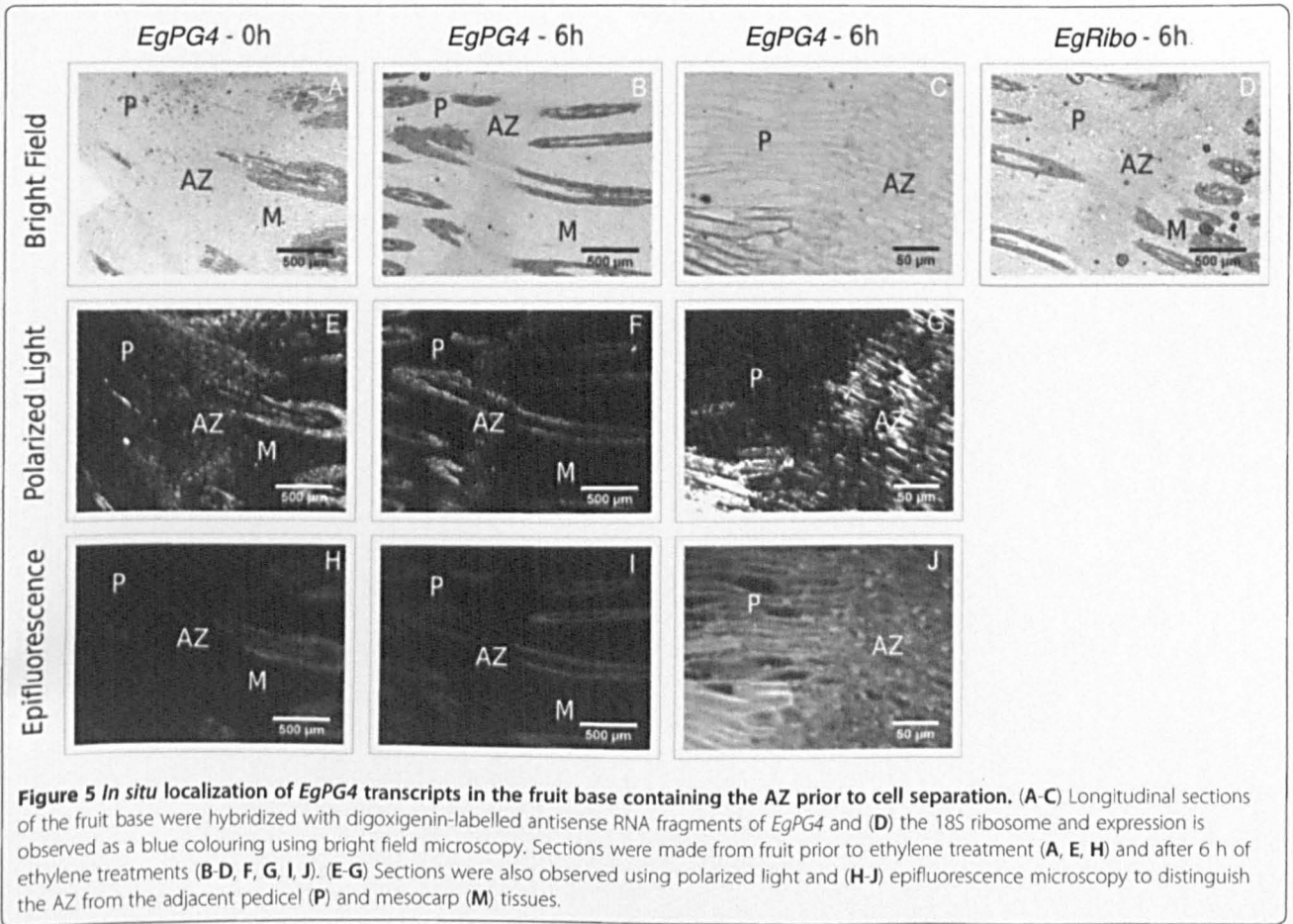
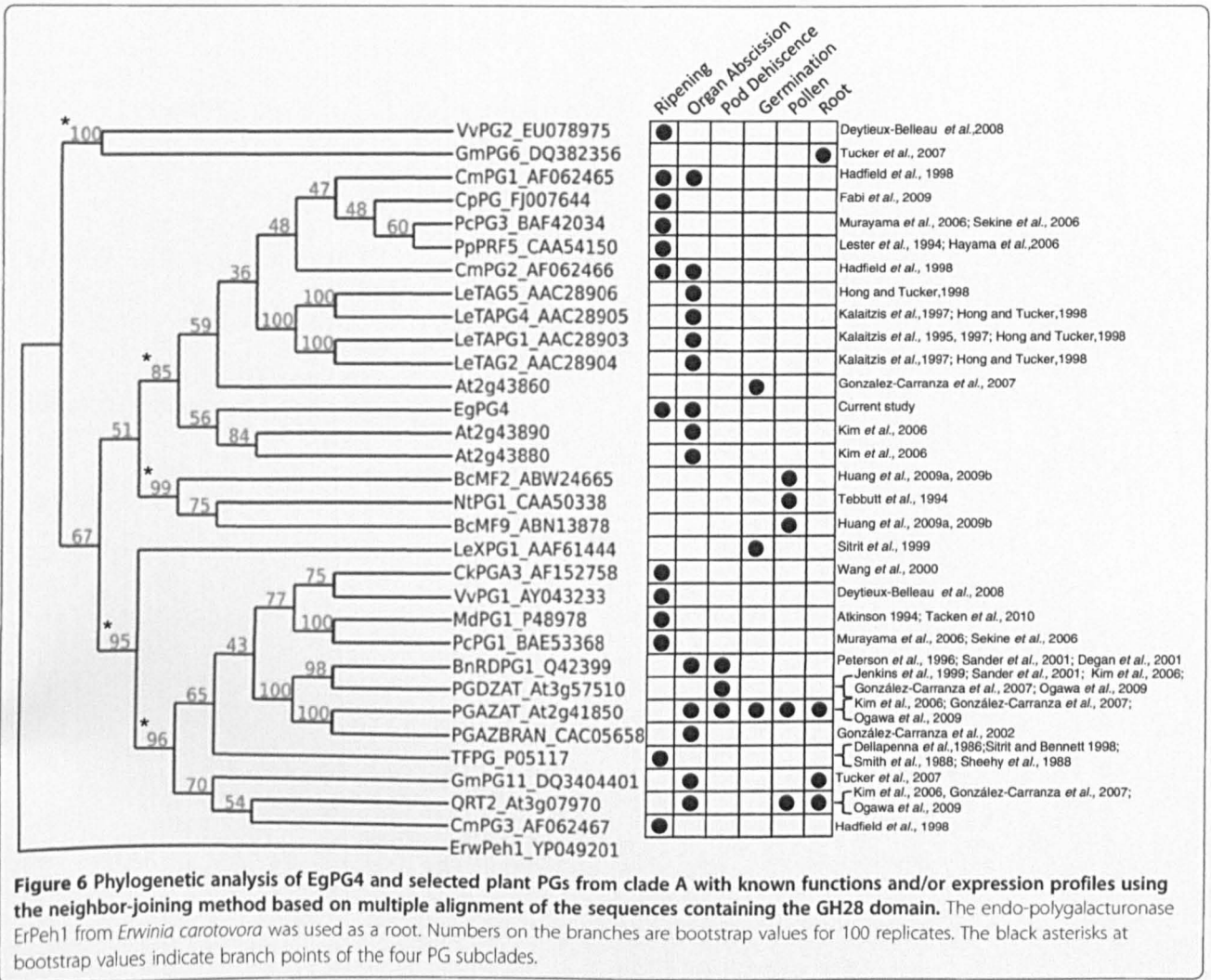


Figure 5 *In situ* localization of *EgPG4* transcripts in the fruit base containing the AZ prior to cell separation. (A-C) Longitudinal sections of the fruit base were hybridized with digoxigenin-labelled antisense RNA fragments of *EgPG4* and (D) the 18S ribosome and expression is observed as a blue colouring using bright field microscopy. Sections were made from fruit prior to ethylene treatment (A, E, H) and after 6 h of ethylene treatments (B-D, F, G, I, J). (E-G) Sections were also observed using polarized light and (H-J) epifluorescence microscopy to distinguish the AZ from the adjacent pedicel (P) and mesocarp (M) tissues.

from *Arabidopsis* and rice was performed. Firstly, *EgPG4* groups within the PG clade A3 formed with members from both rice and *Arabidopsis* previously defined [32] (Additional file 4). Notably, *EgPG4* does not group with the PGs from *Arabidopsis* in clade A15 shown to function during floral organ abscission, silique or anther dehiscence including At2g41850 (PGAZAT/ADPG2), At3g07970 (QUARTET2), and At3g57510 (PGDZAT/ADPG1) [31-33]. However, *EgPG4* is grouped in the A3 clade with two other *Arabidopsis* PGs (At2g43880 and At2g43890) that are expressed during floral organ abscission [32].

To examine possible structure-function relationships of the *EgPG4* amino acid sequence with those of known PGs from a variety of species, including those producing fleshy fruits (apple, plum, peach, tomato, kiwi, grape, papaya), and dry fruits (soybean, *B. napus*, *Arabidopsis*), a phylogenetic analysis was performed with selected plant PGs with expression associated with or shown to function during germination, root or pollen development, fruit ripening, organ abscission, and anther and pod dehiscence [19-21,23,25-27,31,33-55]. Firstly, the reconstructed tree and bootstrap values confirm earlier analyses that PGs can be separated into three major

subclades, two that consist of PGs involved in fruit ripening and abscission and one with PGs involved in pollen development [18,19] (Figure 6). The presence of a fourth clade containing soybean (GmPG6_DQ382356) and grape (VvPG2_EU078975) PGs supports more recent studies that indicate this gene family consists of more than three subclades [36,56]. In addition, the bootstrap analysis confirms a close phylogenetic relationship between *EgPG4* and two *Arabidopsis* PGs expressed during floral organ abscission [32]. Notably, in the same subclade there are also four abscission related tomato PGs (TAPG1, TAPG2, TAPG4 and TAPG5) [20,21,38] in addition to two PGs expressed during ripening and abscission of melon (CmPG1 and CmPG2) [19], and PGs expressed during ripening of papaya (CpPG) [37], pear (PcPG3) [53,54] and peach (PpPRF5) [42]. An additional *Arabidopsis* PG (At2g43860) that functions in cell separation between endosperm cells when the radicle emerges during germination [31] was also found within this subclade. The analysis also revealed that the *Arabidopsis* PGs involved in abscission or dehiscence including PGDZAT, PGAZAT, and QTR2, are grouped within a distinct subclade with other PGs that function during fruit ripening, floral organ abscission and pod



dehiscence [31,33,35]. Notably, no PG involved in abscission of a fleshy fruit is found in this clade, only those from species with dry fruit such as *Arabidopsis*, *B. napus* and soybean.

Discussion

Sequence and expression analysis of EgPG4 suggests functional conservation and divergences between monocots and eudicots

PGs are thought to play a central role in the disassembly of pectin in the middle lamella or primary cell wall during cell separation and cell elongation [18]. In particular, PGs have been extensively studied during fruit ripening, organ abscission and pollen development, yet how divergence has occurred between species in order to fulfil different roles in these various tissues is still not completely understood. In particular, very little data is available from monocot species to compare the ripening and abscission processes with those of eudicots.

Our phylogenetic and bootstrap analyses confirmed several previous phylogenetic studies that revealed PGs involved in organ abscission and fruit ripening to be found mainly in two distinct subclades, with a third subclade containing only pollen related PGs [18,19,31,32]. A fourth minor subclade that contained a PG from ripening grape skin was also observed as previously [36]. While the current phylogenetic analysis was done with the complete GH28 domain, not including the prosequences characteristic of some PGs, the results support a previous conclusion that the presence or lack of prosequences are not the basis for the divergence of these sequences into distinct clades [18]. The first notable observation is that all the known tomato abscission PGs group closely within a subclade that also contains the two closely related *Arabidopsis* floral organ abscission associated PGs (At2g43890 and At2g43880), in addition to an *Arabidopsis* PG (At2g43860) implicated in radicle emergence [31,32]. The presence of At2g43860, a PG expressed during the separation of endosperm cells

when the radicle emerges during germination, suggests structural relationships between PGs with functions beyond fruit ripening and organ abscission. It is interesting that EgPG4 groups closest with these *Arabidopsis* abscission PGs, which suggests functional conservation, and that these sequences are derived from a common ancestral PG that existed prior to the separation of monocots and eudicots. A second notable observation is that the tomato fruit PG (TFPG) is more closely associated with the abscission and dry fruit dehiscence PGs than with the tomato PGs involved in organ abscission. This contrasts with sequences from melon that are in the same subclade as the tomato abscission PGs, and have expression profiles associated with both fruit ripening and abscission [19]. Similarly, the *EgPG4* transcript does not only increase in the AZ in relation to abscission, but also is highly expressed in the portion of the ripening mesocarp. Together, it appears that some PGs may function both in ripening fruit tissues, in addition to during cell separation in the AZ that leads to fruit organ abscission in monocots and eudicots.

The sequence and expression of EgPG4 suggest functional divergence between dry and fleshy fruit

Another notable observation is that PGs related to fleshy fruit abscission are not found within the clade containing the well-characterized abscission and/or dehiscent related PGs including QRT2, PGAZAT, PGDZAT, BnRDPG1 and PGAZBRAN [33,34]. By contrast, PGs involved in fleshy fruit ripening, such as the tomato (TFPG), grape (VvPG1), apple (MdPG1), kiwi (CkPGA3) and pear (PcPG1) are also found within this clade [23,25-27,36,43,44,48,50,51]. In addition, only the melon PG (CmPG3) that has an expression profile related to ripening is found in the same subclade as the dry fruit dehiscence and abscission PGs, while the other two melon PGs (CmPG1 and CmPG2) associated with organ abscission and ripening are in the same subclade as *EgPG4* [19]. While there is no current data that suggests that the fleshy fruit PGs within this subclade are involved in fruit or other organ abscission, it is possible their involvement in cell separation during organ abscission has not been sufficiently investigated. Indeed, the analysis and results discussed here are based on the two best-characterized organ abscission model systems available, namely tomato and *Arabidopsis*, and it should be emphasised that many gaps exist in our current knowledge about the functional diversity of plant PGs. Nevertheless, the results suggest that dry fruit species may have PGs from at least two divergent subclades involved in cell separation for dehiscence, while fleshy fruit may have PGs specialized in ripening or abscission, or, that may function in both contexts. Overall, the results suggest that divergence may have occurred between PGs

involved in dry fruit dehiscence and fleshy fruit abscission, an area that merits further investigation.

The high expression and induction of EgPG4 by ethylene suggests functions during both fruit ripening and abscission

The most notable result of this study is the high accumulation of the *EgPG4* transcript in the base of the fruit containing the AZ prior to cell separation. Importantly, *EgPG4* transcript accumulates prior to the occurrence of cell separation, and also accumulates less and in correlation to the timing of the slower separation in fruit at earlier stages of development. However, the *EgPG4* transcript is also highly expressed in the mesocarp tissue near the apex of the fruit that suggests a role in the ripening of this tissue. Our data also indicate that the regulation of *EgPG4* is closely associated with the capacity for cells to respond to ethylene. This in turn is related to the developmental stage of ripening, and may be an important factor that controls the spatial and temporal functionality of *EgPG4* during mesocarp ripening and cell separation in the AZ. Indeed, the mesocarp produces an increasing amount of ethylene during ripening, and production progresses from the apex of the fruit to the fruit base, where it may act as the signal to initiate the separation events within the AZ [9,57]. Studies on fruit ripening and floral pedicel abscission of tomato provide examples of how individual members of this gene family may have distinct functions in adjacent tissues undergoing cell separation processes in a fleshy fruit species, and highlight the central importance of tissue specific transcriptional regulation of PGs during these developmental processes. Indeed, the tomato fruit *TFPG* is the only PG gene expressed in the ripening fruit tissues, its transcription is positively regulated by ethylene, and the encoded protein is responsible for the PG activity required for pectin depolymerisation that occurs during ripening [23-27]. Notably, the *TFPG* mRNA accounts for up to 2.3% of the total RNA in ripening tomato fruit, and down regulation of *TFPG* has no effect on the timing or rate of leaf abscission, indicating a specific function of this enzyme during fruit ripening but not organ abscission [22,58]. In contrast, in the pedicel where the AZ is located at the base of the tomato floral organs, there are at least four abscission-related PG genes (*TAPG1*, *TAPG2*, *TAPG4* and *TAPG5*) expressed, three of which are induced by ethylene and correlate well with the cell separation that occurs in the flower and leaf AZs [20,21,38]. Furthermore, silencing of the tomato abscission-related PGs using a *TAPG1* fragment, delayed abscission and increased break strength of the leaf petiole AZs in explants treated with ethylene. These studies suggest that a combination of tissue specific transcriptional regulation and/or localized cellular

differences in response to ethylene are important factors that determine the spatial and temporal specificities related to their functional roles during fruit ripening and organ abscission.

Oil palm fruit shedding has some similarities but also notable differences from that seen in tomato. Firstly, the timing of separation induced by ethylene in oil palm is comparable to that in tomato. In the presence of ethylene, cell separation begins to occur by 9 h, while 80–100% of ripe fruit are shed by 12 h, whereas in tomato, flower shedding begins at 6 h and is complete by 12 h [59]. This result is striking given the surface area of the primary AZ of ripe oil palm, up to 10 mm (Figure 3) is approximately 20 times larger than the tomato pedicel AZ, up to 0.55 mm [59]. Secondly, we observe a greater diversity of PGs expressed in the oil palm fruit tissues than that of tomato during ripening or abscission. Notably, of the 14 transcripts expressed in the base of the fruit containing the AZ, five are regulated positively, and four others negatively in response to ethylene. In addition, five PG mRNAs displayed no significant change in abundance during the ethylene treatments. A previous study with banana fruit revealed that at least four PG genes are expressed during ripening [60]. However, none of the PGs identified in that study contained the full-length GH28 domain and thus we were not able to compare their phylogenetic relationship with the oil palm PGs and other PGs presented in Figure 6. The expression of the banana PG genes was also analyzed during finger drop, a process that also involves pectin disassembly [60,61]. The results indicated that the four banana PGs were also expressed in the finger drop zone where cell separation takes place, while *MaPG4* was the most highly expressed with a profile of accumulation correlated to the decrease in the pedicel rupture force observed. Together with the present results, the mechanisms of pectin disassembly during banana and oil palm fruit ripening may involve a larger number of PGs than with eudicot species examined thus far. The current study allows a more complete view of PG expression in relation to ethylene in a monocot fruit, given that the earlier studies with banana included fewer and shorter PG sequences [60,61]. In addition, whereas both are monocots, the banana is a parthenocarpic berry-type fruit that accumulates large amounts of starch, while the oil palm is a drupe with the high oil content, which may also dictate different ripening regulatory mechanisms between these two species. Future work will require new molecular resources for more complete comparative studies of fruit ripening and abscission in these two diverse monocots, in addition to the well-characterized eudicot tomato model.

In comparison to tomato, the diversity and complexity of PG expression in the oil palm fruit tissues is far

greater than that observed in the AZs or during ripening. In the oil palm, all 14 *EgPG* transcripts are detected to some extent in the ripening mesocarp tissue, in contrast to the single *TFFPG* expressed during tomato fruit ripening. Notably, none of the *EgPGs* mRNAs identified appears to be completely tissue specific, as observed with the tomato PGs involved in abscission and ripening. However, the data presented here suggest that differences in their tissue and developmental stage dependent response to ethylene may be important for spatial and temporal control. The most notable example is that of *EgPG4*, which is not only the most abundant PG transcript in the mesocarp of untreated ripe fruit, but also undergoes the most dramatic increase in abundance in the base of the fruit containing the AZ in response to ethylene. The high abundance of *EgPG4* in the mesocarp and the massive increase in response to ethylene is similar to PG expression in tomato; however, *EgPG4* is highly expressed in both the ripening mesocarp and the AZ after ethylene treatment prior to fruit shedding. Furthermore, our *in situ* hybridization experiments indicate the increase in *EgPG4* transcript abundance in the base of the fruit occurs preferentially in the AZ compared with the adjacent mesocarp and pedicel tissues. Importantly, a delayed and less significant increase in *EgPG4* transcript is also observed in the AZ of untreated fruit, as well as in 30 and 120 DAP fruit treated with ethylene, which corresponds to the delay in shedding observed at these stages of ripening.

Conclusions

Together, these results provide evidence that *EgPG4* participates in cell wall pectin modifications during both mesocarp ripening and in the AZ cells during fruit shedding, in close relation to a developmentally regulated cell sensitivity or competence to respond to ethylene. Future work will be aimed at identifying the regulatory factors that control the ripening and abscission related expression of *EgPG4*, to provide a basis to compare these processes not only between monocots and eudicots, but in particular between fleshy and dry fruit species. Finally, the identification of genes involved in oil palm fruit shedding will also be helpful for oil palm improvement selection strategies.

Methods

Plant material, ethylene treatment and RNA extraction

Oil palm (*Elaeis guineensis* Jacq) fruits were harvested at Krabi Golden Tenera plantation, from a *tenera* clone (clone C) produced in Thailand. For each stage of development studied, independent bunches were collected from distinct individuals of the same genotype. Spikelets were then collected in the centre of each bunch and sets of 6 spikelets were randomly sampled from them and

put in individual hermetically sealed 50 l volume boxes. Spikelets with fruits at 150 days after pollination (DAP) were treated with different concentrations of ethylene (0, 0.001, 0.01, 0.1, 1, 10 $\mu\text{l l}^{-1}$). In absence of ethylene treatment, ethylene absorber (ETHYL-GONE, <http://www.biosafes.com/ethyl-gone.php>) was added in the box. All the boxes were kept at ambient temperature (approximately 30°C), and after 24 h of treatment the number of fruit separating from the spikelets were counted. Using the concentration of ethylene (10 $\mu\text{l l}^{-1}$) that induced and synchronized the highest amount of fruit shedding, a time course analysis was then conducted that used the same process with fruit from 30, 120 and 180 DAP. Spikelets were treated with or without ethylene, and every 3 h, treated or untreated spikelets were collected and shedding was quantified for each stage of development. For each time point, the mesocarp, pedicel and the base of the fruit containing the primary and adjacent AZs were isolated and frozen immediately in liquid nitrogen. Samples from two independent experiments were collected immediately after bunches were harvested.

Total RNA from mesocarp, pedicel and the base of the fruit enriched in AZs, treated or not with ethylene was extracted as previously described [62]. Total RNA (1 μg) was used to synthesize cDNA using the first-strand cDNA synthesis kit (ImProm-IITM Reverse Transcription System, Promega).

Identification of oil palm non-redundant PG nucleotide sequences from fruit

To identify oil palm PG cDNA sequences a number of molecular resources were used. First, the tblastn program was used to search available databases that contain *Elaeis guineensis* sequences, including NCBI (<http://www.ncbi.nlm.nih.gov>), local 454 pyrosequencing derived oil palm mesocarp contigs [57] and contigs derived from tissues enriched in the AZ (Jantasuriyarat *et al.*, unpublished), for sequences with high similarity to PGs from *Arabidopsis* and rice previously described [32]. Additional sequences were also kindly contributed by Dr Arondel [63]. A complementary approach utilized degenerate primers [34] to amplify cDNAs from AZ tissues treated with or without ethylene at different developmental stages and from oil palm genomic DNA. Primers from the oil palm PEST643 (accession number N° AY291341) were designed in the most conserved regions of PGs and also used to amplify PG cDNAs from fruit tissues. For sequences lacking the 3' regions, RACE (Clontech) amplification was performed and from sequences obtained, sequence specific primer pairs were designed and used to amplify non-redundant PGs from the oil palm fruit tissues. A total of 35 putative non-redundant PG sequences were identified from these complementary approaches

and were compared to confirm similarity to plant PGs, in particular the presence of a partial or complete glycoside hydrolase 28 (GH28) domain that covers approximately 75% of each PG coding sequence [35]. The accession numbers for *EgPG1* and *EgPG4* are JX233615 and JX233616 respectively, while other PG sequences are from previous datasets [57,63].

Quantitative Real-Time RT-PCR

qPCR was conducted on a LightCycler 480 (Roche) in 96 well plates in a volume of 10 μl containing 2 μl of cDNA diluted 1/100, 1.5 μl of primer forward (2 μM), 1.5 μl of reverse primer (2 μM) and 5 μl SYBR[®] Green Mastermix (Roche). Additional file 5 lists the primers used. PCR was initiated by denaturation at 95°C for 10 min, followed by 45 cycles of 95°C for 15 s, 60°C for 15 s, and a final extension at 70°C for 1 min. All expression was normalized to the *EgEfa1* (accession number: AY550990) mRNA from *Elaeis guineensis*, and relative mRNA abundance was determined with the formula as described previously [64]. No change of *EgEfa1* transcript accumulation was found in the fruit tissues treated or not treated with ethylene. Control using RNA matrices were also conducted to validate the absence of DNA in each sample. Each time point was replicated three times from 2 independent biological samples, and all amplified cDNA fragments were sequenced by Beckman-Cogenics to check the specificity of the amplified products. Gene abundance is expressed as mean and standard error bars are calculated from the technical replicates of one of the biological repetitions.

Phylogenetic analysis

Phylogenetic trees were constructed based on similarity searches performed with BLASTp programs with default parameters in protein sequence databases provided by the NCBI server (<http://www.ncbi.nlm.nih.gov>). Phylogenetic analyses were performed on the Phylogeny.fr platform (<http://www.phylogeny.fr>) [65]. Amino acid sequences from the GH28 domain were aligned with ClustalW (v2.0.3) [66]. After alignment, ambiguous regions (i.e. containing gaps and/or poorly aligned) were removed with Gblocks (v0.91b). The phylogenetic tree was constructed using the neighbour joining method implemented in Neighbor from the PHYLIP package (v3.66) [67]. Distances were calculated using ProtDist. The Jones-Taylor-Thornton substitution model was selected for the analysis [68]. The robustness of the nodes was assessed by bootstrap proportion analysis computed from 100 replicates [69]. Graphical representation and edition of the phylogenetic tree were performed with TreeDyn (v198.3) and Inkscape respectively.

RNA *in situ* hybridization

To obtain DNA templates for the RNA probe synthesis, PCR amplifications were performed with gene-specific antisense primers tailed with a T7 RNA polymerase binding site. PCRs were performed with the EgPG4qS1–EgPG4qAS1T7 and EgPG4S1T7–EgPG4qAS1, and the EgRiboS–EgRiboAST7 and EgRiboST7–EgRiboAS primer pairs for *EgPG4*, and *EgRibo*-specific probes, respectively (Additional file 6). The resulting DNA fragments were used directly as templates to synthesize antisense probes, with the incorporation of UTP–digoxigenin (Roche) as the label using the MAXIscript® T7 Kit (Ambion). Each amplification product was sequenced to check the specificity of the products amplified. *In situ* hybridization experiments were carried out as described previously [70] with some modifications. The fruit bases from untreated fruits and fruits treated with 10 $\mu\text{l l}^{-1}$ of ethylene for 6 h were fixed overnight in the dark at 4°C in fixation buffer (4% paraformaldehyde, 0.1 M phosphate buffer pH 7). After 16h, they were washed two times in 0.1 M phosphate buffer with 2% glycine, then two times in 0.1 M phosphate buffer before dehydration through an increasing series of ethanol and butanol concentrations. After 15 days in butanol to soften the tissues, the samples were embedded in Paraplast plus (Paraplast X-Tra, Oxford Labware) and sectioned to 12 μm with a microtome. Tissue sections were deparaffinised with Safesol (LaboNord, France), rehydrated through an ethanol series of decreasing concentrations, and then pre-treated with proteinase K (100 U μl^{-1} , Roche) in Tris–HCl (100 mM, pH 7.5), EDTA (50 mM) at 37°C for 35 min. Digestion was stopped by washing twice for 5 min each with TRIS–HCL (20 mM, pH 7.5, CaCl₂ (2mM) and MgCl₂ (50 mM), then phosphate-buffered saline (0.1 M PBS) with 0.2% glycine for 2 min, and then twice with 0.1 M PBS. After ethanol baths, hybridization was performed at 45°C overnight with 200 ng of the digoxigenin-labelled RNA probe in 100 μl of hybridization solution (50 μl formamide, 10 μl 20X SSC, 1 μl Denhardt 100X, 20 μl dextran sulphate 50%, 1 μl tRNA at 100 mg ml^{-1}). After hybridization, slides were washed in 2X SSC at 25°C for 5 min, in 2X SSC at 50°C for 45 min and in 1X NTE (Tris–HCl 10 mM, NaCl 0.5 M, EDTA 1 mM, pH 7.5) at 25°C then 37°C for 5 min each. An RNase A digestion (20 $\mu\text{g ml}^{-1}$) was carried out for 30 min at 37°C and stopped by washing with 1X NTE at 37°C. Final washes were conducted twice in 1X SSC for 30 min each at 55°C. Detection was performed using the Vector Blue Alkaline Phosphatase Substrate Kit III (Vector Laboratories). Control without probe was conducted to valid the absence of endogenous alkaline phosphate activity. Samples were incubated in blocking reagent [Roche; 10% (w/v) in PBS] for 1 h and afterwards for 45 min at 37°C containing antidigoxigenin alkaline phosphatase-conjugated Fab fragment antibody (Roche) diluted at 1:500 in blocking

reagent. After three washes for 10 min in 0.1 M PBS, tissues were equilibrated in detection buffer (100 mM Tris–HCl pH 8.2) then several batches of 3 h at 37°C with Blue vector. Finally the detection was amplified by ethanol vapour for 20 min and samples were mounted on slides with Mowiol and observed with a bright-field microscope (Leica DM6000) using the 40X/0.75 numeric aperture. To visualize the abscission zone, tissue sections were also observed under polarized light and epifluorescence with a TXR filter. Photographs were taken with a Retiga 2000R camera (Qimaging). *In situ* hybridization and microscopy analysis were conducted at the “Plate-Forme d’Histocytologie et Imagerie Cellulaire Végétale” (PHIV platform; <http://phiv.cirad.fr/>).

Additional files

Additional file 1: List of the 28 sequences that contain either a partial or complete GH28 PG signature domain.

Additional file 2: Standard errors for Figure 3. Percentages were calculated from gene expression data derived from qPCR analysis that included individual values (3 technical repetitions) compared to the average expression of the reference gene (*EgEF1a*, elongation factor 1 α), together with the standard deviation (SD) for the following three tissue regions of the fruit: AZ, Abscission Zone; M, Mesocarp; P, Pedicel.

Additional file 3: Control experiments for *in situ* hybridization studies. Longitudinal sections of the fruit base were hybridized with digoxigenin-labelled RNA fragments of *EgPG4* antisense (A) and sense (B), and the 18S ribosome antisense (C) and sense (D) probes after 6h ethylene treatment.

Additional file 4: Phylogenetic analysis of *EgPG4*, *EgPG8* and *EgPG10* with sequences from *Arabidopsis* and rice.

Additional file 5: List of primers used for expression analysis of oil palm PG genes by qPCR.

Additional file 6: List of primers used for the synthesis of *in situ* hybridization probes.

Abbreviations

PG: Polygalacturonase; AZ: Abscission zone; GH28: Glycoside hydrolase family 28; DAP: Days after pollination.

Competing interests

There are no competing interests to declare.

Authors' contributions

TJT and FM devised and participated in all aspects of the study. TJT and ST coordinated the logistics for study. TJT, FM, PR, CJ and MP performed the ethylene experiments and collected samples for RNA isolation and *in situ* hybridization studies. PR extracted total RNA, isolated polygalacturonase cDNAs, performed cloning, designed gene specific primers and performed preliminary RT-PCR expression studies. ZHGC participated in the identification of putative polygalacturonase cDNAs. MP and FM performed the qPCR analysis. ST and PA participated in the data analysis and critically read the manuscript. SM and FM performed the phylogenetic analysis. JLV, SM, DJ and MC prepared samples for histological analysis and performed *in situ* hybridizations. TJT, JLV, FM, ZHGC, JWT and PR participated in writing the article. All authors read and approved the final submitted manuscript.

Acknowledgments

This work was supported by a Fondation Agropolis RTRA doctoral grant to PR. Financial support for the project also came from PHC Thaïlande projects 2007–2010 (codes 16589YK and 16589YK) to TJT and ST, and from PalmElit SAS/IRD/CIRAD to FM and TJT. We thank Jerry Roberts for helpful discussions

and advice on the project. We especially thank Anek Limsrivilai and the staff at GoldenTenera Oil Palm Plantation in Thailand for the excellent plant material used in the study. We also appreciate Marc Lebrun's excellent technical assistance with ethylene experiment set-up.

Author details

¹Institut de Recherche pour le Développement, IRD Centre de Montpellier, IRD/CIRAD Palm Development Group, DIADE 911 avenue agropolis BP 64501, 34394 Montpellier cedex 5, France. ²Centre de Coopération Internationale en Recherche Agronomique pour le Développement, CIRAD, UMR DIADE, Montpellier F-34398, France. ³Department of Genetics, Faculty of Science, Kasetsart University, Bangkok Campus, 50 Phahonyothin Road, Jatujak, Thailand. ⁴Division, Loughborough, The University of Nottingham, Sutton Bonington Campus, School of Biosciences, Plant Science, Leicestershire LE12 5RD, United Kingdom. ⁵PalmElit SAS, Montferrier-sur-Lez F-34980, France. ⁶Genome Institute, National Center for Genetic Engineering and Biotechnology, BIOTEC, 113 Thailand Science Park, Phahonyothin Road, Klong 1, Klong Luang, Pathumthani 12120, Thailand. ⁷Centre de Coopération Internationale en Recherche Agronomique pour le Développement CIRAD, UMR AGAP, MRI-PHIV, Montpellier F-34398, France.

Received: 23 November 2011 Accepted: 26 July 2012

Published: 25 August 2012

References

- Addicott FT: *Abscission*. Berkeley and Los Angeles, California: University of California Press; 1982.
- Leslie ME, Lewis MW, Liljegren SJ: **Organ Abscission**. In *Plant Cell Separation and Adhesion, Annual Plant Reviews*. Edited by Roberts JA, Gonzalez-Carranza ZH. Oxford, UK: Blackwell Publishing; 2007. vol. 25.
- Roberts JA, Elliott KA, Gonzalez-Carranza ZH: **Abscission, dehiscence, and other cell separation processes**. *Annu Rev Plant Biol* 2002, **53**:131–158.
- Sexton R, Roberts JA: **Cell Biology of Abscission**. *Annual Review of Plant Physiology* 1982, **33**(1):133–162.
- Osborne DJ, Henderson J, Corley RHV: **Controlling Fruit Shedding in the Oil Palm**. *Endeavour* 1992, **16**(4):173–177.
- Rival A: *Oil Palm*, Volume 61. Berlin Heidelberg: Springer; 2007.
- Henderson J, Davies HA, Heyes SJ, Osborne DJ: **The study of a monocotyledon abscission zone using microscopic, chemical, enzymatic and solid state C-13 CP/MAS NMR analyses**. *Phytochemistry* 2001, **56**(2):131–139.
- Henderson J, Osborne DJ: **Cell Separation and Anatomy of Abscission in the Oil Palm, *Elaeis guineensis* Jacq.** *J Exp Bot* 1990, **41**(2):203–210.
- Henderson J, Osborne DJ: **Intertissue Signaling during the 2-Phase Abscission in Oil Palm Fruit**. *J Exp Bot* 1994, **45**(276):943–951.
- Taylor JE, Whitelaw CA: **Signals in abscission**. *New Phytol* 2001, **151**(2):323–340.
- Burr CA, Leslie ME, Orłowski SK, Chen I, Wright CE, Daniels MJ, Liljegren SJ: **CAST AWAY, a membrane-associated receptor-like kinase, inhibits organ abscission in Arabidopsis**. *Plant Physiol* 2011, **156**(4):1837–1850.
- Liljegren SJ, Leslie ME, Darnielle L, Lewis MW, Taylor SM, Luo R, Geldner N, Chory J, Randazzo PA, Yanofsky MF, et al: **Regulation of membrane trafficking and organ separation by the NEVERSHED ARF-GAP protein**. *Development* 2009, **136**(11):1909–1918.
- Berger RK, Reid PD: **Role of polygalacturonase in bean leaf abscission**. *Plant Physiol* 1979, **63**(6):1133–1137.
- Bonghi C, Rascio N, Ramina A, Casadoro G: **Cellulase and Polygalacturonase Involvement in the Abscission of Leaf and Fruit Explants of Peach**. *Plant Mol Biol* 1992, **20**(5):839–848.
- Taylor JE, Webb STJ, Coupe SA, Tucker GA, Roberts JA: **Changes in Polygalacturonase Activity and Solubility of Poluronides during Ethylene-Stimulated Leaf Abscission in *Sambucus-Nigra***. *J Exp Bot* 1993, **44**(258):93–98.
- Tucker GA, Schindler B, Roberts JA: **Flower abscission in mutant tomato plants**. *Planta* 1984, **160**:164–167.
- Giovannoni JJ, DellaPenna D, Bennett AB, Fischer RL: **Expression of a chimeric polygalacturonase gene in transgenic rin (ripening inhibitor) tomato fruit results in polyuronide degradation but not fruit softening**. *Plant Cell* 1989, **1**(1):53–63.
- Hadfield KA, Bennett AB: **Polygalacturonases: Many genes in search of a function**. *Plant Physiol* 1998, **117**(2):337–343.
- Hadfield KA, Rose JKC, Yaver DS, Berka RM, Bennett AB: **Polygalacturonase gene expression in ripe melon fruit supports a role for polygalacturonase in ripening-associated pectin disassembly**. *Plant Physiol* 1998, **117**(2):363–373.
- Kalaitzis P, Koehler SM, Tucker ML: **Cloning of a Tomato Polygalacturonase Expressed in Abscission**. *Plant Mol Biol* 1995, **28**(4):647–656.
- Kalaitzis P, Solomos T, Tucker ML: **Three different polygalacturonases are expressed in tomato leaf and flower abscission, each with a different temporal expression pattern**. *Plant Physiol* 1997, **113**(4):1303–1308.
- Taylor JE, Tucker GA, Lasslett Y, Smith CJS, Arnold CM, Watson CF, Schuch W, Grierson D, Roberts JA: **polygalacturonase expression during leaf abscission of normal and transgenic tomato plants**. *Planta* 1990, **183**(1):133–138.
- Dellapenna D, Alexander DC, Bennett AB: **Molecular cloning of tomato fruit polygalacturonase: Analysis of polygalacturonase mRNA levels during ripening**. *Proc Natl Acad Sci USA* 1986, **83**(17):6420–6424.
- Dellapenna D, Lincoln JE, Fischer RL, Bennett AB: **Transcriptional analysis of polygalacturonase and other ripening associated genes in rutgers, rin, nor, and Nr Tomato Fruit**. *Plant Physiol* 1989, **90**(4):1372–1377.
- Sheehy RE, Kramer M, Hiatt WR: **Reduction of polygalacturonase activity in tomato fruit by antisense RNA**. *Proc Natl Acad Sci USA* 1988, **85**(23):8805–8809.
- Sitrit Y, Bennett AB: **Regulation of tomato fruit polygalacturonase mRNA accumulation by ethylene: A Re-examination**. *Plant Physiol* 1998, **116**(3):1145–1150.
- Smith CJS, Watson CF, Ray J, Bird CR, Morris PC, Schuch W, Grierson D: **Antisense RNA inhibition of polygalacturonase gene expression in transgenic tomatoes**. *Nature* 1988, **334**:724–726.
- Cooley MB, Yoder JI: **Insertional inactivation of the tomato polygalacturonase gene**. *Plant Mol Biol* 1998, **38**(4):521–530.
- Smith CJ, Watson CF, Morris PC, Bird CR, Seymour GB, Gray JE, Arnold C, Tucker GA, Schuch W, Harding S, et al: **Inheritance and effect on ripening of antisense polygalacturonase genes in transgenic tomatoes**. *Plant Mol Biol* 1990, **14**(3):369–379.
- Jiang CZ, Lu F, Imsabai W, Meir S, Reid MS: **Silencing polygalacturonase expression inhibits tomato petiole abscission**. *J Exp Bot* 2008, **59**(4):973–979.
- Gonzalez-Carranza ZH, Elliott KA, Roberts JA: **Expression of polygalacturonases and evidence to support their role during cell separation processes in *Arabidopsis thaliana***. *J Exp Bot* 2007, **58**(13):3719–3730.
- Kim J, Patterson SE: **Expression divergence and functional redundancy of polygalacturonases in floral organ abscission**. *Plant Signal Behav* 2006, **1**(6):281–283.
- Ogawa M, Kay P, Wilson S, Swain SM: **Arabidopsis dehiscence zone polygalacturonase1 (ADPG1), ADPG2, and QUARTET2 are Polygalacturonases required for cell separation during reproductive development in Arabidopsis**. *Plant Cell* 2009, **21**(1):216–233.
- Gonzalez-Carranza ZH, Whitelaw CA, Swarup R, Roberts JA: **Temporal and spatial expression of a polygalacturonase during leaf and flower abscission in oilseed rape and Arabidopsis**. *Plant Physiol* 2002, **128**(2):534–543.
- Kim J, Shiu SH, Thoma S, Li WH, Patterson SE: **Patterns of expansion and expression divergence in the plant polygalacturonase gene family**. *Genome Biol* 2006, **7**(9):R87.
- Deytieux-Belleau C, Vallet A, Doneche B, Geny L: **Pectin methylesterase and polygalacturonase in the developing grape skin**. *Plant Physiol Biochem* 2008, **46**(7):638–646.
- Fabi JP, Cordenunsi BR, Seymour GB, Lajolo FM, do Nascimento JR: **Molecular cloning and characterization of a ripening-induced polygalacturonase related to papaya fruit softening**. *Plant Physiol Biochem* 2009, **47**(11–12):1075–1081.
- Hong SB, Tucker ML: **Genomic organization of six tomato polygalacturonases and 5' upstream sequence identity with tap1 and win2 genes**. *Mol Gen Genet* 1998, **258**(5):479–487.
- Huang L, Cao J, Zhang A, Ye Y, Zhang Y, Liu T: **The polygalacturonase gene BcMF2 from *Brassica campestris* is associated with intine development**. *J Exp Bot* 2009, **60**(1):301–313.
- Huang L, Ye Y, Zhang Y, Zhang A, Liu T, Cao J: **BcMF9, a novel polygalacturonase gene, is required for both *Brassica campestris* intine and exine formation**. *Ann Bot* 2009, **104**(7):1339–1351.
- Jenkins ES, Paul W, Coupe SA, Bell SJ, Davies EC, Roberts JA: **Characterization of an mRNA encoding a polygalacturonase expressed during pod development in oilseed rape (*Brassica napus* L.)**. *J Exp Bot* 1996, **47**(294):111–115.

42. Lester DR, Speirs J, Orr G, Brady CJ: **Peach (*Prunus persica*) endopolygalacturonase cDNA isolation and mRNA analysis in melting and nonmelting peach cultivars.** *Plant Physiol* 1994, **105**(1):225–231.
43. Murayama H, Sekine D, Yamauchi Y, Gao M, Mitsuhashi W, Toyomasu T: **Effect of girdling above the abscission zone of fruit on 'Bartlett' pear ripening on the tree.** *J Exp Bot* 2006, **57**(14):3679–3686.
44. Sekine D, Munemura I, Gao M, Mitsuhashi W, Toyomasu T, Murayama H: **Cloning of cDNAs encoding cell-wall hydrolases from pear (*Pyrus communis*) fruit and their involvement in fruit softening and development of melting texture.** *Physiol Plant* 2006, **126**(2):163–174.
45. Sitrit Y, Hadfield KA, Bennett AB, Bradford KJ, Downie AB: **Expression of a polygalacturonase associated with tomato seed germination.** *Plant Physiol* 1999, **121**(2):419–428.
46. Tebbutt SJ, Rogers HJ, Lonsdale DM: **Characterization of a tobacco gene encoding a pollen-specific polygalacturonase.** *Plant Mol Biol* 1994, **25**(2):283–297.
47. Tucker ML, Burke A, Murphy CA, Thai VK, Ehrenfried ML: **Gene expression profiles for cell wall-modifying proteins associated with soybean cyst nematode infection, petiole abscission, root tips, flowers, apical buds, and leaves.** *J Exp Bot* 2007, **58**(12):3395–3406.
48. Wang ZY, MacRae EA, Wright MA, Bolitho KM, Ross GS, Atkinson RG: **Polygalacturonase gene expression in kiwifruit: relationship to fruit softening and ethylene production.** *Plant Mol Biol* 2000, **42**(2):317–328.
49. Hayama H, Shimada T, Fujii H, Ito A, Kashimura Y: **Ethylene-regulation of fruit softening and softening-related genes in peach.** *J Exp Bot* 2006, **57**(15):4071–4077.
50. Atkinson RG: **A cDNA clone for endopolygalacturonase from apple.** *Plant Physiol* 1994, **105**(4):1437–1438.
51. Tacken E, Ireland H, Gunaseelan K, Karunairetnam S, Wang D, Schultz K, Bowen J, Atkinson RG, Johnston JW, Putterill J, et al: **The role of ethylene and cold temperature in the regulation of the apple POLYGALACTURONASE1 gene and fruit softening.** *Plant Physiol* 2010, **153**(1):294–305.
52. Petersen M, Sander L, Child R, vanOnckelen H, Ulvskov P, Borkhardt B: **Isolation and characterisation of a pod dehiscence zone-specific polygalacturonase from *Brassica napus*.** *Plant Mol Biol* 1996, **31**(3):517–527.
53. Sander L, Child R, Ulvskov P, Albrechtsen M, Borkhardt B: **Analysis of a dehiscence zone endo-polygalacturonase in oilseed rape (*Brassica napus*) and *Arabidopsis thaliana*: evidence for roles in cell separation in dehiscence and abscission zones, and in stylar tissues during pollen tube growth.** *Plant Mol Biol* 2001, **46**(4):469–479.
54. Degan FD, Child R, Svendsen I, Ulvskov P: **The cleavable N-terminal domain of plant endopolygalacturonases from clade B may be involved in a regulated secretion mechanism.** *J Biol Chem* 2001, **276**(38):35297–35304.
55. Jenkins ES, Paul W, Craze M, Whitelaw CA, Weigand A, Roberts JA: **Dehiscence-related expression of an *Arabidopsis thaliana* gene encoding a polygalacturonase in transgenic plants of *Brassica napus*.** *Plant Cell Environ* 1999, **22**(2):159–167.
56. Torki M, Mandaron P, Mache R, Falconet D: **Characterization of a ubiquitous expressed gene family encoding polygalacturonase in *Arabidopsis thaliana*.** *Gene* 2000, **242**(1–2):427–436.
57. Tranbarger TJ, Dussert S, Joet T, Argout X, Summo M, Champion A, Cros D, Omore A, Nouy B, Morcillo F: **Regulatory mechanisms underlying oil palm fruit mesocarp maturation, ripening, and functional specialization in lipid and carotenoid metabolism.** *Plant Physiol* 2011, **156**(2):564–584.
58. Dellapenna D, Kates DS, Bennett AB: **Polygalacturonase Gene Expression in Rutgers, rin, nor, and Nr Tomato Fruits.** *Plant Physiol* 1987, **85**(2):502–507.
59. Roberts JA, Schindler B, Tucker GA: **Ethylene-promoted tomato flower abscission and the possible involvement of an inhibitor.** *Planta* 1984, **160**:159–163.
60. Asif MH, Nath P: **Expression of multiple forms of polygalacturonase gene during ripening in banana fruit.** *Plant Physiol Bioch* 2005, **43**(2):177–184.
61. Mbeugue AMD, Hubert O, Baurens FC, Matsumoto T, Chillet M, Fils-Lycaon B, Sidibe-Bocs S: **Expression patterns of cell wall-modifying genes from banana during fruit ripening and in relationship with finger drop.** *J Exp Bot* 2009, **60**(7):2021–2034.
62. Morcillo F, Gagneur C, Adam H, Richaud F, Singh R, Cheah SC, Rival A, Duval Y, Tregear JW: **Somaclonal variation in micropropagated oil palm. Characterization of two novel genes with enhanced expression in epigenetically abnormal cell lines and in response to auxin.** *Tree Physiol* 2006, **26**(5):585–594.
63. Bourgis F, Kilaru A, Cao X, Ngando-Ebongue GF, Drira N, Ohlrogge JB, Arondel V: **Comparative transcriptome and metabolite analysis of oil palm and date palm mesocarp that differ dramatically in carbon partitioning.** *P Natl Acad Sci USA* 2011, **108**(30):12527–12532.
64. Pfaffl MW: **A new mathematical model for relative quantification in real-time RT-PCR.** *Nucleic Acids Res* 2001, **29**(9):e45.
65. Dereeper A, Guignon V, Blanc G, Audic S, Buffet S, Chevenet F, Dufayard JF, Guindon S, Lefort V, Lescot M: **Phylogeny.fr: robust phylogenetic analysis for the non-specialist.** *Nucleic Acids Res* 2008, **36**(Web Server issue):W465–469.
66. Thompson JD, Higgins DG, Gibson TJ: **CLUSTAL W: improving the sensitivity of progressive multiple sequence alignment through sequence weighting, position-specific gap penalties and weight matrix choice.** *Nucleic Acids Res* 1994, **22**(22):4673–4680.
67. Saitou N, Nei M: **The neighbor-joining method: a new method for reconstructing phylogenetic trees.** *Mol Biol Evol* 1987, **4**(4):406–425.
68. Jones DT, Taylor WR, Thornton JM: **The rapid generation of mutation data matrices from protein sequences.** *Comput Appl Biosci* 1992, **8**(3):275–282.
69. Felsenstein: **Limits on Phylogenies: An Approach Using the Bootstrap.** *Evolution* 1985, **39**(4):783–791.
70. Jabnourne M, Espeout S, Mieulet D, Fizames C, Verdeil JL, Conejero G, Rodriguez-Navarro A, Sentenac H, Guiderdoni E, Abdely C, et al: **Diversity in expression patterns and functional properties in the rice HKT transporter family.** *Plant Physiol* 2009, **150**(4):1955–1971.

doi:10.1186/1471-2229-12-150

Cite this article as: Roongsattham et al.: Temporal and spatial expression of polygalacturonase gene family members reveals divergent regulation during fleshy fruit ripening and abscission in the monocot species oil palm. *BMC Plant Biology* 2012 **12**:150.

Submit your next manuscript to BioMed Central and take full advantage of:

- Convenient online submission
- Thorough peer review
- No space constraints or color figure charges
- Immediate publication on acceptance
- Inclusion in PubMed, CAS, Scopus and Google Scholar
- Research which is freely available for redistribution

Submit your manuscript at
www.biomedcentral.com/submit

